



## **NEW RUTHENIUM, MANGANESE AND COBALT DINUCLEAR COMPLEXES AS REDOX CATALYSTS. UNFOLDING THE ESSENTIAL STEPS FOR THE GENERATION OF SOLAR FUELS**

**Carlo Di Giovanni**

**Dipòsit Legal: T. 1429-2012**

**ADVERTIMENT.** L'accés als continguts d'aquesta tesi doctoral i la seva utilització ha de respectar els drets de la persona autora. Pot ser utilitzada per a consulta o estudi personal, així com en activitats o materials d'investigació i docència en els termes establerts a l'art. 32 del Text Refós de la Llei de Propietat Intel·lectual (RDL 1/1996). Per altres utilitzacions es requereix l'autorització prèvia i expressa de la persona autora. En qualsevol cas, en la utilització dels seus continguts caldrà indicar de forma clara el nom i cognoms de la persona autora i el títol de la tesi doctoral. No s'autoritza la seva reproducció o altres formes d'explotació efectuades amb finalitats de lucre ni la seva comunicació pública des d'un lloc aliè al servei TDX. Tampoc s'autoritza la presentació del seu contingut en una finestra o marc aliè a TDX (framing). Aquesta reserva de drets afecta tant als continguts de la tesi com als seus resums i índexs.

**ADVERTENCIA.** El acceso a los contenidos de esta tesis doctoral y su utilización debe respetar los derechos de la persona autora. Puede ser utilizada para consulta o estudio personal, así como en actividades o materiales de investigación y docencia en los términos establecidos en el art. 32 del Texto Refundido de la Ley de Propiedad Intelectual (RDL 1/1996). Para otros usos se requiere la autorización previa y expresa de la persona autora. En cualquier caso, en la utilización de sus contenidos se deberá indicar de forma clara el nombre y apellidos de la persona autora y el título de la tesis doctoral. No se autoriza su reproducción u otras formas de explotación efectuadas con fines lucrativos ni su comunicación pública desde un sitio ajeno al servicio TDR. Tampoco se autoriza la presentación de su contenido en una ventana o marco ajeno a TDR (framing). Esta reserva de derechos afecta tanto al contenido de la tesis como a sus resúmenes e índices.

**WARNING.** Access to the contents of this doctoral thesis and its use must respect the rights of the author. It can be used for reference or private study, as well as research and learning activities or materials in the terms established by the 32nd article of the Spanish Consolidated Copyright Act (RDL 1/1996). Express and previous authorization of the author is required for any other uses. In any case, when using its content, full name of the author and title of the thesis must be clearly indicated. Reproduction or other forms of for profit use or public communication from outside TDX service is not allowed. Presentation of its content in a window or frame external to TDX (framing) is not authorized either. These rights affect both the content of the thesis and its abstracts and indexes.

UNIVERSITAT ROVIRA I VIRGILI

NEW RUTHENIUM, MANGANESE AND COBALT DINUCLEAR COMPLEXES AS REDOX CATALYSTS.

UNFOLDING THE ESSENTIAL STEPS FOR THE GENERATION OF SOLAR FUELS

Carlo Di Giovanni

Dipòsit Legal: T. 1429-2012

UNIVERSITAT ROVIRA I VIRGILI

NEW RUTHENIUM, MANGANESE AND COBALT DINUCLEAR COMPLEXES AS REDOX CATALYSTS.

UNFOLDING THE ESSENTIAL STEPS FOR THE GENERATION OF SOLAR FUELS

Carlo Di Giovanni

Dipòsit Legal: T. 1429-2012



**New Ruthenium, Manganese and Cobalt  
dinuclear complexes as redox catalysts.**

**Unfolding the essential steps  
for the generation of solar fuels**

**Ph.D. Thesis presented by**

*Carlo Di Giovanni*

In candidacy for the degree of  
Doctor of Philosophy in Chemistry

Supervised by

*Prof. Antoni Llobet Dalmases*

2012



UNIVERSITAT ROVIRA I VIRGILI

NEW RUTHENIUM, MANGANESE AND COBALT DINUCLEAR COMPLEXES AS REDOX CATALYSTS.

UNFOLDING THE ESSENTIAL STEPS FOR THE GENERATION OF SOLAR FUELS

Carlo Di Giovanni

Dipòsit Legal: T. 1429-2012

**Antoni Llobet Dalmases**, Group Leader at the Institute of Chemical Research of Catalonia (ICIQ) in Tarragona and Full Professor of Chemistry at the Universitat Autònoma de Barcelona (UAB), CERTIFIES that the present research work entitled **“New Ruthenium, Manganese and Cobalt dinuclear complexes as redox catalysts. Unfolding the essential steps for the generation of solar fuels”** contains the work carried out by Carlo Di Giovanni under my supervision, constitutes the memory for the candidacy for the degree of Doctor of Philosophy in Chemistry and fulfils all the requirements to be eligible for the European Doctorate Award.

Tarragona, October 2012



UNIVERSITAT ROVIRA I VIRGILI

UNIVERSITAT ROVIRA I VIRGILI

NEW RUTHENIUM, MANGANESE AND COBALT DINUCLEAR COMPLEXES AS REDOX CATALYSTS.

UNFOLDING THE ESSENTIAL STEPS FOR THE GENERATION OF SOLAR FUELS

Carlo Di Giovanni

Dipòsit Legal: T. 1429-2012

UNIVERSITAT ROVIRA I VIRGILI

NEW RUTHENIUM, MANGANESE AND COBALT DINUCLEAR COMPLEXES AS REDOX CATALYSTS.

UNFOLDING THE ESSENTIAL STEPS FOR THE GENERATION OF SOLAR FUELS

Carlo Di Giovanni

Dipòsit Legal: T. 1429-2012

*a mia nonna che non c'è più*

*e a mio nipote che non c'è ancora*

## Acknowledgements

This thesis resumes all the work of my years at ICIQ but there is not an experiment that I would have been able to perform without the help of all the people that have worked, lived and shared these years with me. For this reason in this section I would like to thank to all of them for their important contribution to my Ph.D. inside and outside ICIQ.

First of all I would like to thank my supervisor Prof. Antoni Llobet for the opportunity he gave me to come at ICIQ and work in his group and for being the door of his office always open every time I needed. I want to thank “my group”, this sort of second family made of people of the most different nationalities and cultures linked by the common quest for “oxygen”. I want to start from those who welcomed me in the long gone March 2008. Thank you to Lydia, who has been my best friend during these years, to Xavi, who has always followed my career even after he left ICIQ, to Stephan, my eternal “desk mate”, to Sophie, who helped me from my first day in the lab, to Chiara, for her perpetual smile, to Fernando, who always had time for my questions, to Nora, for helping me in becoming part of the group, to Matías, for his happy character and attitude. Moreover I want say thank you to the people arrived after I did, like Isidoro P, for all the funny moments in the lab, Laura, who became an ever-present friend even from great distances, Somnath, the friend came from far away to teach us how to grow crystals, Pau, who helped me to “catch the light”, Laia, who I always considered as a friend rather than a lab mate, and Takashi, Tomek, Lorenzo, Roc, Pablo and Sukanta. I want to thank those who might arrived later but helped me as if they had always been there like Craig, for telling me “how to say”, Carolina, for teaching me so much in so little time and Joan for the great company in “the office”. I also want to thank

all the people who had spent short stays in the lab, in particular Maribel and Arianna. Then I want to say thanks to those of my Master course, in particular Nuria, Moira, Miriam, Oriol, Cristina and Merce because I will always remember that period as one of the most funny of my Ph.D. And I also want to thank all the ICIQ people I have met in these years who I spent nice moments with. In addition, many thanks to all the people of the research and administrative support units for their help to my work.

Also, a special thank you to Dr Erwin Reisner and his entire group especially Fezile and Masaru, for the help during my stay in Cambridge.

Finally I want to thank Daniele, who made possible that our flat in Tarragona always would remind me of Palermo, my beloved hometown. And I cannot forget my family and my best friends Ugo, Enrico, Silvia, Giorgio and Claudio for their help and support.

The work performed in the present doctoral thesis has been possible thanks to the funding of:

- ❑ Institut Català d'Investigació Química (ICIQ)
- ❑ Ministerio de Ciencia e Innovación CTQ2010-21497
- ❑ AGAUR
- ❑ Ministerio de Ciencia e Innovación dentro del Programa Nacional de Internacionalización de la I+D (Proyectos y Acciones Internacionales )
- ❑ European Commission, SOLAR-H2



UNIVERSITAT ROVIRA I VIRGILI

NEW RUTHENIUM, MANGANESE AND COBALT DINUCLEAR COMPLEXES AS REDOX CATALYSTS.

UNFOLDING THE ESSENTIAL STEPS FOR THE GENERATION OF SOLAR FUELS

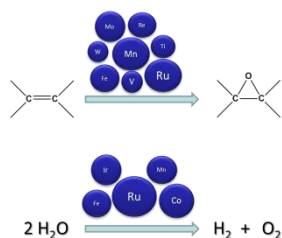
Carlo Di Giovanni

Dipòsit Legal: T. 1429-2012



# Graphical Abstracts

## Chapter I. General introduction

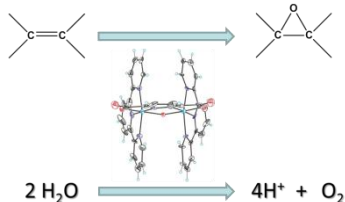


General introduction about the chemistry of ruthenium and its application in catalysis. An overview of the most representative catalysts for water oxidation and alkenes epoxidation.

## Chapter II. Objectives

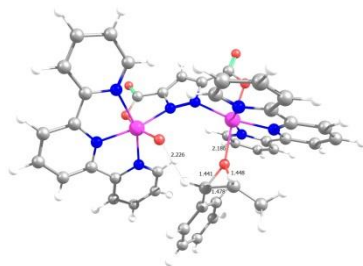


## Chapter III. Synthesis and characterization of two new dinuclear ruthenium complexes based on the pyridazine-3,6-dicarboxylic acid ligand. Reactivity in homogeneous oxidations



A Ru  $\mu$ -chloro and a  $\mu$ -hydroxo complexes containing the pyridazine-3,6-dicarboxylic acid ligand have been synthesized and characterized. Study of the catalytic activity toward water oxidation and olefins epoxidation.

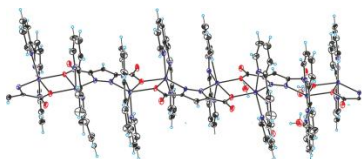
## Chapter IV. Synthesis and characterization of new dinuclear ruthenium complexes based on the pyrazole-3,5-dicarboxylic acid ligand. Reactivity in homogeneous oxidations



A new Ru  $\mu$ -OOCCH<sub>3</sub> complex containing the pyrazole-3,5-dicarboxylic acid ligand has been synthesized, characterized and tested in the epoxidation of olefins. Electrochemical study and DFT calculation of the transition states for the investigation of the reaction mechanism.

---

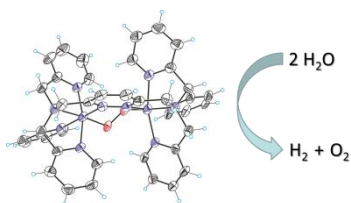
### Chapter V. A new dinuclear manganese bis-aqua complex containing the ligand pyrazole-3,5-dicarboxylic acid. Structural, magnetic characterization and application in the oxidation of *cis*- $\beta$ -methylstyrene



A dinuclear Mn bis-aqua complex containing the pyrazole-3,5-dicarboxylic acid ligand has been synthesized and characterized. Re-crystallization into its polymeric form and study of the magnetic properties of the dimer. Study of the catalytic activity toward epoxidation of *cis*- $\beta$ -methylstyrene with peracetic.

---

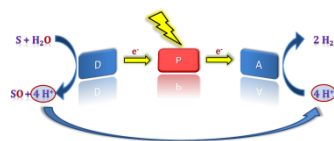
### Chapter VI. Synthesis and characterization of a new polypyridyl decadentate ligand, L. Preparation of cobalt dinuclear complexes based on L and investigation of their catalytic activity



A new a polypyridyl decadentate ligand has been designed and prepared. Two relative Co dinuclear complexes have been synthesized and studied as catalysts for the generation of solar fuels.

---

### Chapter VII. Assembly of a cell for artificial photosynthesis via two-electron oxidation processes



A photocatalytic system for oxidation of organic substrates has been optimized and employed for the assembly of a cell for light-driven  $H_2$  generation.

---

### Chapter VIII. Summary and Conclusions





## Table of Contents

Graphical Abstract	II
Tables of Contents	V
Glossary of Terms and Abbreviations	XI
<b>Chapter I. General Introduction</b>	<b>1-75</b>
<i>i. Ruthenium</i>	3
<i>ii. Ruthenium aqua complexes</i>	4
<i>iii. Ruthenium polypyridyl aqua complexes</i>	5
<i>iv. Higher oxidation states of Ru complexes</i>	9
<i>v. Epoxidation</i>	17
<i>vi. Water Oxidation</i>	39
<i>vii. References</i>	65
<b>Chapter II. Objectives</b>	<b>77-80</b>
<b>Chapter III. Synthesis and characterization of two new dinuclear ruthenium complexes based on the pyridazine-3,6-dicarboxylic acid ligand. Reactivity in homogeneous oxidations</b>	<b>83-111</b>
<i>i. Introduction</i>	85
<i>ii. Experimental Section</i>	87

<i>iii.</i>	<i>Results and discussion</i>	92
<i>iv.</i>	<i>Conclusions</i>	109
<i>v.</i>	<i>Associated content</i>	111
<i>vi.</i>	<i>References</i>	111
<b>Chapter III. Supporting Information</b>		<b>119-137</b>
<b>Chapter IV. Synthesis and characterization of new dinuclear ruthenium complexes based on the pyrazole-3,5-dicarboxylic acid ligand.</b>		<b>139-180</b>
<b>Reactivity in homogeneous oxidations.</b>		
<i>i.</i>	<i>Introduction</i>	141
<i>ii.</i>	<i>Experimental Section</i>	143
<i>iii.</i>	<i>Results and discussion</i>	148
<i>iv.</i>	<i>Conclusions</i>	175
<i>v.</i>	<i>Associated content</i>	177
<i>vi.</i>	<i>Acknowledgements</i>	177
<i>vii.</i>	<i>References</i>	178
<b>Chapter IV. Supporting Information</b>		<b>183-193</b>
<b>Chapter V. A new dinuclear manganese bis-aqua complex containing the pyrazole-3,5-dicarboxylic acid ligand. Structural, magnetic characterization and application in the oxidation of <i>cis</i>-<math>\beta</math>-methylstyrene</b>		<b>195-214</b>

<i>i.</i>	<i>Introduction</i>	197
<i>ii.</i>	<i>Experimental Section</i>	199
<i>iii.</i>	<i>Results and discussion</i>	203
<i>iv.</i>	<i>Conclusions</i>	212
<i>v.</i>	<i>Associated content</i>	213
<i>vi.</i>	<i>Acknowledgements</i>	213
<i>vii.</i>	<i>References</i>	213
	<b>Chapter V. Supporting Information</b>	<b>217-221</b>
	<b>Chapter VI. Synthesis and characterization of a new polypyridyl decadentate ligand, L. Preparation of cobalt dinuclear complexes based on L and investigation of their catalytic activity</b>	<b>223-279</b>
<i>i.</i>	<i>Introduction</i>	225
<i>ii.</i>	<i>Experimental Section</i>	231
<i>iii.</i>	<i>Results and discussion</i>	242
<i>iv.</i>	<i>Conclusions</i>	275
<i>v.</i>	<i>Associated content</i>	276
<i>vi.</i>	<i>Acknowledgements</i>	276
<i>vii.</i>	<i>References</i>	277

<b>Chapter VI. Supporting Information</b>	<b>281-296</b>
<b>Chapter VII. Assembly of a cell for artificial photosynthesis via two-electron oxidation processes</b>	<b>299-331</b>
<i>i. Introduction</i>	301
<i>ii. Experimental Section</i>	304
<i>iii. Photochemical oxidation of organic substrate</i>	308
<i>iii. i. Results and discussion</i>	309
<i>iii. ii. Conclusions</i>	314
<i>iv. Assembly of a system for photochemical sulfide oxidation and proton reduction</i>	315
<i>iv. i. Results and discussion</i>	317
<i>iv. ii. Conclusions</i>	328
<i>v. Associated content</i>	330
<i>vi. Acknowledgments</i>	330
<i>vii. References</i>	331
<b>Chapter VII. Supporting Information</b>	<b>333-340</b>
<b>Chapter VIII. Summary and Conclusions</b>	<b>343-346</b>

UNIVERSITAT ROVIRA I VIRGILI  
NEW RUTHENIUM, MANGANESE AND COBALT DINUCLEAR COMPLEXES AS REDOX CATALYSTS.  
UNFOLDING THE ESSENTIAL STEPS FOR THE GENERATION OF SOLAR FUELS  
Carlo Di Giovanni  
Dipòsit Legal: T. 1429-2012



UNIVERSITAT ROVIRA I VIRGILI  
NEW RUTHENIUM, MANGANESE AND COBALT DINUCLEAR COMPLEXES AS REDOX CATALYSTS.  
UNFOLDING THE ESSENTIAL STEPS FOR THE GENERATION OF SOLAR FUELS  
Carlo Di Giovanni  
Dipòsit Legal: T. 1429-2012

## Glossary of Terms and Abbreviations

$\delta$ :	chemical shift (units: ppm)
$\Delta E$	difference of potential
$\lambda$	wavelength
$\mu$	ionic force
A	ampere
abs:	absorbance
AcO	Acetate
bpy	2,2'-bipyridine
C	Coulomb
COSY	correlation
CPE	Controlled potential electrolysis
CV	cyclic voltammetry
d	Doublet
DCM	Dichloromethane
dcpd <sup>2-</sup>	pyridazine-3,6-dicarboxylate anion
dcpz <sup>3-</sup>	Pyrazole-3,5-dicarboxylate anion
DFT	Density Functional Theory
dmsO	dimethyl sulfoxide
DPV	Differential Pulse Voltammetry
d	doublet
E	potential
E <sup>o</sup>	standard redox potential
E <sub>1/2</sub>	half-wave potential
E <sub>p,a</sub>	anodic peak potential
E <sub>p,c</sub>	cathodic peak potential

ESI-MS	electrospray ionization mass spectroscopy
EtOAc	ethyl acetate
FT-IR	fourier transform infrared spectroscopy
J	coupling constant
GC	Gas Chromatography
H <sub>2</sub> dcpd	pyridazine-3,6-dicarboxylic acid
H <sub>3</sub> dcpz	Pyrazole-3,5-dicarboxylic acid
m	multiplet
m/z	mass-to-charge ratio
MALDI	Matrix assisted lased desorption/ionization
Me	methyl
MeCN	acetonitrile
MLCT	metal-to-ligand charge-transfer
MS	Mass spectroscopy
NHE	Normal Hydrogen Electrode
NMR	nuclear magnetic resonance
NOE	nuclear overhauser effect
NOESY	nuclear overhauser spectroscopy
ORTEP	Oak Ridge thermal ellipsoid plot
PCET	Proton Coupled Electron Transfer
Ph	Phenyl
py	pyridine
RT	Room Temperature
s	singlet
SSCE	Sodium Saturated Calomel Electrode
SPS	Solvent Purification System
t	triplet

TBAH	tetrabutylammonium hexafluorophosphate
TFA	Trifluoroacetic acid
TMS	tetramethylsilane
TN	Turnover number
TOF	Turnover frequency
trpy	2,2' :6', 2''-terpyridine
UV-vis	Ultraviolet-visible spectroscopy
V	Volt

UNIVERSITAT ROVIRA I VIRGILI  
NEW RUTHENIUM, MANGANESE AND COBALT DINUCLEAR COMPLEXES AS REDOX CATALYSTS.  
UNFOLDING THE ESSENTIAL STEPS FOR THE GENERATION OF SOLAR FUELS  
Carlo Di Giovanni  
Dipòsit Legal: T. 1429-2012



UNIVERSITAT ROVIRA I VIRGILI  
NEW RUTHENIUM, MANGANESE AND COBALT DINUCLEAR COMPLEXES AS REDOX CATALYSTS.  
UNFOLDING THE ESSENTIAL STEPS FOR THE GENERATION OF SOLAR FUELS  
Carlo Di Giovanni  
Dipòsit Legal: T. 1429-2012

# Chapter I

## General introduction

- i. Ruthenium*
- ii. Ruthenium aqua complexes*
- iii. Ruthenium polypyridyl aqua complexes*
- iv. Higher oxidation states of Ru complexes*
- v. Epoxidation*
  - v. i. Mechanism*
- vi. Water Oxidation*
  - vi. i. Climate changes and energy demand*
  - vi. ii. Photosystem II*
  - vi. iii. Assembly of a cell for artificial photosynthesis*
  - vi. iv. Photosensitizer*
  - vi. v. Ruthenium water oxidation catalysts*
  - vi. vi. Other water oxidation catalysts*
- vii. References*





## I. i. Ruthenium

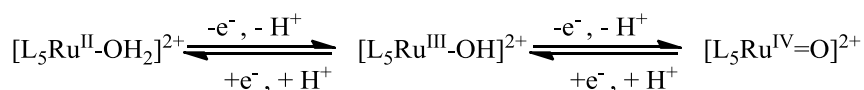
Discovered more than 150 years ago in Siberia by Karl Klaus, ruthenium is one of the rarest elements on the Earth's crust with, an abundance of  $10^{-7}\%$ , but also one of the most sought after by investigators. The great interest that this element generates in scientists is mainly due to its wide range of accessible oxidation states, from -2 in  $[\text{Ru}(\text{CO})_2]^{2-}$  to +8 in  $\text{RuO}_4$ . Lastly its price (\$ 4.2 per gram) makes it fairly cheap compared to platinum (\$ 54.4 per g) and Rh (\$ 49.0 per g)<sup>1</sup>.

Compounds of ruthenium often show a perfect balance between reactivity and stability that make them attractive catalysts. Good  $\sigma$ -donors like  $\text{F}^-$ ,  $\text{O}^{2-}$  and  $\text{N}^{3-}$  stabilize higher oxidation states while  $\pi$ -acceptors such as CO and  $\text{NO}^+$  stabilize low oxidation state<sup>2</sup>. The nature of the coordinated ligand strongly affects the application of ruthenium complexes in catalysis ranging from oxidation to reduction. Complexes with phosphine and diphosphine ligands are employed in  $\text{CO}_2$  reduction<sup>3-14</sup> and enantioselective hydrogenations<sup>15-23</sup>. Sulfoxide complexes of ruthenium have showed activity against tumors often comparable to platinum compounds but with host toxicity of some order of magnitude lower<sup>24</sup>. Incorporation of oxazoline ligands led to the preparation of several ruthenium catalysts active for the epoxidation of alkenes<sup>25,26</sup>. Compounds containing  $\pi$ -conjugated ligands have been studied due to their properties in nonlinear optics<sup>27-29</sup>, magnetism<sup>30,31</sup>, molecular sensors<sup>32</sup> and liquid crystals<sup>33</sup>. Nevertheless the ruthenium compounds that most have attracted the attention in recent years are the polypyridyl based complexes. Their spectroscopic, photophysical, photochemical and electrochemical properties has allowed their use in the construction of supramolecular systems and in the development of photochemically driven molecular devices<sup>34-36</sup>. The large expansion of polypyridyl ruthenium catalysts has been facilitated by the

extensive synthetic chemistry behind these compounds. Several synthetic ways have been improved allowing the systematic removal of some ligands and the maintenance of others leading to the synthesis of well characterized precursors and wide families of related compounds. The elevated melting point, together with the stability in hard conditions, like strong acids, have permitted the preparation of advanced molecular assemblies often not accessible for first row transition metals<sup>37</sup>. Ruthenium polypyridyl complexes have also received attention as functional models for water-oxidation catalysis and photochemical cleavage of water<sup>34,38,39</sup>. In recent years probably the most investigated ruthenium complex has been  $[\text{Ru}(2,2'\text{-bipyridine})_3]^{2+}$ ; thanks to the long-lived photo excited triplet generated under visible light irradiation and to its stability in water it has been the most employed photosensitizer in photocatalytic processes<sup>40-42</sup>. More recently, related complexes have found wide employment as dyes, often attached into semiconductors like  $\text{TiO}_2$ <sup>43-49</sup>. After more than 150 years from its discovery, ruthenium is still one of the elements most attractive for chemists.

## I. ii. Ruthenium aqua complexes

The electrochemical and spectroscopic properties related to ruthenium aqua complexes are two of the major factors that have contributed to the increasing interest into this family of compounds. These complexes undergo proton coupled electron transfer (PCET) making high oxidation states of the metal center more accessible over a relatively narrow range in redox potentials<sup>50</sup> (Scheme 1).



**Scheme 1.** PCET reactions of ruthenium aqua complexes.

Ru(II) aqua complexes present an ideal compromise between softness and acidity of the bound  $\text{H}_2\text{O}$ , and back-bonding into  $\pi^*$  orbitals of carbon  $\pi$  ligands. One of the protons of the aqua ligand can be easily removed in basic media leading to a well define change in the absorption spectra.

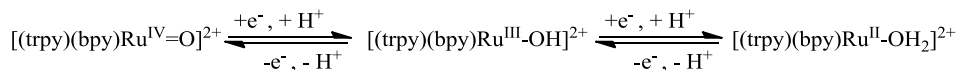
The simplest aqueous species,  $[\text{Ru}(\text{H}_2\text{O})_6](\text{tos})_2$ , is an ideal precursor for a series of aqua complexes with several ligands like polypyridyl groups, phosphines, arenes, olefins and small gaseous molecules. Aebischer et al. reported that the rate constants for the mono-complex formation between  $[\text{Ru}(\text{H}_2\text{O})_6]_2$  and several ligands were almost independent of the nature of the ligand indicating that the entering group has little influence on the transition state<sup>51</sup>. However, the substitution of a weak  $\sigma$ -donating effect, as for  $\text{H}_2\text{O}$ , by ligands with withdrawing and donating properties, strongly influences the redox potential of the metal center resulting in remarkable implications for catalysis. As a general rule the Ru(II) species is stabilized by the  $d\pi$ - $\pi^*$  back-bonding effect (in the presence of ligand like  $\text{PPh}_3$  and  $\text{CH}_3\text{CN}$ ) having low acceptor levels. Contrarily electron-donating ligands like acetylacetonate and oxalate stabilize the Ru(III) oxidation state<sup>52,53</sup>. Ru(IV) oxidation state is less sensitive to ligand modification but gains its stability from the interaction with the O group in a  $\text{Ru}=\text{O}$  bond (see below).

### I. iii. Ruthenium polypyridyl aqua complexes

Thomas J. Meyer, in the early 1980's, deeply studied the redox chemistry of polypyridyl ruthenium aqua complexes starting with  $[\text{Ru}^{\text{II}}(\text{OH}_2)(\text{trpy})(\text{bpy})]^{2+}$ <sup>54-58</sup>. The main effect of oxidation of an aqua complex is the enhanced acidity of the bound  $\text{Ru}-\text{O}-\text{H}$  protons. Both the proton loss and the donation of the freed  $p$ - $\pi$  oxygen electron density to the metal to form the  $\text{M}=\text{O}$  double bond increase the stability of higher oxidation states in the complex<sup>59</sup>.

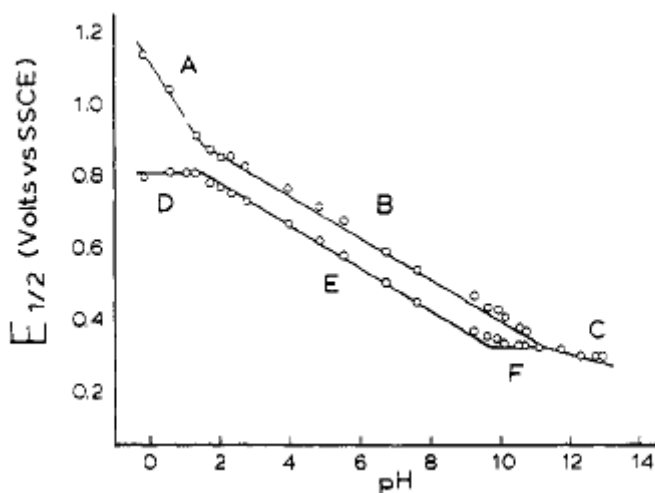
## General Introduction

Spectrophotometric and electrochemical titrations were performed for investigating the PCET processes described by the following reactions:



**Scheme 2.** PCET reactions of  $[\text{Ru}^{\text{II}}(\text{OH}_2)(\text{trpy})(\text{bpy})]^{2+}$

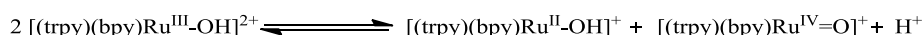
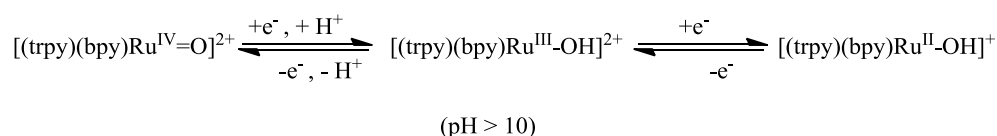
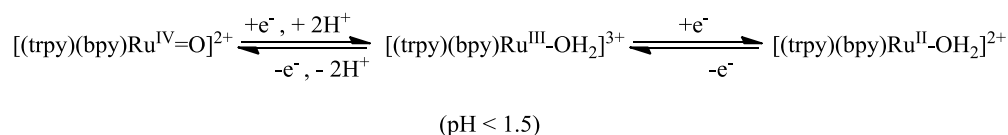
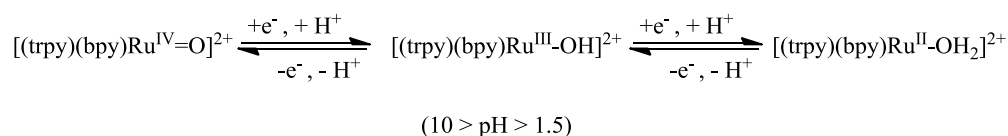
The resulting Pourbaix diagram<sup>58</sup> (Figure 1) shows that over the range of pH from 1.5 to 10 the potentials for the Ru(IV/III) and the Ru(III/II) couples form two straight lines with slopes close to the Nerstian prediction of -0.059 V/pH unit, indicative of a one-electron oxidation accompanied by one proton loss ( $E_{1/2} = E_{1/2}^0 - 0.059(m/n) \text{ pH}$ ).

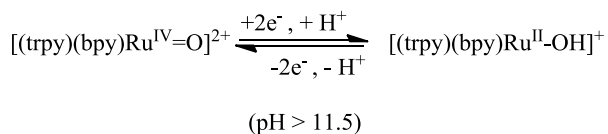


**Figure 1.** Pourbaix diagram of  $[\text{Ru}^{\text{II}}(\text{OH}_2)(\text{trpy})(\text{bpy})]^{2+}$ .

For  $\text{pH} < 1.5$  the  $E_{1/2}$ -pH variation for the Ru(IV/III) couple is linear with a slope close to -0.118 V/pH units, indicative of a one-electron oxidation accompanied by the dissociation of two protons. On the other hand the Ru(III/II) couple the trend is linear but with zero slope, indicative of a one-electron couple with no

proton loss upon oxidation. At  $\text{pH} > 10$ , the potentials for the Ru(IV/III) couple vary linearly with the  $\text{pH}$ , with a slope near  $-0.059 \text{ V/pH}$  units, while the Ru(III/II) couple becomes  $\text{pH}$  independent as a consequence of a proton loss from  $[(\text{trpy})(\text{bpy})\text{Ru}^{\text{II}}\text{-OH}_2]^{2+}$ . Because of the different  $\text{pH}$  dependences for the two couples, a crossing point (defined by a  $\Delta E_{1/2}=0$  between the two oxidations) at  $\text{pH} 11.5$  appears. After this  $\text{pH}$  value the Ru(III) species become unstable with respect to disproportionation due to the fact that the potential for the Ru(IV/III) couple falls below the potential for the Ru(III/II) couple. The  $\text{pH}$  dependence is now of  $-0.030\text{V/pH}$  units, consistent with a two-electron/one proton loss process and the relative voltammogram is characterized by a single wave. The reactions for the processes described above are the following<sup>58</sup>:





**Scheme 3.** PCET reactions of  $[\text{Ru}^{\text{II}}(\text{OH}_2)(\text{trpy})(\text{bpy})]^{2+}$  at different pH values.

The results obtained by a Pourbaix diagram like the one described above are of great importance in the context of potential photoredox applications where excitation by a single photon and excited-state quenching could lead to a net two electron redox reagent depending of the reaction conditions.

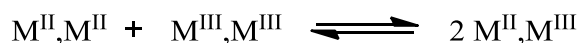
An important remark is that variations in the coordinated ligands provoke systematic variation in the redox potentials of the aqua species.

Meyer and co-workers also gave one of the first examples of an electrochemical study on a bimetallic ruthenium aqua complex,  $\{[(\text{trpy})(\text{pic})\text{Ru}^{\text{III}}]_2\text{O}\}^{2+}$ , where the two metal centers are linked by a  $\mu\text{-O}$  atom<sup>60</sup>. This work demonstrated that the complex could stabilize higher oxidation states when an electronic communication between the metal centers exists across the bridge. A main feature of bimetallic complexes is their ability to generate mixed valence states after oxidation of the first metal center. According to the Robin and Day classification<sup>61</sup> the mixed valence compounds can be sorted into three classes:

- ✓ Class I: the metals of the complex have little or no communication across the ligand bridge.
- ✓ Class II: a communication between the metal centers exists and influences the electrochemical properties of the complex. A typical voltammogram of a class II compound presents discrete redox waves for each metal center.

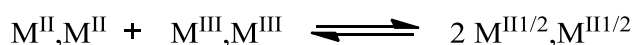
- ✓ Class III: the metals own identity because the short distance between them allows delocalization of the orbitals of each metal across the bridge.

The mixed valence state for a class II complex can be described by the following comproportionation equilibrium:



**Scheme 4.** Comproportionation equilibrium for class II complexes.

while for a class III compound it would be:



**Scheme 5.** Comproportionation equilibrium for class III complexes.

The values of constants for the reactions displayed above define the class of a bimetallic complex.

#### I. iv. Higher oxidation states of Ru complexes

As already mentioned above, the ability to achieve stable higher oxidation state species of ruthenium has important implications for reaction mechanisms and catalysis. The presence of an oxo group directly bound to the metal center offers different approaches for catalysis:

1. An O atom transfer pathway
2. A site for attack on a substrate
3. An acceptor site for hydride transfer

Thanks to these features the Ru(IV)=O species are able to oxidize a wide range of organic<sup>62-68</sup> and inorganic<sup>69-73</sup> substrates.



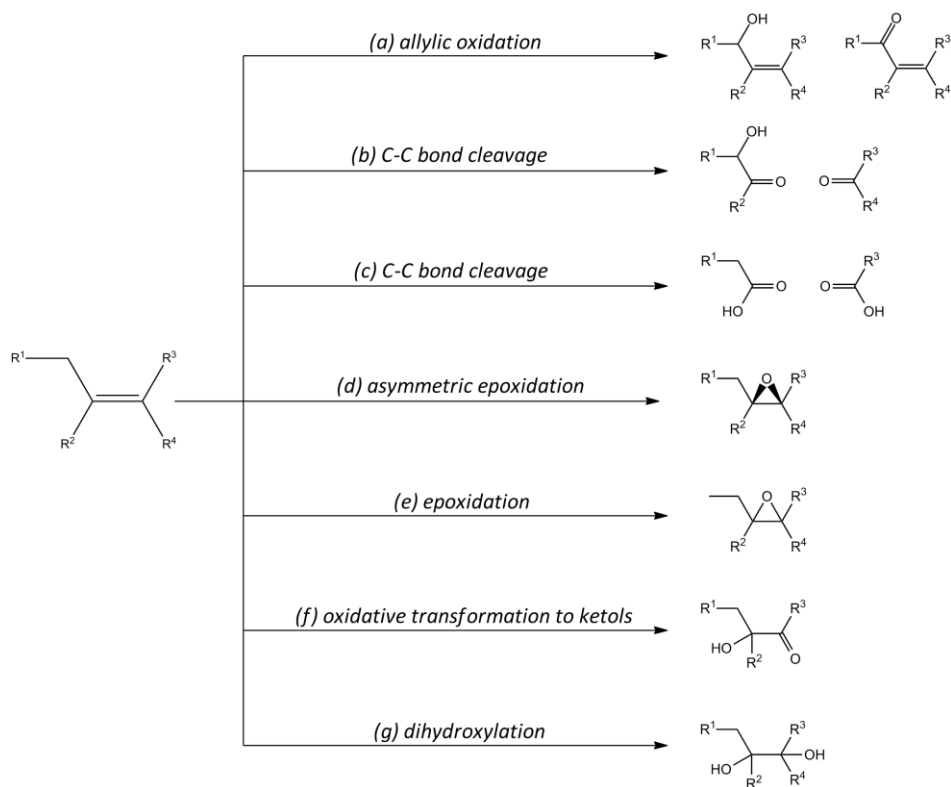
## ✓ Organic

### • Alkanes

The oxidation of alkanes catalyzed by ruthenium complexes can be performed by complexes containing porphyrins<sup>74-77</sup>, phthalocyanine<sup>78</sup>, phosphine<sup>79</sup>, sulfoxide, pyridyl<sup>80,81</sup> and or other ligands<sup>82-88</sup> but the TNs are usually low. Recently oxidation to alcohols and ketones in high TN has been obtained by Neumann and Mizuno employing a POM with formula  $[(\eta\text{-C}_4\text{H}_9)_4\text{N}]_4\text{H}[\text{SiW}_{11}\text{Ru}^{\text{III}}(\text{H}_2\text{O})\text{O}_{39}]\cdot 2\text{H}_2\text{O}$ <sup>89</sup>. Another POM, with formula  $[(\text{Ru}(\text{C}_6\text{Me}_6))_3\text{Mo}_5\text{O}_{18}]$ , for the hydroxylation of adamantane has been published by Bonchio and coworkers<sup>90</sup>. Conversion up to 94% has been obtained and kinetic evidence of in-situ formation of high valent Ru-oxo species has been presented.

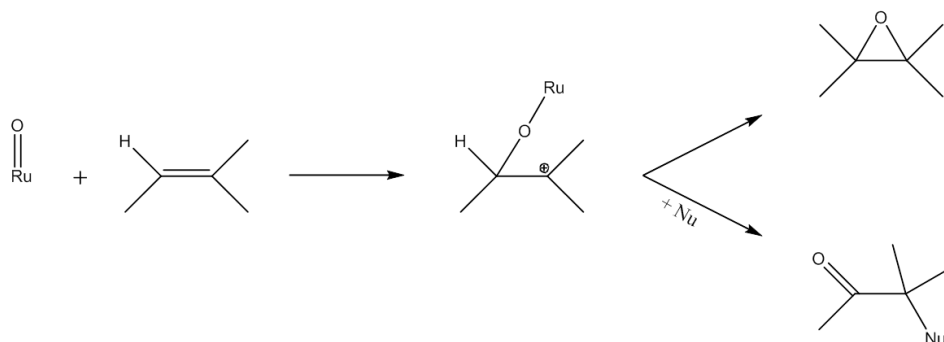
### • Alkenes

Alkenes can be converted into different products depending on the nature of the substrate and if the oxidation involves the C=C bond cleavage or not. No cleavage reactions lead to the formation of epoxides, diols,  $\alpha$ -hydroxyketones and cyclization products (Figure 2).



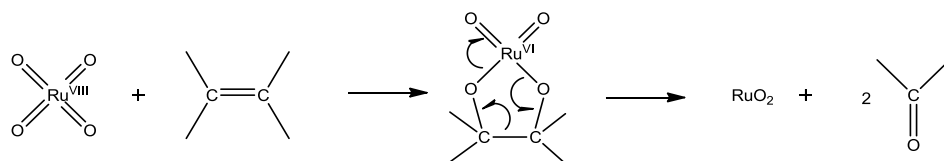
**Figure 2.** Oxidation reactions of alkenes.

Epoxidation (Figure 2, *d* and *e*) will be treated in more detail in I.v. Formation of ketols (Figure 2, *f*) can be explained by the electrophilic attack of a  $R=O$  (Scheme 6) species to the double bond and formation of a cationic intermediate that, treated with water undergoes  $\beta$ -elimination of  $M-H$ , to evolve the  $\alpha$ -hydroxyketone<sup>91</sup>.



**Scheme 6.** Electrophilic attack of oxoruthenium species to C=C double bond.

Oxidations that involve the C=C bond cleavage give aldehydes, ketones, and carboxylic acids as products (Figure 2, *b* and *c*). It is commonly accepted that the mechanism proceeds through coordination of Ru-dioxo species to the double bond<sup>92</sup> (Scheme 7).



**Scheme 7.** Coordination of Ru-dioxo species to C=C double bond.

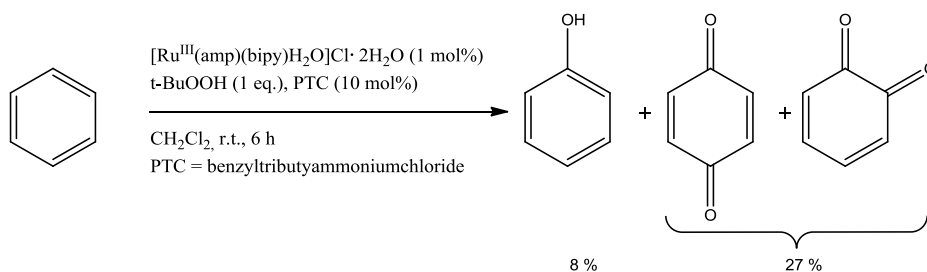
Several systems that employ ruthenium catalysts and NaIO<sub>4</sub>, PhIO, *tert*-BuOOH and O<sub>2</sub> as oxidants have been described for the oxidation of alkenes via C=C bond cleavage; epoxidation is usually a competitive reaction<sup>93-97</sup>.

- *Alkynes*

Similarly to alkenes, alkynes can be oxidized through pathways that involve the acetylenic bond, giving diketones as products, or through C≡C bond cleavage leading to the formation of carboxylic acids.

- *Benzene*

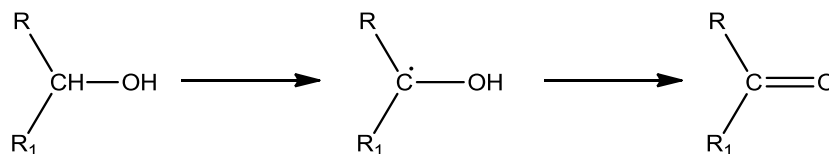
Recently, Chatterjee and coworkers described the oxidation of benzene by a Ru(III) mononuclear aqua complex using tert-BuOOH as the oxidant<sup>98</sup>. Even if the yield and the selectivity are moderate, the reaction has great importance for industrial purposes (phenol is used as disinfectant in surgery)



**Scheme 8.** Benzene oxidation catalyzed by [Ru<sup>III</sup>(amp)(bipy)H<sub>2</sub>O]Cl · 2H<sub>2</sub>O.

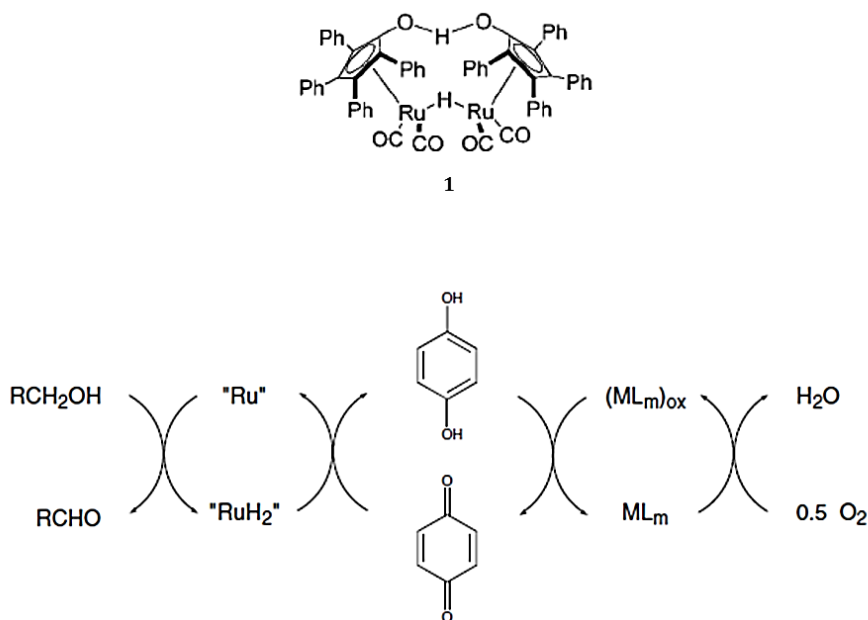
- *Alcohols*

The oxidation of alcohols is one of the widest studied topics in ruthenium-catalyzed chemistry. Primary alcohols are oxidized to aldehydes and carboxylic acids; secondary alcohols to ketones; and diols and polyols to lactones and acids. Different mechanisms have been proposed for the oxidation of alcohols. For one electron oxidants like Co(III), Ce(IV), V(V), Mn(III), Fe(III), Cu(III) the mechanism proceeds via an electron transfer between the substrate and the metal accompanied by the rate-determining breaking of an  $\alpha$ -CH bond and relative formation of a radical species.



**Scheme 9.** Oxidation of alcohols via formation of radical species.

For two-electron oxidants the different pathways have been described: (a) two successive one-electron transfer via radical species; (b) concerted two-electron transfer from substrate to metal, coupled with deprotonation of the substrate; (c) deprotonation of the substrate followed by hydride transfer from the substrate to the metal<sup>99</sup>. An interesting system has been developed by Bäckvall and coworkers for the Ru-catalyzed oxidation of alcohol with O<sub>2</sub><sup>100-102</sup>. A low valent Ru complex (**1**, Figure 3) reacts with the substrate giving an aldehyde (or ketone) and the ruthenium dihydride species as products. The presence of benzoquinone assures the regeneration of the catalyst via hydrogen transfer, while an iron phthalocyanine or a cobalt salen (ML<sub>m</sub>) converts the resulting hydroquinone again to benzoquinone via aerobic oxidation (Figure 3).



**Figure 3.** Aerobic oxidation of alcohol catalyzed by **1**.

- *Other organics substrates*

Ruthenium catalysts have been proven to be capable of oxidizing a wide variety of other organic substrates beyond those mentioned above. Some of them are presented in Table 1 with their relative products<sup>2</sup>:

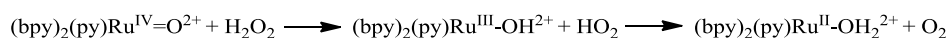
**Table 1.** Substrates of Ru catalyzed oxidation reactions.

Substrate	Product
Ether	Ester
Sulfide	Sulfoxide
Sulfoxide	Sulfone
Amine (primary and secondary)	Imine, nitrile
Amine (tertiary)	Amine-N-oxide
Amide	$\alpha$ -oxygenated amide <sup>103</sup>
$\beta$ -lactam	Acyloxy- $\beta$ -lactam
Phosphine	Phosphine oxide

### ✓ Inorganic

- *Hydrogen peroxide*

Hydrogen peroxide can be oxidized by high valence Ru species, like  $(bpy)_2(py)Ru=O^{2+}$ , giving  $O_2$  and a  $Ru(II)-OH_2$  species. The mechanism of two sequential one-electron transfer steps<sup>59,104,105</sup>, proposed by Meyer and coworkers, is shown in Scheme 10.

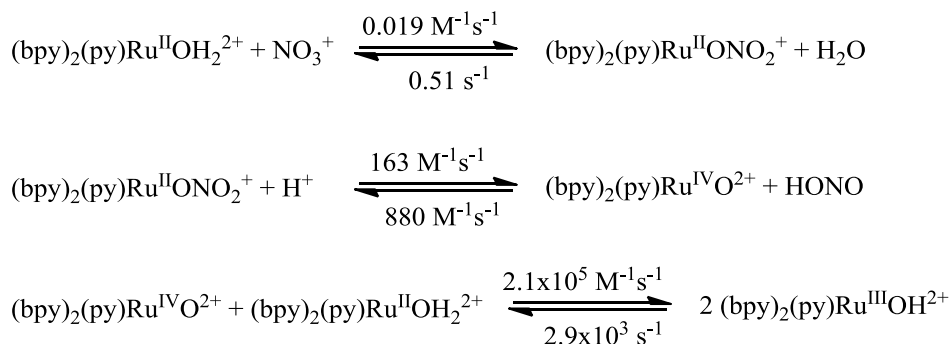


**Scheme 10.** Proposed mechanism for  $H_2O_2$  oxidation catalyzed by  $(bpy)_2(py)Ru^{IV}=O^{2+}$ .

## General Introduction

- *Nitrates*

Conversion of nitrates into nitrites is an important process from a mechanistic point of view since it supports the existence of multiple electron steps pathways. Mechanistic and kinetic studies have been done in order to obtain a clear scheme of the reaction course:

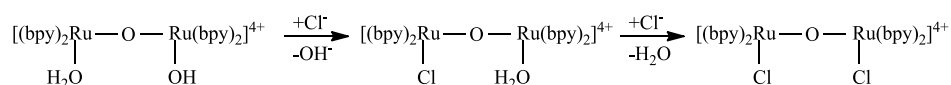


**Scheme 11.** Conversion of nitrates into nitrites catalyzed by  $(\text{bpy})_2(\text{py})\text{Ru}^{\text{II}}\text{OH}_2^{2+}$ .

In such a scheme an initial ligand substitution occurs in the first step, one water molecule is displaced by a  $\text{NO}_3^-$ , giving an intermediate nitrate ion. The latter undergoes an intramolecular redox reaction giving free  $\text{HNO}_2$  after uptake of one proton. The last reaction is a rapid comproportionation equilibrium that leads to the Ru(III) species. If the reaction is carried out in an electrochemical cell,  $(\text{bpy})_2\text{pyRu}^{\text{III}}(\text{OH}_2)^{3+}$  can be electrochemically reduced back to  $(\text{bpy})_2\text{pyRu}^{\text{II}}(\text{OH}_2)^{2+}$ , and the net process becomes catalytic<sup>57,59</sup>.

- *Chloride*

Some ruthenium complexes in high valence states have been proven to be able to oxidize chloride to chlorine<sup>59</sup>. One example is the dimer  $[(\text{bpy})_2(\text{OH}_2)\text{Ru}]_2\text{O}^{4+}$ . The first step consists of the coordination of  $\text{Cl}^-$  in the inner coordination sphere (Scheme 12).

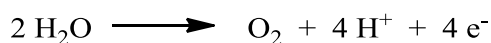


**Scheme 12.** Coordination of  $Cl^-$  to  $[(bpy)_2(OH_2)Ru]_2O^{4+}$ .

The active ruthenium species has been demonstrated, by electrochemical studies, to be the Ru(IV)-Ru(V) dimer<sup>106-108</sup>.

- *Water*

The most interesting inorganic substrate that ruthenium complexes are able to oxidize is undoubtedly water.



**Scheme 13.** Reaction of water oxidation.

The process, which leads to the formation of  $O_2$  and  $4H^+$ , is a highly energy demanding reaction ( $\Delta G = 113.38$  kcal / 4.92 eV) and the mechanism is one of the more complex in catalysis since it includes the removal of four protons and four electrons and the formation of an oxygen-oxygen bond. A more in depth description of the oxidation of water and a resume of the more representative catalysts is given in I.vi.

## I. v. Epoxidation

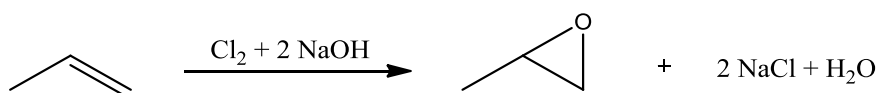
Epoxides are compounds containing a three-membered ring that gives them peculiar properties especially in terms of reactivity. The strained ring is inclined to open, leading to the formation, by attack of a nucleophile, of compounds that contains two adjacent functional groups (diols, alkoxy alcohol, amino alcohol). Epoxides can also be used to assemble polymers known as epoxies, which are excellent adhesives and useful surface coatings. The reactivity of the three-membered ring has great importance also in



## General Introduction

biochemistry; squalene 2,3-epoxide, for example, is the biological precursor to cholesterol and the steroid hormones, including testosterone, progesterone, estrone and cortisone.

The catalytic epoxidation of alkenes is therefore an industrial process of great importance. The formation of epoxides via the catalytic reaction of molecular oxygen with alkenes is the most elegant and environmentally friendly route; however it is not viable for the majority of alkenes. The production of simple epoxides, like propylene oxide, is still now the chlorohydrin process in which alkenes react with chlorine in the presence of sodium hydroxide.



**Scheme 14.** Chlorohydrin process.

1,2-dichloropropane is a by-product of the reaction and its generation on an industrial scale is certainly unattractive from an environmental point of view.

The development of catalytic systems based on transition metals catalysts has been for long time a topic of investigation. One important factor in the transition metal-catalyzed epoxidation of alkenes is the terminal oxidant. Most used compounds able to oxidize the catalyst to the active species are alkyl hydroperoxides, hypochlorite, iodosylbenzene, peracetic acid, hydrogen peroxide and molecular oxygen. Three factors affect the choice of the oxidant:

- Compatibility with the metal
- Active oxygen content
- Waste product

$\text{O}_2$  is certainly the most desirable oxidant for active oxygen content and waste generations, however just a few examples of catalysts are able to be oxidized by  $\text{O}_2$  and the resulting selectivity is often very low.  $\text{H}_2\text{O}_2$  presents the same

problem of selectivity and, in addition, in some cases can cause decomposition of the catalyst or it can be decomposed by the latter<sup>109-116</sup>. Organic oxidants have the advantage of being compatible with the majority of metal-based epoxidation systems but present a low content of active oxygen. Some of the most used oxidants are sorted in the following table<sup>116</sup>:

**Table 2.** Oxidants used in transition metal-catalyzed epoxidations, and their active oxygen content.

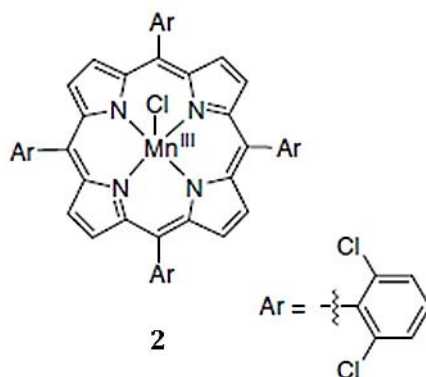
Oxidant	Active oxygen content (wt. %)	Waste product
Oxygen (O <sub>2</sub> )	100	Nothing or H <sub>2</sub> O
Oxygen (O <sub>2</sub> )/reductor	50	H <sub>2</sub> O
H <sub>2</sub> O <sub>2</sub>	47	H <sub>2</sub> O
NaOCl	21.6	NaCl
CH <sub>3</sub> CO <sub>3</sub> H	21.1	CH <sub>3</sub> CO <sub>2</sub> H
<i>t</i> -BuOOH (TBHP)	17.8	<i>t</i> -BuOH
KHSO <sub>5</sub>	10.5	KHSO <sub>4</sub>
BTSP <sup>a)</sup>	9	Hexamethyldisiloxane
PhIO	7.3	PhI

a) Bistrimethylsilyl peroxide.

Several transition metals have been used for the epoxidation of alkenes, some of them for their elevated efficiency, others for their easy preparations, and some for their affinity with “green” oxidants. A short description of the most famous and recent catalysts is summarized below.

### ✓ Manganese

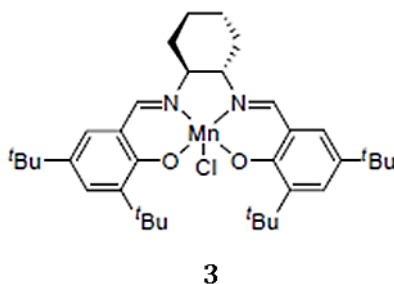
Manganese based catalysts generally have good affinity with oxidants like iodossylbenzene, sodium hypochlorite, alkyl peroxides and hydroperoxides, N-oxides, KHSO<sub>5</sub>, and oxaziridines. Mansuy and coworkers demonstrated that chlorinated manganese porphyrins (Figure 4, **2**) are suitable catalysts for alkene epoxidation with H<sub>2</sub>O<sub>2</sub> as the terminal oxidant<sup>117</sup>.



**Figure 4.** Manganese chlorinated porphyrin **2**.

A drawback of this catalyst was however its stereospecificity for *cis*-alkenes, *trans*-alkenes are not suitable substrates.

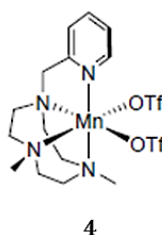
The introduction of salen ligands (Figure 5, **3**), discovered by the groups of Jacobsen and Katsuki, represented a breakthrough in the field of epoxidation by manganese catalysts.



**Figure 5.** Mn-salen complex **3**.

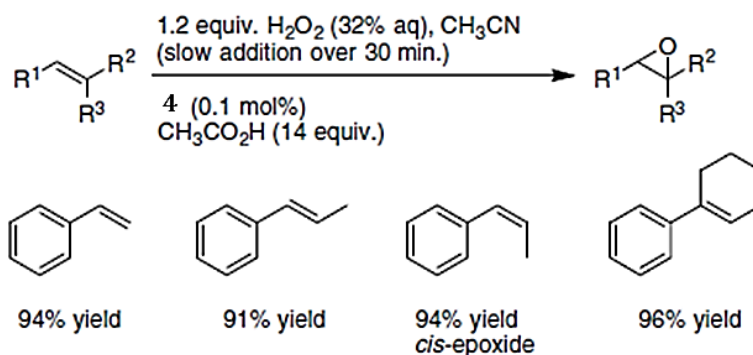
Chiral Mn-salen complexes catalyze the enantioselective formation of epoxides<sup>118-120</sup> using NaOCl and H<sub>2</sub>O<sub>2</sub><sup>121,122</sup> as terminal oxidants. However for these catalysts better results were also obtained in the oxidation of *cis* isomers (>90% *ee*) than *trans* isomers (<40%). Another common problem in the

epoxidation with  $\text{H}_2\text{O}_2$  catalyzed by Mn-salen complexes is the decomposition of the oxidant and catalyst deactivation caused by the presence of water<sup>123-125</sup>. Recently Ribas and Costas presented a manganese triflate complex based on a tetradentate ligand (Figure 6, **4**) derived from triazoacyclononane as a robust and efficient catalyst for epoxidations of alkenes using peracetic acid and  $\text{H}_2\text{O}_2$  as oxidants<sup>126,127</sup>.



**Figure 6.** Manganese triflate complex **4**.

High TN and short reaction time have been obtained employing this catalyst with a series of differently functionalized alkenes (Scheme 15).

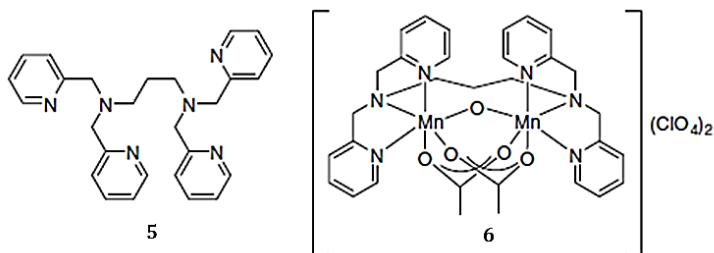


**Scheme 15.** Catalytic scheme of alkenes epoxidation catalyzed by **4**.

Feringa and coworkers in 2000 studied the catalytic activity toward epoxidation of simple alkenes of a dinuclear Mn catalyst<sup>128</sup> (**6**, Figure 7) based

## General Introduction

on the polypyridyl ligand **5** (Figure 7). An excess of  $\text{H}_2\text{O}_2$  was necessary to compensate for the peroxide decomposition.

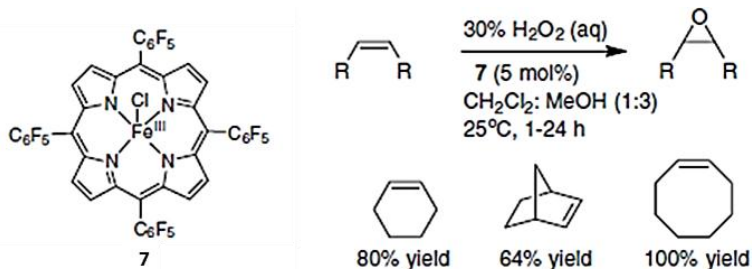


**Figure 7.** Mn dinuclear complex **6** containing polypyridyl ligand **5**.

### ✓ Iron

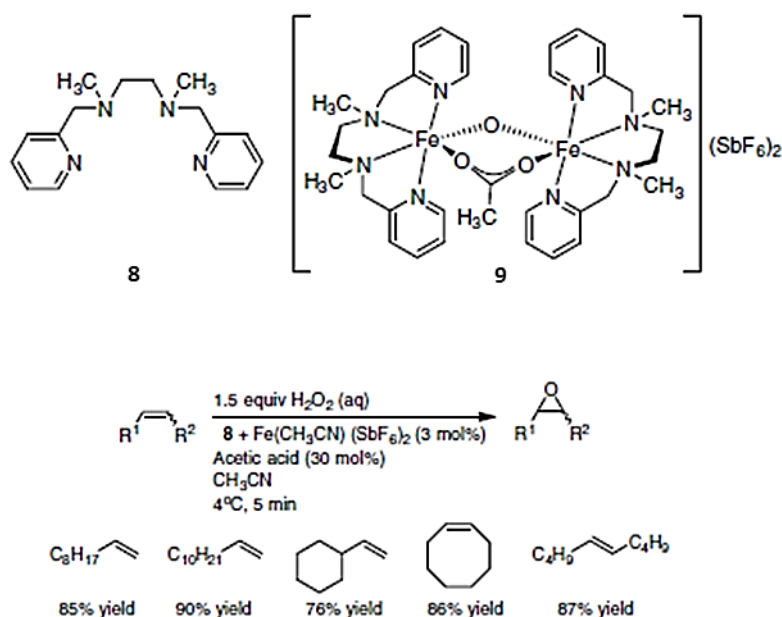
Iron porphyrins have been described as catalysts for alkene epoxidation although conversion and selectivity are lower than for manganese porphyrins. Hydrogen peroxide is generally excluded as an oxidant due to its rapid decomposition catalyzed by iron. However, Beller and coworkers have recently optimized a suitable system for the epoxidation of aromatic alkenes with a slight excess of  $\text{H}_2\text{O}_2$ <sup>129</sup>.

A polyfluorinated iron porphyrin **7** described by Traylor<sup>130</sup> resulted in the highly efficient oxidation of cyclooctene and other cyclic alkenes but elevated catalyst loading and slow addition of the oxidant ( $\text{H}_2\text{O}_2$ ) are drawbacks of this systems (Figure 8).



**Figure 8.** Polyfluorinated Fe porphyrin **7** and catalytic scheme of cyclic alkenes epoxidation.

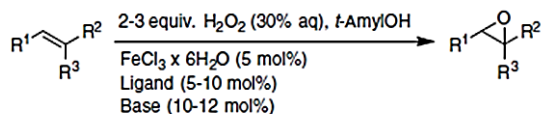
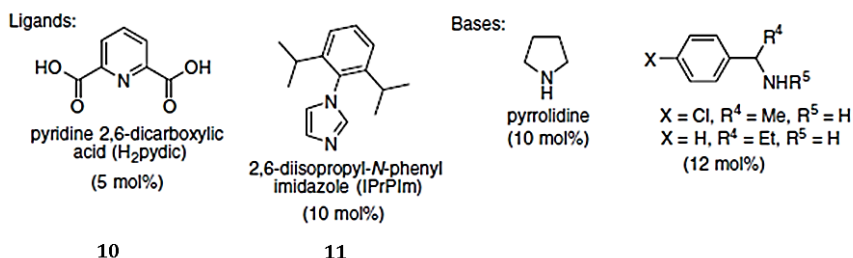
In the epoxidation of terminal alkenes, generally the most difficult substrates to oxidize, excellent results have been obtained with a dinuclear iron catalyst described by Jacobsen and coworkers<sup>131</sup> (Figure 9).



**Figure 9.** Dinuclear Iron complex **9** containing ligand **8** and catalytic scheme of alkenes epoxidation.

An important contribution to iron-catalyzed alkene epoxidation has been the study of Beller and coworkers where they developed a system made by iron(III) chloride hexahydrate, a ligand, and an organic base. After screening several carboxylic acids and imidazoles, the two systems based on ligands **10** and **11** were found to be most efficient for the epoxidation of mono-substituted, trans-1,2-disubstituted aromatic alkenes<sup>132-136</sup> (Figure 10).

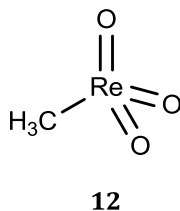
## General Introduction



**Figure 10.** Catalytic scheme for epoxidation of alkenes catalyzed by FeCl<sub>3</sub>/10(11)/base.

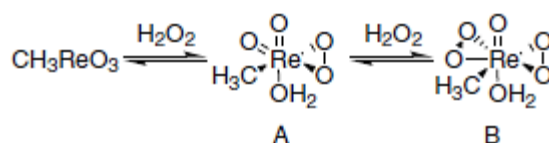
### ✓ Rhenium

The first example of Re catalyzed alkenes epoxidation has been given by Herrmann in 1991<sup>137</sup> who demonstrated the high efficiency as catalyst of the methyltrioxorhenium (MTO) **12** in the presence of H<sub>2</sub>O<sub>2</sub>.



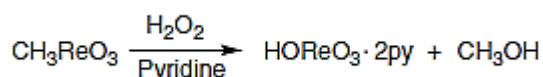
**Figure 11.** Methyltrioxorhenium **12**.

The most attractive feature of this organorhenium oxide is its ability to reduce the hydrogen peroxide decomposition thanks to the rapid equilibrium showed in Scheme 16.



**Scheme 16.** Reaction of **12** with  $\text{H}_2\text{O}_2$ .

The reaction with one equivalent of  $\text{H}_2\text{O}_2$  leads to the formation of a mono-peroxo (A), which further reacts with a second equivalent of oxidant to form a bis-peroxorhenium complex (B). Both of these result in active oxygen transfer but in presence of a base a rapid and irreversible decomposition has been detected in accordance with the reaction show in Scheme 17.



**Scheme 17.** Decomposition of **12** in presence of  $\text{H}_2\text{O}_2$  and base.

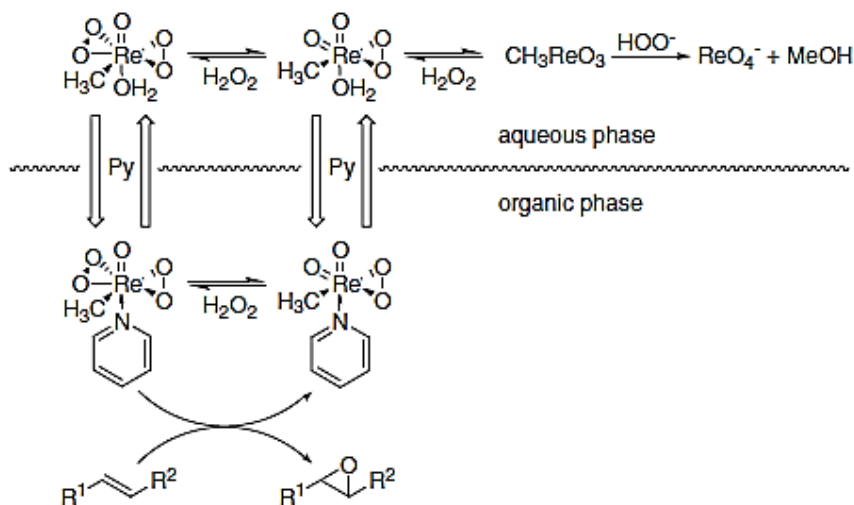
Another drawback of employing **12** is given by the ring opening reaction that often occurs leading to the formation of significant amounts of *trans*-1,2-diol. In 1997 Sharpless and coworkers demonstrated that addition of substoichiometric amounts of pyridine as a co-catalyst reduces the reaction time and increases the efficiency of the catalyst<sup>138</sup>. A reasonable explanation of the advantages gained by the presence of pyridine has been given by Espenson and Wang. As already mentioned, **12** is stable under acidic conditions but undergoes into decomposition at higher pH. The Brønsted basicity of pyridine leads to increased amounts of  $\text{HO}_2^-$ , which speeds up the formation of the peroxo-complexes and the decomposition of the catalyst. The net effect is an improvement in rate and selectivity for epoxide at the expense of catalyst lifetime. The oxidation of highly reactive substrates (tetra-, tri- and *cis*-disubstituted alkenes) were therefore favored by the addition of pyridine due to



## General Introduction

the fact that the conversion rate is higher than the rate of catalyst decomposition. On the contrary, less electron-rich substrates like terminal alkenes, that require longer reaction times, are not fully converted into the relative epoxides on the reaction time scale.


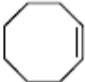
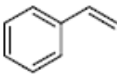
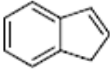
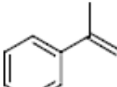
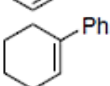
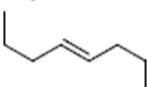
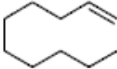
The basic nature of the co-catalyst also prevents the acid-catalyzed ring-opening reactions. It is also believed that the additive acts as a phase-transfer agent from the aqueous layer into the organic phase where the alkenes is in higher concentration<sup>116</sup> (Scheme 18).



**Scheme 18.** Scheme of the two-phase epoxidation catalyzed by **12**.

The use of other additives, studied by the groups of Sharpless, Herrmann and Yamazaki<sup>139-141</sup> strongly influenced the performance of **12** in terms of rate, selectivity and stability (Table 3).

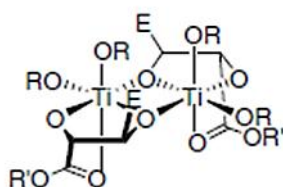
**Table 3.** Epoxidation catalyzed by **12**.

Alkene	No additive <sup>a)</sup>	Pyridine <sup>b)</sup>	3-Cyanopyridine <sup>b)</sup>	Pyrazole <sup>b)</sup>	3-Methylpyrazole <sup>b)</sup>
	90 (5)	96 (6)			96 (5) <sup>d)</sup>
	100 (2) <sup>b)</sup>	99 (2)		89 (0.02)	99(4) <sup>d)</sup>
		84 (16)	96 (5) <sup>c)</sup>	96 (5)	92 (5) <sup>e)</sup>
	48 (37)	96 (5)			87 (1) <sup>e)</sup>
		82 (6)	74 (1.5) <sup>c)</sup>	93 (1.5)	92 (3) <sup>f)</sup>
		98 (1)	96 (1) <sup>c)</sup>	95 (1)	95 (5) <sup>f)</sup>
	95 (2)	91 (24)	97 (12)		98 (8) <sup>f)</sup>
	75 (72)	82 (48)	99 (14)	99 (14)	91 (8)

Yields (%) of alkenes epoxidation catalyzed by **12** and H<sub>2</sub>O<sub>2</sub>. Catalytic loading: 0.5 mol% **12** unless otherwise stated. Reaction times values (h) within parentheses. a) Anhydrous H<sub>2</sub>O<sub>2</sub> in t-BuOH; b) Aqueous H<sub>2</sub>O<sub>2</sub> (30%); c) Pyridine and 3-cyanopyridine (6 mol% of each); d) 0.05 mol% **12**; e) 0.2 mol% **12**; f) 0.1 mol% **12**.

### ✓ Titanium

The Sharpless-Katsuki asymmetric epoxidation is one of the most famous system for conversion of allylic alcohol in their relative epoxides<sup>142</sup>. The system is based on a dimeric complex of titanium (Figure 12, **13**) and TBHP as terminal oxidant.



13

Figure 12. Titanium complex 13.

Enichem in '90s developed an heterogeneous titanium(IV)-silicate catalyst that react with  $H_2O_2$  forming titanium peroxocompounds able to transfer O atoms to alkenes. The system acts throughout adsorption of the substrate into the micropores of the catalyst and works with a wide range of alkenes<sup>116</sup>. Katsuki and coworkers recently published the asymmetric epoxidation of non-functionalized alkenes by a titanium salen complex 14 (Figure 13)<sup>143-145</sup>:

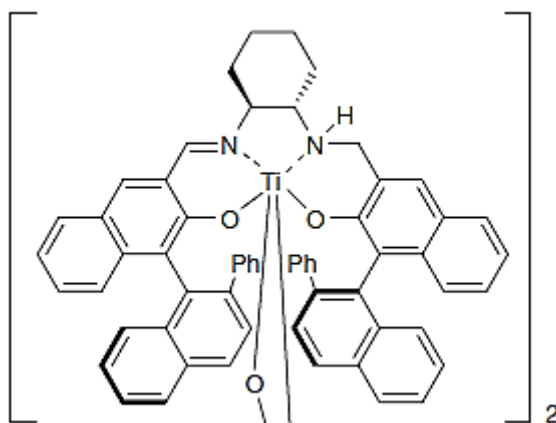
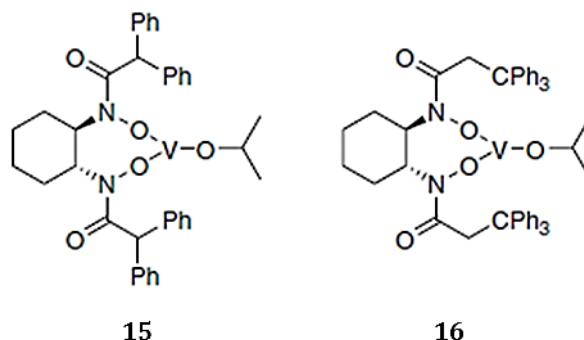


Figure 13. Ti-salen complex 14.

This catalyst gave good yield and high enantioselectivity with terminal alkenes like styrene and 1-octene using a slight excess of hydrogen peroxide as terminal oxidant.

### ✓ Vanadium

Yamamoto and coworkers recently reported the epoxidation of a series of substituted allylic alcohols by two new vanadium catalysts, **15** and **16** (Figure 14), and TBHP as terminal oxidant.

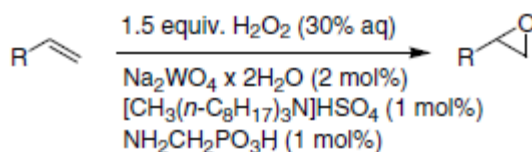


**Figure 14.** Vanadium catalysts **15** and **16**.

A vanadium polyoxometalate,  $[\gamma\text{-}1,2\text{-H}_2\text{SiV}_2\text{W}_{10}\text{O}_{40}]^{4-}$ , has been recently reported by Mizuno as efficient catalyst for epoxidation with  $\text{H}_2\text{O}_2$ <sup>146</sup> of a series of unfunctionalized alkenes, dienes and hydroxyl functionalized alkenes. Due to steric interaction between the substituent and the POM frameworks poor performance resulted for the oxidation of *trans*-disubstituted alkenes<sup>147</sup>.

### ✓ Tungsten

Noyori and coworkers developed a completely solvent free system based on tungsten that provides a green way to obtain epoxides of terminal alkenes<sup>148,149</sup>. Sodium tungstate, (aminomethyl)phosphonic acid and methyltri-*n*-octylammonium bisulfate are employed as catalyst,  $\text{H}_2\text{O}_2$  as terminal oxidant (Scheme 19 and table 4). The lack of solvents allows the isolation of the products by distillation.



**Scheme 19.** Catalytic scheme of Noyori system.

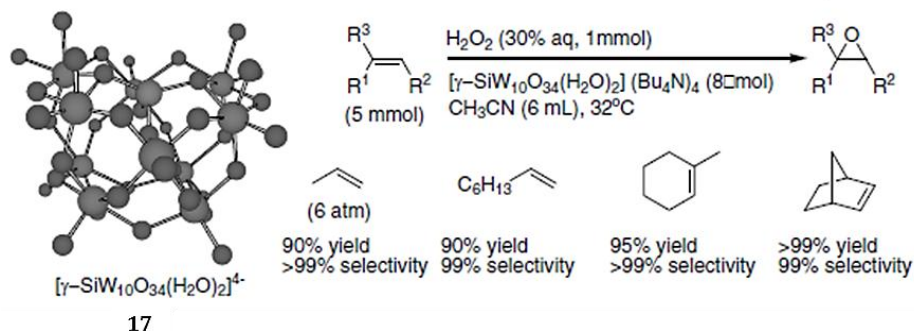
**Table 4.** Epoxidation of terminal alkenes using the Noyori system.

Entry	Alkene	Time (h)	Conversion (%)	Yield (%)
1	1-octene	2	89	86
2	1-decene	2	94	93
3 <sup>a)</sup>	1-decene	4	99	99
4 <sup>a)</sup>	allyl octyl ether	2	81	64
5 <sup>a)</sup>	styrene	3	70	2

a) 20 mmol alkene in 4 mL toluene.

Main limitation of this system is the acidic conditions in which it operates that may cause ring-opening reactions in the products.

A very efficient tungsten catalyst was recently presented by Mizuno<sup>150,151</sup>. It consists of a tetrabutylammonium salt of a Keggin-type silicodecatungstate [ $\gamma$ -SiW<sub>10</sub>O<sub>34</sub>(H<sub>2</sub>O)<sub>2</sub>]<sup>4-</sup> able to oxidize various alkenes with elevated selectivity and efficiency using H<sub>2</sub>O<sub>2</sub> as oxidant.



**Scheme 20.** Alkenes epoxidation catalyzed by **17**.

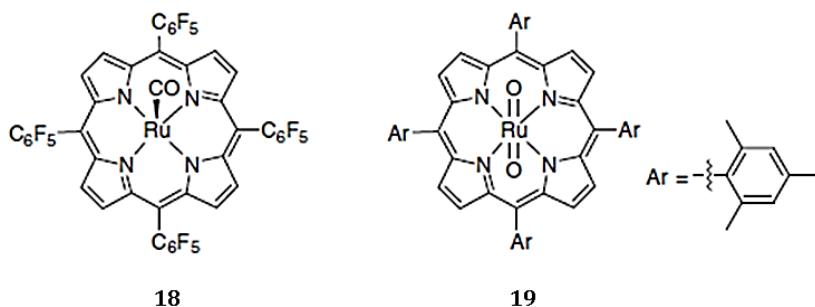
### ✓ Molybdenum

A series of monodentate ligands have been described by Sundermeyer and coworkers for neutral molybdenum peroxy complexes<sup>152</sup> able to oxidize 1-octene and cyclooctene with hydrogen peroxide. The system operates under biphasic conditions (CHCl<sub>3</sub>) giving high yields and good selectivity. Another example is given by the catalyst described by Bhattacharyya<sup>153</sup>, an oxodiperoxomolybdenum(VI) complex that shows excellent catalytic activity for the oxidation of cyclooctene, cinnamyl alcohol, allyl alcohol and 1-hexene.

### ✓ Ruthenium

Epoxidation catalyzed by ruthenium complexes have been largely described with oxidants like periodate<sup>154,155</sup>, iodosylbenzene<sup>156-163</sup>, pyridine-N-oxides<sup>164-166</sup>, hypochlorite<sup>163,167</sup>, hydrogen peroxide<sup>168</sup>, TBHP<sup>161</sup>, and even dioxygen<sup>169-173</sup>. As mentioned above high-valent ruthenium oxides are powerful oxidants. Their reaction with alkenes has been described for various catalysts and terminal oxidants; however the main inconvenience in these catalytic systems is the double bond cleavage<sup>174</sup>.

Two ruthenium porphyrins catalysts<sup>164,175,176</sup> (Figure 15, **18** and **19**) have been described for the oxidations of 1,2-octene (96% yield) and styrene (100% yield) employing 2,6-dichloropyridine N-oxide as terminal oxidant.



**Figure 15.** Ruthenium porphyrins **18** and **19**.

## General Introduction

Nishiyama<sup>177</sup> and coworkers reported a series of ruthenium pyridine-2,6-dicarboxylate complexes of terpyridine and chiral bis(oxazoliny)pyridines (Figure 16, **20-22**) that exhibit efficient catalytic activity (yield up to 92%) in the oxidation of trans-stilbene when treated with [bis(acetoxy)iodo]benzene as oxidant.

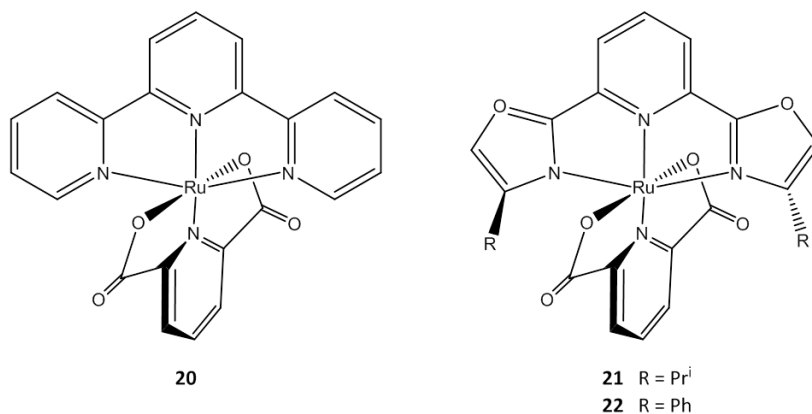
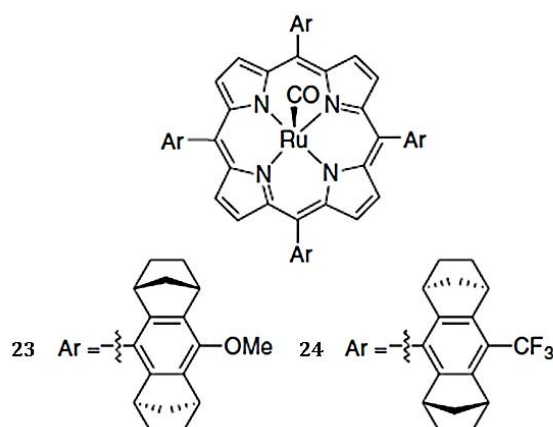


Figure 16. Ruthenium catalysts **20-22**.

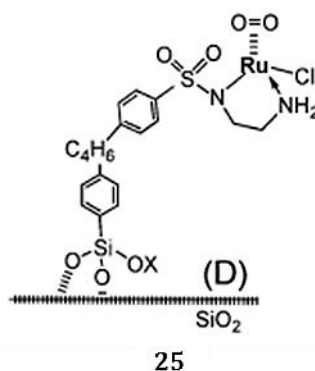
Beller and coworkers have recently demonstrated that Nishiyama catalysts are active also in presence of H<sub>2</sub>O<sub>2</sub> as terminal oxidant. Several alkenes have been tested giving highly conversions and selectivity<sup>178</sup>.

Catalysts **23** and **24** (Figure 17), described by Berkessel<sup>179</sup>, resulted to be efficient catalyst for the enantioselective epoxidation of arylsubstituted alkenes (*ee* up to 83 for 1,2-dihydronaphthalen and catalyst **24**).



**Figure 17.** Catalysts **23** and **24**.

An interesting example of supported catalyst has been recently given by Mizuki and coworkers<sup>180</sup>. The new Ru-monomer supported on SiO<sub>2</sub> (Figure 18) was found to be highly active (up to 2100000 TNs for *trans*-stilbene) for the selective epoxidation of several alkenes using O<sub>2</sub> as oxidant.



**Figure 18.** Mizuki catalyst **25**.

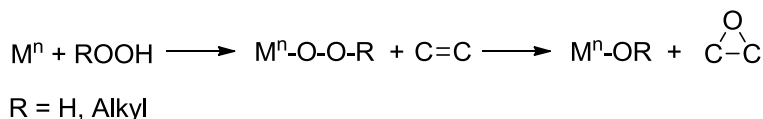
### I. v. i. Mechanism

As already mentioned, the epoxidation of alkenes is an oxygen transfer processes. According with the examples of active catalyst given above this



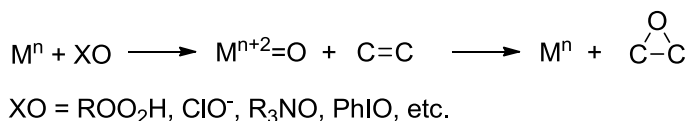
## General Introduction

process can be divided in two major mechanistic categories: one that involve peroxometal species (Scheme 21) and the other that concerns oxometal complexes (Scheme 22). The first is generally observed with early transition metals like Mo(VI), W(VI), V(V), Ti(IV).



**Scheme 21.** Mechanism of epoxidation via peroxometal species.

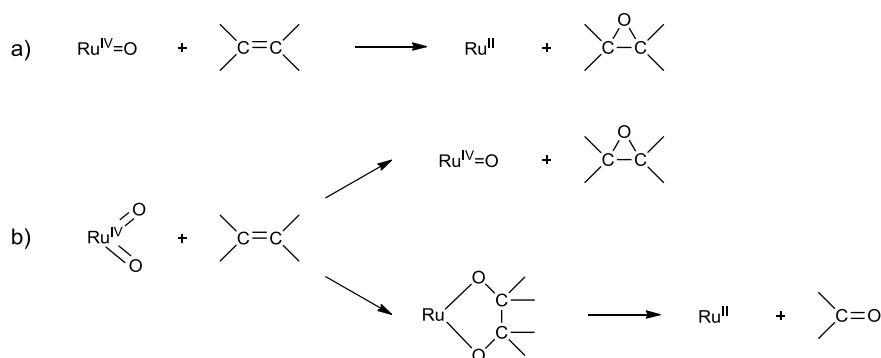
Manganese, Iron and Ruthenium, on the other hand, usually involve high-valent oxometal species, generated in situ via oxidation.



**Scheme 22.** Mechanism of epoxidation via oxometal species.

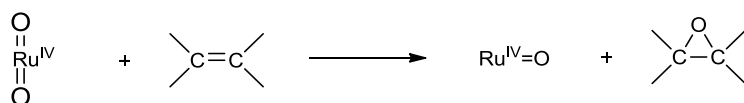
Epoxidation catalyzed by salen and porphyrin complexes of iron and manganese with various oxygen donors has been shown to involve oxometal (V) species as active oxidant<sup>181-185</sup>, but in the case of ruthenium the exact nature of the active oxidant is less clear. Moreover, the oxidative cleavage process is a competing side reaction that may involve different species.

Drago and coworkers proposed that monoxoruthenium (IV) species is responsible for epoxidation whereas *cis*-dioxoruthenium (VI) species for competing epoxidation and oxidative cleavage<sup>87,186,187</sup> (Scheme 23 *a* and *b*):



**Scheme 23.** Epoxidation catalyzed by monooxoruthenium; b) competitive epoxidation and oxidative cleavage catalyzed by *cis*-dioxoruthenium species.

Moreover, assuming that the oxidative cleavage involves initial [3 + 2] cycloaddition of the olefin to a dioxoruthenium (VI), *trans*-dioxo isomers should prevent the oxidative cleavage and favor the epoxidation (Scheme 24)

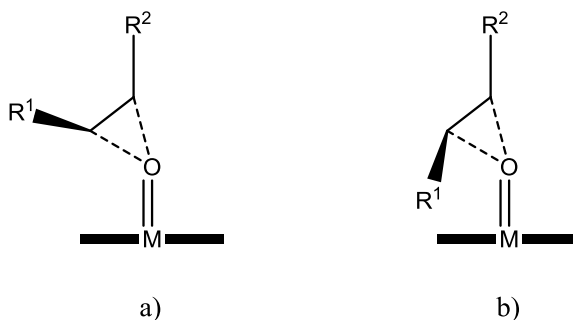


**Scheme 24.** Epoxidation catalyzed by *trans*-dioxoruthenium species.

In porphyrins ruthenium complexes, where the metal is coplanar to the ligand, oxo ligands are forced in *trans* disposition favoring the epoxidation process<sup>188,189</sup>.

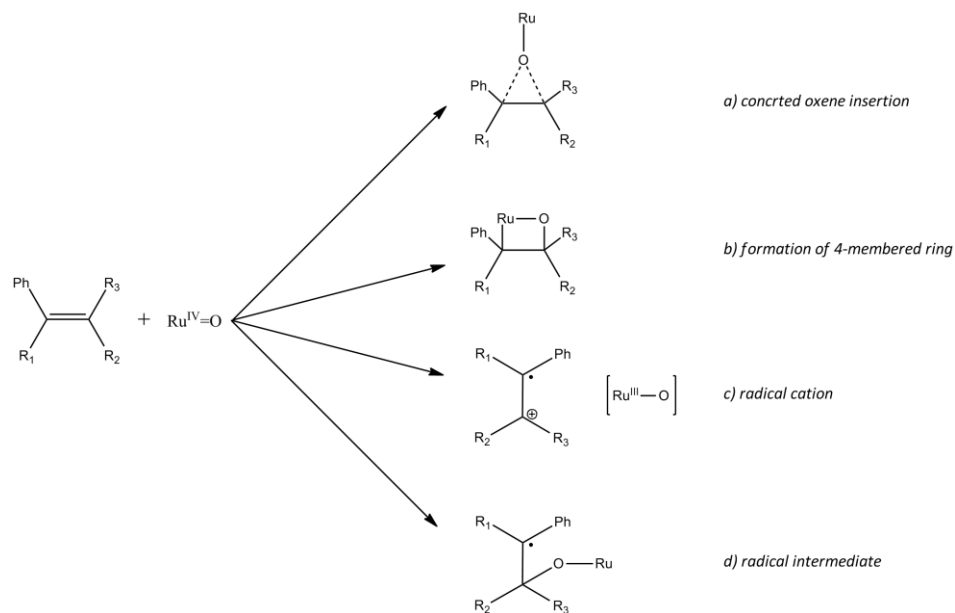
It is generally accepted<sup>183,190-192</sup> that the oxygen transfer to the double bond proceeds via a side-on approach of the oxoruthenium species. This assumption agrees with the lower enantioselectivities generally observed with *trans*-olefins, both with porphyrin-based complexes and Jacobsen type manganese salen ligands, due to the higher hindering of the approach to a *trans*-alkene respect to a *cis*-alkene (Scheme 25).

## General Introduction



**Scheme 25.** Side-on approach of oxoruthenium species to *cis*-alkenes (a) and *trans*-alkenes (b).

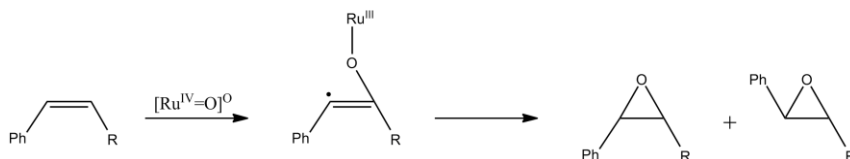
Different pathways have been proposed for the oxygen transfer, both concerted and non-concerted (Scheme 26)



**Scheme 26.** Proposed pathways for oxygen transfer.

The investigation of the stereoselectivity furnishes an important starting point for the interpretation of the mechanism of epoxidation of aromatic alkenes. If the oxidation of *cis*-alkenes via a non-concerted pathway involves breakage of

C=C bond, the resulting acyclic intermediate rapidly undergoes to isomerization into the more stable *trans*-species via C-C bond rotation (Scheme 27). The net result is the production of both *cis*- and *trans*-epoxides.

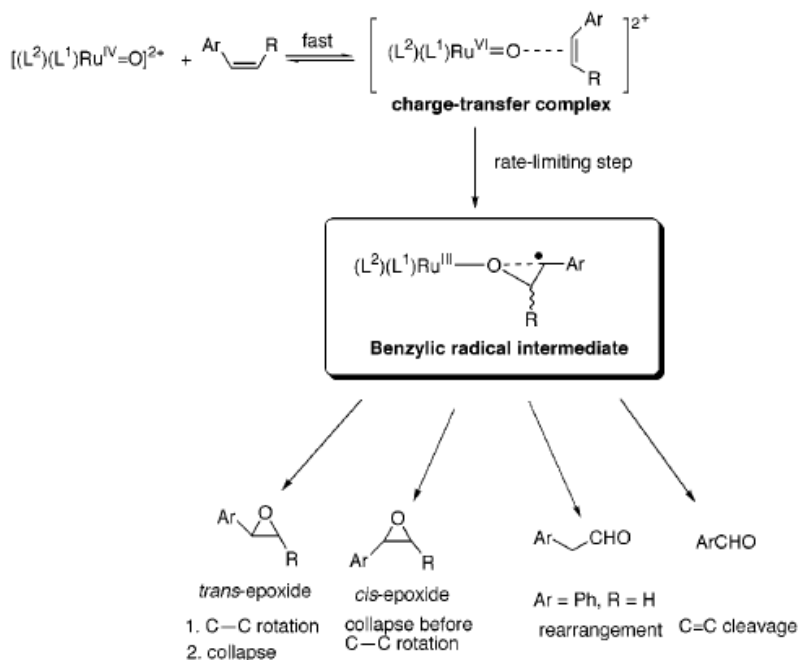


**Scheme 27.** Oxidation of *cis*-alkenes via non-concerted pathway.

A high degree of stereoretention for the oxidation of *cis*-stilbene by  $[\text{Ru}^{\text{IV}}(\text{bpy})_2(\text{py})\text{O}]^{2+}$  has been described by Meyer who suggested an oxene insertion mechanism<sup>193</sup> (Scheme 26 a).

The group of Che has studied the mechanism of alkenes epoxidation catalyzed by a series of monoxoruthenium(IV) complexes<sup>84</sup> detecting almost completely stereoretention for *cis*-stilbene oxidation and mixture of *cis*- and *trans*-epoxides in the case of *cis*- $\beta$ -methylstyrene. A non-concerted mechanism is then strongly probable for the oxidation of *cis*- $\beta$ -methylstyrene as well for styrene. Inverse secondary kinetic effect (KIE) was observed only for the  $\beta$ -*d*<sub>2</sub>-styrene and not for the  $\alpha$ -deuteriostyrene suggesting that not both  $\alpha$  and  $\beta$  olefinic carbon atoms undergo into rehybridization as required by a 4-membered ring formation pathway (Scheme 26 b). According to kinetic results Che and coworkers proposed that the oxidation of aromatic alkenes by oxoruthenium(IV) complexes would generate a benzyl radical intermediate that could involve isomerization via C-C rotation followed by cyclization (or formation of byproducts) (Figure 19).

## General Introduction



**Figure 19.** Proposed mechanism for the oxidation of aromatic alkenes by oxoruthenium(IV) species.

It is important to consider that stereoselectivities for *cis*-alkenes oxidation vary with both the substrate and the ruthenium oxidant as well the reaction mechanism.

## I. vi. Water oxidation

### I. vi. i. Climate changes and Energy demand

The climate changes and the strong energy demand have in the last decade reduced even more the list of candidate as universal source of energy. If for many years oil and carbon have ensured abundant and accessible energy for the world population, at the same time, their unrestrained use has caused remarkable climatic perturbations, often in an irreversible way.

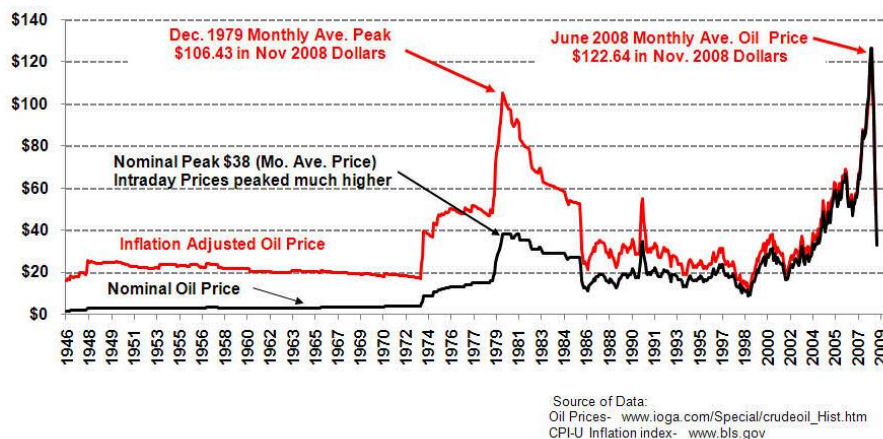
The natural equilibriums that for centuries have regulated the levels of O<sub>2</sub> and CO<sub>2</sub> in the atmosphere are by now ineffective in front of the huge amounts of carbon dioxide generated by the fossil fuels combustion.

Taking into account what mentioned above, the first requisite of a modern energy source is to be clean and safe. It must be clean by the mean that its employment does no generate dangerous chemicals for people and environment, like CO<sub>2</sub> and CO. This energy should be also safe in its production as well in its application and by-products disposal. Recent disasters occurred on nuclear plants, oil plants and coalmines around the world have drawn the attention of people and governments and raised many doubts about their employment.

Another necessary characteristic is the availability of energy. The world population is estimated to be of almost 7 billion of persons with a high growth rate especially in developing countries. An increment of population and living standards is always accompanied by a rise in energy use. Today *ca.* the 80% of the energy demand is satisfied by fossil based energy. The employment of fossil fuels produces every year *ca.* 31.6 billion tonnes of CO<sub>2</sub><sup>194</sup> that is more or less the double of the amount of carbon dioxide that the planet can absorb. Also, fossil fuels are no renewable energies, destined hence to run out. This

## General Introduction

factor, together with the political aspects of the fossil fuels business, has caused a steady rise of the prices in particular concerning the oil (Figure 20).



**Figure 20.** Monthly crude oil prices for barrel 1946-2008 (inflation adjusted in red).

Nuclear power seems to have been for many years the most valid alternative to fossil fuels. The amount of energy produced by nuclear reactors is the main advantages of this source but several drawbacks are frequently controversial:

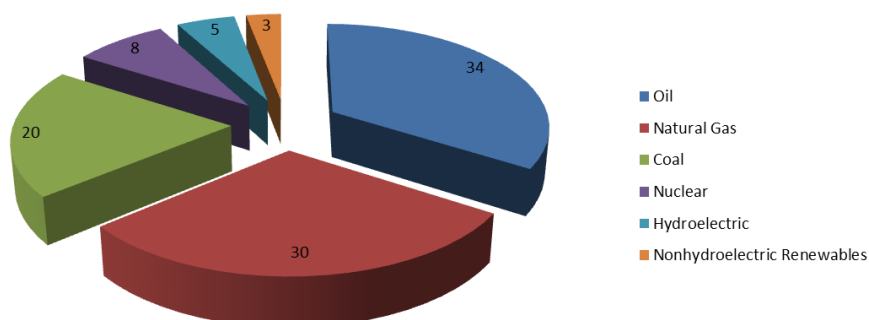
- The cost of construction (6-9 billion dollar for 1.100 MW plant)<sup>195</sup>.
- The cost of maintenance, and decommissioning costs.
- The waste disposal.
- The high risk of accident and the related effect on public opinion.

As of 30 March 2012 in 31 countries 436 nuclear power plant units with an installed electric net capacity of about 370 GW are in operation and 63 plants with an installed capacity of 60 GW are in 15 countries under construction<sup>196</sup> even if some governments are thinking about a total decommissioning of all the installations.

In addition the actual number of nuclear plants can supply just for the 8% of global energy consumption (Figure 21), the same percentage is covered by

renewable energies<sup>197</sup>. However, while an increment in the employments of renewable energy is possible and desirable, a world with ten-times more nuclear plants appears somewhat unlikely.

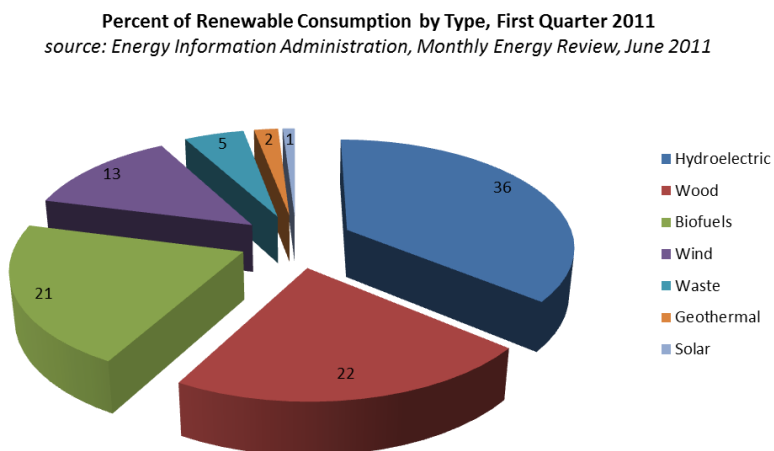
**Percent Energy Consumption by Fuel Type, First Quarter 2011**  
*source: Energy Information Administration, Monthly Energy Review, June 2011*



**Figure 21.** Percent energy consumption by fuel type, first quarter 2011.

Inside the 8% of renewable energy is difficult to believe that just the 1% come from solar energy, that is actually the most abundant renewable resource (Figure 22).





**Figure 22.** Percent of renewable consumption by type, first quarter 2011.

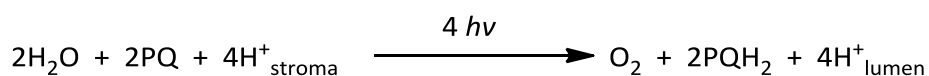
Every hour the earth receives from the sun an amount of energy comparable to the yearly human energy consumption. The last 30-40 years have been characterized by the effort of chemists, physics and biologists to develop different ways to collect this energy. In the most warmed areas of the world, systems for the achievement of high temperature and conversion of heat into energy (concentrated solar power CSP), have been built and operate regularly producing up to 354 MW of energy (Solar Energy Generating Systems, SEGS, in Mojave Desert, California). The photovoltaics are another valid option: solar energy is caught and used for operating an electrolyzer able to split water into  $H_2$  and  $O_2$ . Another working but less promising alternative is the biomass. The energy of the sun is used for growing a plant that can be then harvested and treated for producing alternative fuel (char coal, alcohol). The yields for the conversion of solar energy into biomass (usually less than 2%) and the wide spaces of this kind of farming are considerable disadvantages. The so called artificial photosynthesis is the light driven process that reproduces the ability

of some plants and organisms to split water producing oxygen and release electrons.

### I. vi. ii. Photosystem II

In Nature the process is realized by Photosystem II (PSII), an integral part of the thylakoid membrane; in the thermophilic cyanobacterium *Thermosynechococcus elongatus* it consists of about 20 protein subunits that include 77 cofactors<sup>198</sup>. PSII has the ability to capture and turn into chemical energy photons of sun thanks to a series of charge transfer processes.

The overall reaction of PSII is that of a light-driven (400-700 nm) water plastoquinone oxidoreductase (Scheme 28).

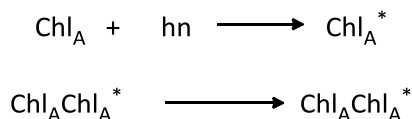


**Scheme 28.** Light-driven water splitting in PSII.

The net process can be divided into four steps:

- I. Light harvesting and energy transfer.
- II. Primary charge separation and stabilization.
- III. Reduction of plastoquinone QB by QA<sup>•-</sup> and protonation at the acceptor side of PSII.
- IV. Accumulation of oxidizing equivalents and water-splitting.

(I) Chlorophyll and carotenoid molecules of the *antenna* complexes Chl<sub>A</sub> capture the light energy and transfer it to the reaction centre by excitation transfer (Scheme 29).



**Scheme 29.** Light absorption by chlorophyll and carotenoid molecules of antenna  $\text{Chl}_A$ .

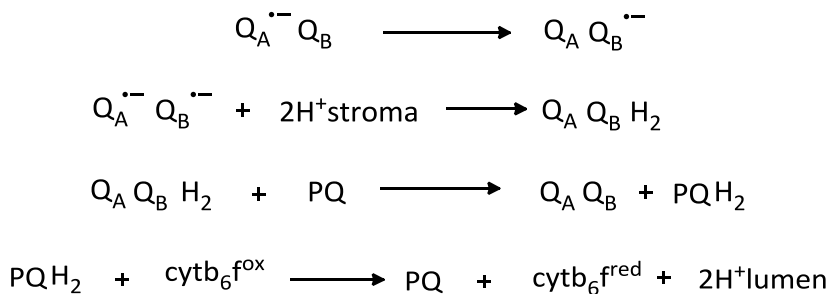
(II) The charge moves among the reaction centre, an arrangement of four  $\text{Chl}_A$  and two Pheo (Scheme 30).



**Scheme 30.** Charge rearrangement.

The charge separation is stabilized by electron transfer from  $\text{Pheo}^{\cdot\cdot}$  to the bound plastoquinone (PQ) molecule  $Q_A$  and by the reduction of  $\text{Chl}_{\text{RC}}^{\cdot\cdot}$ , also called P680<sup>-</sup>, by a red-ox active tyrosine side chain  $Y_z$ .

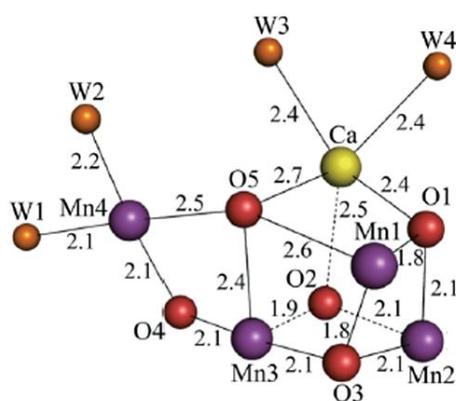
(III)  $Q_A$  is a firmly bound PQ molecule that can be reduced only to the semiquinone level.  $Q_B$ , a mobile PQ molecule, is then twice reduced and protonated (in stroma) by  $Q_A^{\cdot\cdot}$  and leaves its binding pocket and transfers the two electrons to the cytochrome  $b_6f$  complex under the release of its two protons into the lumen.



**Scheme 31.** Electrons transfer to cytochrome  $b_6f$ .

(IV) At the same time the tyrosine radical  $Y'$ , formed during the reduction of  $P680^-$ , oxidizes the  $Mn_4O_5Ca$  cluster, core of the OEC. After four sequential oxidations of the  $Mn_4O_5Ca$  cluster two molecules of water are split releasing molecular oxygen into the medium.

In 2011 a breakthrough in the study of photosynthesis has been reached with determination of the crystal structure of PSII to a 1.9 Å resolution that revealed the molecular structure of the  $CaMn_4$  complex together with 4 water molecules bound<sup>199</sup> (Figure 23)

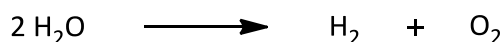


**Figure 23.** Structure of  $Mn_4CaO_5$  cluster (distances in Å).

The attempts to develop an efficient system for artificial photosynthesis range in different fields of science, from chemistry to biology. Chemists and material scientists have designed working systems with molecular and non-molecular catalysts. The first represent the best option in terms of mechanism interpretation and determination of active species, the second are characterized by higher stability under illumination and are more resistant against degradation and deactivation.

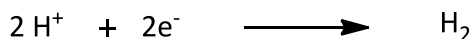
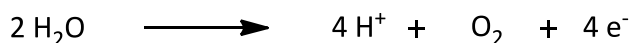
### I. vi. iii. Assembly of cell for artificial photosynthesis

The aim of a photochemical system is, as already mentioned, to use the solar energy, quantified in *photons*, to carry out a chemical reaction in which a substrate is converted in the desired product. If the substrate is water, abundant and cheap, and the product is hydrogen, rich in energy and environmentally friendly, the system in question is a cell for artificial photosynthesis. The net reaction for this device is showed in Scheme 32.



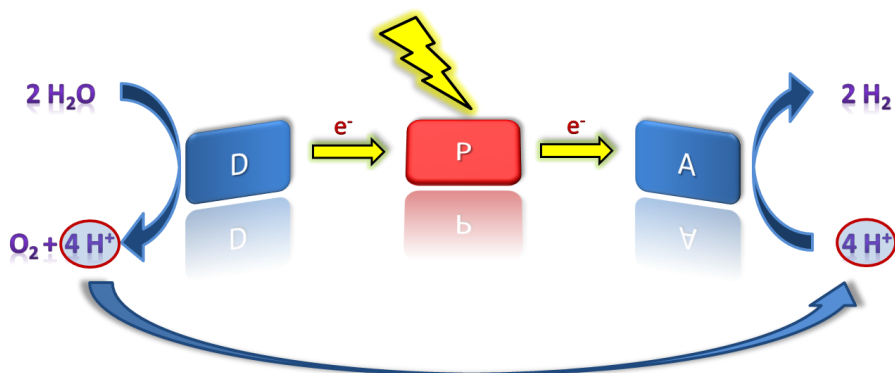
**Scheme 32.** Water splitting reaction.

Being this reaction constituted of the two semi-reactions indicated in Scheme 33.



**Scheme 33.** Water oxidation and proton reduction reactions.

An ideal cell must be able to run both of them at the same time. A scheme of this type of assembly is showed in Figure 24.



**Figure 24.** Scheme for artificial photosynthesis.

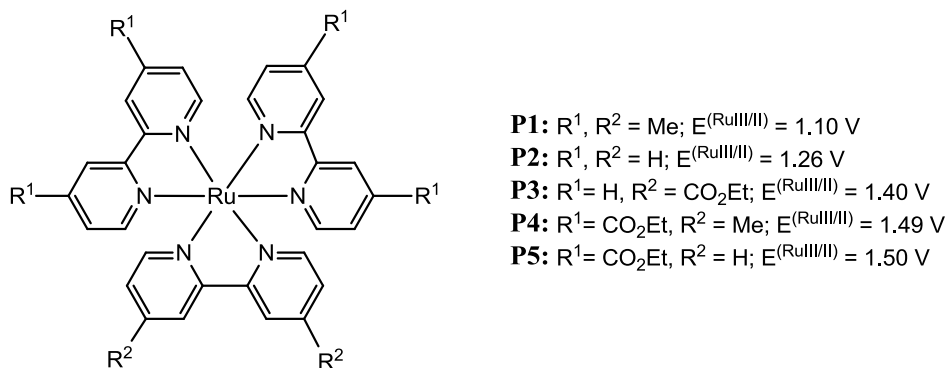
The first step that has to be accomplished by the cell is the absorption of a photon. This task is performed by the photosensitizer (**P**), a photoactive material that is excited by light absorption triggering a charge separation reaction. A highly energetic and unstable radical pair is formed and the electron is separated from the electron hole. The photosensitizer is coupled, via chemical links or through a metal oxide supporting material to the two catalytic systems **A** and **D**. **A**, defined as electron acceptor, receives the radical pair generated on the photosensitizer while the corresponding electron hole is filled again by a new electron coming from the electron donor, **D**. A well-coordinated and enough fast functioning avoid the recombination processes in any step of the system. At the edges of the system take place the two semi-reactions described in Scheme 33. The donor **D** consisting of a water oxidation catalyst, after having acquired the electron holes from the photosensitizer reaches its oxidized active form able to extract electrons from water. At the same time, on the opposite side, the acceptor **A**, consisting of a proton reduction catalyst, after having acquired the electrons from the photosensitizer reaches its reduced active form able to transfer electrons to the protons  $H^+$  coming from the water splitting.

#### I. vi. iv. Photosensitizer

$[Ru(bpy)_3]^{2+}$  ( $bpy = 2,2'$ -bipyridine) derivatives are the most commonly used sensitizers because they own intense  $^3MLCT$  absorption bands in the range of visible light, outstanding thermo-stability and high enough oxidation potentials ( $E > 0.82$  V vs. NHE) to drive water oxidization reaction thermodynamically at pH 7<sup>200,201</sup>. Modification of the *para* position of the bipyridine ligand of  $[Ru(bpy)_3]^{2+}$  leads to variation of the oxidation potential as well influence the

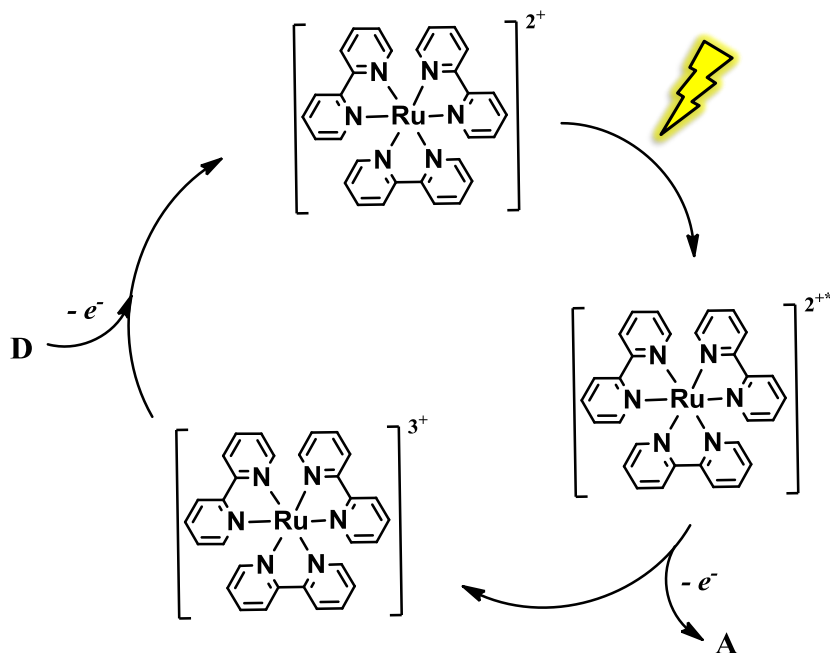
## General Introduction

stability of the photosensitizer. Some Ru-bpy type complexes are showed in Figure 25 with their relative oxidation potentials.



**Figure 25.** Ru-bpy type complexes and relative oxidation potentials.

The assumed cycle for the photooxidation of  $[\text{Ru}(\text{bpy})_3]^{2+}$  is represented in Figure 26.



**Figure 26.** Mechanism of photooxidation of  $[\text{Ru}(\text{bpy})_3]^{2+}$ .

The photoexcitation generates the excited dye  $[\text{Ru}(\text{bpy})_3]^{2+*}$  that reacts with the  $e^-$  acceptor (a proton reduction catalyst or a sacrificial oxidant agent like  $\text{S}_2\text{O}_8^{2-}$  or  $[\text{Co}(\text{NH}_3)_5\text{Cl}]^{2+}$ ) generating the oxidized species  $[\text{Ru}(\text{bpy})_3]^{3+}$ . The latter after reduction by the  $e^-$  donor (a water oxidation catalyst or a sacrificial reducing agent like EDTA or triethanolamine) regenerates the initial species  $[\text{Ru}(\text{bpy})_3]^{2+}$ .

### I. vi. v. Ruthenium water oxidation catalysts

Although in the last thirty years several steps forwards have been made, the lack of an efficient and sturdy catalyst for water oxidation remains the weak point in the assembly of a photoelectrochemical cell. Many complexes based on first and second transition metals like Ru, Ir, Co, Mn and Fe have been described as efficient catalysts for water oxidation when strong chemical oxidants like Ce(IV), Oxone, NaClO are employed<sup>202-210</sup>. Although only a few of them can work in an efficient and enduring light driven process.

The first homogeneous and non-protein catalyst for water oxidation has been described by Thomas J. Meyer in 1982<sup>211,212</sup> (Figure 27).

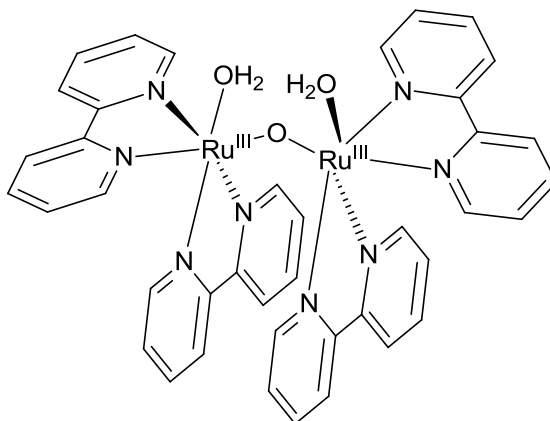
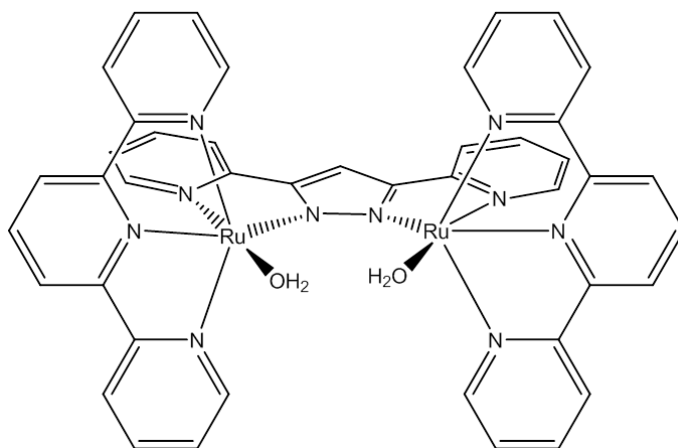


Figure 27. Structure of blue dimer, 26.



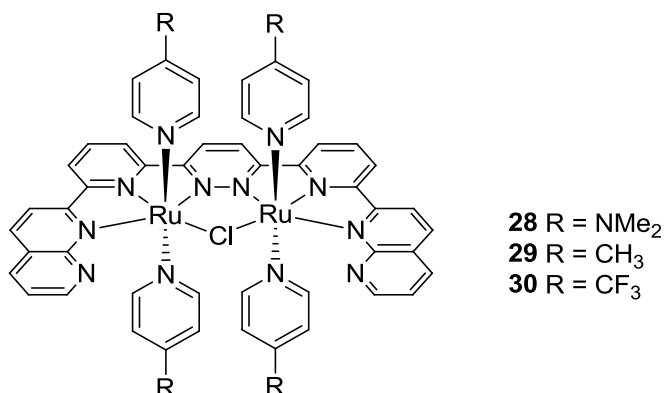
## General Introduction

The dinuclear Ru complex *cis,cis*- $\{[\text{Ru}(\text{bpy})(\text{H}_2\text{O})]_2(\mu\text{-O})\}^{4+}$  (**26**), commonly known as blue dimer, is able to oxidize water with a total turnover number of 13 and TOF of  $0.24 \text{ min}^{-1}$  using Ce(IV) as oxidant at pH 1.0. Hurst and co-workers recently published the photochemical water oxidation catalyzed by the blue dimer in presence of  $[\text{Ru}(\text{bpy})_3]^{2+}$  as photosensitizer and  $\text{S}_2\text{O}_8^{2-}$  as sacrificial electron acceptor. Later on, in 2004, Llobet and co-workers presented a new dinuclear Ru catalyst based on the bis(2-pyridyl)-3,5-pyrazolate anionic bridging ligand ( $\text{bpp}^-$ )<sup>213</sup> (**27**, Figure 28).



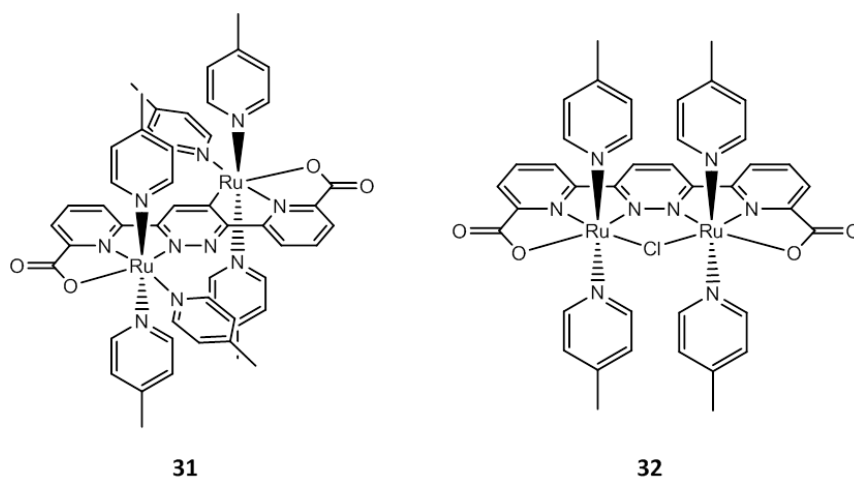
**Figure 28.** Structure of **27**.

The latter provides a more resistant linkage between the two metal centres in the place of the flexible  $\mu\text{-oxo}$  bridge preventing eventual cleavage. This catalyst has been proven to catalyzed water splitting up to  $250 \text{ TN}^{214}$  in presence of Ce(IV) as terminal oxidant. More recently Thummel published a series of dinuclear Ru complexes based on polypyridyl bridging ligands that oxidize water with elevated turnover number<sup>215</sup> (up to 600) (**28-30**, Figure 29).



**Figure 29.** Structures of **28-30**.

The group of Sun later developed new catalysts based on bridging ligands containing carboxylic groups<sup>206,216</sup> (**31** and **32**, Figure 30).



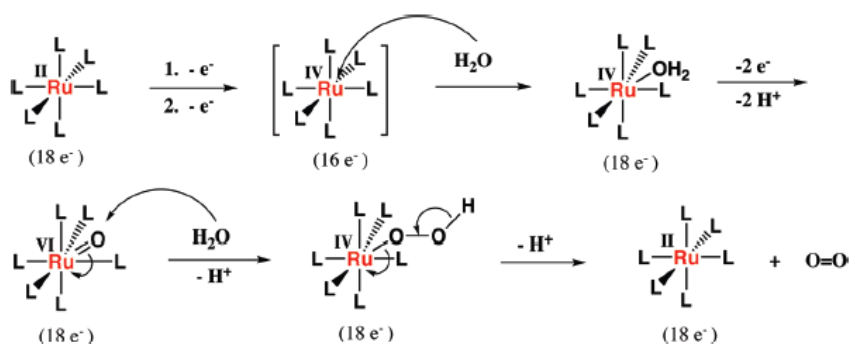
**Figure 30.** Structure of **31** and **32**.

These complexes, in presence of Ce(IV) as oxidant, are able to produce 1690 (complex **31**) and 10400 TN (complex **32**) of O<sub>2</sub> under optimized conditions. Both catalysts were also tested for photochemical water oxidation. A system constituted by **31** as WOC, **P5** as photosensitizer and S<sub>2</sub>O<sub>8</sub><sup>2-</sup> as sacrificial electron acceptor achieved 1270 TN of oxygen. **32** showed a low overpotential

## General Introduction

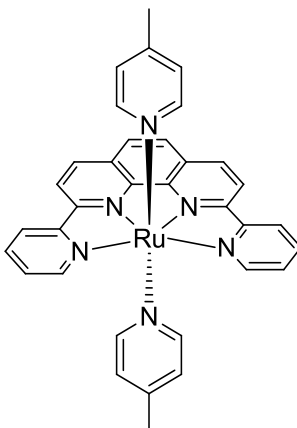
for water oxidation with an onset of catalytic current at *ca.* 1.20 V that makes this catalyst suitable for a A-P-C system. In presence of  $[\text{Ru}(\text{bpy})_3]^{2+}$  as photosensitizer *ca.* 60 TN of oxygen have been detected. Both **31** and **32** resulted stable in aqueous solutions indicating that the breakdown in  $\text{O}_2$  evolution is mainly due to the pH decrease (that causes a rise in the value of red-ox potential) and to the decomposition of the photosensitizer.

More recently the groups of Thummel and Meyer demonstrated that the presence of two metal centres is not a necessary condition for the design of an efficient water oxidation catalyst<sup>217,218</sup>. Thummel and coworkers have published a series of non-aqua  $\text{Ru}^{\text{II}}\text{N6}$  complexes<sup>217,219,220</sup> that presents a saturated first coordination sphere of  $\text{Ru}^{\text{II}}$ . The oxidation of this species generates a 16-electron  $[\text{Ru}^{\text{IV}}\text{N6}]$  highly predisposed to an attack by water molecule. According to mechanism proposed by Thummel<sup>217</sup> after two-step PCET oxidation of the  $\text{Ru}^{\text{IV}}$ -aqua complex a high-valent  $\text{Ru}^{\text{VI}}$ -oxo is generated. The nucleophilic attack of a second molecule of water leads then to the formation  $[\text{Ru}^{\text{IV}}\text{N6}(\text{OOH})]$  hydroperoxide intermediate. An intramolecular electron transfer from peroxide to  $\text{Ru}^{\text{IV}}$  results in the generation of oxygen (Scheme 34).



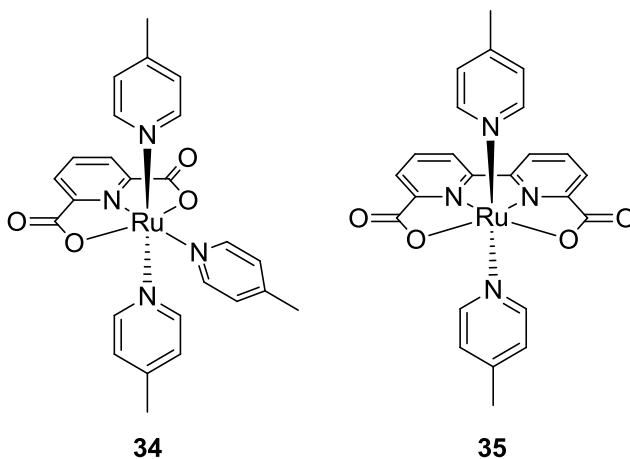
**Scheme 34.** Proposed mechanism for water oxidation catalyzed by mononuclear  $\text{Ru}(\text{II})\text{N6}$  complexes.

An example of a mononuclear Ru(II)N<sub>6</sub> catalyst is showed in Figure 31.



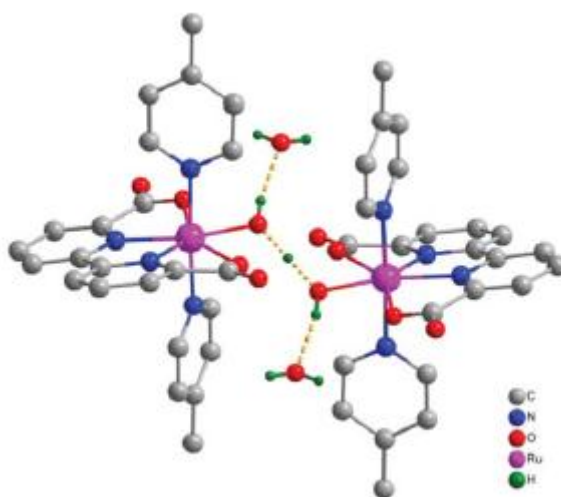
**Figure 31.** Structure of **33**.

$[\text{Ru}(\text{dpp})(\text{pic})_2]^{2+}$  (**33**) is able to generate 416 TN of O<sub>2</sub> using Ce(IV) as terminal oxidant<sup>217</sup>. The group of Sun later developed two mononuclear Ru catalysts **34** and **35** (Figure 32) based on the dicarboxylic ligands  $\text{pdc}^{2-}$  ( $\text{H}_2\text{pdc}$  = 2,6-pyridine dicarboxylic acid) and  $\text{bda}^{2-}$  ( $\text{H}_2\text{bda}$  = 2,2'-bipyridine-6,6'-dicarboxylic acid).



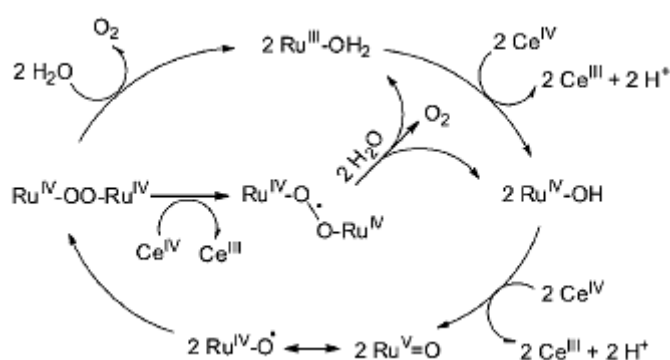
**Figure 32.** Structures of **34** and **35**.

**34** resulted an active catalyst for water oxidation both using Ce(IV) (TN of 550 and TOF of  $13.8 \text{ min}^{-1}$ ) and in a A-P-C system with **P3** and  $\text{S}_2\text{O}_8^{2-}$  (TN 62)<sup>208</sup>. Complex **35** represented a real breakthrough in the theme of mononuclear water oxidation catalysts insofar as its unique conformation of a O-Ru-O moiety with bite angle  $122.99^\circ$  allows Sun and coworkers to isolate and describe by X-Ray diffraction a seven coordinated species (**36**, Figure 33) previously proposed by Meyer and Thummel<sup>217,218,221</sup>.



**Figure 33.** Crystal structure of **36**.

The catalytic cycle proposed for the water oxidation by **35** and Ce(IV) is showed in Figure 34 and described below.<sup>222</sup>

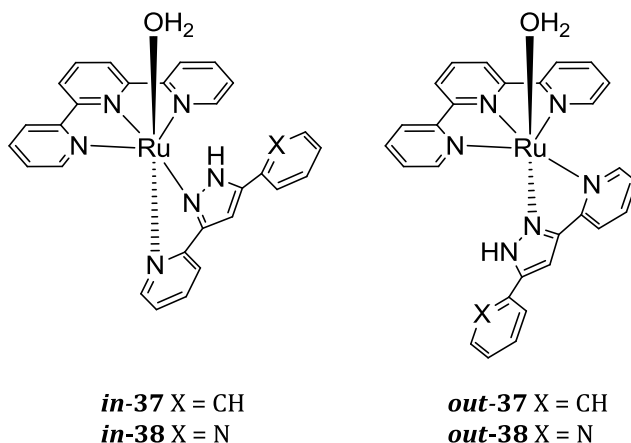


**Figure 34.** Proposed catalytic cycles for **35** in  $\text{Ce}^{\text{IV}}$ -pH 1 conditions.

In aqueous solution **35** generates a  $\text{Ru}^{\text{II}}\text{-OH}_2$  species, from which the removal of protons and electrons takes place in a sequential manner. The active species was proved as  $\text{Ru}^{\text{V}}=\text{O} \leftrightarrow \text{Ru}^{\text{IV}}\text{-O}^{\bullet}$ . Treated with stoichiometric  $\text{Ce}^{\text{IV}}$ ,  $\text{O}_2$  releases from the  $\text{Ru}^{\text{IV}}\text{-OO-Ru}^{\text{IV}}$  species which is regarded as the rate determining step. In the presence of excess  $\text{Ce}(\text{IV})$ ,  $[\text{Ru}^{\text{IV}}\text{-OO-Ru}^{\text{IV}}]^{2+}$  is further oxidized to  $[\text{Ru}^{\text{IV}}\text{-O}^{\bullet}\text{-O-Ru}^{\text{IV}}]^{3+}$  which decomposes fast to  $\text{Ru}^{\text{III}}$ ,  $\text{Ru}^{\text{IV}}$  and  $\text{O}_2$ . In presence of  $\text{Ce}(\text{IV})$  the catalyst resulted extremely active (TN  $\approx$  2000 and TOF  $>$  2500  $\text{min}^{-1}$ ). Lastly, the strong electron donating nature of the  $\text{bda}^{2-}$  ligand and the seven coordinate intermediates bear a very low onset potential toward water oxidation (about 1.0 V vs. NHE at pH 7.0) that makes of **35** a suitable catalyst also for light driven water oxidation. 100 TN of  $\text{O}_2$  with a TOF of 3.7  $\text{min}^{-1}$  were obtained when  $[\text{Ru}(\text{bpy})_3]^{2+}$  is used as photosensitizer and  $[\text{Co}(\text{NH}_3)_5\text{Cl}]\text{Cl}_2$  as sacrificial electron acceptor<sup>210</sup>. The drop in the pH value during the catalysis is the cause of the deactivation of the catalyst; neutralization of the solution restores the catalytic system for several cycles. In 2011 Llobet and co-workers reported a series of isomeric, mononuclear Ru-aqua complexes **37** and **38** (Figure 35) containing the tridentate meridional  $\text{trpy}$  ligand and either a

## General Introduction

bidentate ligand H3p (H3p = 2-(5-phenyl-1H-pyrazol-3-yl) pyridine) or a Hbpp ligand<sup>223</sup>.



**Figure 35.** Structure of complexes **37** and **38**.

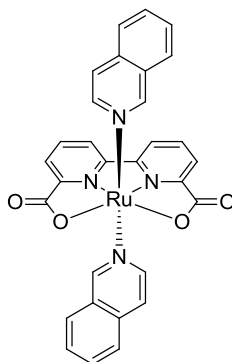
Toward water oxidation both ***out-37*** and ***out-38*** resulted more active than *in*-isomers when Ce(IV) is employed as terminal oxidant:

**Table 5.** TNs for water oxidation catalyzed by **37** and **38** in Ce<sup>IV</sup>-pH 1 conditions

	<b><i>in-37</i></b>	<b><i>out-37</i></b>	<b><i>in-38</i></b>	<b><i>out-38</i></b>
<b>TN</b>	10	12.7	8	14

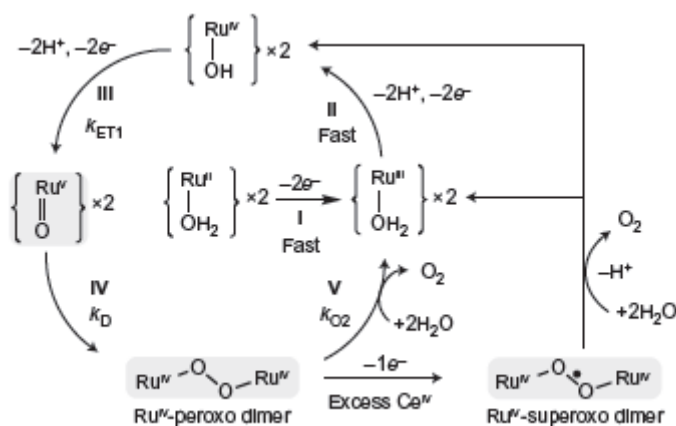
Light driven water oxidation with **37** and **38** was also tested in presence of [Ru(bpy)<sub>3</sub>]<sup>2+</sup> and [Co(NH<sub>3</sub>)<sub>5</sub>Cl]<sup>2+</sup>. In this case ***in-38*** resulted the best catalyst of the series with a TN of 4.

Very recently Sun and Llobet described the catalytic activity of the Ru mononuclear complex [Ru(bda)(isoq)<sub>2</sub>] (H<sub>2</sub>bda= 2,2'-bipyridine-6,6'-dicarboxylic acid; isoq= isoquinoline; **39**, Figure 36) toward water oxidation in presence of an excess of Ce(IV)<sup>224</sup>.



**Figure 36.** Structure of **39**.

The high catalytic activity achieved with **39** (TN = 8360 ± 91) in a very short reaction time (TOF = 303 s<sup>-1</sup>) significantly reduces the gap in reaction rate between the Mn<sub>4</sub>CaO<sub>5</sub> cluster of photosystem II (TOF 100-400 s<sup>-1</sup>) and the best molecular catalyst described till now<sup>225</sup> (TOF > 5 s<sup>-1</sup>). A combination of different techniques has been carried on in order to elucidate the reaction mechanism for water oxidation catalyzed by **39**. A likely catalytic cycle that involves a seven coordinate dinuclear complex has been proposed and showed below:

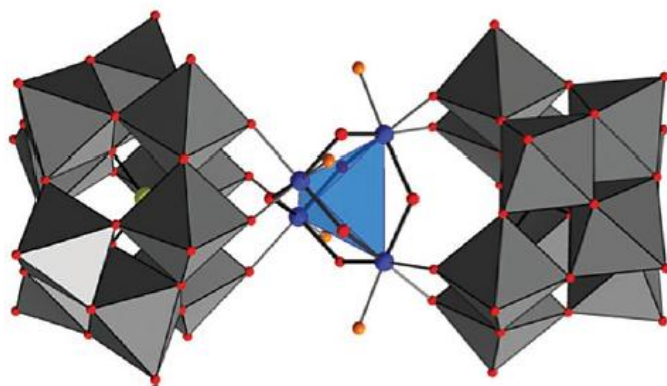


**Figure 37.** O<sub>2</sub> generation pathways of complex **39** with stoichiometric and excess amounts of Ce<sup>IV</sup> at pH 1 (the circular pathway in the middle and further to the right, respectively).



The stacking of isoquinolines, that facilitate the formation of the O-O bonds in the radical dimerization of  $\text{Ru}^{\text{V}}=\text{O}$  active species, and the generation of a superoxo species  $[\text{Ru}^{\text{IV}}-\text{O}^{\bullet}-\text{O}-\text{Ru}^{\text{IV}}]^{3+}$ , that easily liberates oxygen via a reduction-coupled process, are the features that makes **39** highly fast and efficient catalyst for water oxidation.

Lastly the groups of Hill and Bonchio independently reported a Ru-POM, with formula  $\text{Rb}_8\text{K}_2[\{\text{Ru}_4\text{O}_4(\text{OH})_2(\text{H}_2\text{O})_4\}(\gamma\text{-SiW}_{10}\text{O}_{36})_2]\cdot 25\text{H}_2\text{O}$  (**40**, Figure 38), that catalyzes the oxidation of water among 500 TN with a TOF of  $7.5 \text{ min}^{-1}$  in presence of  $\text{Ce}(\text{IV})$ <sup>226,227</sup>.



**Figure 38.** Structure of polyanion in **40**.

350 TN of  $\text{O}_2$  were obtained when  $[\text{Ru}(\text{bpy})_3]^{2+}$  and  $\text{S}_2\text{O}_8^{2-}$  were used as oxidant and sacrificial acceptor.

### I. vi. vi. Other water oxidation catalysts

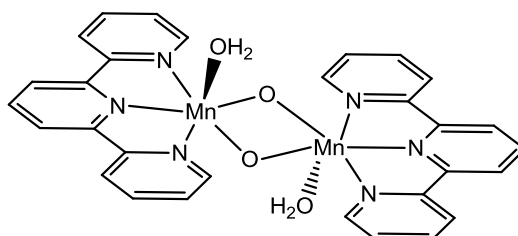
The chemistry of ruthenium water oxidation catalysts has been the most widely studied thanks to some characteristic features:

- A broad synthetic panorama that allows preparation of countless different complexes.
- Elevated performance in terms of TN and TOF.

- Incomparable suitability with several spectroscopic techniques for mechanistic studies.

However it is important to keep in mind that for a world wide scale application an earth abundant, environmentally friendly and inexpensive element based catalyst is required. Unfortunately the number of efficient water oxidation catalysts is considerably lower respect to ruthenium. In order to mimic the PSII several research groups have pointed their efforts of the development of Mn based catalysts. Among all the catalysts described as water splitting complex just some of them are reported to catalyze the water oxidation without using an oxygen-transferring oxidant.

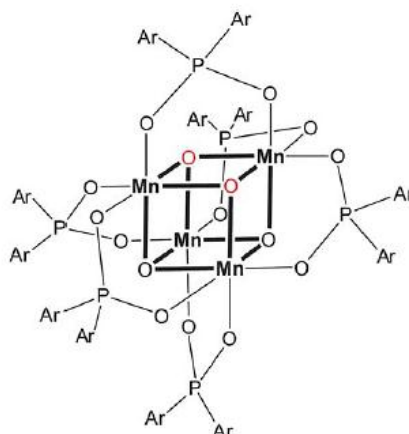
The  $\{[\text{Mn}(\text{trpy})(\mu\text{-O})(\text{H}_2\text{O})]_2(\text{NO}_3)_3\}$  **41** (Figure 39) described by Crabtree and Brudvig in 1999<sup>228</sup> was initially tested in presence of oxidants like hypochlorite and peroxymonosulfate giving 4 TN of oxygen during 6 hours reaction.



**Figure 39.** Structure of **41**.

Later, Yagi and co-workers, after adsorbing **41** on Kaolin, mica and montmorillonite K10, reported a catalytic activity of 17 TN of  $\text{O}_2$  using Ce(IV) as terminal oxidant<sup>229</sup>. More recently **41** was also combined with  $[\text{Ru}(\text{bpy})_3]^{2+}$  and  $\text{S}_2\text{O}_8^{2-}$  for a light driven water oxidation experiment leading to 4 TN of oxygen. An efficient manganese cubane core type catalyst has been prepared by Dismukes and coworkers through self-assembly in solution of a  $[\text{Mn}_2\text{O}_2]^{3+}$  core

complex and bidentate ligand diarylphosphinates which bridge pairs of Mn atoms on each cube face ( $\text{Mn}_4\text{O}_4\text{L}_6$ , **42**, Figure 40)<sup>230</sup>.



**Figure 40.** Structure of **42**.

Catalytic evolution of  $\text{O}_2$  in a TN of 1000 was achieved by suspending **42** into a proton-conducting membrane (Nafion) preadsorbed onto a conducting electrode and electroxidizing by application of an external bias<sup>231</sup>. Recently Spiccia and Hocking demonstrated, by in situ X-ray absorption spectroscopy and transmission electron microscopy studies, that the active species derives from the dissociation of **42** into Mn(II) compounds in the Nafion, which are then reoxidized to form dispersed nanoparticles of a disordered Mn(III/IV)-oxide phase<sup>232</sup>.

The chemistry of manganese oxide includes a wide variety of  $\text{MnO}_x$  materials that can be easily synthesized; some of them are moreover characterized by the presence of alkali metal cations. Kurz and coworkers prepared a series of these “biomimetic oxides” and tested toward water oxidation employing different oxidants (Table 6)<sup>233</sup>.

**Table 6.** Oxidation of water catalyzed by “biomimetic oxides”

Catalyst	$S_{\text{BET}}^{[b]}$	$\text{H}_2\text{O}_2$	Oxidation agent <sup>[a]</sup>		
			$\text{HSO}_5^-$	$\text{Ce}^{\text{IV}}$	$\text{Ru}^{\text{III}}_{\text{photo}}^{[c]}$
commercial $\text{Mn}_2\text{O}_3$	1.09	0.3	traces	traces	0.022
$\alpha\text{-Mn}_2\text{O}_3$ (1)	16.6	0.2	traces	0.027	0.023
$\text{CaMn}_2\text{O}_4 \cdot 4\text{H}_2\text{O}$ (2)	303	$> 5.0^{[d]}$	0.325	0.325	0.325
$\text{CaMn}_2\text{O}_4 \cdot \text{H}_2\text{O}$ (3)	205	4.2	0.255	0.540	0.350
$\text{CaMn}_2\text{O}_4$ (4)	2.62	0.9	0.024	traces	0.012
$\text{CaMn}_2\text{O}_4 \cdot 4\text{H}_2\text{O}$ (5)	14.8	$> 5.0^{[d]}$	0.012	0.290	0.225

<sup>a</sup>Concentrations of the oxidants in the reaction mixture (1mL):  $[\text{H}_2\text{O}_2] = 4.4 \text{ mM}$ ,  $[\text{HSO}_5^-] = 7.4 \text{ mM}$ ,  $[\text{Ce}^{\text{IV}}] = 0.24 \text{ M}$ ,  $[\text{Ru}(\text{bpy})_3]^{2+} = 1.5 \text{ mM}/[\text{Co}(\text{NH}_3)_5\text{Cl}]^{2+} = 12.5 \text{ mM}$ . <sup>b</sup>Values in  $\text{m}^2\text{g}^{-1}$ . <sup>c</sup>Rates for the phase of steady  $\text{O}_2$  formation (2–3 min. after the start of the illumination). <sup>d</sup>Rate faster than the upper detection limit of the setup of circa 5  $\text{mmolO}_2 \cdot \text{mol} \cdot \text{Mn}^{-1} \cdot \text{s}^{-1}$ .

Oxygen has been detected for  $\text{CaMn}_2\text{O}_4 \cdot x\text{H}_2\text{O}$  oxide materials even with no-oxygen transfer oxidant like Ce and photogenerated  $[\text{Ru}(\text{bpy})_3]^{2+}$  pointing to the water as the only possible source.

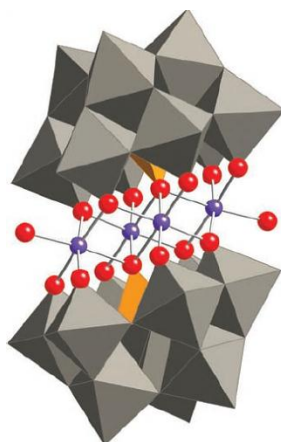
Also Co oxide has been recently described as active water oxidation catalysts. Nocera and coworkers described the electrochemical water oxidation catalyzed by Co oxide film formed *in situ* on ITO surface in phosphate derivate buffer<sup>234</sup>. Dau and coworkers later proposed that the central structural unit likely is a cluster of interconnected  $\text{Co}^{\text{III}}$ -oxo cubanes<sup>235</sup>.

Berlinguette and coworkers have recently pointed out the electrochemical behavior of the mononuclear Co complex,  $[\text{Co}(\text{Py}5)(\text{OH}_2)](\text{ClO}_4)_2$  (**43**; Py5=2,6-bis(bis-2-pyridyl)-methoxymethane)pyridine, Figure 41), that through consecutive (proton-coupled) oxidation steps furnishes a  $\text{Co}^{\text{IV}}$  species that catalyzes the oxidation of water in basic media.



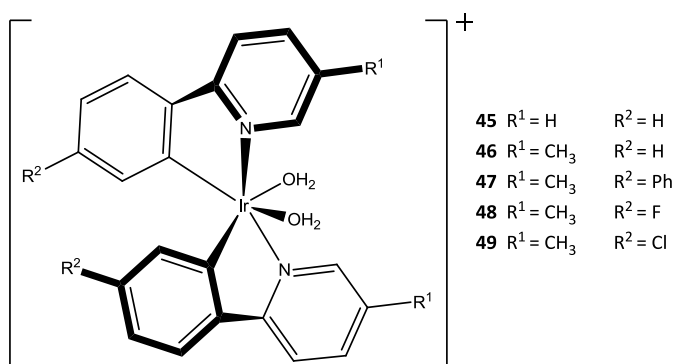
**Figure 41.** Structural representation of **43**.

In 2010 the group of Hill published the catalytic activity of a cubane type  $\text{Co}_4$ -POM complex,  $[\text{Co}_4(\text{H}_2\text{O})_2(\text{PW}_9\text{O}_{34})_2]^{10-}$  (**44**, figure 42), able to generate 70 TN of  $\text{O}_2$  at pH 8 in presence of  $[\text{Ru}(\text{bpy})_3](\text{ClO}_4)_3$  as terminal oxidant<sup>236</sup>. The oxidant was later substituted by the couple  $[\text{Ru}(\text{bpy})_3]^{2+}/\text{S}_2\text{O}_8^{2-}$  resulting in more than 220 TN of oxygen.



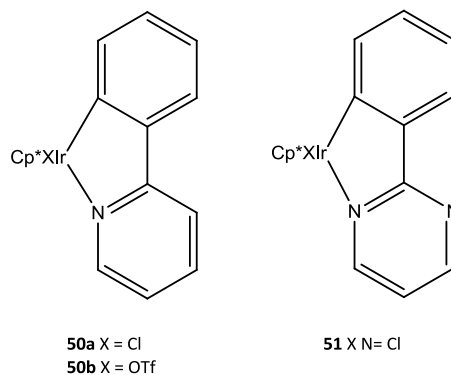
**Figure 42.** Crystal structure of **Na<sub>10</sub>-44**.

Iridium-based water oxidation catalysts are usually characterized by significant robustness. Bis-phenylpyridine iridium complexes **45-49** (Figure 43), described by Bernhard<sup>237</sup>, are able to generate up to 2760 TN (**48**) when an excess of Ce(IV) is employed as oxidant. After one week these catalysts maintain their catalytic activity.



**Figure 43.** Structures of **45-49**.

Later, Crabtree and coworkers reported a new family of Ir complex (**50** and **51**, figure 44) based on the electron donating ligand Cp\* (C<sub>5</sub>Me<sub>5</sub>) able to catalyze water oxidation with a lower TN ( $\approx 1500$ ) respect to Bernhard catalysts but with an enhanced TOF (initial rate of 54 turnover/min)<sup>238</sup>



**Figure 44.** Structures of **50** and **51**.

Further advances in Ir WOCs have been reached by substitution the biphenylpyridine ligand with Me<sub>2</sub>-NHC (Me<sub>2</sub>-NHC = N-dimethylimidazolin-2-ylidene) that resulted in high TOF (1.5 mol mol<sup>-1</sup> s<sup>-1</sup>)<sup>239</sup>, and with a pyridinium-functionalized triazolium salt (**52** and **53**, Figure 45) that leads to the formation

## General Introduction

of a more stable complex even in higher oxidation states like Ir(V) oxo species<sup>240</sup>

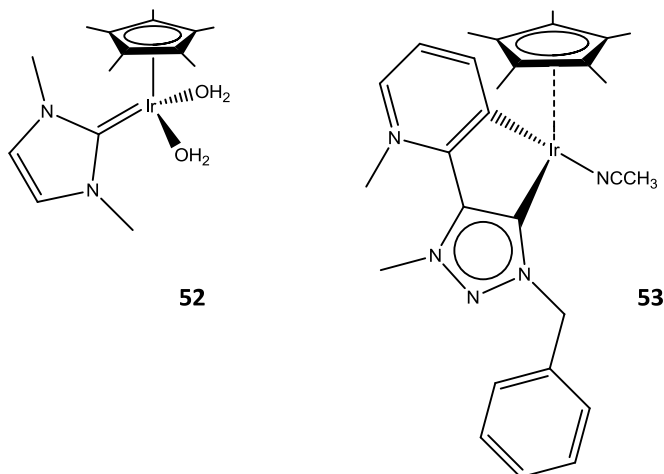


Figure 45. Structures of **52** and **53**.

Catalytic activity reported for **53** was of  $\approx 10000$  TN after 5 days reaction.

Lastly Bernhard and coworkers presented a family of iron containing a tetraamido macrocyclic ligand<sup>241</sup> (Fe-TAML, **54-58**, Figure 46) that efficiently catalyze the oxidative conversion of water to dioxygen in the presence of ceric ammonium nitrate as oxidant. In the case of **58** the turnover frequency exceeds  $1.3 \text{ TN}\cdot\text{s}^{-1}$ .

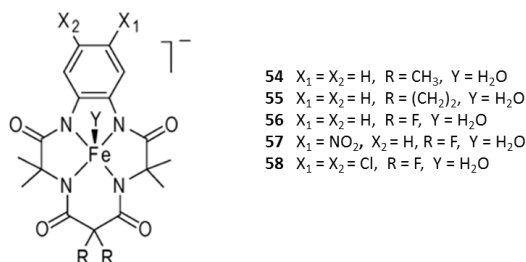


Figure 46. Structures **54-58**.

## I. vii. References

- (1) Johnson Matthey
- (2) Griffith, W. P. *Catalysis By Metal Complexes* **2011**, 34.
- (3) Planas, N.; Ono, T.; Vaquer, L.; Miro, P.; Benet-Buchholz, J.; Gagliardi, L.; Cramer, C. J.; Llobet, A. *Phys. Chem. Chem. Phys.* **2011**, 13, 19480.
- (4) Federsel, C.; Jackstell, R.; Beller, M. *Angew. Chem. Int. Ed.* **2010**, 49, 6254.
- (5) Jessop, P. G. *Handbook Homogeneous Hydrogenation*, H. de Vries, K. Elsevier (eds.), Wiley-VCH, Weinheim, **2007**, 1, 489.
- (6) Jessop, P. G.; Joó, F.; Tai, C. C. *Coord. Chem. Rev.* **2004**, 248, 2425.
- (7) Leitner, W. *J. Am. Chem. Soc.* **1997**, 119, 4432.
- (8) Leitner, W.; Gassner, F.; *J. Chem. Soc. Chem. Commun.* **1993**, 1465.
- (9) Angermund, K.; Baumann, W.; Dinjus, E.; Fornika, R.; Gørls, H.; Kessler, M.; Kruger, C.; Leitner, W.; Lutz, F. *Chem. Eur. J.* **1997**, 3, 755.
- (10) Tanaka, R.; Yamashita, M.; Nazaki, K. *J. Am. Chem. Soc.* **2009**, 131, 14168.
- (11) Ng, S. M.; Yin, C.; Yeung, C. H.; Chan, T. C.; Lau, C. P. *Eur. J. Inorg. Chem.* **2004**, 9, 1788.
- (12) Himeda, Y.; Onozawa-Komatsuzaki, N.; Sugihara, H.; Kasuga, K. *Organometallics* **2007**, 26, 702.
- (13) Jessop, P. G.; Hsiao, Y.; Ikariya, T.; Noyori, R. *J. Am. Chem. Soc.* **1996**, 118, 344.
- (14) Munshi, P.; Denise Main, A.; Linehan, J. C.; Tai, C.-C.; Jessop, P. G. *J. Am. Chem. Soc.* **2002**, 124, 7963.
- (15) Mashima, K.; Kusano, K.-h.; Sato, N.; Matsumura, Y.-i.; Nozaki, K.; Kumobayashi, H.; Sayo, N.; Hori, Y.; Ishizaki, T. *J. Org. Chem.* **1994**, 59, 3064.
- (16) Ohta, T.; Miyake, T.; Seido, N.; Kumobayashi, H.; Takaya, H. *J. Org. Chem.* **1995**, 60, 357.
- (17) Wabnitz, T. C.; Rizzo, S.; Goette, C.; Buschauer, A.; Benincori, T.; Reiser, O. *Tetrahedron Lett.* **2006**, 47, 3733.
- (18) Starodubtseva, E. V.; Vinogradov, M. G.; Pavlov, V. A.; Gorshkova, L. S.; Ferapontov, V. A. *Russ. Chem. Bull.* **2004**, 53, 2172.
- (19) Starodubtseva, E. V.; Turova, O. V.; Vinogradov, M. G.; Gorshkova, L. S.; Ferapontov, V. A. *Russ. Chem. Bull.* **2005**, 54, 2374.
- (20) Doherty, S.; Knight, J. G.; Bell, A. L.; Harrington, R. W.; Clegg, W. *Organometallics* **2007**, 26, 2465.
- (21) Bronze-Uhle, E. S.; Ines, d. S. M.; Donate, P. M.; Frederico, D. *J. Mol. Catal. A: Chem.* **2006**, 259, 103.



## General Introduction

- (22) Daley, C. J. A.; Wiles, J. A.; Bergens, S. H. *Inorg. Chim. Acta* **2006**, *359*, 2760.
- (23) Arai, N.; Azuma, K.; Nii, N.; Ohkuma, T. *Angew. Chem. Int. Ed.* **2008**, *47*, 7457.
- (24) Bratsosa, I.; Jednera, S.; Gianferrara, T.; Alessio, E. *Chimia* **2007**, *61*, 692.
- (25) Serrano, I.; López, M. I.; Ferrer, I. n.; Poater, A.; Parella, T.; Fontrodona, X.; Solà, M.; Llobet, A.; Rodríguez, M.; Romero, I. *Inorg. Chem.* **2011**, *50*, 6044.
- (26) Bhor, S.; Tse, M. K.; Klawonn, M.; Doebler, C.; Maegerlein, W.; Beller, M. *Adv. Synth. Catal.* **2004**, *346*, 263.
- (27) Whittall, I. R.; McDonagh, A. M.; Humphrey, M. G.; Samoc, M. *Advances in Organomet. Chem.* **1999**, *43*, 349.
- (28) Whittall, I. R.; McDonagh, A. M.; Humphrey, M. G.; Samoc, M. *Advances in Organomet. Chem.* **1998**, *42*, 291.
- (29) Verbiest, T. H.; S.; Kauranen, M.; Clays, K.; Persoons, A. *J. Mater. Chem.* **1997**, *7*, 2175.
- (30) Larionova, J. M.; B.; Sanchiz, J. n.; Kahn, O. *Inorg. Chem.* **1998**, *37*, 679.
- (31) Hmyene, M. Y.; A.; Escorne, M.; Percheron-Guegan, A.; Garnier, F. *Adv. Mater.* **1994**, *6*, 564.
- (32) Constable, E. C. *Angew. Chem. Int. Ed.* **1991**, *30*, 407.
- (33) Dembek, A. A.; Burch, R. R.; Feiring, A. *J. Am. Chem. Soc.* **1993**, *115*, 2087.
- (34) Adeloye, A. O.; Ajibade, P. A. *Int. J. Mol. Sci.* **2010**, *11*, 3158.
- (35) Prasanna de Silva, A.; Fox, D. B.; Moody, T.S.; Weir, S.M. *Pure Appl. Chem.* **2001**, *73*, 503.
- (36) Robertson, N.; McGowan, C. A. *Chem. Soc. Rev.* **2003**, *32*, 96.
- (37) Vos, J. G.; Kelly, J. M. *Dalton Trans.* **2006**, 4869.
- (38) Balzani, V. B.; F.; Ciano, M.; Maestri, M. *J. Chem. Ed.* **1983**, *60*.
- (39) Sun, L.; Hammarstrom, L.; Norrby, T.; Berglund, H.; Davydov, R.; Andersson, M.; Borje, A.; Korall, P.; Philouze, C.; Almgren, M.; Styring, S.; Akermark, B. *Chem. Commun.* **1997**, 607.
- (40) Durham, B.; Caspar, J. V.; Nagle, J. K.; Meyer, T. J. *J. Am. Chem. Soc.* **1982**, *104*, 4803.
- (41) Van Houten, J.; Watts, R. J. *J. Am. Chem. Soc.* **1976**, *98*, 4853.
- (42) Van Houten, J.; Watts, R. J. *Inorg. Chem.* **1978**, *17*.
- (43) Chen, H. H.; Tsai, A. Y.; Huang, C. W.; Eternal Chemical Co.; Ltd.; Taiwan, **2009**, p 14pp.

- (44) Park, J. W.; Lee, J. W.; Lee, W. S.; Ahn, K. S.; Choi, J. M.; Shin, B. C.; Seok, W. K.; Samsung SDI Co.; Ltd.; S. Korea, **2007**, p No pp. given.
- (45) Park, N. G. *Hwahak Sekye* **2006**, *46*, 74.
- (46) Yoneda, E.; Graetzel, M.; Nazeeruddin, M. K.; JSR Corporation, Japan, EPFL Ecole Polytechnique Federale de Lausanne . 2009, p 32pp.
- (47) Chandrasekharam, M.; Rajkumar, G.; Rao, C. S.; Suresh, T.; Reddy, P. Y.; Yum, J.-H.; Nazeeruddin, M. K.; Graetzel, M. *Adv. Nat. Sci.: Nanosci. Nanotechnol.* **2011**, *2*, 035016/1.
- (48) Bessho, T.; Constable, E. C.; Graetzel, M.; Hernandez, R. A.; Housecroft, C. E.; Kylberg, W.; Nazeeruddin, M. K.; Neuburger, M.; Schaffner, S. *Chem. Commun.* **2008**, 3717.
- (49) Stengel, I.; Mishra, A.; Pootrakulchote, N.; Moon, S.-J.; Zakeeruddin, S. M.; Graetzel, M.; Baeuerle, P. *J. Mater. Chem.* **2011**, *21*, 3726.
- (50) Seok, W. K.; Kim, M. Y.; Yokomori, Y.; Hodgson, D. J.; Meyer, T. J. *Bull. Korean Chem. Soc.* **1995**, *16*, 619.
- (51) Aebischer, N.; Laurenczy, G.; Ludi, A.; Merbach, A. E. *Inorg. Chem.* **1993**, *32*, 2810.
- (52) Dovletoglou, A.; Adeyemi, S.A.; Meyer, T.J. *Inorg. Chem.* **1996**, *35*.
- (53) Dovletoglou, A.; Adeyemi, S. A.; Meyer, T. J. *Inorg. Chem.* **1996**, *35*, 4120.
- (54) Moyer, B. A.; Thompson, M. S.; Meyer, T. J. *J. Am. Chem. Soc.* **1980**, *102*, 2310.
- (55) Moyer, B. A.; Meyer, T. J. *Inorg. Chem.* **1981**, *20*, 436.
- (56) Moyer, B. A.; Sipe, B. K.; Meyer, T. J. *Inorg. Chem.* **1981**, *20*.
- (57) Moyer, B. A.; Meyer, T. J. *J. Am. Chem. Soc.* **1979**, *101*, 1326.
- (58) Takeuchi, K. J.; Thompson, M. S.; Pipes, D. W.; Meyer, T. J. *Inorg. Chem.* **1984**, *23*, 1845.
- (59) Meyer, T. J. *J. Electrochem. Soc.* **1984**, *131*, 221C.
- (60) Llobet, A.; Doppelt, P.; Meyer, T. J. *Inorg. Chem.* **1988**, *27*, 514.
- (61) Robin, M. B.; Day, P. In *Adv. Inorg. Chem.* Emeléus, H. J.; Sharpe, A. G.; Eds.; Academic Press: 1968, Vol. Volume 10, p 247.
- (62) Arends, I. W. C. E.; Kodama, T.; Sheldon, R. A. *Top. Organomet. Chem.* **2004**, *11*, 277.
- (63) Marmion, M. L.; Tadeuchio, K. J. *J. Am. Chem. Soc.* **1988**, *110*.
- (64) Thompson, M. S.; De Giovanni, W. F.; Moyer, B. A.; Meyer, T. J. *J. Org. Chem.* **1984**, *25*, 4972.
- (65) Catalano, V. J.; Heck, R. A.; Immoos, C. E.; Hill, M. G. *Inorg. Chem.* **1998**, *37*.
- (66) Che, C.-M.; Ho, C.; Lau, T.-C. *J. Chem. Soc. Dalton Trans.* **1991**, *24*.

## General Introduction

- (67) Che, C.-M.; Cheng, K.-W.; Chan, M. C. W.; Lau, T.-C.; Mak, C.-K. *J. Org. Chem.* **2000**, *65*.
- (68) Stultz, L. K.; Huynh H. V.; Binstead, R. A.; Curry, M.; Meyer, T. J. *J. Am. Chem. Soc.* **2000**, *122*.
- (69) Nugent, W. A.; Mayer, J. M. *Metall-Ligand Multiple Bonds*, Wiley: New York, **1988**.
- (70) Meyer, T. J. *Metal Oxo Complexes and Oxygen Activation*, Martell, A. E.; Ed.; Plenum: New York, **1988**.
- (71) Holm, R. H. *Chem. Rev.* **1987**, *87*.
- (72) Gulliver, D. J. L.; W. *Coord. Chem. Rev.* **1982**, *46*.
- (73) Sheldon, R. A.; Kochi, J. K. *Metal-Catalyzed Oxidations of Organic Compounds*, Academic: New York, 1981.
- (74) James, B. R.; Mikkelsen, S. R.; Leung, T. W.; Williams, G. M.; Wong, R. *Inorg. Chim. Acta* **1984**, *85*, 209.
- (75) Groves, J. T.; Bonchio, M.; Carofiglio, T.; Shalyaev, K. *J. Am. Chem. Soc.* **1996**, *118*, 8961.
- (76) Shigeaki, T.; Miura, K.; Higuchi, T.; Hirobe, M.; Nagano, T. *Chem. Commun.* **1997**, 861.
- (77) Ohtake, H.; Higuchi, T.; Hirobe, M. *J. Am. Chem. Soc.* **1992**, *114*, 10660.
- (78) Balkus, K. J.; Jr.; Khanmamedova, A.; Eissa, M. *Stud. Surf. Sci. Catal.* **1995**, *97*, 189.
- (79) Bressan, M.; Morvillo, A. *J. Chem. Soc. Chem. Commun.* **1988**, 650.
- (80) Yamaguchi, M.; Kousaka, H.; Yamagishi, T. *Chem. Lett.* **1997**, 769.
- (81) Yamaguchi, M.; Kousaka, H.; Yamagishi, T. *J. Inorg. Biochem.* **1997**, *67*, 236.
- (82) Lau, T.-C.; Mak, C.-K. *J. Chem. Soc. Chem. Commun.* **1995**, 943.
- (83) Cheng, W.-C.; Yu, W.-Y.; Cheung, K.-K.; Che, C.-M. *J. Chem. Soc. Chem. Commun.* **1994**, 1063.
- (84) Fung, W.-H.; Yu, W.-Y.; Che, C.-M. *J. Org. Chem.* **1998**, *63*, 7715.
- (85) Fung, W.-H.; Yu, W.-Y.; Che, C.-M. *J. Org. Chem.* **1998**, *63*, 2873.
- (86) Murahashi, S.-I.; Oda, Y.; Komiya, N.; Naota, T. *Tetrahedron Lett.* **1994**, *35*, 7953.
- (87) Goldstein, A. S.; Beer, R. H.; Drago, R. S. *J. Am. Chem. Soc.* **1994**, *116*, 2424.
- (88) Neumann, R.; Abu-Gnim, C. *J. Chem. Soc. Chem. Commun.* **1989**, 1324.
- (89) Yamaguchi, K.; Mizuno, N. *New J. Chem.* **2002**, *26*, 972.
- (90) Bonchio, M.; Scorrano, G.; Toniolo, P.; Proust, A.; Artero, V.; Conte, V. *Adv. Synth. Catal.* **2002**, *344*, 841.

- (91) Naota, T.; Takaya, H.; Murahashi, S.-I. *Chem. Rev.* **1998**, *98*, 2599.
- (92) Barf, G. A.; Sheldon, R. A. *J. Mol. Catal. A: Chem.* **1995**, *102*, 23.
- (93) Lin, X.; Xu, J.; Liu, H.; Yue, B.; Jin, S.; Xie, G. *J. Mol. Catal. A: Chem.* **2000**, *161*, 163.
- (94) Zhang, X.; Chen, Q.; Duncan, D. C.; Lachicotte, R. J.; Hill, C. L. *Inorg. Chem.* **1997**, *36*, 4381.
- (95) Neumann, R.; Abu-Gnim, C. *J. Am. Chem. Soc.* **1990**, *112*, 6025.
- (96) Morvillo, A.; Bressan, M. *J. Mol. Catal. A: Chem.* **1997**, *125*, 119.
- (97) Wong, W.-K.; Chen, X.-P.; Pan, W.-X.; Guo, J.-P.; Wong, W.-Y. *Eur. J. Inorg. Chem.* **2002**, 231.
- (98) Chatterjee, D.; Mitra, A.; Mukherjee, S. *J. Mol. Catal. A: Chem.* **2001**, *165*, 295.
- (99) Keene, F. R. *Coord. Chem. Rev.* **1999**, *187*, 121.
- (100) Wang G. Z.; Andreasson. U.; Bäckvall J. E. *J. Chem. Soc. Chem. Commun.* **1994**, 1037.
- (101) Csjernyik G.; Ell, A.; Fadini, L.; Pugin, B.; Backvall, J. E. *J. Org. Chem.* **2002**, *67*, 1657.
- (102) Bäckvall J. E.; Chowdhury, R. L.; Karlsson, U. *J. Chem. Soc. Chem. Commun.* **1991**, 473.
- (103) Murahashi, S.; Naota, T.; Kuwabara, T.; Saito, T.; Kumobayashi, H.; Akutagawa, S. *J. Am. Chem. Soc.* **1990**, *112*, 7820.
- (104) Gilbert, J.; Roecker, L.; Meyer, T. J. *Inorg. Chem.* **1987**, *26*, 1126.
- (105) Gilbert, J. A.; Gersten, S. W.; Meyer, T. J. *J. Am. Chem. Soc.* **1982**, *104*, 6872.
- (106) Vining, W. J.; Meyer, T. J. *J. Electroanal. Chem. Interfacial Electrochem.* **1985**, *195*, 183.
- (107) Ellis, C. D.; Gilbert, J. A.; Murphy, W. R. Jr.; Meyer, T. J. *J. Am. Chem. Soc.* **1983**, *105*, 4842.
- (108) Vining, W. J.; Meyer, T. J. *Inorg. Chem.* **1986**, *25*, 2023.
- (109) Beller, M.; Bolm, C. *Transition Metals for Organic Synthesis*, Wiley-VCH, Weinheim.; **2004**.
- (110) Khenkin, A. M.; Hill, C. L. *Mendeleev Commun.* **1993**.
- (111) Zhang, X.; Chen, Q.; Duncan, D. C.; Lachicotte, R. J.; Hill, C. L. *Inorg. Chem.* **1997**, *36*.
- (112) de Boer, J. W.; Browne, W. R.; Feringa, B. L.; Hage, R. C. *R. Chimie* **2007**, *10*, 351.
- (113) Waldo, G. S.; Yu, S.; Penner-Hahn, J. E. *J. Am. Chem. Soc.* **1992**, *114*, 5869.
- (114) Pessiki, P. J.; Dismukes, G. C. *J. Am. Chem. Soc.* **1994**, *116*, 898.
- (115) Hage, R. *Red. Trav. Chim.* **1996**, *115*, 385.

## General Introduction

- (116) Bäckvall J. E.; Editor *Modern Oxidation Methods, 2nd Completely Revised*, Wiley-VCH Verlag GmbH & Co. KGaA, **2010**.
- (117) Battioni, P.; Renaud, J. P.; Bartoli, J. F.; Reina-Artiles, M.; Fort, M.; Mansuy, D. *J. Am. Chem. Soc.* **1988**, *110*, 8462.
- (118) Zhang, W.; Loebach, J. L.; Wilson, S. R.; Jacobsen, E. N. *J. Am. Chem. Soc.* **1990**, *112*.
- (119) Irie, R.; Noda, K.; Ito, Y.; Matsumoto, N.; Katsuki, T. *Tetrahedron Lett.* **1990**, *31*.
- (120) Jacobsen, E. N.; Wu, M. H. *Comprehensive Asymmetric Catalysis*, Springer, Heidelberg, 1999.
- (121) Berkessel, A.; Frauenkron, M.; Schwenkreis, T.; Steinmetz, A.; Baum, G.; Fenske, D. *J. Mol. Catal. A: Chem.* **1996**, *113*.
- (122) Irie, R.; Hosoya, N.; Katsuki, T. *Synlett.* **1994**.
- (123) Pietikainen, P. *J. Mol. Catal. A: Chem.* **2001**, *165*.
- (124) Kureshy, R. I.; Khan, N. H.; Abdi, S. H. R.; Patel, S. T.; Jasra, R. V. *Tetrahedron: Asymmetr.* **2001**, *12*.
- (125) Kureshy, R. I.; Kahn, N. H.; Abdi, S. H. R.; Singh, S.; Ahmed, I.; Shukla, R. S. Jasra, R. V. *J. Catal.* **2003**, *219*.
- (126) Garcia-Bosch, I.; Company, A.; Fontrodona, X.; Ribas, X.; Costas, M. *Org. Lett.* **2008**, *10*, 2095.
- (127) Garcia-Bosch, I.; Ribas, X.; Costas, M. *Adv. Synth. Catal.* **2009**, *351*.
- (128) Brinksma, J.; Hage, R.; Kerschner, J.; Feringa, B. L. *Chem. Commun.* **2000**.
- (129) Anilkumar, G.; Bitterlich, B.; Gelalcha, F. G.; Tse, M. K.; Beller, M. *Chem. Commun* **2007**, 289.
- (130) Traylor, T. G.; Tsuchiya, S.; Byun, Y.-S.; Kim, C. *J. Am. Chem. Soc.* **1993**, *115*.
- (131) White, M. C.; Doyle, A. G.; Jacobsen, E. N. *J. Am. Chem. Soc.* **2001**, *123*, 7194.
- (132) Anilkumar, G.; Bitterlich, B.; Gelalcha, F. G.; Tse, M. K.; Beller, M. *Chem. Commun.* **2007**.
- (133) Bitterlich, B.; Anilkumar, G.; Gelalcha, F. G.; Spilker, B.; Grotevendt, A.; Jackstell, R.; Tse, M. K.; Beller, M. *Chem. Asian J.* **2007**, *2*.
- (134) Bitterlich, B.; Schroder, K.; Tse, M. K.; Beller, M. *Eur. J. Org. Chem.* **2008**.
- (135) Schröder, K.; Tong, X.; Bitterlich, B.; Tse, M. K.; Gelalcha, F. G.; Brückner, A.; Beller, M. *Tetrahedron Lett.* *48*.
- (136) Schröder, K.; Enthaler, S.; Bitterlich, B.; Schulz, T.; Spannenberg, A.; Tse, M.K.; Junge, K.; Beller, M. *Chem. Eur. J.* **2009**, *15*.

- (137) Herrmann, W.; Fischer, R. W.; Marz, D. W. *Angew. Chem. Int. Ed.* **1991**, *30*.
- (138) Rudolph, J.; Reddy, K. L.; Chiang, J. P.; Sharpless, K. B. *J. Am. Chem. Soc.* **1997**, *119*.
- (139) Copéret, C.; Adolffsson, H.; Khuong, T.-A. V.; Yudin, A. K.; Sharpless, K. B. *J. Org. Chem.* **1998**, *63*.
- (140) Herrmann, W. A.; Kratzer, R. M.; Ding, H.; Thiel, W. R.; Glas, H. *J. Organomet. Chem.* **1998**, *555*.
- (141) Yamazaki, S. *Org. Biomol. Chem.* **2007**, *5*.
- (142) Katsuki, T.; Sharpless, K. B. *J. Am. Chem. Soc.* **1980**, *102*.
- (143) Matsumoto, K.; Sawada, Y.; Saito, B.; Sakai, K.; Katsuki, T. *Angew. Chem. Int. Ed.* **2005**, *44*.
- (144) Sawada, Y.; Matsumoto, K.; Kondo, S.; Watanabe, H.; Ozawa, T.; Suzuki, K.; Saito, B.; Katsuki, T. *Angew. Chem. Int. Ed.* **2006**, *45*.
- (145) Matsumoto, K.; Sawada, Y.; Katsuki, T. *Synlett.* **2006**.
- (146) Mizuno, N.; Nakagawa, Y.; Yamaguchi, K. *J. Mol. Catal. A: Chem.* **2006**, *251*.
- (147) Nakagawa, Y.; Mizuno, N. *Inorg. Chem.* **2007**, *46*.
- (148) Sato, K.; Aoki, M.; Ogawa, M.; Hashimoto, T.; Noyori, R. *J. Org. Chem.* **1996**, *61*.
- (149) Sato, K.; Aoki, M.; Ogawa, M.; Hashimoto, T.; Paynella, D.; Noyori, R. *Bull. Chem. Soc. Jpn.* **1997**, *70*.
- (150) Kamata, K.; Yonehara, K.; Sumida, Y.; Yamaguchi, K.; Hikichi, S.; Mizuno, N. *Science* **2003**, *300*.
- (151) Kamata, K.; Kotani, M.; Yamaguchi, K.; Hikichi, S.; Mizuno, M. *Chem. Eur. J.* **2007**, *13*.
- (152) Wahl, G.; Kleinhenz, D.; Schorm, A.; Sundermeyer, J.; Stowasser, R.; Rummey, C.; Bringmann, G.; Fickert, C.; Kiefer, W. *Chem. Eur. J.* **1999**, *5*.
- (153) Gharah, N.; Drew, M.; Bhattacharya, R. *Transit. Metal Chem.* **2009**, *34*, 549.
- (154) Balavoine G.; E. C.; Meunier F.; Rivière H.; *Tetrahedron Lett.* **1984**, *25*.
- (155) Eskenazi C.; Balavoine, G.; Meunier, F.; Riviere, H.; *J. Chem. Soc. Chem. Commun.* **1985**.
- (156) Leung, T.; James, B. R.; Dolphin, D. *Inorg. Chim. Acta* **1983**, *79*.
- (157) Upadhyay M.J.; B Bhattacharya, P. K.; Ganesphure P.A. Satish S. J. *Mol. Catal.* **1992**, *73*.
- (158) Che C.-M.; Tang, W.-T.; Lee W.-O.; Wong W.-T. Lai T.-F. **1989**, 2011.
- (159) Agarwal D. D.; J. R.; Chakravorty A. Rastogi R. *Polyhedron* **1992**, *11*.

## General Introduction

- (160) Upadhyay, M. J.; Bhattacharya, P. K.; Ganesphure P. A.; Satish, S. J. *Mol. Catal.* **1994**, *88*.
- (161) Che C.-M.; Tang, W.-T.; Wong, W.-T.; Lai, T. F. *J. Am. Chem. Soc.* **1989**, *111*.
- (162) Bressan, M.; Morvillo, A. *Inorg. Chem.* **1989**, *28*.
- (163) Bressan, M.; Morvillo, A. *J. Chem. Soc. Chem. Commun.* **1988**.
- (164) Ohtake, H.; Hihuchi, T.; Hirobe, M. *Tetrahedron Lett.* **1992**, *32*.
- (165) Ohtake, H.; Hihuchi, T.; Hirobe, M. *Tetrahedron Lett.* **1991**, *32*.
- (166) Ohtake, H.; Hihuchi, T.; Hirobe, M. *Tetrahedron Lett.* **1989**, *30*.
- (167) Dobson, J. C.; Seok, W. K.; Meyer, T. J. *Tetrahedron Lett.* **1984**, *25*.
- (168) Fisher J.M.; Fulford, A. Bennett, P. S. *J. Mol. Catal.* **1992**, *77*.
- (169) Drago, R. S. *Coord. Chem. Rev.* **1992**, *117*.
- (170) Goldstein A. S.; Beer, R. H.; Drago, R. S. *J. Am. Chem. Soc.* **1994**, *116*.
- (171) Bailey, C. L.; Drago, R. S. *J. Chem. Soc. Chem. Commun.* **1987**.
- (172) Groves, J. T.; Quinn, R. *J. Am. Chem. Soc.* **1985**, *107*.
- (173) Marchon, J. C.; Ramasseul, R. *J. Chem. Soc. Chem. Commun.* **1988**.
- (174) Murahashi, S.-I.; Komiya.; N. *Ruthenium in Organic Synthesis*, Wiley-VCH, Weinheim, **2004**.
- (175) Groves, J. T.; Bonchio, M.; Carofiglio, T.; Shalyaev, K. *J. Am. Chem. Soc.* **1996**, *118*.
- (176) Higuchi, T.; Othake, H.; Hirobe, M. *Tetrahedron Lett.* **1989**, *30*.
- (177) Nishiyama, H.; Shimada, T.; Itoh, H.; Sugiyama, H.; Motoyama, Y. *Chem. Commun.* **1997**, *1863*.
- (178) Tse, M. K.; Klawonn, M.; Bhor, S.; Dobler, C.; Anilkumar, G.; Hugl, H.; Magerlein, W.; Beller, M. *Org Lett* **2005**, *7*, 987.
- (179) Berkessel, A.; Kaiser, P.; Lex, J. *Chem. Eur. J.* **2003**, *9*.
- (180) Tada, M.; Muratsugu, S.; Kinoshita, M.; Sasaki, T.; Iwasawa, Y. *J. Am. Chem. Soc.* **2010**, *132*, 713.
- (181) Barf, G. A.; Sheldon, R. A. *J. Mol. Catal. A: Chem.* **1995**, *102*, 23.
- (182) Srinivasan K.; Michaud, P.; Kochi, J. K. *J. Am. Chem. Soc.* **1986**, *108*.
- (183) Jacobsen, E. N. *Catalytic Asymmetric Synthesis*; VCH, New York,, 1993.
- (184) Srinivasan K.; Perrier, S. Kochi, J. K. *J. Mol. Catal.* **1986**, *36*.
- (185) Srinivasan, K.; Kochi, J. K. *Inorg. Chem.* **1985**, *24*, 4671.
- (186) Bailey, C. L.; Drago, R. S. *J. Chem. Soc. Chem. Commun.* **1987**, *179*.
- (187) Drago, R. S. *Coordination Chemistry Reviews* **1992**, *117*, 185.
- (188) Groves, J. T.; Quinn, R. *J. Am. Chem. Soc.* **1985**, *107*, 5790.
- (189) Groves, J. T.; Quinn, R. *Inorg. Chem.* **1984**, *23*, 3844.
- (190) Sheldon, R. A. *J. Mol. Catal.* **1980**, *7*.
- (191) Bruce, T. *Acc. Chem. Res.* **1991**, *24*.



- (192) Groves, J. T.; Meyers R. S. *J. Am. Chem. Soc.* **1983**, *105*.
- (193) Stultz, L. K.; Binstead, R. A.; Reynolds, M. S.; Meyer, T. J. *J. Am. Chem. Soc.* **1995**, *117*, 2520.
- (194) International Energy Agency.
- (195) David Schlissel, B. B. Nuclear Power Plant Construction Costs **2008**.
- (196) European Nuclear Society.
- (197) Institute for Energy Research.
- (198) Lubitz, W.; Reijerse, E. J.; Messinger, J. *Energy Environ. Sci.* **2008**, *1*, 15.
- (199) Umena, Y.; Kawakami, K.; Shen, J.-R.; Kamiya, N. *Nature* **2011**, *473*, 55.
- (200) Juris, A.; Balzani, V.; Barigelletti, F.; Campagna, S.; Belser, P.; Von, Z. *A. Coord. Chem. Rev.* **1988**, *84*, 85.
- (201) Duan, L.; Tong, L.; Xu, Y.; Sun, L. *Energy Environ. Sci.* **2011**, *4*, 3296.
- (202) Geletii, Y. V.; Huang, Z.; Hou, Y.; Musaev, D. G.; Lian, T.; Hill, C. L. *J. Am. Chem. Soc.* **2009**, *131*, 7522.
- (203) Huang, Z.; Luo, Z.; Geletii, Y. V.; Vickers, J. W.; Yin, Q.; Wu, D.; Hou, Y.; Ding, Y.; Song, J.; Musaev, D. G.; Hill, C. L.; Lian, T. *J. Am. Chem. Soc.* **2011**, *133*, 2068.
- (204) Cape, J. L.; Hurst, J. K. *J. Am. Chem. Soc.* **2008**, *130*, 827.
- (205) Tong, L.; Duan, L.; Xu, Y.; Privalov, T.; Sun, L. *Angew. Chem. Int. Ed.* **2011**, *50*, 445.
- (206) Xu, Y.; Fischer, A.; Duan, L.; Tong, L.; Gabrielsson, E.; Aakermark, B.; Sun, L. *Angew. Chem. Int. Ed.* **2010**, *49*, 8934.
- (207) Xu, Y.; Duan, L.; Tong, L.; Aakermark, B.; Sun, L. *Chem. Commun.* **2010**, *46*, 6506.
- (208) Duan, L.; Xu, Y.; Gorlov, M.; Tong, L.; Andersson, S.; Sun, L. *Chem. Eur. J.* **2010**, *16*, 4659.
- (209) Duan, L.-L.; Xu, Y.-H.; Tong, L.-P.; Sun, L.-C. *ChemSusChem* **2011**, *4*, 238.
- (210) Duan, L.-L.; Xu, Y.-H.; Zhang, P.; Wang, M.; Sun, L.-C. *Inorg. Chem.* **2010**, *49*, 209.
- (211) Gersten, S. W.; Samuels, G. J.; Meyer, T. J. *J. Am. Chem. Soc.* **1982**, *104*, 4029.
- (212) Gilbert, J. A.; Eggleston, D. S.; Murphy, W. R.; Jr.; Geselowitz, D. A.; Gersten, S. W.; Hodgson, D. J.; Meyer, T. J. *J. Am. Chem. Soc.* **1985**, *107*, 3855.
- (213) Sens, C.; Romero, I.; Rodríguez, M.; Llobet, A.; Parella, T.; Benet-Buchholz, J. *J. Am. Chem. Soc.* **2004**, *126*, 7798.



## General Introduction

- (214) Bozoglian, F.; Romain, S.; Ertem, M. Z.; Todorova, T. K.; Sens, C.; Mola, J.; Rodriguez, M.; Romero, I.; Benet-Buchholz, J.; Fontrodona, X.; Cramer, C. J.; Gagliardi, L.; Llobet, A. *J. Am. Chem. Soc.* **2009**, *131*, 15176.
- (215) Deng, Z.; Tseng, H.-W.; Zong, R.; Wang, D.; Thummel, R. *Inorg. Chem.* **2008**, *47*, 1835.
- (216) Xu, Y.; Aakermark, T.; Gyollai, V.; Zou, D.; Eriksson, L.; Duan, L.; Zhang, R.; Aakermark, B.; Sun, L. *Inorg. Chem.* **2009**, *48*, 2717.
- (217) Tseng, H.-W.; Zong, R.; Muckerman, J. T.; Thummel, R. *Inorg. Chem.* **2008**, *47*, 11763.
- (218) Concepcion, J. J.; Jurss, J. W.; Templeton, J. L.; Meyer, T. J. *J. Am. Chem. Soc.* **2008**, *130*, 16462.
- (219) Zhang, G.; Zong, R.; Tseng, H.-W.; Thummel, R. P. *Inorg. Chem.* **2008**, *47*, 990.
- (220) Zong, R.; Thummel, R. P. *J. Am. Chem. Soc.* **2005**, *127*, 12802.
- (221) Duan, L.; Fischer, A.; Xu, Y.; Sun, L. *J. Am. Chem. Soc.* **2009**, *131*, 10397.
- (222) Xu, Y.; Wang, M.; Yang, X.; Privalov, T.; Duan, L.; Sun, L. *Presented in part at JSPS-RSAS Joint Conference "Capturing the Sun" Stockholm, Sweden, May 30–31, 2011.*
- (223) Roeser, S.; Farras, P.; Bozoglian, F.; Martinez-Belmonte, M.; Benet-Buchholz, J.; Llobet, A. *ChemSusChem* **2011**, *4*, 197.
- (224) Duan, L.; Bozoglian, F.; Mandal, S.; Stewart, B.; Privalov, T.; Llobet, A.; Sun, L. *Nat. Chem.* **2012**, *4*, 418.
- (225) Yin, Q.; Tan, J. M.; Besson, C.; Geletii, Y. V.; Musaev, D. G.; Kuznetsov, A. E.; Luo, Z.; Hardcastle, K. I.; Hill, C. L. *Science* **2010**, *328*, 342.
- (226) Geletii, Y. V.; Botar, B.; Kogerler, P.; Hillesheim, D. A.; Musaev, D. G.; Hill, C. L. *Angew. Chem. Int. Ed.* **2008**, *47*, 3896.
- (227) Sartorel, A.; Carraro, M.; Scorrano, G.; De, Z. R.; Geremia, S.; McDaniel, N. D.; Bernhard, S.; Bonchio, M. *J. Am. Chem. Soc.* **2008**, *130*, 5006.
- (228) Limburg, J.; Vrettos, J. S.; Liable-Sands, L. M.; Rheingold, A. L.; Crabtree, R. H.; Brudvig, G. W. *Science* **1999**, *283*, 1524.
- (229) Yagi, M.; Narita, K. *J. Am. Chem. Soc.* **2004**, *126*, 8084.
- (230) Ruettinger, W. F.; Campana, C.; Dismukes, G. C. *J. Am. Chem. Soc.* **1997**, *119*, 6670.
- (231) Dismukes, G. C.; Brimblecombe, R.; Felton, G. A. N.; Pryadun, R. S.; Sheats, J. E.; Spiccia, L.; Swiegers, G. F. *Acc. Chem. Res.* **2009**, *42*, 1935.

- (232) Hocking, R. K.; Brimblecombe, R.; Chang, L.-Y.; Singh, A.; Cheah, M. H.; Glover, C.; Casey, W. H.; Spiccia, L. *Nat Chem* **2011**, *3*, 461.
- (233) Najafpour, M. M.; Ehrenberg, T.; Wiechen, M.; Kurz, P. *Angew. Chem. Int. Ed.* **2010**, *49*, 2233.
- (234) Kanan, M. W.; Nocera, D. G. *Science* **2008**, *321*, 1072.
- (235) Risch, M.; Khare, V.; Zaharieva, I.; Gerencser, L.; Chernev, P.; Dau, H. *J. Am. Chem. Soc.* **2009**, *131*, 6936.
- (236) Yin, Q.; Tan, J. M.; Besson, C.; Geletii, Y. V.; Musaev, D. G.; Kuznetsov, A. E.; Luo, Z.; Hardcastle, K. I.; Hill, C. L. *Science* **2010**, *328*, 342.
- (237) McDaniel, N. D.; Coughlin, F. J.; Tinker, L. L.; Bernhard, S. *J. Am. Chem. Soc.* **2008**, *130*, 210.
- (238) Hull, J. F.; Balcells, D.; Blakemore, J. D.; Incarvito, C. D.; Eisenstein, O.; Brudvig, G. W.; Crabtree, R. H. *J. Am. Chem. Soc.* **2009**, *131*, 8730.
- (239) Hettterscheid, D. G. H.; Reek, J. N. H. *Chem. Commun.* **2011**, *47*, 2712.
- (240) Lalrempuia, R.; McDaniel, N. D.; Mueller-Bunz, H.; Bernhard, S.; Albrecht, M. *Angew. Chem. Int. Ed.* **2010**, *49*, 9765.
- (241) Ellis, W. C.; McDaniel, N. D.; Bernhard, S.; Collins, T. J. *J. Am. Chem. Soc.* **2010**, *132*, 10990.

UNIVERSITAT ROVIRA I VIRGILI

NEW RUTHENIUM, MANGANESE AND COBALT DINUCLEAR COMPLEXES AS REDOX CATALYSTS.

UNFOLDING THE ESSENTIAL STEPS FOR THE GENERATION OF SOLAR FUELS

Carlo Di Giovanni

Dipòsit Legal: T. 1429-2012

# Chapter II

## Objectives



Dinuclear complexes of transition metals have been widely employed in catalysis due to their tendency of promote intramolecular catalytic mechanisms between the two active sites that often results in better efficiency and performance of the catalyst. The electronic communication between the metal centers in dinuclear complexes mainly influences their ground and excited state properties as well as their redox properties<sup>1</sup>. The bridging ligand in such complexes regulates several factors like the  $\sigma$  and  $\pi$  donor/acceptor properties, the distance between the metal centers, the rigidity and flexibility of the whole structure and the net charge of the complex. N-heterocyclic bridging ligands have been widely used for chelating Ru, Os, Mn, Fe and other transition metals into dinuclear highly stable species. These ligands vary from electron-poor type, that mediate metal-metal interactions through low-lying  $\pi^*$  orbitals (LUMOs) by promoting electron transfer mechanisms, to electron-rich anionic bridging ligands that operate via hole transfer mechanisms, taking advantage of relatively high lying filled molecular orbitals (HOMOs)<sup>1,2</sup>. The main topic of this thesis is the study of the structural, electrochemical and catalytic properties of new dinuclear complexes of ruthenium, manganese and cobalt containing polypyridyl bridging ligands.

- (1) Giuffrida, G.; Campagna, S. *Coord. Chem. Rev.* **1994**, 135–136, 517.
- (2) Baitalik, S.; Flörke, U.; Nag, K. *Inorg. Chem.* **1999**, 38, 3296.

## Objectives

The objectives of this thesis can be then summarized as:

- Synthesis of new ruthenium dinuclear complexes containing the pyridazine-3,6-dicarboxylate bridging ligand. Structural, spectroscopic and electrochemical characterization. Application as redox catalyst.
- Synthesis of new ruthenium and manganese dinuclear complexes containing the pyrazole-3,5-dicarboxylate bridging ligand. Structural, spectroscopic and electrochemical characterization. Application in chemical and photochemical oxidation of organic substrates.
- Synthesis and characterization of a new polypyridyl decadentate ligand.
- Synthesis and characterization of dinuclear cobalt complexes containing a decadentate ligand. Structural, spectroscopic and electrochemical characterization. Application in electrochemical water oxidation and proton reduction.
- Assembly of a cell for artificial photosynthesis via two-electron processes.

UNIVERSITAT ROVIRA I VIRGILI

NEW RUTHENIUM, MANGANESE AND COBALT DINUCLEAR COMPLEXES AS REDOX CATALYSTS.

UNFOLDING THE ESSENTIAL STEPS FOR THE GENERATION OF SOLAR FUELS

Carlo Di Giovanni

Dipòsit Legal: T. 1429-2012



UNIVERSITAT ROVIRA I VIRGILI

NEW RUTHENIUM, MANGANESE AND COBALT DINUCLEAR COMPLEXES AS REDOX CATALYSTS.

UNFOLDING THE ESSENTIAL STEPS FOR THE GENERATION OF SOLAR FUELS

Carlo Di Giovanni

Dipòsit Legal: T. 1429-2012

# Chapter III

Synthesis and characterization of two new  
dinuclear ruthenium complexes based on the  
pyridazine-3,6-dicarboxylic acid ligand.  
Reactivity in homogeneous oxidations

- i. Introduction*
- ii. Experimental Section*
- iii. Results and discussion*
- iv. Conclusions*
- v. Associated content*
- vi. References*



### III. i. Introduction

Ruthenium complexes are attracting a great deal of attention because of their multiple applications in many fields of science.<sup>1-5</sup> Polypyridylruthenium complexes are proposed as basic electronic devices because they can act as molecular wires and switches.<sup>6-8</sup> They are also used as building blocks for the development of macromolecular assemblies,<sup>9-17</sup> as well as for the design and construction of molecular machines.<sup>18-21</sup> Furthermore, during the past decades, the application of ruthenium complexes as light harvesters in dye sensitized solar cells<sup>22,23</sup> has been a key issue for the development of new solar-energy conversion schemes.<sup>24</sup> Catalysis is also a field in which Ru complexes have broad applications given the rich chemistry of Ru that has compounds known in 11 different oxidation states.<sup>25-32</sup> A variety of reactions have been reported where Ru complexes behave as catalysts including: nitrile hydrolysis, olefin metathesis, CO<sub>2</sub> reduction<sup>33-44</sup>, enantioselective hydrogenations<sup>45-53</sup>. Ru complexes are also excellent catalyst for redox transformations such as alcohol oxidation<sup>54-57,58-62</sup>, epoxidation<sup>63-72</sup>, sulfoxidation<sup>73-76</sup> and water oxidation<sup>77-86</sup>. In these cases the active site of the metal center is invariably a Ru-O group where the metal is in a formal high oxidation state. Most of the Ru literature related to redox catalysis is based on mononuclear complexes since they are generally easily accessible from a synthetic view point. This has fostered the preparation of families of related Ru-aqua complexes with different auxiliary ligands that have allowed to understand how their steric and electronic properties perturbations influence the reactivity. We have set up a project to design dinuclear Ru complexes as redox catalysts containing a bridging ligand. The bridging ligand can act as electronic communicators among the metal centers or depending on its nature it can act as electronic insulator. Furthermore the

## Ru dinuclear complexes containing the pyridazine-3,6-dicarboxylic acid ligand

geometry of the ligand can allow two metals to cooperate through space. Therefore a large number of complexes with different properties can be envisaged depending on the bridging ligand together with the rest of the auxiliary ligands filling up the first coordination sphere.

In the present chapter we reported report the preparation of new family of Ru complexes of general formula  $\{[Ru^{II}(trpy)]_2(\mu-dcpd)(\mu-L)\}^+$  (where  $dcpd^{2-}$  is the pyridazine-3,6-dicarboxylate anion; trpy is 2,2':6',2''-terpyridine; L = Cl, **1**<sup>+</sup>; L = OH, **2**<sup>+</sup>) and  $\{[Ru^{II}(trpy)(L')]_2(\mu-dcpd)\}^{2+}$  (L' = H<sub>2</sub>O, **3**<sup>2+</sup> or **RuPDZ**; L' = MeCN, **4**<sup>2+</sup>) and we test them as redox catalysts for epoxidation and water oxidation reactions.

### III. ii. Experimental section

**Materials.** All reagents used in the present work were obtained from Aldrich Chemical Co. or Alfa Aesar and were used without further purification. Synthesis-grade organic solvents were obtained from SDS and were routinely degassed with argon. Ethanol was dried with a 3.5 Å molecular sieves, and acetonitrile, dichloromethane (DCM), hexane, and diethyl ether were used from the SPS. High-purity deionized water was obtained by passing distilled water through a nanopure Milli-Q water purification system.

Sodium pyridazine-3,6-dicarboxylate<sup>87</sup> ligand (dcpd) and  $[\text{Ru}^{\text{III}}\text{Cl}_3(\text{trpy})]^{88}$  were prepared as described in the literature. All synthetic manipulations were routinely performed under an argon atmosphere using Schlenk and vacuum-line techniques.

$\{[\text{Ru}^{\text{II}}(\text{trpy})]_2(\mu\text{-dcpd})(\mu\text{-Cl})\}(\text{PF}_6)\cdot 6\text{H}_2\text{O}$ ,  $[\mathbf{1}(\text{PF}_6)\cdot 6\text{H}_2\text{O}]$ . 200 mg (0.454 mmol) of  $[\text{RuCl}_3(\text{trpy})]$  and 130 mg (3.067 mmol) of LiCl were dissolved in 50 mL of a mixture ethanol/water (3:1). 133  $\mu\text{L}$  (0.954 mmol) of triethylamine were added and the mixture was stirred for 20 minutes at RT. 10 mL of EtOH/H<sub>2</sub>O (3:1) containing 48 mg (0.226 mmol) of sodium 3,6-pyridazinedicarboxylate sodium salt (Na<sub>2</sub>dcpd) were added and the mixture was heated at reflux for 4 h and then stirred in the presence of a 200 W tungsten lamp for 12 h. The resulting solution was filtered and 1 mL of a saturated aqueous NH<sub>4</sub>PF<sub>6</sub> solution was added. The precipitate formed was filtered and washed with dichloromethane until colorless filtrate. Recrystallization from acetone/ether yielded small dark-brown crystals. Yield: 56 mg (22%). Anal. Calcd for C<sub>36</sub>H<sub>36</sub>ClF<sub>6</sub>N<sub>8</sub>O<sub>10</sub>PRu<sub>2</sub>: C, 38.49; H, 3.23; N, 9.90. Found: C, 38.48; H, 2.98; N, 9.77. <sup>1</sup>H-NMR (500 MHz, Acetone-d<sub>6</sub>)  $\delta$  8.94 (d,  $J = 5.4$  Hz, 1H, H1-H15), 8.54 (d,  $J = 6.3$  Hz, 2H, H7-H9), 8.52 (s, 1H, H17), 8.46 (d,  $J = 7.93$  Hz, 2H, H4-H12), 8.08 (t,  $J = 8.0$  Hz, 1H, H8),

## Ru dinuclear complexes containing the pyridazine-3,6-dicarboxylic acid ligand

7.99 (td,  $J = 7.9, 1.5$  Hz, 2H, H3-H13), 7.68 (ddd,  $J = 7.4, 5.5, 1.4$  Hz, 2H, H2-H14).  $^{13}\text{C-NMR}$  (125 MHz, Acetone- $d_6$ )  $\delta$  159.3 (C20), 158.8 (C16), 158.3 (C5,C11, C6, C10), 154.5 (C1, C15), 138.1 (C3, C13), 135.5 (C8), 127.4 (C17), 127.8 (C2, C14), 124.0 (C4, C12), 122.5 (C7, C9). UV-vis ( $(\text{CH}_3)_2\text{CO}$ ) [ $\lambda_{\text{max}}$ , nm ( $\epsilon$ ,  $\text{M}^{-1} \text{cm}^{-1}$ ): 420 (4695), 484 (4525), 536 (5038), 675 (1623).  $E_{1/2}$  ( $\text{CH}_3\text{CN}$ , V vs SSCE): 0.796 V and 1.264 V. MALDI(+)-MS: ( $\text{CH}_3\text{CN}$ ):  $m/z = 870.9$  ( $[\text{M} - \text{PF}_6]^{-}$ ).

$\{[\text{Ru}^{\text{II}}(\text{trpy})]_2(\mu\text{-dcpd})(\mu\text{-OH})\}(\text{PF}_6)_4 \cdot 4\text{H}_2\text{O}$ , **[2(PF<sub>6</sub>)]·4H<sub>2</sub>O**. All the synthesis has been carried on under strictly Ar atmosphere in a schlenk line. 400 mg (0.908 mmol) of  $[\text{RuCl}_3(\text{trpy})]$  and 96 mg (0.453 mmol) of  $\text{Na}_2\text{dcpd}$  were dissolved in 50 mL of water. 400  $\mu\text{L}$  (2.869 mmol) of triethylamine were added and the mixture refluxed for 4 h under Ar. The solution was then filtered and 1 mL of  $\text{KPF}_6$  added. A black solid precipitated after reduction of the volume. The dark solid obtained was washed with cold degassed acetone and dried under vacuum. Yield = 184 mg (38%). Anal. Calcd for  $\text{C}_{36}\text{H}_{33}\text{F}_6\text{N}_8\text{O}_9\text{PRu}_2$ : C, 40.46; H, 3.11; N, 10.48. Found: C, 40.38 H, 2.85; N, 10.43.  $^1\text{H-NMR}$  (400 MHz, Acetone- $d_6$ )  $\delta$  8.84 (d,  $J = 5.4$  Hz, 2H, H22-36), 8.51 (s, 1H, H3), 8.33 (d,  $J = 8.1$  Hz, 2H, H28-H30), 8.27 (d,  $J = 8.1$  Hz, 2H, H25-H33), 7.87 – 7.75 (m, 3H, H3-H34-H29), 7.54 (dd,  $J = 7.5, 5.6$  Hz, 2H, H23-H35).  $^{13}\text{C-NMR}$  (100 MHz, Acetone- $d_6$ )  $\delta$  171.7 (C1), 159.8 (C26-C32), 158.7 (C27-C31), 157.1 (C2), 154.3 (C22-C36), 137.5 (C24-C34), 133.7 (C29), 127.9 (C23-C35), 126.8 (C3), 123.8 (C25-C33), 121.9 (C28-C30). UV-vis ( $\text{CH}_3\text{CN}$ ) [ $\lambda_{\text{max}}$ , nm ( $\epsilon$ ,  $\text{M}^{-1} \text{cm}^{-1}$ ): 277 (7871), 314 (8921), 421 (3826), 527 (3213), 560 (3238), 743 (1254).  $E_{\text{p,a}}$  ( $\text{CF}_3\text{SO}_3\text{H}$ , V vs SSCE): 0.290 V, 0.490 V, 0.680 V and 1.047 V. MALDI(+)-MS: ( $(\text{CH}_3)_2\text{CO}/\text{CH}_2\text{Cl}_2$ ):  $m/z = 852.2$  ( $[\text{M} - \text{PF}_6]^{-}$ );  $m/z = 997.2$  ( $[\text{M} + \text{H}]^{+}$ ).

**Equipment and Measurements.** All electrochemical experiments were performed in a PAR 263A EG&G potentiostat or in an IJ-Cambria HI-660 potentiostat, using a three-electrode cell. Glassy carbon (3 mm diameter) from

BAS was used as the working electrode, a platinum wire as the auxiliary electrode, and SSCE as the reference electrode. Cyclic voltammograms were recorded at a  $100 \text{ mV}\cdot\text{s}^{-1}$  scan rate. The complexes were dissolved in previously degassed MeCN containing the necessary amount of  $(n\text{-Bu}_4\text{N})(\text{PF}_6)$ , used as the supporting electrolyte, to yield a 0.1 M ionic strength solution. All  $E_{1/2}$  values reported in this work were estimated from cyclic voltammetry (CV) as the average of the oxidative and reductive peak potentials  $(E_{p,a} + E_{p,c})/2$  or from differential pulse voltammetry (DPV; pulse amplitudes of 0.05 V, pulse widths of 0.05 s, sampling width of 0.02 s, and a pulse period of 0.1 s). Unless explicitly mentioned, the concentrations of the complexes were approximately 1 mM. A 400 MHz Bruker Avance II spectrometer and a Bruker Avance 500 MHz were used to carry out NMR spectroscopy at room temperature. Samples were run in acetone- $d_6$ . The electrospray ionization (ESI) and matrix-assisted laser desorption ionization (MALDI) mass spectrometry (MS) experiments were performed on a Waters Micromass LCT Premier equipment and a Bruker Daltonics Autoflex equipped with a nitrogen laser (337 nm), respectively. UV-vis spectroscopy was performed on a Cary 50 Bio (Varian) UV-vis spectrophotometer with 1 cm quartz cells. Manometric measurements were performed with homemade water-jacket glass reactor coupled to a Testo 521 manometer. Composition of the gaseous phase was determined by online mass-spectrometry with an OmniStar GSD 301 C (Pfeiffer) quadrupole mass-spectrometer. In a typical experiment, 1 mL of a 1 mM complex solution in  $\text{CF}_3\text{SO}_3\text{H}$  (pH 1.0) was degassed with nitrogen until no oxygen could be detected. The reactor was then closed with a septum-sealed adapter that excluded the gas phase. A 0.2 mL of previously degassed  $(\text{NH}_4)_2\text{Ce}^{\text{IV}}(\text{NO}_3)_6$  solution, was then added directly into the reaction solution with a Hamilton syringe. Blank experiments were performed by addition of  $(\text{NH}_4)_2\text{Ce}^{\text{IV}}(\text{NO}_3)_6$



## Ru dinuclear complexes containing the pyridazine-3,6-dicarboxylic acid ligand

solution to neat  $\text{CF}_3\text{SO}_3\text{H}$  (pH 1.0) in absence of catalyst. Epoxidation catalytic experiments were analyzed in an Agilent 6890N gas chromatograph coupled to a mass selective detector with ionization by electronic impact and in an Agilent 6890 with a FID detector using a HP5 column. In a typical experiment the catalyst (1.4 mg;  $1,31 \cdot 10^{-3}$  mmol; final concentration = 1 mM), the substrate (2.6 mmol, final concentration = 2 M), dodecane (50  $\mu\text{L}$ ; 0.22 mmol; final concentration = 170 mM) as internal reference, and (diacetoxyiodo)benzene (1.67 g; 5.2 mmol; final concentration = 4 M) were mixed together in 1 mL of a 1:1 dichloromethane/ethanol solution (final volume  $\approx 1.3$  mL). First aliquot was taken, filtered through a Pasteur pipette filled with celite, diethyl ether was added in order to elute the organic compounds and the filtrate analyzed by GC. The reaction mixture was stirred at RT for 30 min and a second aliquot was taken and treated as described above. No epoxide or just traces were detected at this time. Water (94  $\mu\text{L}$ ; 5.2 mmol; final concentration = 4 M) was added and aliquots taken every 5, 10, 15, 20, 25, 30 or until completion of reaction. The characterization of the reaction products were done by comparison with commercial products or by GC-MS spectrometry. GC conditions: initial temperature 40  $^\circ\text{C}$  for 10 min, ramp rate variable for each substrate (typically from 10  $^\circ\text{C}/\text{min}$  to 20  $^\circ\text{C}/\text{min}$ ), final temperature 250  $^\circ\text{C}$ , injection temperature 220  $^\circ\text{C}$ , detector temperature 250 $^\circ\text{C}$ . Yield of epoxide and substrate conversion were calculated with regard to the initial concentration of substrate. Substrate conversion =  $\frac{[\text{substrate}]_{\text{initial}} - [\text{substrate}]_{\text{final}}}{[\text{substrate}]_{\text{initial}}} \cdot 100$ . Yield epoxide =  $\frac{[\text{epoxide}]_{\text{final}}}{[\text{substrate}]_{\text{initial}}} \cdot 100$ . Epoxide selectivity =  $\frac{[\text{epoxide}]_{\text{final}}}{[\text{substrate}]_{\text{initial}} - [\text{substrate}]_{\text{final}}} \cdot 100$

### Single-Crystal X-Ray Structure Determination. *Crystal Preparation.*

Crystals for **1**( $\text{PF}_6$ ) were grown by the slow evaporation of a water solution of the complex. Crystals for complexes **2**( $\text{PF}_6$ ) were grown by the slow

evaporation of an acetonitrile solution of the complex. All measured crystals were prepared under inert conditions immersed in perfluoropolyether as the protecting oil for manipulation.

*Data collection:* Crystal structure determinations for  $\mathbf{1}^+$  and  $\mathbf{2}^+$  were carried out using a Bruker-Nonius diffractometer equipped with an APEX 2 4K CCD area detector, a FR591 rotating anode with  $\text{MoK}_\alpha$  radiation, Montel mirrors as monochromator and an Oxford Cryosystems low temperature device Cryostream 700 plus ( $T = -173^\circ\text{C}$ ). Full-sphere data collection was used with  $\omega$  and  $\varphi$  scans. *Programs used:* Data collection APEX-2<sup>89</sup>, data reduction Bruker Saint<sup>90</sup> V/.60A and absorption correction SADABS<sup>91</sup> or TWINABS<sup>92</sup>.

*Structure Solution and Refinement:* Crystal structure solution was achieved using direct methods as implemented in SHELXTL<sup>93</sup> and visualized using the program XP. Missing atoms were subsequently located from difference Fourier synthesis and added to the atom list. Least-squares refinement on  $F^2$  using all measured intensities was carried out using the program SHELXTL. All non-hydrogen atoms were refined including anisotropic displacement parameters. In order to avoid highly disordered solvent molecules the program SQUEEZE<sup>94</sup> was used.

The Ortep-plot of  $\mathbf{2}^+$  was drawn exceptionally with an occupancy of 30 %. The asymmetric unit contains four independent molecules of the complex, four  $\text{PF}_6$  anions and 32 different positions of disordered water molecules. In order to avoid the highly disordered solvent molecules the program SQUEEZE was applied leading to a refined model with a R1 value of 7.87 %. One of the  $\text{PF}_6$  anions is also disordered in two positions with a ratio of 83:17. In one of the complex molecules a hydrogen atom corresponding to a hydroxide was localized. In the rest of the complex molecules hydroxides could not be

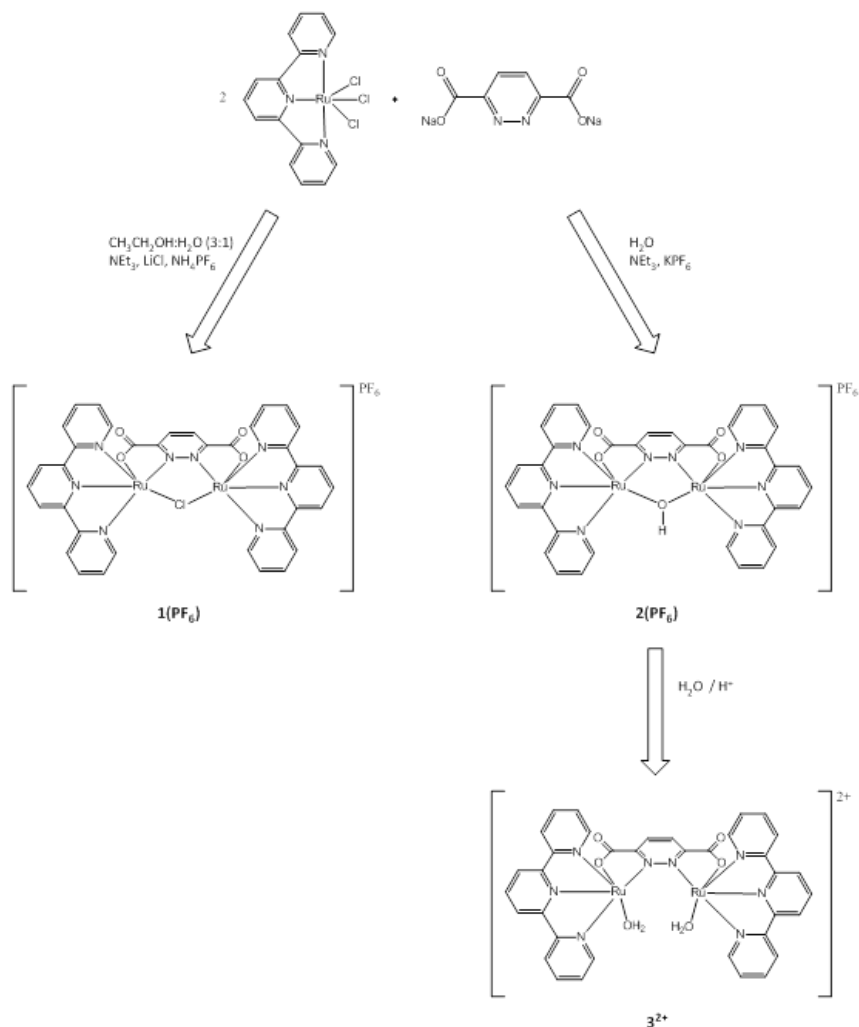
## Ru dinuclear complexes containing the pyridazine-3,6-dicarboxylic acid ligand

localized. In one of the cases the presence of a hydroxide is not possible since there is no space for it.

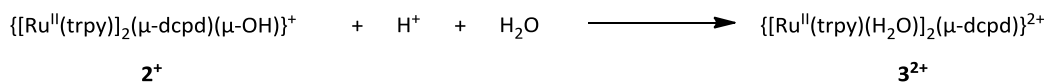
### III. iii. Results and discussion

#### Synthesis

We have chosen the  $\text{dcpd}^{2-}$  ligand because through the pyridazine moiety allows the electronic communication between the ruthenium metals and thus controls their electronic coupling. Furthermore its geometry allows placing two metals in very close proximity so that through space interactions can also occur. Finally the  $\text{trpy}$  ligand with its meridional geometry ensures the possibility of the through space interaction provided there is no isomerization process towards the out isomers. The synthetic strategy followed for the preparation of the complexes described here is depicted in Scheme 1. Addition of the octahedral Ru complex  $[\text{Ru}^{\text{III}}\text{Cl}_3(\text{trpy})]$  to the  $\text{N}_2\text{O}_2$  compartmental dinucleating  $\text{dcpd}^{2-}$  ligand in the presence of triethylamine and LiCl generates the corresponding dinuclear complex  $\{[\text{Ru}^{\text{II}}(\text{trpy})]_2(\mu\text{-dcpd})(\mu\text{-Cl})\}^+$ ,  $\mathbf{1}^+$ , bridged by the  $\text{dcpd}^{2-}$  ligand and by the chloride ligand. The 28% yield obtained in this reaction is low, mainly due to the parallel formation of  $[\text{Ru}^{\text{II}}(\text{trpy})_2]^{2+}$  that could not be avoided. Multiple attempts to remove the Cl and generate the corresponding aqua complex  $\{[\text{Ru}^{\text{II}}(\text{trpy})(\text{H}_2\text{O})]_2(\mu\text{-dcpd})\}^{2+}$ ,  $\mathbf{3}^{2+}$ , from  $\mathbf{1}^+$  failed. In the absence of  $\text{Cl}^-$  and using neat water as solvent, the reaction of  $[\text{Ru}^{\text{III}}\text{Cl}_3(\text{trpy})]$  and  $\text{dpcd}^{2-}$  afforded the hydroxo bridged complex,  $\{[\text{Ru}^{\text{II}}(\text{trpy})]_2(\mu\text{-dcpd})(\mu\text{-OH})\}^+$ ,  $\mathbf{2}^+$ , also in low yields for the same reason as in the previous case. Now acidic treatment of  $\mathbf{2}^+$  in water generates the desired aqua complex,  $\mathbf{3}^{2+}$ , as indicated in Scheme 2. Complexes  $\mathbf{1}^+$  and  $\mathbf{2}^+$  were characterized by the usual spectroscopic techniques as well as by X-Ray diffraction analysis.



**Scheme 1.** Synthetic pathways for **1(PF<sub>6</sub>)**, **2(PF<sub>6</sub>)**, and **3<sup>2+</sup>**.



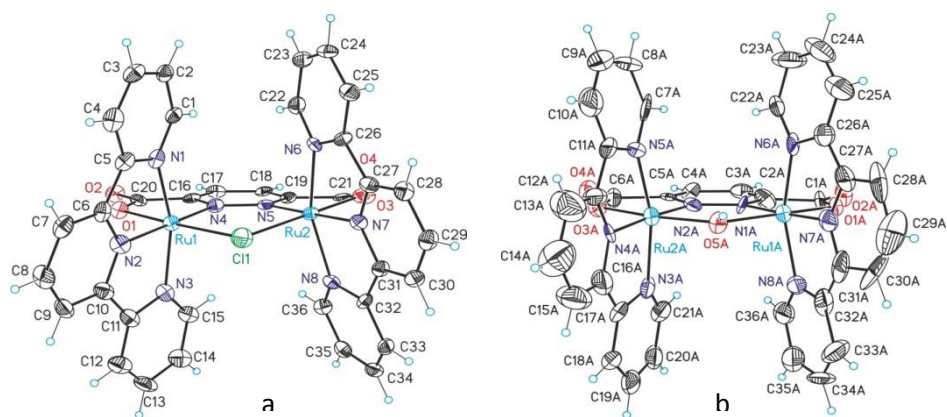
**Scheme 2.** Water coordination in acidic conditions.

## Ru dinuclear complexes containing the pyridazine-3,6-dicarboxylic acid ligand

### Solid state structure

Suitable crystals for X-Ray diffraction analysis of **1(PF<sub>6</sub>)** were obtained by slow evaporation of a solution of complex in water. Slow evaporation of a solution of **2(PF<sub>6</sub>)** in acetonitrile gave suitable crystals for X-Ray. The asymmetric contained four independent molecules of the complex. In one of the complex molecules a hydrogen atom corresponding to a hydroxide was localized. In the rest of the complex molecules hydroxides could not be localized. In one of the cases the presence on a hydroxide is not possible since there is no space for it. In both complexes the Ru centers adopt a distorted octahedral geometry with bond distances and angles comparable to analogous complexes reported earlier in the literature<sup>26,29,31,32,95-105</sup>. Figure 1, displays an Ortep plot for the cationic moiety of these two complexes together with an atom labelling scheme. An interesting feature here is the Ru-N-N-Ru torsion angle of 7.08° for **1<sup>+</sup>** and of 3.21° for **2<sup>+</sup>**, that reflects the need for the dcpd<sup>2-</sup> ligand to adapt to the longer Ru-Cl distance (2.357 Å, average of 2.440 Å<sup>100,106,107</sup>) with regard to that of the bridging Ru-OH distance (2.089 Å). This is also responsible for a longer Ru--Ru distance for the chlorido complex **1<sup>+</sup>** (3.636 Å, average of 3.813 Å<sup>100,106,107</sup>) with regard to hydroxido complex **2<sup>+</sup>** (3.431 Å). In order to adapt to this geometrical constraint a rotation of the carboxylate out of the pyridazine moiety plane takes placing Ru metal center also out of this plane. This is reflected in the N(5)C(19)C(21)O(3) torsion angle of 10.9° whereas for N(4)C(16)C(20)O(1) is only 1.7°. As a consequence of all this the molecular structure of **2<sup>+</sup>** is very close to C<sub>2v</sub> symmetry with the C<sub>2</sub> axis going through the OH bridge and bisecting the pyridazine moiety of the dcpd<sup>2-</sup> ligand whereas **1<sup>+</sup>** has no symmetry. The molecular packing arrangement adopted by complex **1<sup>+</sup>** is very interesting and is exhibited in Figure SI1. In the Figure it is shown the unit cell where two cationic moieties of **1<sup>+</sup>** are hydrogen bonded by several

water molecules. A cubane type of structure is generated where 6 of its vertex are occupied by oxygen atoms of the hydrogen bonded water molecules and the remaining two oxygens come from the non-coordinated oxygen atoms (O4), belonging to the carboxylate moiety of the  $\text{dcpd}^{2-}$  ligand from two symmetric related  $1^+$  units, that are situated in opposite vertexes. Additional water molecules are further connected via hydrogen bonding to the cubane structure. Finally, the other carboxylate of the  $\text{dcpd}^{2-}$  ligand is also hydrogen bonded with an additional water molecule that is not shown in the drawing. The asymmetric unit of **2**( $\text{PF}_6$ ) contains four independent molecules of the complex, four  $\text{PF}_6$  anions and 32 different positions of disordered water molecules. In one of the complex molecules a hydrogen atom corresponding to a hydroxide was localized. In the rest of the complex molecules hydroxides could not be localized. In one of the cases the presence on a hydroxide is not possible since there is no space for it (Figure S12).



**Figure 1.** Ortep plots (ellipsoid at 30% probability) X-Ray structure of the  $1^+$  (a) and  $2^+$  (b) together with labeling scheme.

Ru dinuclear complexes containing the pyridazine-3,6-dicarboxylic acid ligand

**Table 1.** Crystal Data for compounds **1<sup>+</sup>** and **2<sup>+</sup>**.

	<b>1<sup>+</sup></b>		<b>2<sup>+</sup></b>	
Empirical formula	C <sub>36</sub> H <sub>38</sub> ClF <sub>6</sub> N <sub>8</sub> O <sub>11</sub> PRu <sub>2</sub>		C <sub>144</sub> H <sub>97</sub> F <sub>24</sub> N <sub>32</sub> O <sub>20</sub> P <sub>4</sub> Ru <sub>8</sub>	
Formula weight	1141.30		3983.98	
Temperature	296(2)K		100(2)K	
Wavelength	0.71073 Å		0.71073 Å	
Crystal system	Triclinic		Monoclinic	
Space group	P-1		P2(1)n	
Unit cell dimensions	a = 13.292(11) Å	α = 72.08(2)°	a = 16.0198(19) Å	α = 90.00°
	b = 13.351(13) Å	β = 68.04(2)°	b = 34.255(5) Å	β = 97.256(4)°
	c = 14.855(14) Å	γ = 60.72(2)°	c = 30.625(4) Å	γ = 90.00°
Volume	2107(3) Å <sup>3</sup>		16671(4) Å <sup>3</sup>	
Z	2		4	
Density (calculated)	1.799 Mg/m <sup>3</sup>		1.587 Mg/m <sup>3</sup>	
Absorption coefficient	0.914 mm <sup>-1</sup>		0.840 mm <sup>-1</sup>	
F(000)	1144		7892	
Crystal size	0.06 x 0.04 x 0.02 mm <sup>3</sup>		0.2 x 0.1 x 0.02 mm <sup>3</sup>	
Theta range for data collection	1.50 to 25.40 °.		1.34 to 25.15 °.	
Index ranges	-15 <=h<=15, -15 <=k<=16, -17 <=l<=17		-19 <=h<=15, -40 <=k<=25, -32 <=l<=36	
Reflections collected	20779		62722	
Independent reflections	7231 [R(int) = 0.0961 ]		26196 [R(int) = 0.0844 ]	
Completeness to theta =25.40 °	0.933 %		0.878 %	
Absorption correction	Empirical		Empirical	
Max. and min. transmission	0.98 and 0.81		1.00 and 0.92	
Refinement method	Full-matrix least-squares on F <sup>2</sup>		Full-matrix least-squares on F <sup>2</sup>	
Data / restraints / parameters	7231 / 21 / 628		26196 / 216 / 2106	
Goodness-of-fit on F <sup>2</sup>	0.978		0.950	
Final R indices [I>2sigma(I)]	R1 = 0.0471, wR2 = 0.0989		R1 = 0.0787, wR2 = 0.1937	
R indices (all data)	R1 = 0.0936, wR2 = 0.1159		R1 = 0.1552, wR2 = 0.2174	
Largest diff. peak and hole	1.064 and -0.877 e.Å <sup>-3</sup>		1.067 and -0.876 e.Å <sup>-3</sup>	

**Table 2.** Selected metric parameters for complex **1<sup>+</sup>**.

Selected bond (Å)		Selected Angle (°)	
Ru(1)-N(1)	2.067(6)	N(4)-Ru(1)-Cl(1)	95.28(16)
Ru(1)-N(2)	1.976(5)	N(2)-Ru(1)-N(4)	174.40(2)
Ru(1)-N(3)	2.060(6)	O(1)-Ru(1)-Cl(1)	173.74(12)
Ru(1)-N(4)	2.032(5)	N(1)-Ru(1)-N(3)	158.28(19)
Ru(1)-O(1)	2.077(4)	Ru(1)-N(4)-N(5)-Ru(2) <sup>a</sup>	-7.1(6)
Ru(1)-Cl(1)	2.357(2)		

<sup>a</sup> Torsion angle that involves the two N atoms belonging to the pyridazinedicarboxylate-bridged group and the two metal centers.

**Table 3.** Selected metric parameters for complex **2<sup>+</sup>**.

Selected bond (Å)		Selected Angle (°)	
Ru(1A)-N(6A)	2.037(9)	N(1A)-Ru(1A)-O(5A)	93.7(3)
Ru(1A)-N(7A)	1.952(8)	N(7A)-Ru(1A)-N(1A)	79.3(4)
Ru(1A)-N(8A)	2.071(9)	O(1A)-Ru(1A)-O(5A)	170.5(2)
Ru(1A)-N(1A)	1.985(7)	N(6A)-Ru(1A)-N(8A)	157.6(3)
Ru(1A)-O(1A)	2.074(6)	Ru(1A)-N(1A)-N(2A)-Ru(2A) <sup>a</sup>	-3.5(10)
Ru(1A)-O(5A)	2.080(6)		

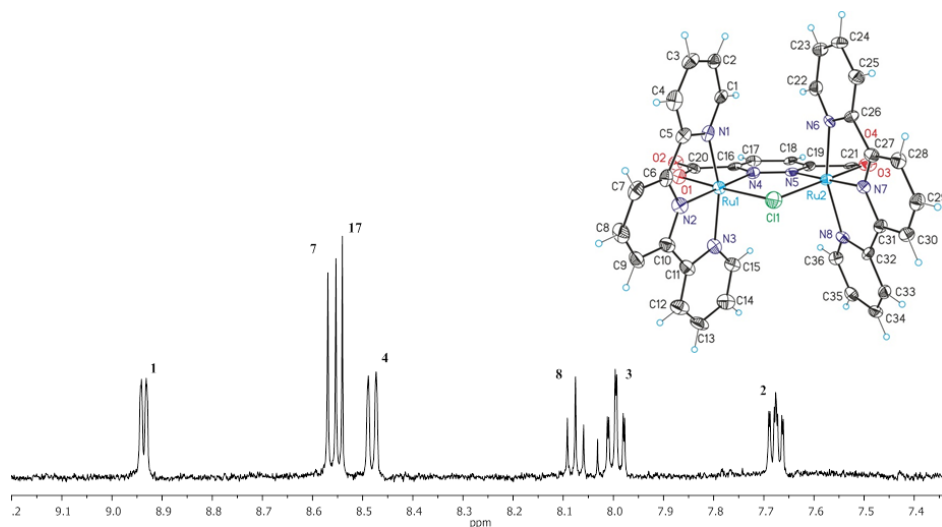
<sup>a</sup> Torsion angle that involves the two N atoms belonging to the pyridazinedicarboxylate-bridged group and the two metal centers.



## Ru dinuclear complexes containing the pyridazine-3,6-dicarboxylic acid ligand

### NMR Spectroscopic properties

1D and 2D NMR spectroscopy for complexes  $\mathbf{1}^+$  and  $\mathbf{2}^+$  was carried out in acetone- $d_6$ . The  $^1\text{H}$ -NMR spectra are displayed in Figure 2 and Figure 3 whereas the rest of the spectra are presented as Supporting Information. All the resonances displayed could be unambiguously assigned based on their multiplicity integrals and thanks to the 2D spectra. For the chlorido bridging complex  $\mathbf{1}^+$  the spectrum obtained is consistent as if  $\mathbf{1}^+$  had  $C_{2v}$  symmetry, due to fast interconversion of conformomers at room temperature<sup>108,109</sup>. As can be observed in the spectrum in solution  $\mathbf{2}^+$  behaves as having  $C_{2v}$  symmetry as is the case in the solid state.



**Figure 2.**  $^1\text{H}$ -NMR spectra of  $\mathbf{1}^+$  (500 MHz, 298 K, acetone- $d_6$ ).

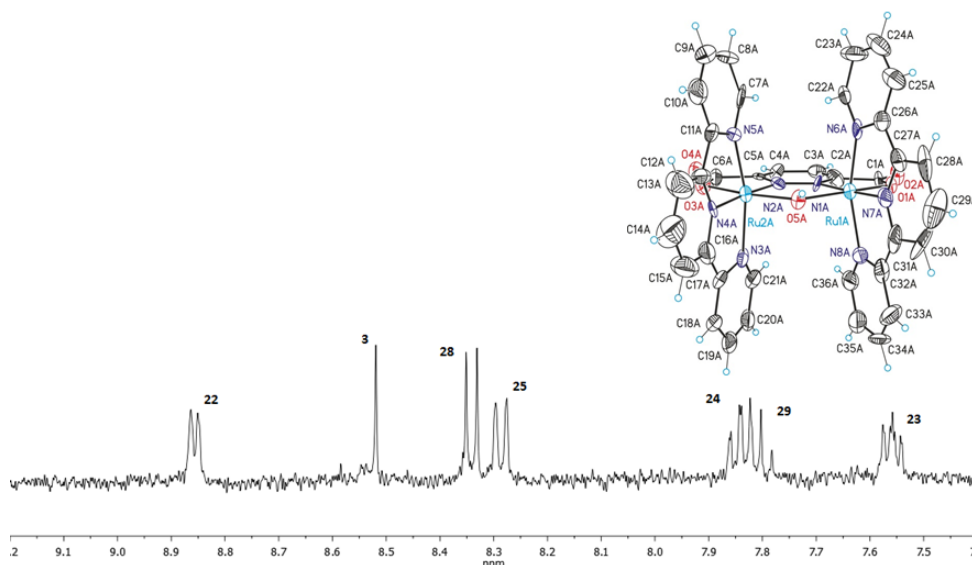
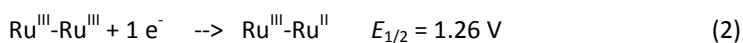
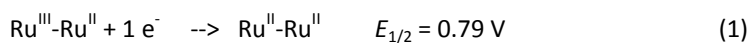


Figure 3.  $^1\text{H-NMR}$  spectra of  $\mathbf{2}^+$  (400 MHz, 298 K, acetone- $d_6$ ).

### Redox properties and electrocatalytically active species.

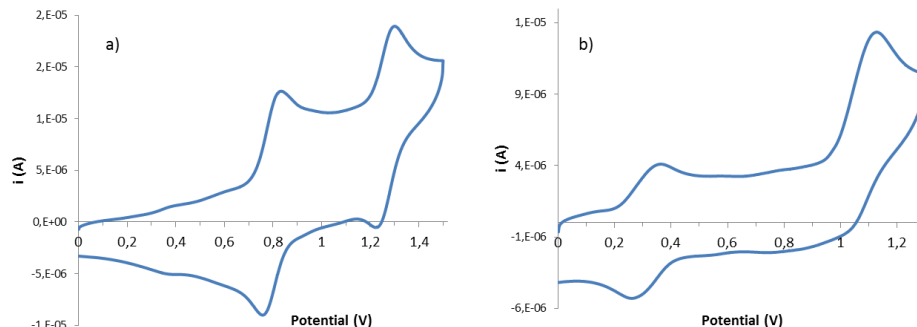
The redox properties of the complexes described were investigated by means of CV and DPV. The CV of  $\mathbf{1}^+$  and  $\mathbf{2}^+$  in MeCN (0.1 M TBAH) at 100 mV/s scan rate vs. SSCE are exhibited in Figure 4. As can be observed in the figure complex  $\mathbf{1}^+$  presents two chemically reversible redox waves at  $E_{1/2} = 0.79$  V ( $\Delta E_p = 57$  mV) and at  $E_{1/2} = 1.26$  V ( $\Delta E_p = 55$  mV) that are assigned to the following one electron processes,



CV of  $\mathbf{2}^+$  in MeCN shows a reversible wave at  $E_{1/2} = 0.31$  V ( $\Delta E_p = 110$  mV) and a chemically irreversible wave at  $E_{1/2} = 1.05$  V as can be observed in Figure 4. The  $\Delta E_{1/2}$ , defined as  $E_{1/2}^{\text{III,III}} - E_{1/2}^{\text{III,II}}$ , is 740 mV for  $\mathbf{2}^+$  and 530 mV for  $\mathbf{1}^+$  that under comparable conditions and is indicative of a stronger electronic coupling between the metal centers for  $\mathbf{2}^+$  with regard to  $\mathbf{1}^+$ . This is in agreement with a

## Ru dinuclear complexes containing the pyridazine-3,6-dicarboxylic acid ligand

much stronger magnetic coupling obtained for related dinuclear Cu complexes bridged by hydroxido units with regard to similar ones bridged by chlorido ligands<sup>110-115</sup>.

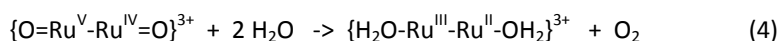
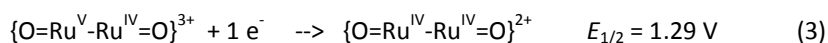


**Figure 4.** Cyclic voltammograms of  $1^+$  (a) and  $2^+$  (b) in MeCN (0.1 mM TBAH).

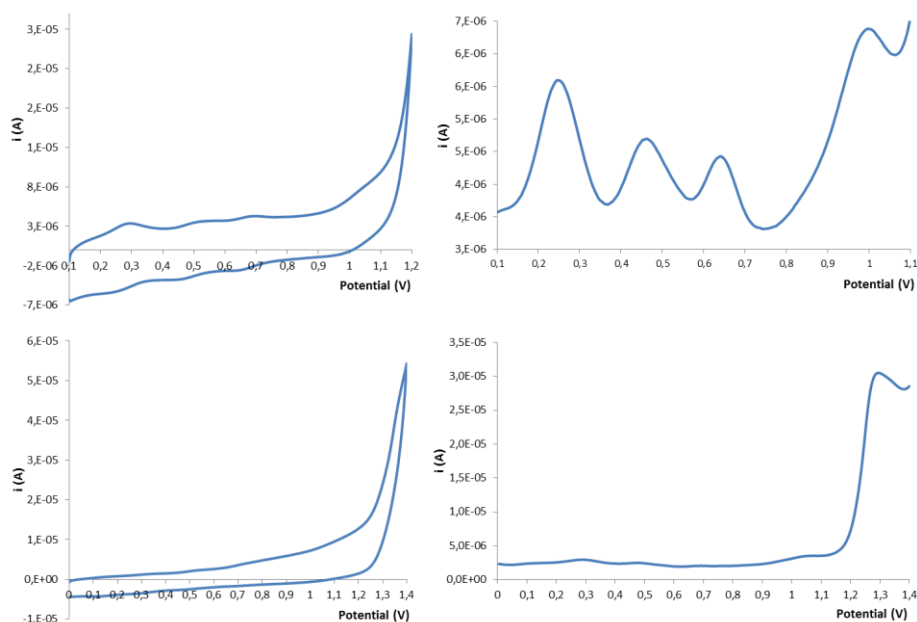
The electrochemistry of  $3^{2+}$  has been investigated at pH = 1.0 in 0.1 M triflic acid aqueous solution using  $2^+$  as a precursor (Scheme 2) and its CV and DPV are presented in Figure 5. As it can be observed four redox processes are obtained within the potential range of 0 to 1.10 V, that are tentatively assigned to the redox couples shown in Table 4, based on related complexes previously described in the literature<sup>81</sup>.

As it can be seen in the table, in this case a cathodic shift is observed as expected when comparing the potentials of  $3^{2+}$  with regard to those of the related Hbpp complex  $\{[Ru^{II}(trpy)(H_2O)]_2(\mu\text{-bpp})\}^{3+}$ . When the potential is increased further to 1.4 V a large anodic current is observed in the CV that is associated with a further one electron oxidation of the complex concomitant with the electrocatalytic oxidation of water to dioxygen in agreement with equations 3 and 4 (the trpy and dcpd<sup>2-</sup> ligands are not shown).

## Ru dinuclear complexes containing the pyridazine-3,6-dicarboxylic acid ligand



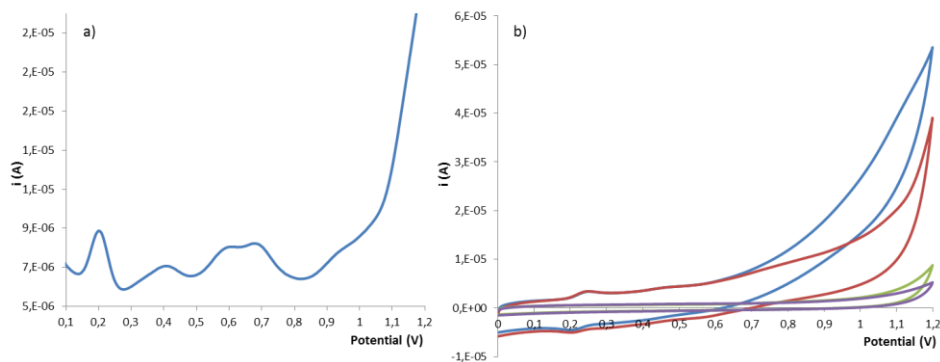
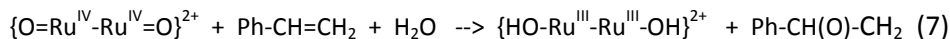
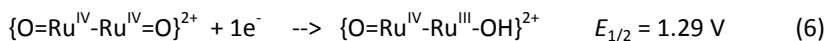
The redox potential for the  $Ru^{V,IV}-Ru^{IV,IV}$  couple is extracted from the DPV shown in Figure 5.



**Figure 5.** CV (left) and DPV (right) at different potential range for  $3^{2+}$  at pH = 1.0 in 0.1 M triflic acid aqueous solution.

The CV of  $3^{2+}$  was also carried out at pH = 7.0 and is shown in Figure 6. The redox potentials extracted from CV and DPV are displayed in Table 4 together with those of complex  $\{[Ru^{II}(trpy)(H_2O)]_2(\mu-bpp)\}^{3+}$  for comparison purposes. The CV of  $3^{2+}$  was also run in the presence of styrene and an increase of current intensity is observed at approximately 0.75 V that is consistent with an electrocatalytic oxidation of styrene to styrene oxide according to the following equations,

Ru dinuclear complexes containing the pyridazine-3,6-dicarboxylic acid ligand



**Figure 6.** (a) DPV of  $3^{+}$  in pH 7 phosphate buffer. (b) CV of  $3^{2+}$  (1 mM) in pH 7 phosphate buffer (red line) and of  $3^{2+}$  (1 mM) in the presence of styrene (60 mM, blue line). Cyclic voltammogram of styrene (60 mM, green line) and blank (purple line).

Lastly addition of MeCN to a solution of  $3^{2+}$  in triflic acid resulted in the formation of new species with two main reversible waves at  $E_{1/2} = 0.294 \text{ V}$  and  $0.484 \text{ V}$  assigned to the formation of a bis-MeCN species,  $4^{2+}$ . (Figure SI16).

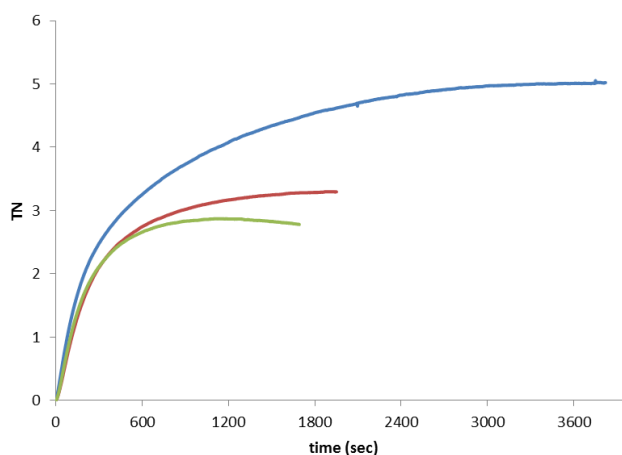
**Table 4.** Redox potentials in V (vs. SSCE) for  $3^{2+}$  and  $\{[Ru^{II}(trpy)(H_2O)]_2(\mu-bpp)\}^{3+}$  at pH = 1.0 and at pH = 7.0<sup>a</sup>

Complex	$E_{1/2}$				
	pH	III,II-II,II	III,III-III,II	IV,III-III,III	IV,IV-IV,III <sup>b</sup>
$\{[Ru^{II}(trpy)(H_2O)]_2(\mu-bpp)\}^{3+}$	1.0	0.59	0.65	0.88	1.10
	7.0	0.28	0.52	--	--
$\{[Ru^{II}(trpy)(H_2O)]_2(\mu-dcpd)\}^{2+}, 3^{2+}$	1.0	0.25	0.46	0.64	1.00
	7.0	0.21	0.40 <sup>b</sup>	0.58 <sup>b</sup>	0.66 <sup>b</sup>

<sup>a</sup>pH = 1.0 triflic acid 0.1 M; pH = 7.0 phosphate buffer 0.1 M. <sup>b</sup> $E_{p,a}$

### Catalysis of water oxidation

Oxygen evolution can be observed in a 0.1 M triflic acid solution containing  $(\text{NH}_4)_2\text{Ce}^{\text{IV}}(\text{NO}_3)_6$  and  $\mathbf{3}^{2+}$  in an airtight degassed cell. Addition of a 25 to 100-fold molar excess of  $\text{Ce}^{\text{IV}}$  to 0.94 mM solution of  $\mathbf{3}^{2+}$  in triflic acid resulted in an immediate release of  $\text{O}_2$  (Figure 7) confirmed by on-line mass detection of evolved gas (Figure SI17). In the presence of 100 equivalents of oxidant 5 TN of oxygen were produced after 1 h reaction corresponding to an efficiency of the 20 % (respect to the oxygen expected based on the amount of  $\text{Ce}^{\text{IV}}$  added). The efficiency increased at lower amounts of oxidant, 29% when 50 equivalents of  $\text{Ce}^{\text{IV}}$  are mixed with  $\mathbf{3}^{2+}$  and 44.5% in the presence of 25 eqs of  $\text{Ce}^{\text{IV}}$  (Figure 7 red and green line). Blank experiments carried out in a similar manner did not generate any molecule of oxygen. The moderate activity in terms of turnover number and the results at different concentration of oxidant point at some potential deactivation processes that can involve the degradation of  $\mathbf{3}^{2+}$  via intermolecular pathways or by the same  $\text{Ce}^{\text{IV}}$ .

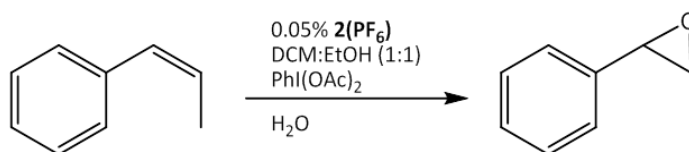


**Figure 7.** Gas evolution measured with a manometer from the reaction of 0.94 mM  $\mathbf{3}^{2+}$  and 24  $\mu\text{M}$  (green line), 47  $\mu\text{M}$  (red line), and 94  $\mu\text{M}$  (blue line)  $(\text{NH}_4)_2\text{Ce}^{\text{IV}}(\text{NO}_3)_6$  at pH = 1.0 in 0.1 M triflic acid solution.

## Ru dinuclear complexes containing the pyridazine-3,6-dicarboxylic acid ligand

### Olefins Epoxidation

The reactivity of  $3^{2+}$  towards epoxidation was initially studied for the oxidation of *cis*- $\beta$ -methylstyrene (Scheme 3), being this substrate useful for extraction information about the mechanism pathways. The reaction was performed in a mixture of dichloromethane:ethanol (1:1), using (diacetoxyiodo)benzene as terminal oxidant. A concentration of 1 mM of catalyst and a relation of cat:sub:ox of 1:2000:4000 was used. A 4000-fold excess of water, that is needed to generate PhIO from PhIOAc<sub>2</sub><sup>116</sup> and to transform precursor  $2^+$  into catalyst  $3^{2+}$  as described in previous sections, was added after stirring the mixture for 30 min. This time has been found to be essential for triggering the catalysis.



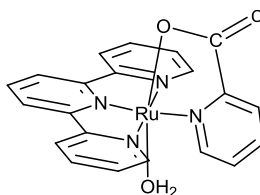
**Scheme 3.** Epoxidation of *cis*- $\beta$ -methylstyrene.

The corresponding *cis*-epoxide (1-phenyl-propyleneoxide) was detected as the major product, with no formation of the *trans*-epoxide. 92 % of substrate was converted after 210 min of reaction, at the same time 62 % of epoxide was generated corresponding to a selectivity of 67%. After 22 h of reaction no further oxidation of the epoxide was detected (Figure 9a).

The catalytic activity has been compared with the analogous mononuclear complex [Ru(trpy)(pic)(H<sub>2</sub>O)]<sup>+</sup>,  $5^+$ , (where pic is picolate anion or pyridine-2-carboxylate) represented in Figure 8. This catalyst has been described to catalyzed the epoxidation of *cis*- $\beta$ -methylstyrene in a relation cat:sub:ox:water of 1:100:200:200<sup>117</sup>. Under identical catalytic conditions the epoxidation of *cis*- $\beta$ -methylstyrene catalyzed by  $3^{2+}$  proceed with similar yield but with an

## Ru dinuclear complexes containing the pyridazine-3,6-dicarboxylic acid ligand

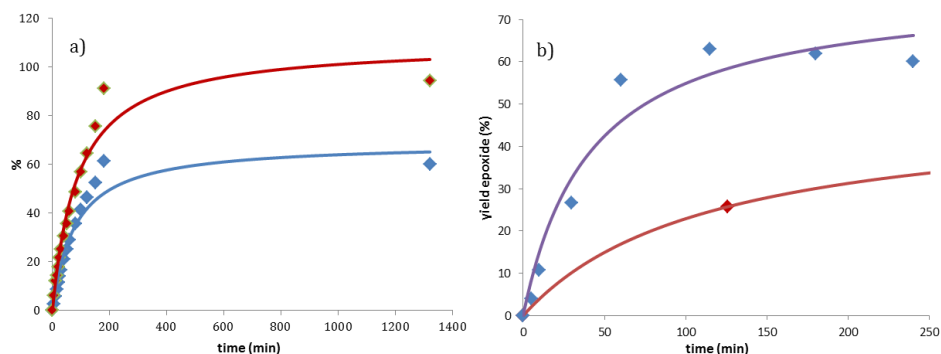
enhanced catalytic rate (Figure 9b). After 2 hours of reaction the system based on the dinuclear complex  $3^{2+}$  showed a conversion of more than 72 % with a yield of epoxide corresponding to 63 %; at the same time the yield of epoxide for the system with mononuclear catalyst  $5^+$  was almost 26 %. The maximum yield of 65 for the mononuclear system has been reached after more than 25 hours of reaction. In the case of the reaction catalyzed by  $3^{2+}$  a slight decrease in the yield of epoxide has been detected when the conversion exceeded the 86%, probably due to a ring opening reaction catalyzed by  $3^{2+}$  or independent decomposition of the product, the nature of this reaction was not further investigated because not present under optimized reaction conditions . Final conversion of 100% and yield of epoxide of 52% resulted after 5 h of reaction. The fact that  $3^{2+}$  is about 5 times faster than its mononuclear homologue  $5^+$  suggests a cooperation effect between the two metal centers. Given that the simultaneous oxidation of two molecule of alkene on each  $Ru^{IV}=O$  sites results highly unlikely, cause the steric hindrance that would take place around the metal centers, a one site approach result the most plausible mechanism for the catalysis. However the non-innocent role of the adjacent  $Ru^{IV}=O$  is valid hypothesis for explaining the high catalytic activity of  $3^{2+}$  in respect to complex  $5^+$ . Potentially one of the  $Ru=O$  groups generates a hydrogen bonding with the alkene, fixing the substrate, while the other  $Ru=O$  group can be responsible for the oxygen atom transfer.



**Figure 8.** Structure of  $[Ru(trpy)(pic)(H_2O)]^+$ ,  $5^+$ .



## Ru dinuclear complexes containing the pyridazine-3,6-dicarboxylic acid ligand

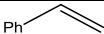
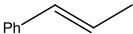
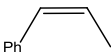
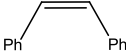
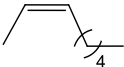
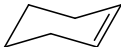


**Figure 9.** (a) Conversion of the *cis*-alkene (red) and formation of *cis*-epoxide (blue); reaction conditions: **2(PF<sub>6</sub>)** (1.4 mg;  $1,31 \cdot 10^{-3}$  mmol; final concentration = 1 mM) in dichloromethane/ethanol (1:1, 1 mL), *cis*- $\beta$ -methylstyrene (340  $\mu$ L; 2.62 mmol; final concentration = 2 M), PhI(OAc)<sub>2</sub> (1,69 g; 5,25 mmol; final concentration = 4 M), H<sub>2</sub>O (94  $\mu$ L, 5.23 mmol; final concentration = 4 M), dodecane (50  $\mu$ L; 0.22 mmol; final concentration = 165 mM); final volume  $\approx$ 1.33 mL. (b) evolution of *cis*-epoxide catalyzed by **2(PF<sub>6</sub>)** (blue) and by **5(PF<sub>6</sub>)** (red); reaction conditions: catalyst (2.8 mg **2(PF<sub>6</sub>)** or 1.5 mg of **5(PF<sub>6</sub>)**;  $2,62 \cdot 10^{-3}$  mmol; final concentration = 2.5 mM) in dichloromethane (1 mL), *cis*- $\beta$ -methylstyrene (34  $\mu$ L; 0.26 mmol; final concentration = 0.25 M), PhI(OAc)<sub>2</sub> (169 mg; 0.52 mmol; final concentration = 0.5 M), H<sub>2</sub>O (9.5  $\mu$ L, 0.52 mmol; final concentration = 0.5 M), dodecane (10  $\mu$ L; 0.044 mmol; final concentration = 42 mM), final volume  $\approx$ 1.05 mL.

The reactivity of **3<sup>2+</sup>** was further investigated with regards to the epoxidation of different alkenes. An example of linear, cyclic, sterically hindered, and *trans*-isomer has been tested. Catalytic data are reported in Table 5. A first general glance at the table shows that **3<sup>2+</sup>** is very powerful catalyst for the epoxidation reaction of alkenes and that with electron-donor groups the catalyst performs much better than with electron-withdrawers. Thus *cis*-octene and cyclohexene (Entries 5 and 6) resulted the best substrates whereas *cis*-stilbene (Entry 4) the worst. The latter also suffers from potential steric effects due to the bulkiness

of the two phenyl rings. These electronic effects are in agreement with an electrophilic character of the  $\text{Ru}^{\text{IV}}=\text{O}$  active group proposed in the electrochemical section.

**Table 5.** Catalytic performance of  $\mathbf{3}^{2+}$  for the epoxidation of several alkenes using

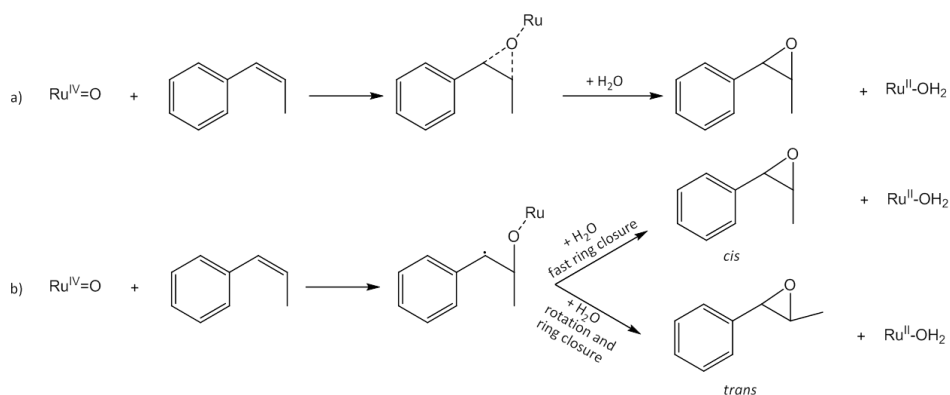
Entry	Alkene	Substrate	Conversion (%) <sup>b</sup>	[Epoxide], M; (Selectivity %) <sup>c</sup>	TN/TOF <sub>i</sub> <sup>d</sup>
1	Styrene		87	0.88 (51)	880/0.288
2	<i>trans</i> - $\beta$ -methylstyrene		93	1.47 (79) <sup>e</sup>	1470/0.261
3	<i>cis</i> - $\beta$ -methylstyrene		92	1.32 (72) <sup>f</sup>	1320/0.275
4	<i>cis</i> -stilbene		44	0.32 (36) <sup>f</sup>	320/0.007
5	<i>cis</i> -2-octene		99	1.54 (78) <sup>f</sup>	1540/0.164
6	Cyclohexene		100	1.58 (79)	1580/0.676

$\text{PhI}(\text{AcO})_2$  as oxidant in  $\text{CH}_2\text{Cl}_2:\text{EtOH}$  1:1 (Cat:Subs:Ox. 1:2000:4000).<sup>a</sup>

<sup>a</sup>Reaction conditions:  $\mathbf{2}(\text{PF}_6)$  (1.4 mg;  $1,31 \cdot 10^{-3}$  mmol; final concentration = 1 mM) in dichloromethane/ethanol (1:1, 1 mL), substrate (2.62 mmol; final concentration = 2 M),  $\text{PhI}(\text{OAc})_2$  (1.69 g; 5,25 mmol; final concentration = 4 M),  $\text{H}_2\text{O}$  (94  $\mu\text{L}$ , 5.23 mmol; final concentration = 4 M), dodecane (50  $\mu\text{L}$ ; 0.22 mmol; final concentration = 165 mM); final volume  $\approx 1.33$  mL. <sup>b</sup>Substrate conversion =  $\frac{[\text{substrate}]_{\text{initial}} - [\text{substrate}]_{\text{final}}}{[\text{substrate}]_{\text{initial}}} \cdot 100$ . <sup>c</sup>Epoxide selectivity =  $\frac{[\text{epoxide}]_{\text{final}}}{([\text{substrate}]_{\text{initial}} - [\text{substrate}]_{\text{final}})} \cdot 100$ . <sup>d</sup>TN is the turnover number with regard to epoxide. TOF<sub>i</sub> is the initial turnover frequency expressed in epoxide cycles per second. <sup>e</sup>100% of *trans*-epoxide. <sup>f</sup>100% of *cis*-epoxide.

## Ru dinuclear complexes containing the pyridazine-3,6-dicarboxylic acid ligand

Another interesting feature of the systems studied here are the stereospecific nature of the catalysis performed in the sense that no *cis/trans* isomerization takes place for the *cis*-alkenes (Entries 3-5). This points towards a mechanism that either a concerted oxygen atom transfer from the Ru<sup>IV</sup>=O active site to the double bond of the alkene or a radical path were the C-C rotation of the generated radical is much slower than the ring closing that generates the final epoxide<sup>118-122</sup> (Scheme 4).

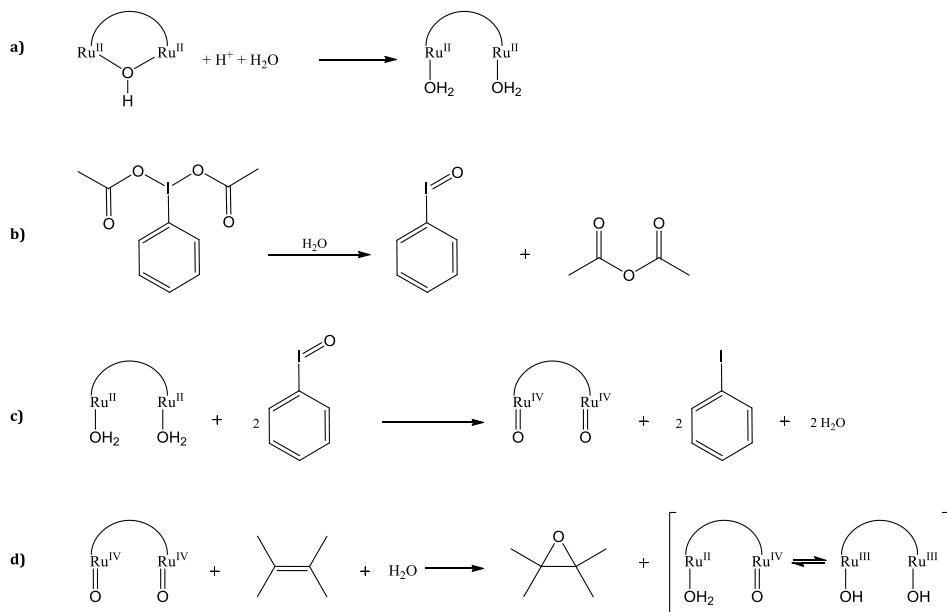


**Scheme 4.** Proposed reaction pathway for the epoxidation of *cis*- $\beta$ -methylstyrene by Ru<sup>IV</sup>=O.

### III. iv. Conclusions

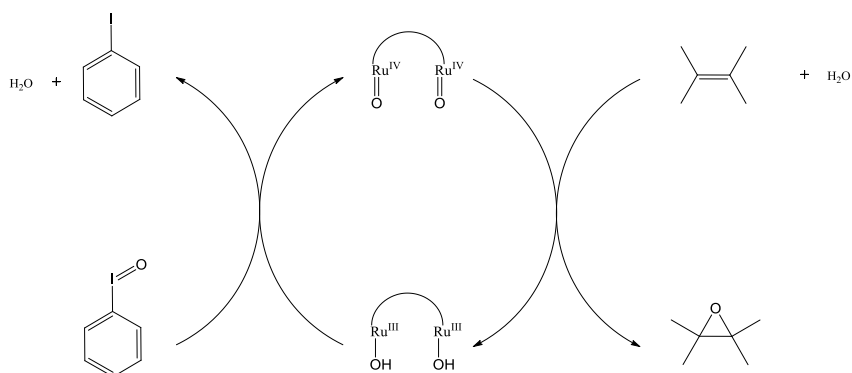
Two new Ru dinuclear complexes **1**<sup>+</sup> and **2**<sup>+</sup> containing the bridging ligand pyridazine-3,6-dicarboxylic acid have been synthesized and fully characterized, both in the solid state and in solution. From electrochemical study it was demonstrated that **2**<sup>+</sup> undergoes in aqueous media into *in situ* formation of a bis-aqua complex **3**<sup>2+</sup>. The latter has been proven to be an active catalyst both towards oxidation of water and epoxidation of different olefins. It is interesting to compare the rate of the epoxidation reactions with **3** with that of the mononuclear [Ru(trpy)(pic)(OH<sub>2</sub>)]<sup>+</sup>, **5**<sup>+</sup>, which results ≈12 times slower under similar conditions. The higher activity of the dinuclear species respect to the analogous mononuclear compound can be attributed to a supramolecular interaction via hydrogen bond between the hydrogen in β to the double bond of the alkene with the O atom of the adjacent metal centre. The higher selectivity of **3**<sup>2+</sup> for the formation of *cis*-epoxide and *trans*-epoxide from the relative *cis* and *trans* alkenes point at a concerted mechanism via direct oxene insertion. The presence of water resulted necessary for the catalytic process. According to previously proposed mechanisms its role consists in a) generate the initial Ru bis-aqua species b) generate the oxidant species iodosyl benzene from the starting (diacetoxyiodo)benzene (Scheme 5 *a* and *b*). Once formed, the iodosyl benzene is then supposed to oxidized the Ru(II,II) bis-aqua species to the Ru(IV,IV) bis-oxo compound, active species in the oxidation of alkenes (Scheme 5 *c* and *d*).

Ru dinuclear complexes containing the pyridazine-3,6-dicarboxylic acid ligand



**Scheme 5.** Independent stoichiometric reaction steps of the for epoxidation of alkenes catalyzed by  $2^+$  in the presence of an excess of  $\text{PhI}(\text{OAc})_2$  and water.

Considering the reaction described above the catalytic cycle proposed for the epoxidation of alkenes catalyzed by  $3^{2+}$  is showed in Scheme 6.



**Scheme 6.** Proposed global catalytic reaction paths the for epoxidation of alkenes catalyzed by  $3^{2+}$  in the presence of an excess of  $\text{PhI}(\text{OAc})_2$  and water.

### III. v. Associated content

#### Supportin Information

X-Ray crystallographic data in CIF format, additional spectroscopic and electrochemical data.

### III. vi. References

- (1) Baranoff, E.; Collin, J.-P.; Furusho, J.; Furusho, Y.; Laemmel, A.-C.; Sauvage, J.-P. *Inorg. Chem.* **2002**, *41*, 1215.
- (2) Kelley, S. O.; Barton, J. K. *Science* **1999**, *283*, 375.
- (3) Schuster, G. B. *Acc. Chem. Res.* **2000**, *33*, 253.
- (4) Venturi, M.; Balzani, V.; Ballardini, R.; Credi, A.; Gandolfi, M. T. *Int. J. Photoenergy* **2004**, *6*, 1.
- (5) Weatherly, S. C.; Yang, I. V.; Thorp, H. H. *J. Am. Chem. Soc.* **2001**, *123*, 1236.
- (6) Brennaman, M. K.; Alstrum-Acevedo, J. H.; Fleming, C. N.; Jang, P.; Meyer, T. J.; Papanikolas, J. M. *J. Am. Chem. Soc.* **2002**, *124*, 15094.
- (7) Sauvage, J. P.; Collin, J. P.; Chambron, J. C.; Guillerez, S.; Coudret, C.; Balzani, V.; Barigelletti, F.; De, C. L.; Flamigni, L. *Chem. Rev.* **1994**, *94*, 993.
- (8) Scandola, V. B. F. *Supramol. Chem.*, **1991**.
- (9) Friedman, A. E.; Chambron, J. C.; Sauvage, J. P.; Turro, N. J.; Barton, J. K. *J. Am. Chem. Soc.* **1990**, *112*, 4960.
- (10) Holmlin, R. E.; Stemp, E. D. A.; Barton, J. K. *Inorg. Chem.* **1998**, *37*, 29.
- (11) Jenkins, Y.; Friedman, A. E.; Turro, N. J.; Barton, J. K. *Biochemistry* **1992**, *31*, 10809.
- (12) Li, L.; Szmecinski, H.; Lakowicz, J. R. *Biospectroscopy* **1997**, *3*, 155.
- (13) Li, L.; Szmecinski, H.; Lakowicz, J. R. *Anal. Biochem.* **1997**, *244*, 80.
- (14) Murtaza, Z.; Chang, Q.; Rao, G.; Lin, H.; Lakowicz, J. R. *Anal. Biochem.* **1997**, *247*, 216.
- (15) Santos, T. M.; Madureira, J.; Goodfellow, B. J.; Drew, M. G. B.; Pedrosa, d. J. J.; Felix, V. *Met.-Based Drugs* **2001**, *8*, 125.
- (16) Terpetschnig, E.; Szmecinski, H.; Lakowicz, J. R. *Anal. Biochem.* **1995**, *227*, 140.
- (17) Youn, H. J.; Terpetschnig, E.; Szmecinski, H.; Lakowicz, J. R. *Anal. Biochem.* **1995**, *232*, 24.
- (18) Balzani, V.; Credi, A.; Raymo, F. M.; Stoddart, J. F. *Angew. Chem., Int. Ed.* **2000**, *39*, 3348.

## Ru dinuclear complexes containing the pyridazine-3,6-dicarboxylic acid ligand

- (19) Balzani, V.; Gomez-Lopez, M.; Stoddart, J. F. *Acc. Chem. Res.* **1998**, *31*, 405.
- (20) Collin, J.-P.; Dietrich-Buchecker, C.; Gavina, P.; Jimenez-Molero, M. C.; Sauvage, J.-P. *Acc. Chem. Res.* **2001**, *34*, 477.
- (21) Sauvage, J.-P. *Acc. Chem. Res.* **1998**, *31*, 611.
- (22) Gratzel, M. *Inorg. Chem.* **2005**, *44*, 6841.
- (23) Saito, Y.; Azechi, T.; Kitamura, T.; Hasegawa, Y.; Wada, Y.; Yanagida, S. *Coord. Chem. Rev.* **2004**, *248*, 1469.
- (24) Gratzel, M. *Nature* **2001**, *414*, 338.
- (25) Greenwood, N. N.; Earnshaw, A. *Chemistry of Elements*; VCH Verlagsgesellschaft, **1988**.
- (26) Laurent, F.; Plantalech, E.; Donnadiou, B.; Jimenez, A.; Hernandez, F.; Martinez-Ripoll, M.; Biner, M.; Llobet, A. *Polyhedron* **1999**, *18*, 3321.
- (27) Llobet, A. *Inorg. Chim. Acta* **1994**, *221*, 125.
- (28) Masllorens, E.; Rodriguez, M.; Romero, I.; Roglans, A.; Parella, T.; Benet-Buchholz, J.; Poyatos, M.; Llobet, A. *J. Am. Chem. Soc.* **2006**, *128*, 5306.
- (29) Mola, J.; Rodriguez, M.; Romero, I.; Llobet, A.; Parella, T.; Poater, A.; Duran, M.; Sola, M.; Benet-Buchholz, J. *Inorg. Chem.* **2006**, *45*, 10520.
- (30) Mola, J.; Romero, I.; Rodriguez, M.; Bozoglian, F.; Poater, A.; Sola, M.; Parella, T.; Benet-Buchholz, J.; Fontrodona, X.; Llobet, A. *Inorg. Chem.* **2007**, *46*, 10707.
- (31) Sens, C.; Rodriguez, M.; Romero, I.; Llobet, A.; Parella, T.; Benet-Buchholz, J. *Inorg. Chem.* **2003**, *42*, 8385.
- (32) Serrano, I.; Sala, X.; Plantalech, E.; Rodriguez, M.; Romero, I.; Jansat, S.; Gomez, M.; Parella, T.; Stoeckli-Evans, H.; Solans, X.; Font-Bardia, M.; Vidjayacoumar, B.; Llobet, A. *Inorg. Chem.* **2007**, *46*, 5381.
- (33) Planas, N.; Ono, T.; Vaquer, L.; Miro, P.; Benet-Buchholz, J.; Gagliardi, L.; Cramer, C. J.; Llobet, A. *Phys. Chem. Chem. Phys.* **2011**, *13*, 19480.
- (34) Federsel, C.; Jackstell, R.; Beller, M. *Angew. Chem., Int. Ed.* **2010**, *49*, 6254.
- (35) Jessop, P. G. *Handbook Homogeneous Hydrogenation* **2007**, *1*, 489.
- (36) Jessop P. G., Joo F., Tai C. C. *Coord. Chem. Rev.* **2004**, *248*, 2425.
- (37) Leitner, W. *J. Am. Chem. Soc.* **1997**, *119*, 4432.
- (38) Leitner, W.; Gassner, F. *J. Chem. Soc., Chem. Commun.* **1993**, 1465.
- (39) Angermund, K.; Baumann, W.; Dinjus, E.; Fornika, R.; Gorgs, H.; Kessler, M.; Kruger, C.; Leitner, W.; Lutz, F. *Chem.-Eur. J.* **1997**, *3*, 755.
- (40) Tanaka R., Yamashita, M.; Nozaki, K. *J. Am. Chem. Soc.* **2009**, *131*, 14168.

- (41) Ng, S. M.; Yin, C.; Yeung, C. H.; Chan, T. C.; Lau C. P. *Eur. J. Inorg. Chem.* **2004**, 2004, 1788.
- (42) Himeda, Y.; Onozawa-Komatsuzaki, N.; Sugihara, H.; Kasuga, K. *Organometallics* **2007**, 26, 702.
- (43) Jessop, P. G.; Hsiao, Y.; Ikariya, T.; Noyori, R. *J. Am. Chem. Soc.* **1996**, 118, 344.
- (44) Munshi, P.; Main, A.D.; Linehan, J. C.; Tai, C. C.; Jessop, P. G. *J. Am. Chem. Soc.* **2002**, 124, 7963.
- (45) Mashima, K.; Kusano, K.-h.; Sato, N.; Matsumura, Y.-i.; Nozaki, K.; Kumobayashi, H.; Sayo, N.; Hori, Y.; Ishizaki, T. *J. Org. Chem.* **1994**, 59, 3064.
- (46) Ohta, T.; Miyake, T.; Seido, N.; Kumobayashi, H.; Takaya, H. *J. Org. Chem.* **1995**, 60, 357.
- (47) Wabnitz, T. C.; Rizzo, S.; Goette, C.; Buschauer, A.; Benincori, T.; Reiser, O. *Tetrahedron Lett.* **2006**, 47, 3733.
- (48) Starodubtseva, E. V.; Vinogradov, M. G.; Pavlov, V. A.; Gorshkova, L. S.; Ferapontov, V. A. *Russ. Chem. Bull.* **2004**, 53, 2172.
- (49) Starodubtseva, E. V.; Turova, O. V.; Vinogradov, M. G.; Gorshkova, L. S.; Ferapontov, V. A. *Russ. Chem. Bull.* **2005**, 54, 2374.
- (50) Doherty, S.; Knight, J. G.; Bell, A. L.; Harrington, R. W.; Clegg, W. *Organometallics* **2007**, 26, 2465.
- (51) Bronze-Uhle, E. S.; Ines, d. S. M.; Donate, P. M.; Frederico, D. *J. Mol. Catal. A: Chem.* **2006**, 259, 103.
- (52) Daley, C. J. A.; Wiles, J. A.; Bergens, S. H. *Inorg. Chim. Acta* **2006**, 359, 2760.
- (53) Arai, N.; Azuma, K.; Nii, N.; Ohkuma, T. *Angew. Chem., Int. Ed.* **2008**, 47, 7457.
- (54) Keene, F. R. *Coord. Chem. Rev.* **1999**, 187, 121.
- (55) Wang, G. Z.; Andreasson, U.; Bäckvall, J. E. *J. Chem. Soc. Chem. Commun.* **1994**.
- (56) Csjernyik, G.; Ell, A.H.; Fadini, L.; Pugin, B.; Backvall, J. E. *J. Org. Chem.* **2002**, 67.
- (57) Bäckvall, J. E.; Chowdhury, R. L.; Karlsson, U. *J. Chem. Soc. Chem. Commun.* **1991**, 47.
- (58) Murahashi, S.-I.; Komiya, N.; Wiley-VCH Verlag GmbH & Co. KGaA: **2004**, p 165.
- (59) Murahashi, S.; Naota, T. *Adv. Met.-Org. Chem.* **1994**, 3, 225.
- (60) Friedrich, H. B. *Platinum Met. Rev.* **1999**, 43, 94.
- (61) Murahashi, S.; Naota, T. *Sekiyu Gakkaishi* **1991**, 34, 1.
- (62) Murahashi, S. I.; Naota, T. *Zh. Org. Khim.* **1996**, 32, 223.



## Ru dinuclear complexes containing the pyridazine-3,6-dicarboxylic acid ligand

- (63) Baeckvall, J.-E.; Editor *Modern Oxidation Methods, 2nd Completely Revised*; Wiley-VCH Verlag GmbH & Co. KGaA, **2010**.
- (64) Murahashi, S.-I.; Komiya, N. *Ruthenium in Organic Synthesis*; Wiley-VCH, Weinheim, **2004**.
- (65) Bhor, S.; Tse, M. K.; Klawonn, M.; Doebler, C.; Maegerlein, W.; Beller, M. *Adv. Synth. Catal.* **2004**, *346*, 263.
- (66) Porter, M. J.; Skidmore, J. *Chem. Commun.* **2000**, 1215.
- (67) Serrano, I.; López, M. I.; Ferrer, I. n.; Poater, A.; Parella, T.; Fontrodona, X.; Solà, M.; Llobet, A.; Rodríguez, M.; Romero, I. *Inorg. Chem.* **2011**, *50*, 6044.
- (68) Groves, J. T.; Quinn, R. *J. Am. Chem. Soc.* **1985**, *107*, 5790.
- (69) Bailey, C. L.; Drago, R. S. *J. Chem. Soc., Chem. Commun.* **1987**, 179.
- (70) Barf, G. A.; Sheldon, R. A. *J. Mol. Catal. A-Chem.* **1995**, *102*, 23.
- (71) Stultz, L. K.; Binstead, R. A.; Reynolds, M. S.; Meyer, T. J. *J. Am. Chem. Soc.* **1995**, *117*, 2520.
- (72) Arends, I. W. C. E.; Kodama, T.; Sheldon, R. A. *Top. Organomet. Chem.* **2004**, *11*, 277.
- (73) Młodnicka, T.; James, B. R. *Catal. Met. Complexes* **1994**, *17*, 121.
- (74) Benet-Buchholz, J.; Comba, P.; Llobet, A.; Roeser, S.; Vadivelu, P.; Wiesner, S. *Dalton Trans.* **2010**, *39*, 3315.
- (75) Hamelin, O.; Ménage, S. p.; Charnay, F.; Chavarot, M.; Pierre, J.-L.; Pécaut, J.; Fontecave, M. *Inorg. Chem.* **2008**, *47*, 6413.
- (76) Huynh, M. H. V.; Witham, L. M.; Lasker, J. M.; Wetzler, M.; Mort, B.; Jameson, D. L.; White, P. S.; Takeuchi, K. J. *J. Am. Chem. Soc.* **2003**, *125*, 308.
- (77) Gersten, S. W.; Samuels, G. J.; Meyer, T. J. *J. Am. Chem. Soc.* **1982**, *104*, 4029.
- (78) Gilbert, J. A.; Eggleston, D. S.; Murphy, W. R., Jr.; Geselowitz, D. A.; Gersten, S. W.; Hodgson, D. J.; Meyer, T. J. *J. Am. Chem. Soc.* **1985**, *107*, 3855.
- (79) Sala, X.; Romero, I.; Rodríguez, M.; Escriche, L.; Llobet, A. *Angew. Chem., Int. Ed.* **2009**, *48*, 2842.
- (80) Xu, Y.; Fischer, A.; Duan, L.; Tong, L.; Gabrielsson, E.; Aakermark, B.; Sun, L. *Angew. Chem., Int. Ed.* **2010**, *49*, 8934.
- (81) Sens, C.; Romero, I.; Rodríguez, M.; Llobet, A.; Parella, T.; Benet-Buchholz, J. *J. Am. Chem. Soc.* **2004**, *126*, 7798.
- (82) Tseng, H.-W.; Zong, R.; Muckerman, J. T.; Thummel, R. *Inorg. Chem.* **2008**, *47*, 11763.
- (83) Xu, Y.; Aakermark, T.; Gyollai, V.; Zou, D.; Eriksson, L.; Duan, L.; Zhang, R.; Aakermark, B.; Sun, L. *Inorg. Chem.* **2009**, *48*, 2717.

- (84) Zong, R.; Thummel, R. P. *J. Am. Chem. Soc.* **2005**, *127*, 12802.
- (85) Concepcion, J. J.; Jurss, J. W.; Templeton, J. L.; Meyer, T. J. *J. Am. Chem. Soc.* **2008**, *130*, 16462.
- (86) Duan, L.; Bozoglian, F.; Mandal, S.; Stewart, B.; Privalov, T.; Llobet, A.; Sun, L. *Nat Chem* **2012**, *4*, 418.
- (87) S. Sueur, M. L., F. Abraham *J. Heterocyclic Chem.* **1987**, *24*, 1285.
- (88) Sullivan, B. P.; Calvert, J. M.; Meyer, T. J. *Inorg. Chem.* **1980**, *19*, 1404.
- (89) Data collection with APEX II versions v1.0-22, Madison, Wisconsin, USA.
- (90) Data reduction with Bruker SAINT versions V.2.10(**2003**), Madison, Wisconsin, USA.
- (91) SADABS: V.2.10(**2003**); V2008 and V2008/1 Bruker (**2001**). Bruker AXS Inc., M., Wisconsin, USA. *Blessing Acta Cryst.* **1995**, *A51*, 33.
- (92) TWINABS Version 2008/4 Bruker AXS; *Blessing Acta Cryst.* **1995**, *A51*, 33.
- (93) Sheldrick, G. M. S. v. V. a. *Acta Cryst.* **2008**, *A64*, 112.
- (94) SQUEEZE implemented in Platon: Spek, A. L. *J. Appl. Cryst.* **2003**, *36*.
- (95) Romero, I.; Rodriguez, M.; Llobet, A.; Collomb-Dunand-Sauthier, M.-N.; Deronzier, A.; Parella, T.; Stoeckli-Evans, H. *Dalton* **2000**, 1689.
- (96) Rodriguez, M.; Romero, I.; Llobet, A.; Deronzier, A.; Biner, M.; Parella, T.; Stoeckli-Evans, H. *Inorg. Chem.* **2001**, *40*, 4150.
- (97) Sens, C.; Rodriguez, M.; Romero, I.; Llobet, A.; Parella, T.; Sullivan, B. P.; Benet-Buchholz, J. *Inorg. Chem.* **2003**, *42*, 2040.
- (98) Sala, X.; Poater, A.; Romero, I.; Rodriguez, M.; Llobet, A.; Solans, X.; Parella, T.; Santos, T. M. *Eur. J. Inorg. Chem.* **2004**, 612.
- (99) Sala, X.; Romero, I.; Rodriguez, M.; Llobet, A.; Gonzalez, G.; Martinez, M.; Benet-Buchholz, J. *Inorg. Chem.* **2004**, *43*, 5403.
- (100) Sens, C.; Romero, I.; Rodriguez, M.; Llobet, A.; Parella, T.; Benet-Buchholz, J. *J. Am. Chem. Soc.* **2004**, *126*, 7798.
- (101) Katz, N. E.; Fagalde, F.; Lis, d. K. N. D.; Mellace, M. G.; Romero, I.; Llobet, A.; Benet-Buchholz, J. *Eur. J. Inorg. Chem.* **2005**, 3019.
- (102) Katz, N. E.; Romero, I.; Llobet, A.; Parella, T.; Benet-Buchholz, J. *Eur. J. Inorg. Chem.* **2005**, 272.
- (103) Dakkach, M.; Lopez, M. I.; Romero, I.; Rodriguez, M.; Atlamsani, A.; Parella, T.; Fontrodona, X.; Llobet, A. *Inorg. Chem.* **2010**, *49*, 7072.
- (104) Mola, J.; Dinoi, C.; Sala, X.; Rodriguez, M.; Romero, I.; Parella, T.; Fontrodona, X.; Llobet, A. *Dalton Trans.* **2011**, *40*, 3640.
- (105) Roeser, S.; Farras, P.; Bozoglian, F.; Martinez-Belmonte, M.; Benet-Buchholz, J.; Llobet, A. *ChemSusChem* **2011**, *4*, 197.

## Ru dinuclear complexes containing the pyridazine-3,6-dicarboxylic acid ligand

- (106) Francas, L.; Sala, X.; Escudero-Adan, E.; Benet-Buchholz, J.; Escriche, L.; Llobet, A. *Inorg. Chem.* **2011**, *50*, 2771.
- (107) Deng, Z.; Tseng, H.-W.; Zong, R.; Wang, D.; Thummel, R. *Inorg. Chem.* **2008**, *47*, 1835.
- (108) Planas, N.; Christian, G. J.; Mas-Marza, E.; Sala, X.; Fontrodona, X.; Maseras, F.; Llobet, A. *Chem.-Eur. J.* **2010**, *16*, 7965.
- (109) Planas, N.; Christian, G.; Roeser, S.; Mas-Marza, E.; Kollipara, M.-R.; Benet-Buchholz, J.; Maseras, F.; Llobet, A. *Inorg. Chem.* **2012**, *51*, 1889.
- (110) Kapoor, P.; Pathak, A.; Kapoor, R.; Venugopalan, P.; Corbella, M.; Rodriguez, M.; Robles, J.; Llobet, A. *Inorg. Chem.* **2002**, *41*, 6153.
- (111) Rodriguez, M.; Llobet, A.; Corbella, M.; Martell, A. E.; Reibenspies, J. *Inorg. Chem.* **1999**, *38*, 2328.
- (112) Company, A.; Jee, J.-E.; Ribas, X.; Lopez-Valbuena, J. M.; Gomez, L.; Corbella, M.; Llobet, A.; Mahia, J.; Benet-Buchholz, J.; Costas, M.; Van, E. R. *Inorg. Chem.* **2007**, *46*, 9098.
- (113) Costa, R.; Moreira, I. d. P. R.; Youngme, S.; Siritwong, K.; Wannarit, N.; Illas, F. *Inorg. Chem.* **2010**, *49*, 285.
- (114) Battle, A. R.; Graham, B.; Spiccia, L.; Moubaraki, B.; Murray, K. S.; Skelton, B. W.; White, A. H. *Inorg. Chim. Acta* **2006**, *359*, 289.
- (115) Benzekri, A.; Dubourdeaux, P.; Latour, J. M.; Laugier, J.; Rey, P. *Inorg. Chem.* **1988**, *27*, 3710.
- (116) In, J.-H.; Park, S.-E.; Song, R.; Nam, W. *Inorg. Chim. Acta* **2003**, *343*, 373.
- (117) Malia, L. V., Universitat Autònoma de Barcelona, **2011**.
- (118) Muray, E.; Illa, O.; Castillo, J. A.; Alvarez-Larena, A.; Bourdelande, J. L.; Branchadell, V.; Ortuno, R. M. *J. Org. Chem.* **2003**, *68*, 4906.
- (119) Kumar, D.; de Visser Sam, P.; Shaik, S. *Chem.-Eur. J.* **2005**, *11*, 2825.
- (120) Baciocchi, E.; Boschi, T.; Cassioli, L.; Galli, C.; Jaquinod, L.; Lapi, A.; Paolesse, R.; Smith, K. M.; Tagliatesta, P. *Eur. J. Org. Chem.* **1999**, 3281.
- (121) Zona, T. A.; Goodman, J. L. *J. Am. Chem. Soc.* **1995**, *117*, 5879.
- (122) Srinivasan, K.; Michaud, P.; Kochi, J. K. *J. Am. Chem. Soc.* **1986**, *108*, 2309.

UNIVERSITAT ROVIRA I VIRGILI

NEW RUTHENIUM, MANGANESE AND COBALT DINUCLEAR COMPLEXES AS REDOX CATALYSTS.

UNFOLDING THE ESSENTIAL STEPS FOR THE GENERATION OF SOLAR FUELS

Carlo Di Giovanni

Dipòsit Legal: T. 1429-2012

UNIVERSITAT ROVIRA I VIRGILI

NEW RUTHENIUM, MANGANESE AND COBALT DINUCLEAR COMPLEXES AS REDOX CATALYSTS.







UNFOLDING THE ESSENTIAL STEPS FOR THE GENERATION OF SOLAR FUELS

Carlo Di Giovanni

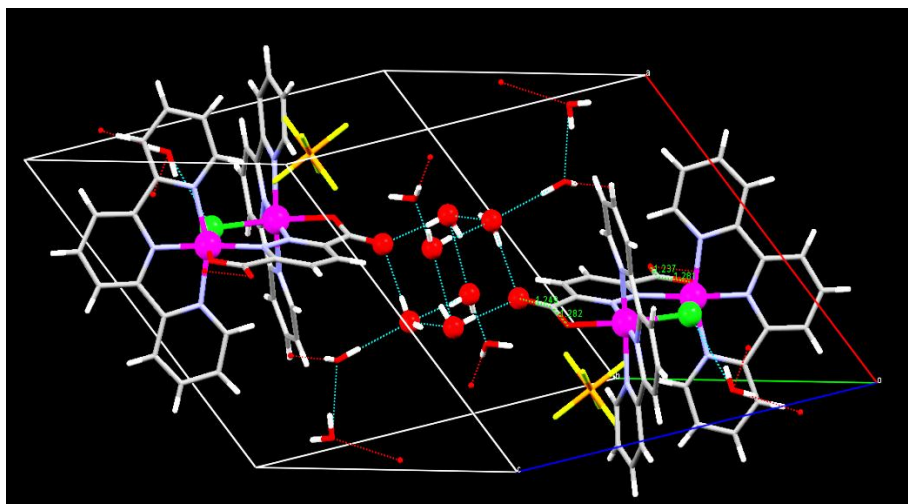
Dipòsit Legal: T. 1429-2012

# Chapter III

## Supporting Information

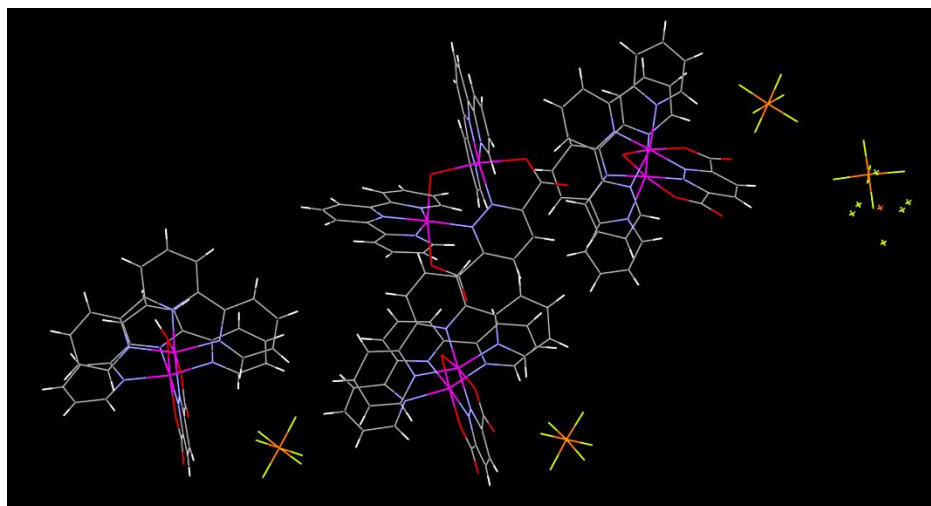
-  *NMR Characterization of  $1^+$ : Figure S11- Figure S16*
-  *MALDI-MS of  $1^+$ : Figure S17*
-  *NMR Characterization of  $2^+$ : Figure S18- Figure S112*
-  *MALDI-MS of  $1^+$ : Figure S113*
-  *Cyclic Voltammetry of  $2^+$ : Figure S14*
-  *On-line MS spectrometry: Figure S15*



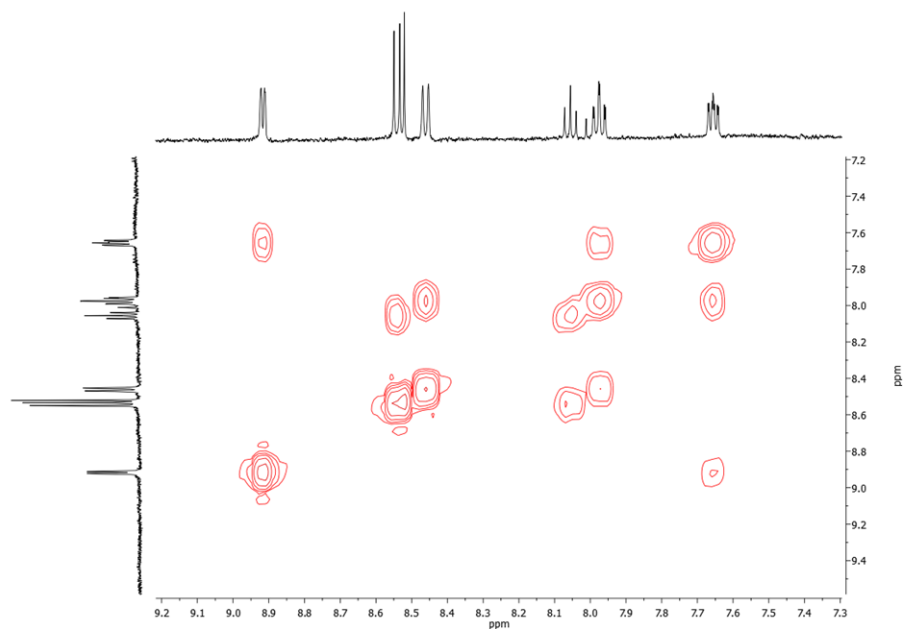


**Figure SI1.** Molecular packing arrangement of **1<sup>+</sup>**.

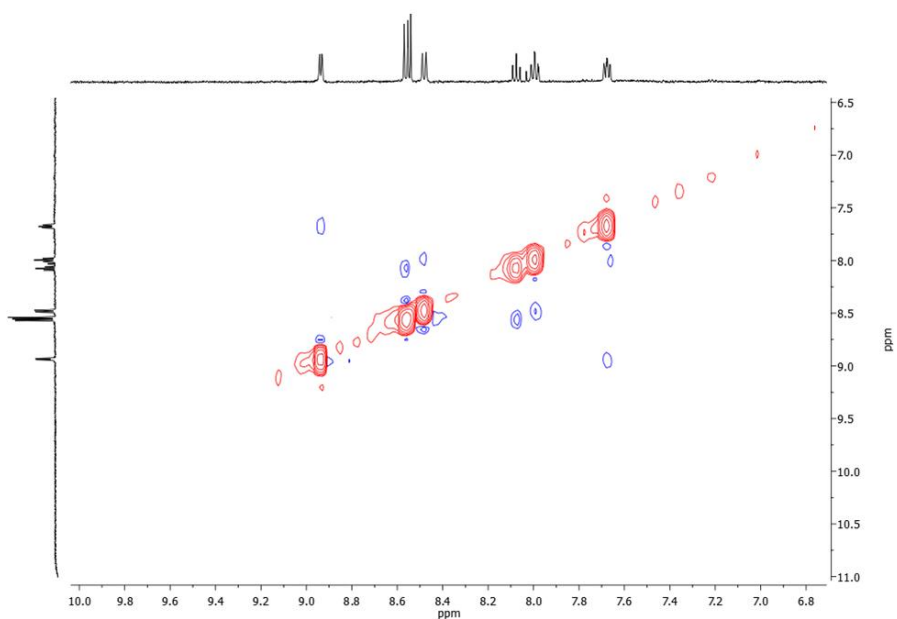




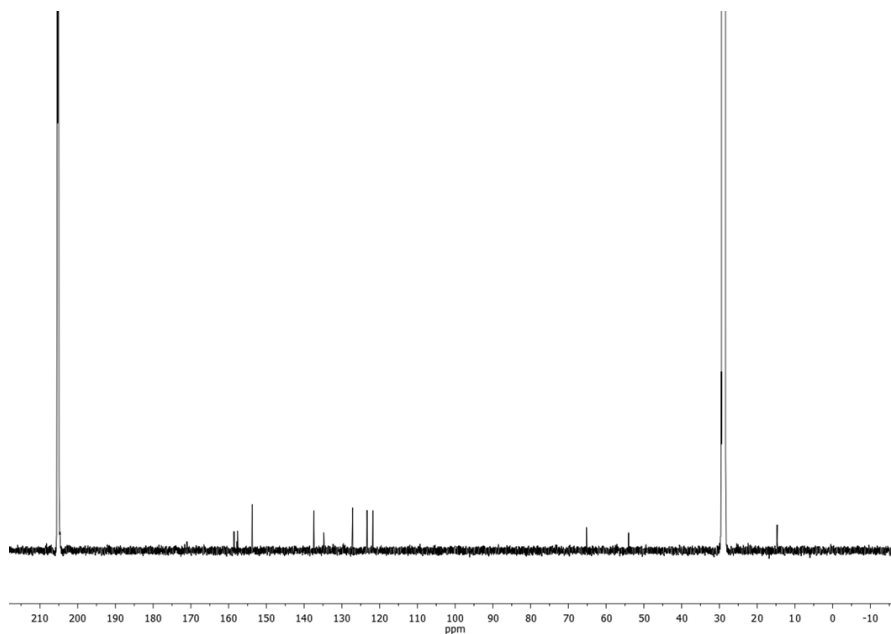
**Figure S12.** Asymmetric units of **2**(PF<sub>6</sub>).



**Figure SI3.** COSY of  $1^+$  (500 MHz, 298 K, acetone- $d_6$ ).



**Figure S14.** NOESY of **1<sup>+</sup>** (500 MHz, 298 K, acetone-d<sub>6</sub>).



**Figure S15.**  $^{13}\text{C}$ -NMR of  $\mathbf{1}^+$  (125 MHz, 298 K, acetone- $d_6$ ).

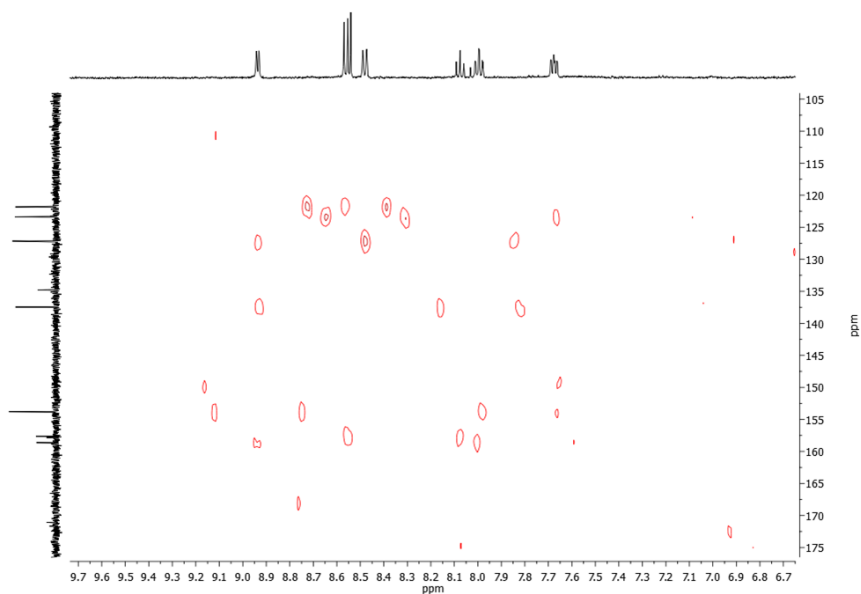


Figure S16. HMBC of  $1^+$  (298 K, acetone- $d_6$ ).

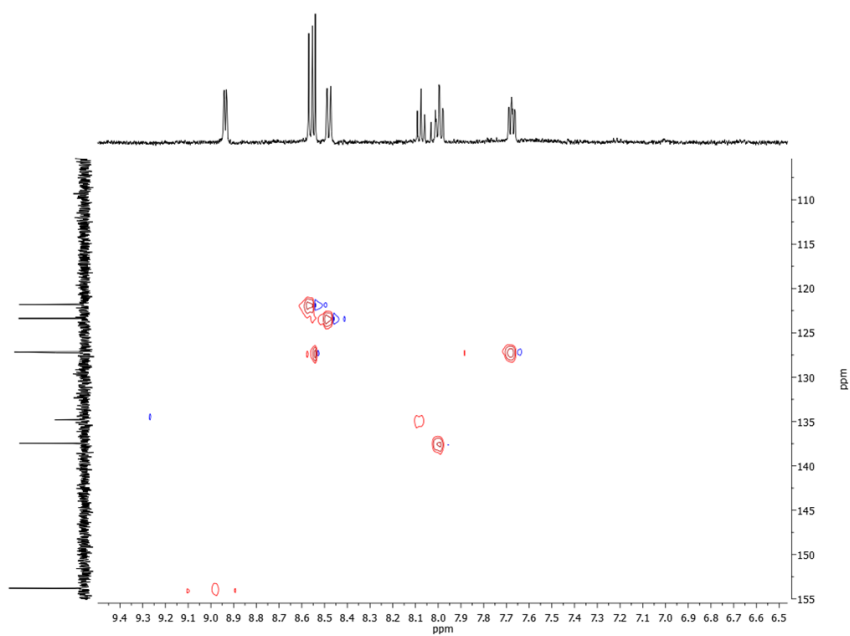
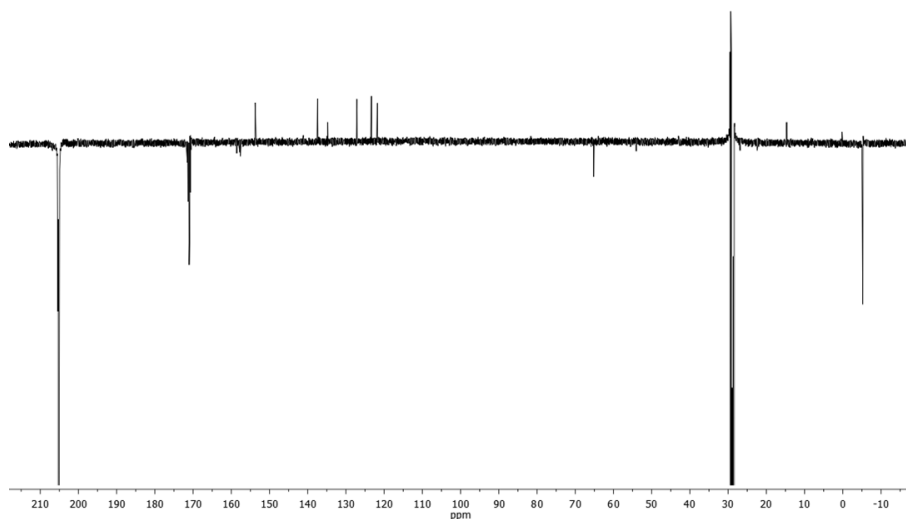


Figure S17. HSQC of  $1^+$  (298 K, acetone- $d_6$ ).



**Figure S18.** DEPTQ-135 of  $\mathbf{1}^+$  (125 MHz, 298 K, acetone- $d_6$ ).

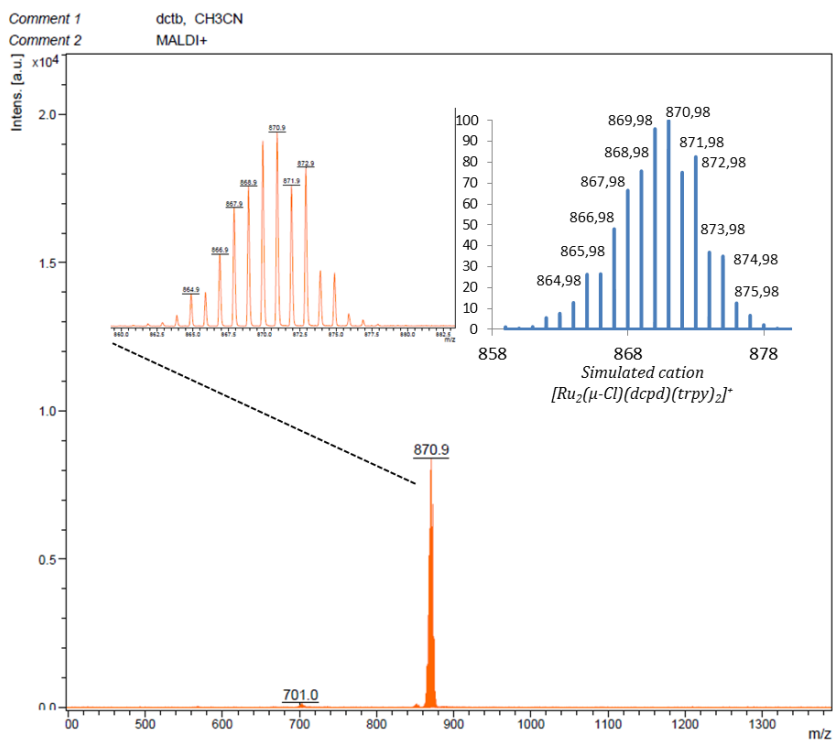
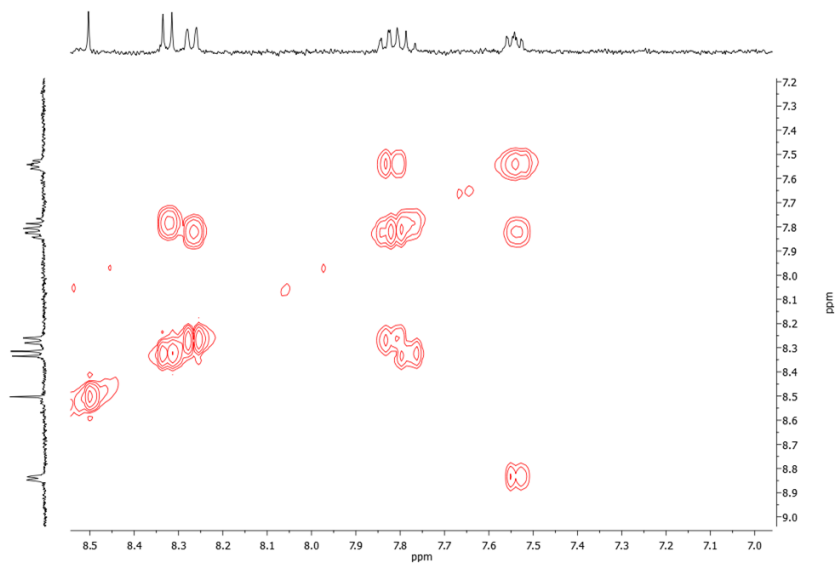
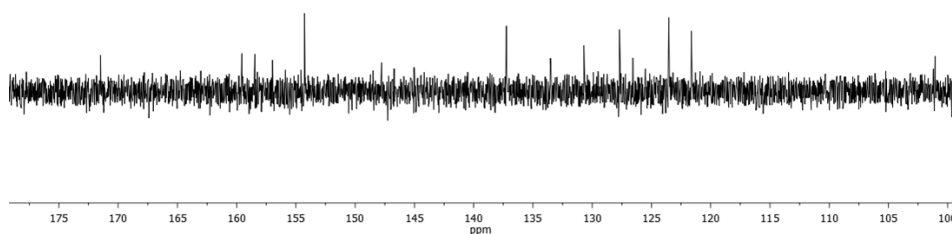


Figure SI9. MALDI-MS of  $1^+$  in  $\text{CH}_3\text{CN}$ .

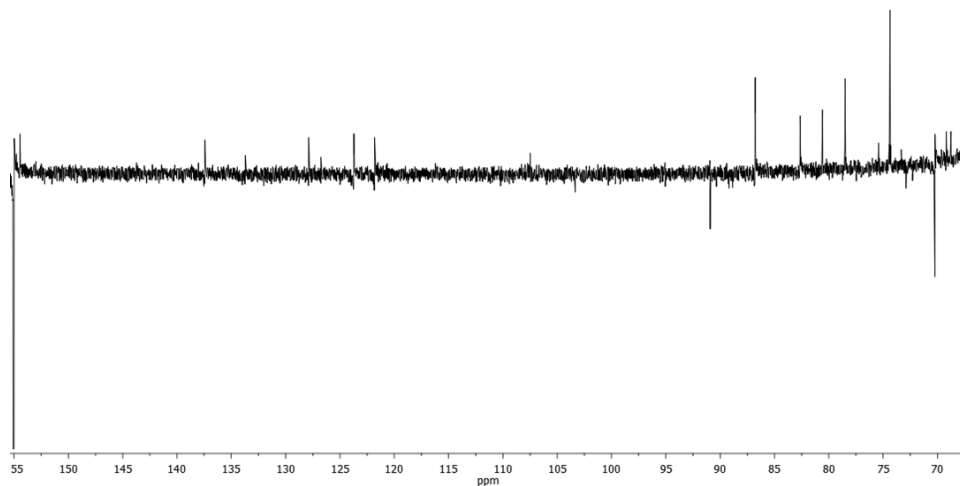




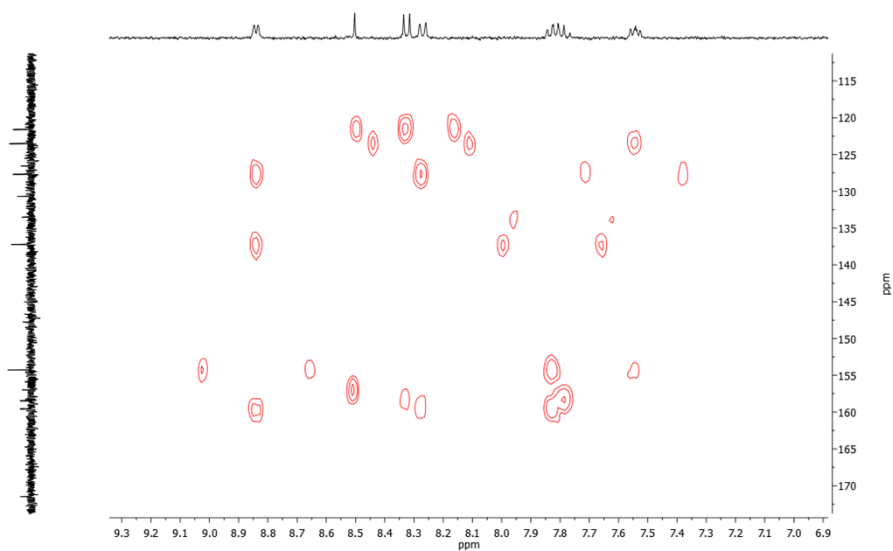
**Figure S110.** COSY of  $2^+$  (400 MHz, 298 K, acetone- $d_6$ ).



**Figure SI11.**  $^{13}\text{C}$ -NMR of  $2^+$  (100 MHz, 298 K, acetone- $\text{d}_6$ ).



**Figure SI12.** DEPTQ-135 of  $2^+$  (100 MHz, 298 K, acetone- $d_6$ ).



**Figure SI13.** HMBC of  $2^+$  (298 K, acetone- $d_6$ ).

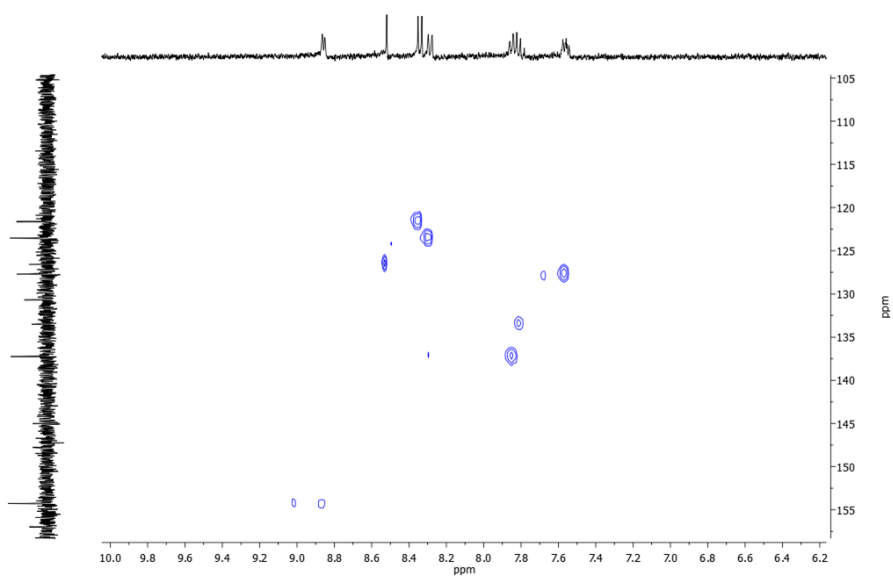


Figure S114. HSQC of  $2^+$  (298 K, acetone- $\text{d}_6$ ).

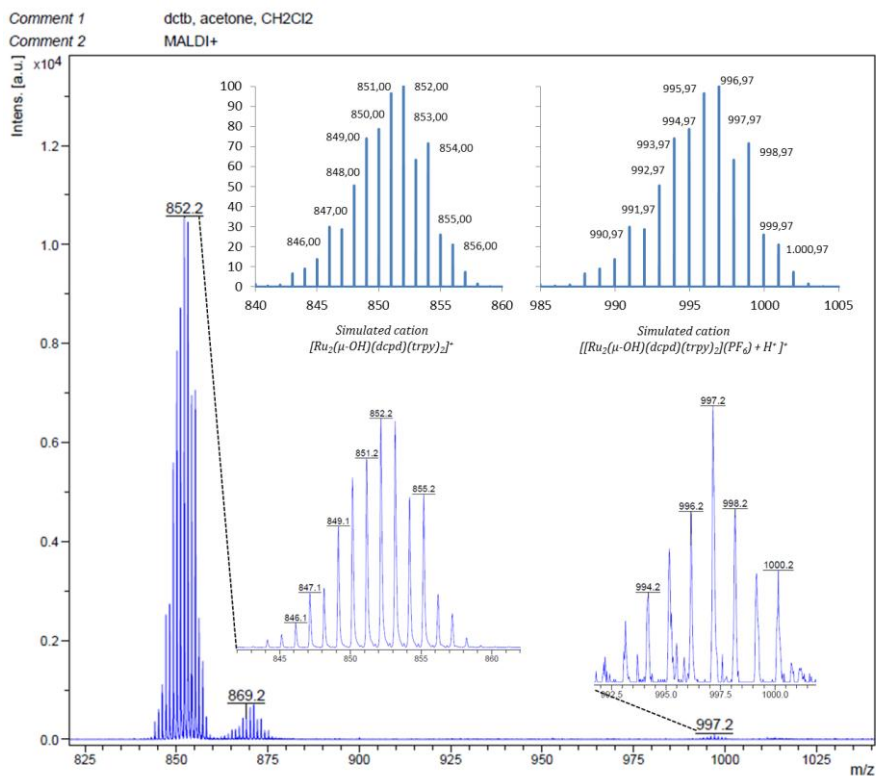
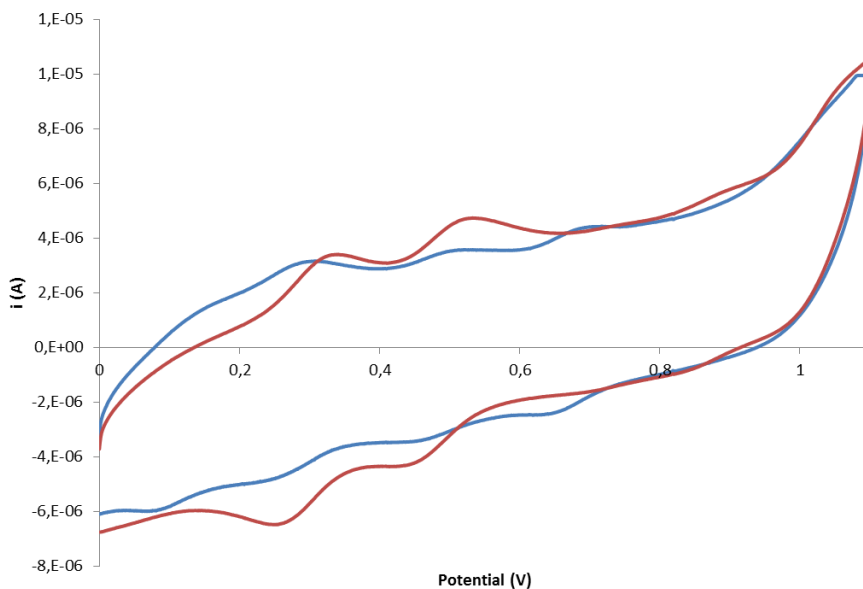
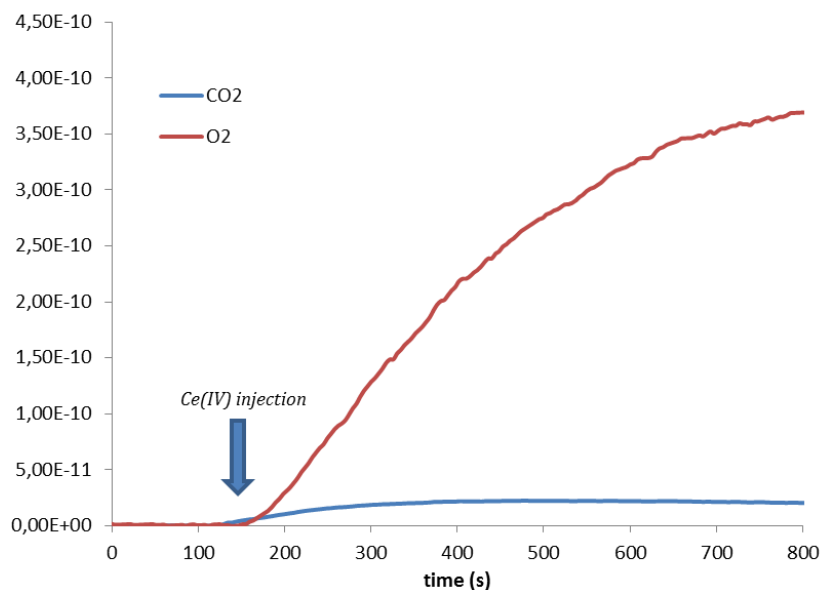


Figure S15. MALDI-MS of 2<sup>+</sup> in Acetone/CH<sub>2</sub>Cl<sub>2</sub>.



**Figure S116.** Cyclic voltammograms of  $2^+$  in triflic acid 0.1 M pH 1 (blue line) and triflic acid 0.1 M pH 1+ MeCN (1:1, red line); vs SSCE, scan rate: 100mV/s.



**Figure SI17.** On-line MS gas evolution of  $2^+$  ( $1.3 \mu\text{M}$ ) with  $\text{Ce}^{\text{IV}}$  ( $130 \mu\text{M}$ ) in triflic acid  $0.1\text{M}$  pH 1 ( $1.2 \text{mL}$  total volume).



UNIVERSITAT ROVIRA I VIRGILI

NEW RUTHENIUM, MANGANESE AND COBALT DINUCLEAR COMPLEXES AS REDOX CATALYSTS.

UNFOLDING THE ESSENTIAL STEPS FOR THE GENERATION OF SOLAR FUELS

Carlo Di Giovanni

Dipòsit Legal: T. 1429-2012

# Chapter IV

Synthesis and characterization of new  
dinuclear ruthenium complexes based on the  
pyrazole-3,5-dicarboxylic acid ligand.  
Reactivity in homogeneous oxidations

- i. Introduction*
- ii. Experimental Section*
- iii. Results and discussion*
- iv. Conclusions*
- v. Associated content*
- vi. Acknowledgements*
- vii. References*



## IV. i. Introduction

Even if in recent years molecular catalysis has reached important advances in the area of organic synthesis, usually, when compared to enzymes, synthetic catalysts result considerably inferior. It is generally considered that enzymes can achieve higher selectivity and turnover frequencies thanks to multiple non-covalent interactions in the active site. Supramolecular catalysis has indeed mainly centered on the assembly of catalysts that works through enzyme-inspired approaches. This strategy may lead to catalysts containing a substrate-binding site or cavitand next to a catalyst-binding site that lead to cage-driven reactions with enhanced selectivity and activity<sup>1,2</sup>. Supramolecular catalysts allow a spatial control over chemical transformations bringing substrates into close proximity, accelerating bimolecular reactions and influencing regiochemistry<sup>3,4</sup>. These assemblies often permit to select the reactive conformations of substrates. Through the combination of a non-covalent binding site with a catalytically oxidative metal, selective oxidation reactions become accessible for a variety of substrates<sup>5-9</sup>. The use of hydrogen bonds for the self-assembly of three-dimensional capsules has been extensively studied since 90s<sup>10</sup> but the use of a remote hydrogen-bonding motif<sup>11-13</sup> for directing the enantioselective approach of a transition-metal catalyst has not yet been deeply investigated. The ability of hydrogen bonds to display the enantiotopic face of a substrate to a transition-metal catalyst was recently probed by Bach and coworkers by combining a hydrogen-bonding motif with a catalytically active metal center for epoxidation of 3-vinylquinolone catalyzed by a ruthenium tricyclic octahydro-1*H*-4,7-methanoisoindol-1-one scaffold<sup>14</sup>. In such a catalyst, the hydrogen bonds provide the orientation of a given substrate with respect to a ligand-bound metal center.

## IV Ru dinuclear complexes containing the pyrazole-3,5-dicarboxylic acid ligand

Here we present a new dinuclear catalyst containing the anionic bridging ligand pyrazole-3,5-dicarboxylic acid able to catalyze the epoxidation of alkenes in higher TNs and TOFs respect to mononuclear ruthenium catalysts in presence of (diacetoxyiodo)benzene as oxidant. A pronounced stereoselectivity and a DFT study of the transition states point at a supramolecular approach via hydrogen bond between the substrate and the one of the metal center.

The synthesis and the characterization of an acetato bridge complex with formula  $\{[\text{Ru}^{\text{II}}(\text{trpy})]_2(\mu\text{-dcpz})(\mu\text{-OOCMe})\}$  (where  $\text{dcpz}^{3-}$  is the pyrazole-3,5-dicarboxylate anion;  $\text{trpy}$  is 2,2':6',2''-terpyridine), **1**, will be presented. The hydrolysis of **1** to form the bis aqua complex  $\{[\text{Ru}^{\text{II}}(\text{trpy})(\text{H}_2\text{O})]_2(\mu\text{-dcpz})\}^+$ , **2<sup>+</sup>** or **RuPYZ**, has been investigated by electrochemical techniques. The catalytic oxidation of water with **2<sup>+</sup>** in the presence of an excess of  $(\text{NH}_4)_2\text{Ce}^{\text{IV}}(\text{NO}_3)_6$  has been also investigated.

## IV. ii. Experimental section

**Materials.** All reagents used in the present work were obtained from Aldrich Chemical Co. or Alfa Aesar and were used without further purification. Synthesis-grade organic solvents were obtained from SDS and were routinely degassed with argon. Methanol (MeOH) was distilled over Mg/I<sub>2</sub>, ethanol was dried with a 3.5 Å molecular sieve, and acetonitrile, dichloromethane (DCM), hexane, and diethyl ether were used from the SPS. High-purity deionized water was obtained by passing distilled water through a nanopure Milli-Q water purification system.

[Ru<sup>III</sup>Cl<sub>3</sub>(trpy)]<sup>15</sup> was prepared as described in the literature. All synthetic manipulations were routinely performed under an argon atmosphere using Schlenk and vacuum-line techniques.

{[Ru<sup>II</sup>(trpy)]<sub>2</sub>(μ-dcpz)(μ-OOCMe)} · 1.5 CHCl<sub>3</sub> · 1.5 CH<sub>3</sub>CH<sub>2</sub>OH·H<sub>2</sub>O, [**1**·1.5 CHCl<sub>3</sub>·1.5 CH<sub>3</sub>CH<sub>2</sub>OH·H<sub>2</sub>O]. 110 mg (0.249 mmol) of [RuCl<sub>3</sub>(trpy)] were dissolved in 20 mL of ethanol:water (3:1) and 44 μL (0.316 mmol) of triethylamine were added. The mixture was stirred at room temperature for 20 minutes under Argon atmosphere and then 2 mL of ethanol containing 19 mg (0.109 mmol) of pyrazole-3,5-dicarboxylic acid monohydrate H<sub>3</sub>dcpz·H<sub>2</sub>O and 50 μL (0.359 mmol) of triethylamine were added. 195 mg (2.38 mmol) of sodium acetate were added last of all and the resulting solution heated at reflux for 4 h. Afterward, the solution was cooled and the purple solid filtered on a frit, washed with diethyl ether and dried in a vacuum. Recrystallization from chloroform/ethanol/diethyl ether yielded small dark blue crystals Yield: 113 mg 91%. Anal. Calcd. for C<sub>37</sub>H<sub>26</sub>N<sub>8</sub>O<sub>6</sub>Ru<sub>2</sub>·1.5 CHCl<sub>3</sub>·1.5 CH<sub>3</sub>CH<sub>2</sub>OH·H<sub>2</sub>O : C, 43.28; H, 3.18; N, 9.97. Found: C, 43.04; H, 2.97; N, 10.15. <sup>1</sup>H-NMR (400 MHz, CF<sub>3</sub>CD<sub>2</sub>OD + NEt<sub>3</sub>) δ 8.47 (d, *J* = 5.3 Hz, H1, H15), 8.27 (d, *J* = 8.1 Hz, H7, H9),

**Ru dinuclear complexes containing the pyrazole-3,5-dicarboxylic acid ligand**

8.23 (d,  $J = 8.1$  Hz, H4, H12), 7.92 – 7.73 (m, H3, H8, H13, H18), 7.38 (t,  $J = 6.5$  Hz, H2, H14), 0.12 (s, H20).  $^{13}\text{C-NMR}$  (100 MHz,  $\text{CF}_3\text{CD}_2\text{OD} + \text{NEt}_3$ )  $\delta$  200.0 (C19), 177.4 (C16), 163.5 (C6, C10), 162.9 (C5, C11), 155.4 (C1, C15), 148.5 (C17), 138.5 (C3, C13), 133.9 (C8), 128.6 (C2, C14), 124.3 (C4, C12), 123.1 (C7, C9), 111.7 (C18), 25.8 (C20). UV-Vis ( $\text{CH}_2\text{Cl}_2\text{-CH}_3\text{CH}_2\text{OH}$ , 9:1) [ $\lambda_{\text{max}}$ , nm ( $\epsilon$ ,  $\text{M}^{-1}\cdot\text{cm}^{-1}$ ): 237 (29340), 280 (29080), 317 (28160), 326 (29440), 392 (8400), 555 (7980), 604 (6600).  $E_{1/2}$  ( $\text{CH}_2\text{Cl}_2\text{:EtOH}$ , V vs SSCE): 0.325 V and 0.633 V.  $E_{1/2}$  ( $\text{CH}_2\text{Cl}_2\text{:EtOH}$ , V vs SSCE): 0.325 V and 0.633 V. ESI-MS ( $\text{CH}_3\text{OH}$ ):  $m/z = 463.9$  ( $[\text{M} + 2 \text{Na}^+]^{2+}$ ).

**Equipment and Measurements.** All electrochemical experiments were performed in a PAR 263A EG&G potentiostat or in an IJ-Cambria HI-660 potentiostat, using a three-electrode cell. Glassy carbon (3 mm diameter) from BAS was used as the working electrode, a platinum wire as the auxiliary electrode, and SSCE as the reference electrode. Cyclic voltammograms were recorded at a  $100 \text{ mV}\cdot\text{s}^{-1}$  scan rate. The complexes were dissolved in previously degassed DCM/EtOH containing the necessary amount of  $(n\text{-Bu}_4\text{N})(\text{PF}_6)$ , used as the supporting electrolyte, to yield a 0.1 M ionic strength solution. All  $E_{1/2}$  values reported in this work were estimated from cyclic voltammetry (CV) as the average of the oxidative and reductive peak potentials  $(E_{p,a} + E_{p,c})/2$  or from differential pulse voltammetry (DPV; pulse amplitudes of 0.05 V, pulse widths of 0.05 s, sampling width of 0.02 s, and a pulse period of 0.1 s). Unless explicitly mentioned, the concentrations of the complexes were approximately 1 mM. A 400 MHz Bruker Avance II spectrometer and a Bruker Avance 500 MHz were used to carry out NMR spectroscopy at room temperature. Samples were run in acetone- $d_6$ . The electrospray ionization (ESI) and matrix-assisted laser desorption ionization (MALDI) mass spectrometry (MS) experiments were performed on a Waters Micromass LCT Premier equipment and a Bruker

Daltonics Autoflex equipped with a nitrogen laser (337 nm), respectively. UV-vis spectroscopy was performed on a Cary 50 Bio (Varian) UV-vis spectrophotometer with 1 cm quartz cells. Manometric measurements were performed with homemade water-jacket glass reactor coupled to a Testo 521 manometer. Composition of the gaseous phase was determined by online mass-spectrometry with an OmniStar GSD 301 C (Pfeiffer) quadrupole mass-spectrometer. In a typical experiment, 1 mL of a 1 mM complex solution in  $\text{CF}_3\text{SO}_3\text{H}$  (pH 1.0) was degassed with nitrogen until no oxygen could be detected. The reactor was then closed with a septum-sealed adapter that excluded the gas phase. A 0.2 mL of previously degassed  $(\text{NH}_4)_2\text{Ce}^{\text{IV}}(\text{NO}_3)_6$  solution, was then added directly into the reaction solution with a Hamilton syringe. Blank experiments were performed by addition of  $(\text{NH}_4)_2\text{Ce}^{\text{IV}}(\text{NO}_3)_6$  solution to neat  $\text{CF}_3\text{SO}_3\text{H}$  (pH 1.0) in absence of catalyst. Epoxidation catalytic experiments were analyzed in an Agilent 6890N gas chromatograph coupled to a mass selective detector with ionization by electronic impact and in an Agilent 6890 with a FID detector using a HP5 column. In a typical experiment the catalyst (1.5 mg;  $1,31 \cdot 10^{-3}$  mmol; final concentration = 1 mM), the substrate (2.6 mmol, final concentration = 2 M), dodecane (50  $\mu\text{L}$ ; 0.22 mmol; final concentration = 170 mM) as internal reference, and (diacetoxyiodo)benzene (1.67 g; 5.2 mmol; final concentration = 4 M) were mixed together in 1 mL of a 1:1 dichloromethane/ethanol solution (final volume  $\approx 1.3$  mL). First aliquot was taken, filtered through a Pasteur pipette filled with celite, diethyl ether was added in order to elute the organic compounds and the filtrate analyzed by GC. The reaction mixture was stirred at RT for 30 min and a second aliquot was taken and treated as described above. No epoxide or just traces were detected at this time. Water (94  $\mu\text{L}$ ; 5.2 mmol; final concentration = 4 M) was added and aliquots taken every 5, 10, 15, 20, 25, 30 or until completion of reaction. The



## IV Ru dinuclear complexes containing the pyrazole-3,5-dicarboxylic acid ligand

characterization of the reaction products were done by comparison with commercial products or by GC-MS spectrometry. GC conditions: initial temperature 40 °C for 10 min, ramp rate variable for each substrate (typically from 10 °C/min to 20 °/min), final temperature 250 °C, injection temperature 220 °C, detector temperature 250°C. Yield of epoxide and substrate conversion were calculated with regard to the initial concentration of substrate. Yield of epoxide and substrate conversion were calculated with regard to the initial concentration of substrate.

Substrate conversion =  $\frac{[\text{substrate}]_{\text{initial}} - [\text{substrate}]_{\text{final}}}{[\text{substrate}]_{\text{initial}}} \cdot 100$ .

Yield epoxide =  $\frac{[\text{epoxide}]_{\text{final}}}{[\text{substrate}]_{\text{initial}}} \cdot 100$ . Epoxide selectivity =  $\frac{[\text{epoxide}]_{\text{final}}}{\{[\text{substrate}]_{\text{initial}} - [\text{substrate}]_{\text{final}}\}} \cdot 100$ .

### **Single-Crystal X-Ray Structure Determination.** *Crystal Preparation.*

Crystals for **1** were grown by the slow evaporation of a chloroform/ethanol solution of the complex. All measured crystals were prepared under inert conditions immersed in perfluoropolyether as the protecting oil for manipulation.

*Data collection:* Crystal structure determinations for **1** was carried out using a Bruker-Nonius diffractometer equipped with an APEX 2 4K CCD area detector, a FR591 rotating anode with MoK $_{\alpha}$  radiation, Montel mirrors as monochromator and an Oxford Cryosystems low temperature device Cryostream 700 plus ( $T = -173$  °C). Full-sphere data collection was used with  $\omega$  and  $\varphi$  scans. *Programs used:* Data collection APEX-2<sup>16</sup>, data reduction Bruker Saint<sup>17</sup> V/.60A and absorption correction SADABS<sup>18</sup> or TWINABS<sup>19</sup>.

*Structure Solution and Refinement:* Crystal structure solution was achieved using direct methods as implemented in SHELXTL<sup>20</sup> and visualized using the program XP. Missing atoms were subsequently located from difference Fourier synthesis and added to the atom list. Least-squares refinement on  $F^2$  using all

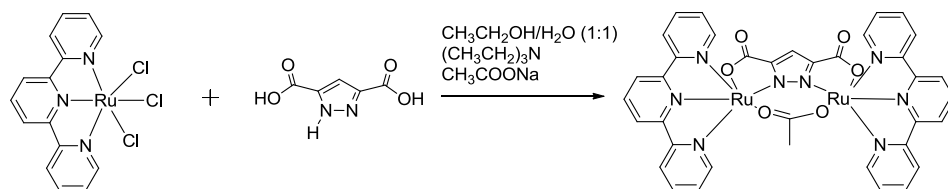
measured intensities was carried out using the program SHELXTL. All non-hydrogen atoms were refined including anisotropic displacement parameters. In order to avoid highly disordered solvent molecules the program SQUEEZE<sup>21</sup> was used.

**Computational method.** All the DFT static calculations were performed at the GGA level with the *Gaussian09* set of programs,<sup>22</sup> using the M06L correlation-exchange functional of Truhlar et al.,<sup>23</sup> which parametrization takes into account the dispersion effect. The electronic configuration of the molecular systems was described with the standard split-valence basis set with a polarization function of Ahlrichs and co-workers for H, C, N, and O (SVP keyword in Gaussian).<sup>24</sup> For Ru we used the small-core, quasi-relativistic Stuttgart/Dresden effective core potential, with an associated valence basis set contracted (standard SDD keywords in gaussian09).<sup>25-27</sup> The geometry optimizations were performed without symmetry constraints, and the characterization of the located stationary points was performed by analytical frequency calculations. The reported energies have been optimized via single point calculations on the M06L geometries with triple zeta valence plus polarization (TZVP keyword in Gaussian) using the M06 functional,<sup>28</sup> however estimating solvent effects with the polarizable continuous solvation model PCM using ethanol as solvent.<sup>29,30</sup>

### IV. iii. Results and discussion

#### Synthesis

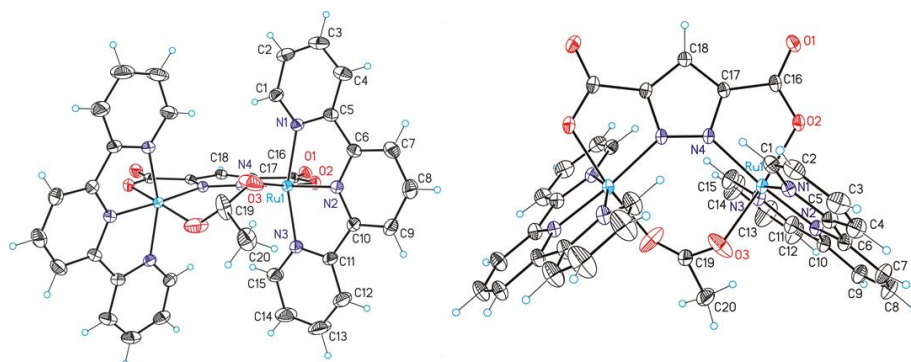
The synthetic procedure followed for the synthesis of **1** was based on the synthesis of analogues ruthenium dinuclear complexes based on  $[\text{Ru}^{\text{III}}\text{Cl}_3(\text{trpy})]$  precursor. The Ru(III) species was reduced with triethylamine and then the bridging ligand was added (Scheme 1).



**Scheme 1.** Synthetic pathway.

#### Solid state and spectroscopic characterization

Suitable crystals for X-Ray diffraction analysis of **1** were obtained by slow evaporation of a chloroform/ethanol solution of the complex. The structure, presented in Figure 1, shows a distorted octahedral geometry around the metal centre.



**Figure 1.** Ortep plot (ellipsoids at 50% probability) X-Ray structure of **1**.

The geometric nature of the acetate bridge produces an inverse relative rotation of the two terpy ligands in order to accommodate its two coordinating oxygen atoms. The effects of this alteration result in the distortion of the planarity of the dcpz<sup>3-</sup> ligand yielding an angle of 3.73° between the carboxylic groups, and in an extended distance of 4.331 Å between the two metal centers. All the bond distances and angles are comparable to analogous complexes reported earlier in the literature<sup>31-45</sup>.

Crystal data and selected bond distances and angles are reported in Table 1 and Table 2, respectively.

**Table 1.** Crystal data for complex **1**.

	<b>1<sup>+</sup></b>	
Empirical formula	$C_{43.70}H_{43.30}Cl_{4.50}N_8O_{8.50}PRu_2$	
Formula weight	1178.23	
Temperature	100(2)K	
Wavelength	0.71073 Å	
Crystal system	Monoclinic	
Space group	C2/c	
Unit cell dimensions	a = 21.9842(9) Å	$\alpha = 90.00^\circ$
	b = 13.4059(6) Å	$\beta = 97.09 (10)^\circ$
	c = 15.7659(6) Å	$\gamma = 90.0^\circ$
Volume	4610.9 (3) Å <sup>3</sup>	
Z	4	
Density (calculated)	1.697 Mg/m <sup>3</sup>	
Absorption coefficient	0.980 mm <sup>-1</sup>	
F(000)	2376	
Crystal size	0.20 x 0.10 x 0.05 mm <sup>3</sup>	
Theta range for data collection	1.78 to 30.11 °.	
Index ranges	-30 ≤ h ≤ 30, -18 ≤ k ≤ 18, -21 ≤ l ≤ 20	
Reflections collected	82069	
Independent reflections	6390 [R(int) = 0.0293]	
Completeness to theta = 25.40 °	0.942 %	
Absorption correction	Empirical	
Max. and min. transmission	0.98526 and 0.8282	
Refinement method	Full-matrix least-squares on F <sup>2</sup>	
Data / restraints / parameters	6390 / 100 / 375	
Goodness-of-fit on F <sup>2</sup>	1.076	
Final R indices [I > 2σ(I)]	R1 = 0.0420, wR2 = 0.1131	
R indices (all data)	R1 = 0.0479, wR2 = 0.1177	
Largest diff. peak and hole	1.029 and -1.408 e.Å <sup>-3</sup>	

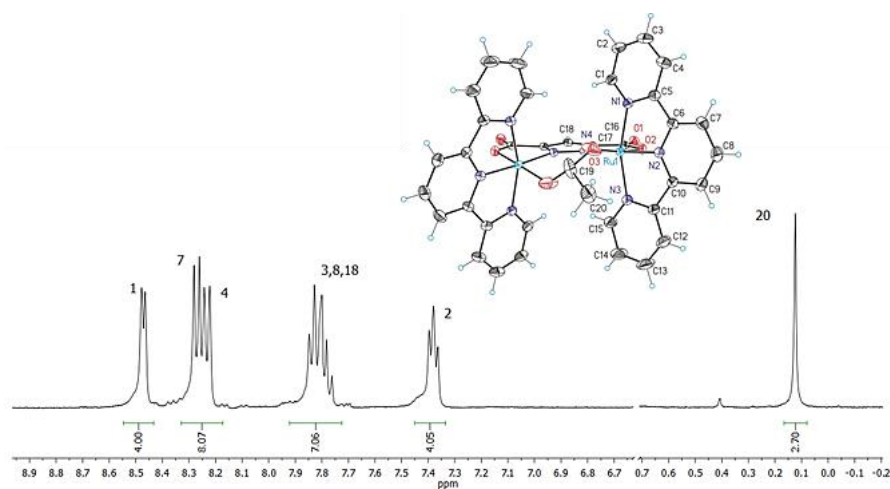
**Table 2.** Selected metric parameters for complex **1**.

Selected bond (Å)		Selected Angle (°)	
Ru(1)-N(1)	2.065(3)	N(4)-Ru(1)-O(3)	96.48(13)
Ru(1)-N(2)	1.942(3)	N(2)-Ru(1)-N(4)	174.44(10)
Ru(1)-N(3)	2.046(3)	O(2)-Ru(1)-O(3)	171.61(12)
Ru(1)-N(4)	2.065(2)	N(1)-Ru(1)-N(3)	159.58(11)
Ru(1)-O(2)	2.090(2)	Ru(1)-N(4)-N(4')-Ru(1') <sup>a</sup>	-15.90
Ru(1)-O(3)	2.076(3)		

<sup>a</sup> Torsion angle that involves the two N atoms belonging to the pyridazinedicarboxylate-bridged group and the two metal centers.

### NMR Spectroscopic properties

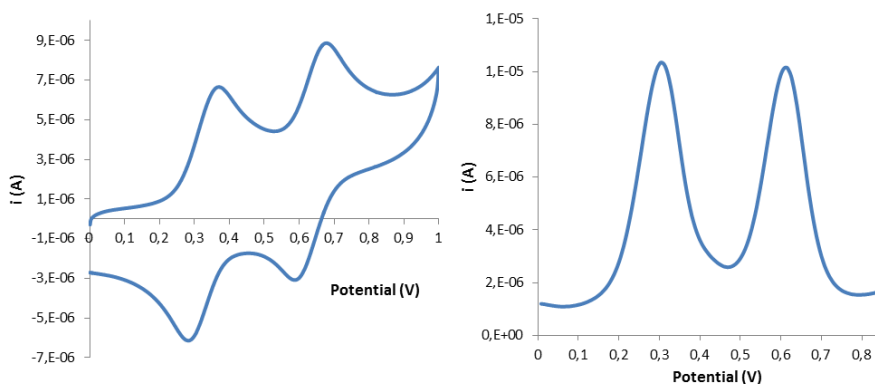
The complex was also characterized by 1D and 2D NMR spectroscopy in deuterated trifluoroethanol. The <sup>1</sup>H-NMR spectra is displayed in Figure 2 whereas the rest of the spectra are presented as Supporting Information. All the resonances displayed could be unambiguously assigned based on their multiplicity integrals and thanks to the 2D spectra.

**Figure 2.** <sup>1</sup>H-NMR of **1** (400 MHz, 298 K, CF<sub>3</sub>CD<sub>2</sub>OD).

## Ru dinuclear complexes containing the pyrazole-3,5-dicarboxylic acid ligand

### Redox properties

With regards to their electrochemical properties **1** in a mixture of 1:1  $\text{CH}_2\text{Cl}_2/\text{CH}_3\text{CH}_2\text{OH}$  (0.1 M TBAH) presented two reversible waves at half wave potential ( $E_{1/2}$ ) of 0.325 V and 0.633 assigned to redox couple  $\text{Ru}^{\text{III,II/II,II}}$  and  $\text{Ru}^{\text{III,III/III,II}}$  (Figure 3). Compared with the analogous dinuclear system containing the bis(2-pyridyl)-3,5-pyrazolate anionic bridging ligand ( $\text{bpp}^-$ )<sup>46</sup> the effect of the two carboxylic groups results in lower half-potentials of the red-ox couples. On the contrary, the similar  $\Delta E_{1/2}$  values (0.323 V for  $[\text{Ru}^{\text{II}}_2(\text{trpy})_2(\mu\text{-bpp})(\mu\text{-OOCMe})]^{2+}$  and 0.308 V for **1**) similar electronic communication between the metal centers. Redox properties for complex **1** and complex  $[\text{Ru}^{\text{II}}_2(\text{trpy})_2(\mu\text{-bpp})(\mu\text{-OOCMe})](\text{PF}_6)_2$  are reported in Table 3.



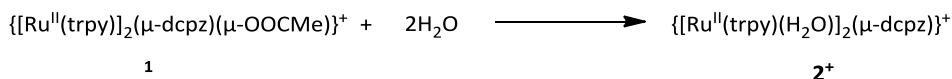
**Figure 3.** CV and DPV of **1** in  $\text{CH}_2\text{Cl}_2:\text{CH}_3\text{CH}_2\text{OH}$  (1:1), 0.1 M TBAH vs SSCE.

**Table 3.** Redox properties for **1** and  $\{[\text{Ru}^{\text{II}}(\text{trpy})]_2(\mu\text{-bpp})(\mu\text{-OOCMe})\}^{2+}$ , values reported vs SSCE.

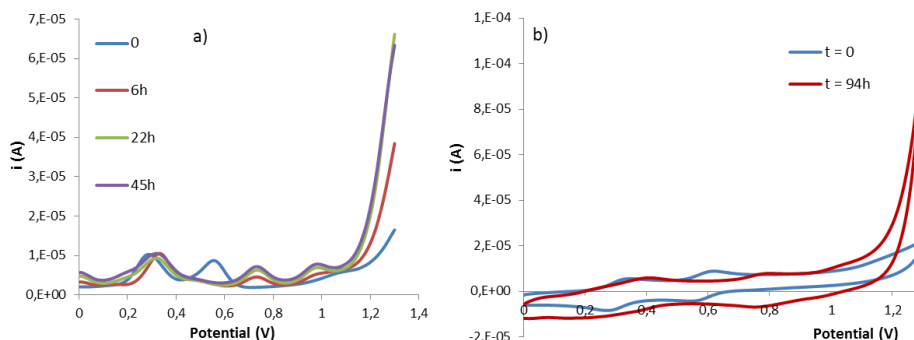
complex	$E_{1/2}(\text{III,II-II,II})$ (V)	$E_{1/2}(\text{III,III-III,II})$ (V)	$\Delta E_{1/2}$ (V)
$\{[\text{Ru}^{\text{II}}(\text{trpy})]_2(\mu\text{-dcpz})(\mu\text{-OOCMe})\}^+$ , <b>1</b>	0.325	0.633	0.308
$\{[\text{Ru}^{\text{II}}(\text{trpy})]_2(\mu\text{-bpp})(\mu\text{-OOCMe})\}^{2+}$	0.728	1.051	0.323

When treated with 0.1 M triflic acid pH 1 a new species formed. Four new waves and an electrochemical wave can be detected after some hours of stirred solution of **1** in trifluoroethanol:triflic acid (1:1) solution (Figure 4).

Substitution of the acetate bridge with two molecules of water take place as consequence of hydrolysis of **1** in aqueous media to form the bis-aqua complex  $\{[\text{Ru}^{\text{II}}(\text{trpy})(\text{H}_2\text{O})]_2(\mu\text{-dcpz})\}^+$ , **2**<sup>+</sup>:



**Scheme 2.** Hydrolysis of **1** in aqueous media.



**Figure 4.** Hydrolysis of **1** in 1:1 trifluoroethanol:triflic acid solution (0.1 M), time evolution of differential pulse voltammogram (a) and cyclic voltammogram (b).



## IV Ru dinuclear complexes containing the pyrazole-3,5-dicarboxylic acid ligand

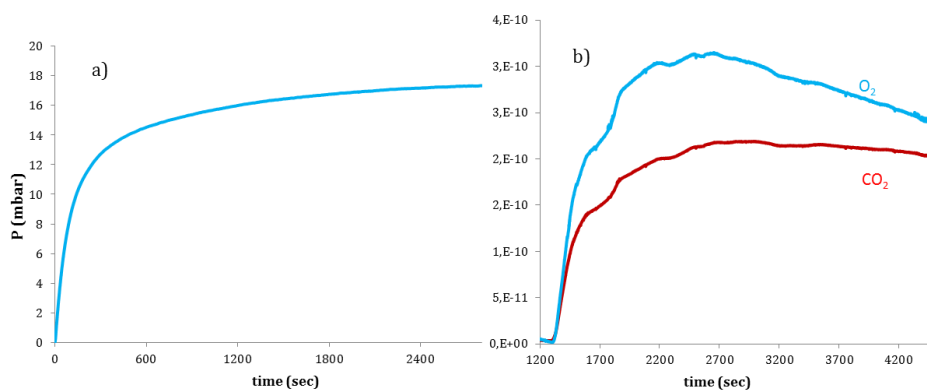
The 4 waves have been assigned to the one-electron oxidation of bis-aqua complex from Ru<sup>II</sup>Ru<sup>II</sup> to Ru<sup>IV</sup>Ru<sup>IV</sup> species and the electrocatalytical wave to the oxidation of water. Also in this case the redox potential have been compared with the ones of the bpp<sup>-</sup> system<sup>46</sup>. All the redox data are reported in table 4.

**Table 4.** Redox properties for **2** and {[Ru<sup>II</sup>(trpy)(H<sub>2</sub>O)]<sub>2</sub>(μ-bpp)}<sup>3+</sup>, values reported vs SSCE.

complex	E <sub>1/2</sub> (III,II-II,II) (V)	E <sub>1/2</sub> (III,III-III,II) (V)	E <sub>1/2</sub> (III,III-III,II) (V)	E <sub>pa</sub> (III,III-III,II) (V)
{[Ru <sup>II</sup> (trpy)(H <sub>2</sub> O)] <sub>2</sub> (μ-dcpz)} <sup>+</sup> , <b>2</b>	0.20	0.35	0.73	0.97
{[Ru <sup>II</sup> (trpy)(H <sub>2</sub> O)] <sub>2</sub> (μ-bpp)} <sup>3+</sup>	0.54	0.61	0.84	1.05

### Catalysis of water oxidation

The activity of  $2^+$  toward water oxidation was tested in a 0.1 M triflic acid solution containing  $(\text{NH}_4)_2\text{Ce}^{\text{IV}}(\text{NO}_3)_6$  and the complex in an airtight degassed cell. Addition of a 100-fold molar excess of  $\text{Ce}^{\text{IV}}$  to  $1.30 \cdot 10^{-6}$  M solution of  $2^+$  in triflic acid resulted in an immediate release of gas (Figure 5a) which resulted to be a mixture of  $\text{O}_2$  and  $\text{CO}_2$  (Figure 5b) by on-line mass detection. A decomposition reaction of the catalyst which involves the organic moiety oxidation, probably catalyzed by higher oxidation states of ruthenium species, likely takes place in competition with the water oxidation process.



**Figure 5.** Chemical water oxidation with  $2^+$  (1 mM) at pH = 1.0 in 0.1 M triflic acid solution in the presence of  $(\text{NH}_4)_2\text{Ce}^{\text{IV}}(\text{NO}_3)_6$  (100 mM). a) Manometric measurement. b) On-line mass spectroscopy ( $\text{O}_2$  evolution blue line,  $\text{CO}_2$  evolution red line).

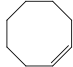
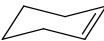
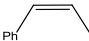
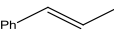
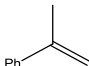
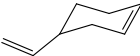
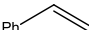
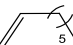
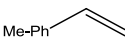
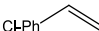
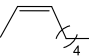
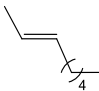
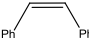
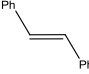
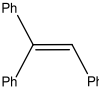
## Olefins epoxidation

The catalytic activity of  $2^+$  was also tested with regards to its capacity to oxidize alkenes. The reaction was performed in a mixture of dichloromethane:ethanol (1:1), using (diacetoxyiodo)benzene as oxidant. A concentration of 1 mM of catalyst and a relation of cat:sub:ox of 1:2000:4000 was used. A 4000-fold excess of water, that is needed to generate PhIO from PhIOAc<sub>2</sub> and to transform precursor **1** into catalyst  $2^+$  as described in previous sections, was added after stirring the mixture for 30 min. This time has been found to be essential for triggering the catalysis. The epoxidation of *cis* alkenes with  $2^+$  resulted stereospecific by the meaning that no *cis/trans* isomerization takes place. In Table 5 are summarized the catalytic performance of  $2^+$  toward the oxidation of several alkenes. Turnover frequencies for each catalytic reaction have been calculated and sorted in Figure 6. High catalytic activity has been detected for cyclic substrate, like cyclooctene and cyclohexene (Entries 1 and 2), as well for alkenes activated by electron-donor groups in  $\beta$ , like the  $\beta$ -methylstyrene and octene (Entries 3, 4, 11 and 12). Substrates with elevated steric hindrance like stilbene and triphenylethylene react slowly and with low turnover numbers and selectivities (Entries 13 and 15). The linear olefins *cis*- and *trans*-2-octene (Entries 11 and 12) have been both oxidized with conversion of 100% and 87% respectively but with remarkable difference in selectivity and turnover frequency. 96% of *cis*-2,3-epoxyoctane has been formed with a turnover frequency of 6.08 TN·s<sup>-1</sup> while the *trans*-epoxide was obtained in 57% of yield (selectivity of 66%) and with a slower TOF of 1.25 TN·s<sup>-1</sup>. 1-octene was converted for the 51% and with a selectivity of 59% with a markedly lower TOF (20 TN·min<sup>-1</sup>). 4-vinyl-1-cyclohexene was fully converted in a mixture 1:1 of the *endo*- and *exo*-epoxide (Entry 6). The oxidation of *cis*- $\beta$ -methylstyrene has been also tested in a catalyst:substrate:oxidant:water ratio

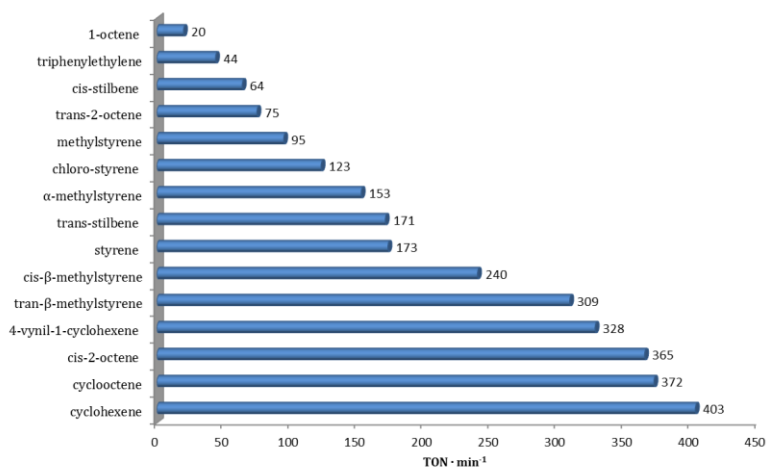
of 1:20000:40000:40000 that results in the formation of corresponding *cis*-epoxide in  $\approx 85\%$  of yield ( $\approx 17000$  TN). **1** has been recovered after the catalytic epoxidation reaction through precipitation by addition of diethyl ether to the reaction mixture. X-Ray diffraction and DPV (Figure S17) measurements confirmed the integrity **1** after reaction.

**Ru dinuclear complexes containing the pyrazole-3,5-dicarboxylic acid ligand**

**Table 5.** Catalytic performance of **2<sup>+</sup>** for the epoxidation of several alkenes using  $\text{PhI}(\text{AcO})_2^{\text{a}}$

Entry	substrate	Substrate conversion <sup>b</sup> (%)	[Epoxide], M; selectivity <sup>c</sup> (%)	TN/TOF <sup>d</sup>	
1	<i>cis</i> -cyclooctene <sup>e</sup>		100	1.88 (94)	1880/6.20
2	Cyclohexene		100	1.94 (97)	1940/6.72
3	<i>cis</i> - $\beta$ -methylstyrene <sup>e</sup>		100	1.74 (87)	1740/4.00
4	<i>trans</i> - $\beta$ -methylstyrene <sup>f</sup>		100	1.8 (90)	1800/5.15
5	$\alpha$ -methylstyrene		100	0.98 (49)	980/2.55
6	4-vinyl-1-cyclohexene		100	(1.64) 82 <sup>h</sup>	1640/5.47
7	Styrene		99	1.15 (58)	1150/2.88
8	1-octene		51	0.60 (59)	602/0.33
9	<i>para</i> -methylstyrene		100	(0.48) 24	480/1.58
10	<i>para</i> -chloro-styrene		80	1.09 (68)	1090/2.05
11	<i>cis</i> -2-octene <sup>e</sup>		100	1.92 (96)	1920/6.08
12	<i>trans</i> -2-octene <sup>f</sup>		87	1.15 (66)	1150/1.25
13	<i>cis</i> -stilbene <sup>e,g</sup>		32	0.26 (40)	130/1.07
14	<i>trans</i> -stilbene <sup>f,g</sup>		61	0.70 (57)	350/2.85
15	Triphenylethylene		25	0.24 (48)	240/0.73

<sup>a</sup>Reaction conditions: [**1**·1.5 CHCl<sub>3</sub>·1.5 CH<sub>3</sub>CH<sub>2</sub>OH·H<sub>2</sub>O] (1.5 mg; 1,31·10<sup>-3</sup> mmol; final concentration = 1 mM) in dichloromethane/ethanol (1:1, 1 mL), substrate (2.62 mmol; final concentration = 2 M), PhI(OAc)<sub>2</sub> (1.69 g; 5,25 mmol; final concentration = 4 M), H<sub>2</sub>O (94 μL, 5.23 mmol; final concentration = 4 M), dodecane (50 μL; 0.22 mmol; final concentration = 165 mM); final volume ≈1.33 mL. <sup>b</sup>Substrate conversion =  $\frac{[\text{substrate}]_{\text{initial}} - [\text{substrate}]_{\text{final}}}{[\text{substrate}]_{\text{initial}}} \cdot 100$ . <sup>c</sup>Epoxide selectivity =  $\frac{[\text{epoxide}]_{\text{final}}}{([\text{substrate}]_{\text{initial}} - [\text{substrate}]_{\text{final}})} \cdot 100$ . <sup>d</sup>TN is the turnover number with regard to epoxide. TOF<sub>i</sub> is the initial turnover frequency expressed in epoxide cycles per second. <sup>e</sup>100% of *cis*-epoxide is obtained. <sup>f</sup>100% of *trans*-epoxide is obtained. <sup>g</sup>Relation of cat:sub:ox:water 1:1000:2000:2000. <sup>h</sup>1:1 mixture of *endo*- and *exo*-epoxide was detected.

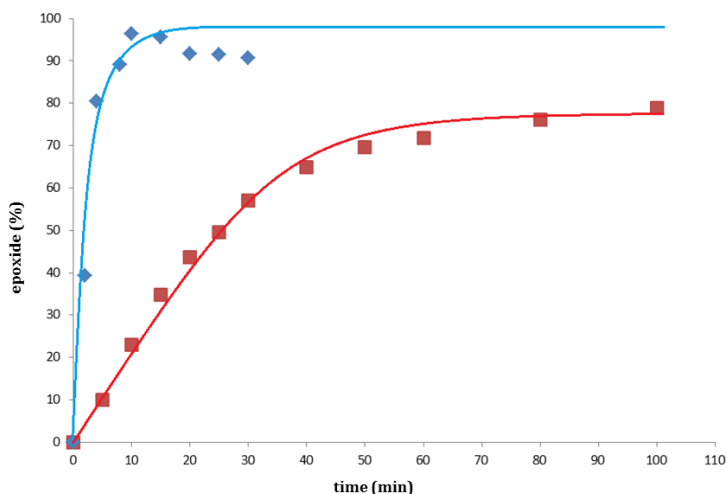


**Figure 6.** Turnover frequencies for epoxidation of alkenes catalyzed by **1** reported in TN·min<sup>-1</sup>.

The best catalytic activity in terms of TN and TOF has been detected in the epoxidation of cyclohexene with **2**<sup>+</sup>. The epoxide evolution trend is plotted in Figure 7 together with the trend of the reaction catalyzed by  $\{[\text{Ru}^{\text{II}}(\text{trpy})(\text{H}_2\text{O})]_2(\mu\text{-dcpd})\}^{2+}$  (**RuPDZ**), where dcpd<sup>2-</sup> is pyridazine-3,6-dicarboxylate anion. The initial rate for the cyclohexene oxide formation

#### Ru dinuclear complexes containing the pyrazole-3,5-dicarboxylic acid ligand

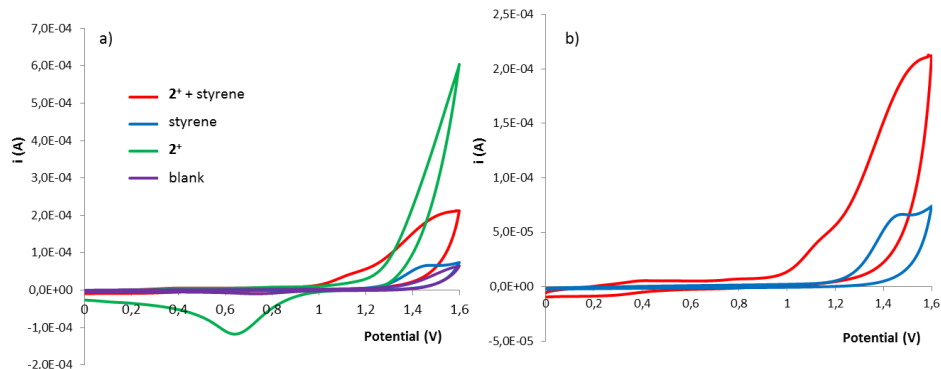
catalyzed by  $\mathbf{2}^+$  resulted of  $6.717 \text{ TN}\cdot\text{s}^{-1}$ , almost 10 times higher than the rate of  $0.676 \text{ TN}\cdot\text{s}^{-1}$  detected with **RuPDZ** (see Chapter III).



**Figure 7.** Evolution of cyclohexene oxide catalyzed by **1** (blue line) and  $\{[\text{Ru}^{\text{II}}(\text{trpy})_2(\mu\text{-dcpd})(\mu\text{-OH})]^+\}$  (red line).

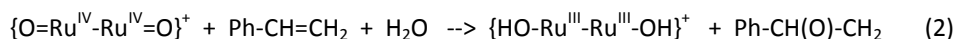
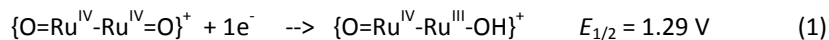
In order to extract information about the active species, the epoxidation of styrene has been investigated by cyclic voltammetry in a trifluoroethanol/triflic solution (Figure 8 a and b). After stirring complex **1** (0.7 mM) for 5 hours in order to ensure the formation the bis-aqua species  $\mathbf{2}^+$ , 5  $\mu\text{L}$  (21 mM) of styrene were added and cyclic voltammogram registered. As consequence of the addition of the substrate the electrocatalytic wave of the oxidation of water at 1.3 V disappeared and two new waves formed at  $E = 1.1 \text{ V}$  and  $1.4 \text{ V}$  (Figure 8a green and red lines). These waves were assigned to the oxidation of styrene catalyzed by  $\mathbf{2}^+$ ; blank experiments have been carried on in absence of catalyst (Figure 8a blue line). The oxidation in presence of  $\mathbf{2}^+$  takes place at lower potential ( $\approx 300 \text{ mV}$ ) respect to the experiment in absence of catalyst (Figure

8b). The anodic current increased linearly with the concentration of styrene, as shown in Figure S18

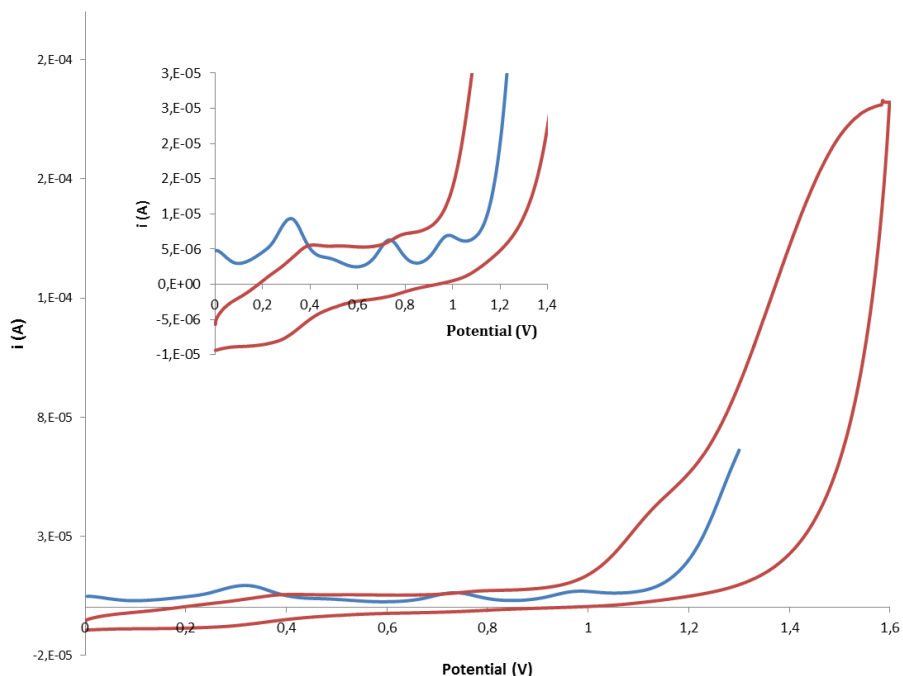


**Figure 8.** Electrochemical oxidation of styrene catalyzed by  $2^+$  in trifluoroethanol/triflic acid 1:1. (a)  $2^+$  (0.7 mM) + styrene (21 mM) (red line);  $2^+$  (0.7 mM) (green line); styrene (21 mM) (blue line); blank (purple line).  
 b)  $2^+$  (0.7 mM) + styrene (21 mM) (red line), styrene (21 mM) (blue line).

In figure 9 the cyclic voltammogram of the oxidation of styrene catalyzed by  $2^+$  is overlapped upon the DPV of  $2^+$ . The catalytic oxidation of styrene coincides with the formation of the  $Ru^{IV}Ru^{IV}$  bis-oxo species at  $E = 0.96$  V vs SSCE, that is consistent with an electrocatalytic oxidation of styrene to styrene oxide according to the following equations (the trpy and dcpz<sup>3-</sup> ligands are not shown),



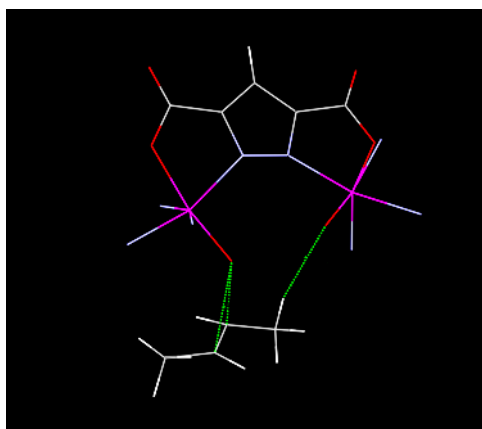




**Figure 9.** Electrochemical oxidation of styrene catalyzed by  $2^+$  in trifluoroethanol:triflic acid 1:1; cyclic voltammogram of  $2^+$  (0.7 mM) + styrene (21 mM) (red line), differential pulse voltammogram of  $2^+$  (0.7 mM).

The maintenance of configuration in the resulting epoxide for all substrates analyzed the electrochemical studies discussed above likely point towards a mechanism of concerted oxygen atom transfer from the  $\text{Ru}^{\text{IV}}=\text{O}$  active site to the double bond or a formation of a radical species followed by fast ring closure<sup>47-51</sup> (see Scheme 4 in Chapter III). In such a type of configuration one  $\text{Ru}=\text{O}$  would be responsible of the coordination and O transfer to the substrate while the other site, again a  $\text{Ru}=\text{O}$  species, would operate a further stabilization of the intermediate by H-bond formation with the hydrogen in  $\alpha$

or  $\beta$  respect to the double bond. The latter would at the same time impede the rotation avoiding the configuration inversion (Figure 10).

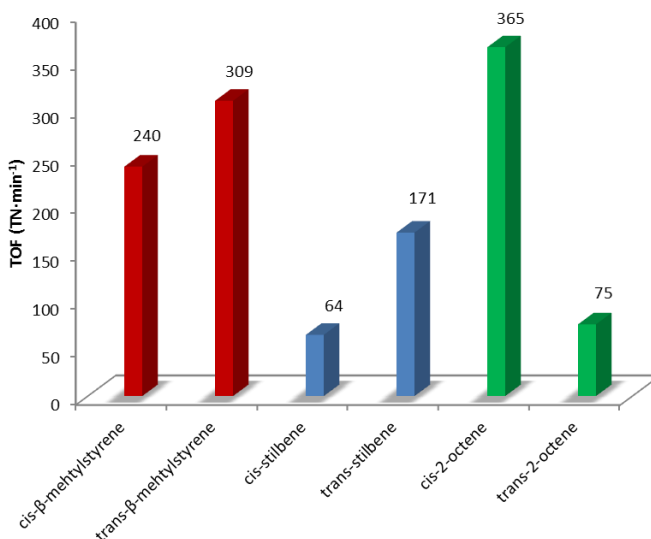


**Figure 10.** Model of side on approach and hydrogen bond of  $\{[\text{Ru}^{\text{IV}}(\text{trpy})(\text{O})]_2(\mu\text{-dcpd})\}^+$  to *trans*-2-butene.

From the TNs and TOFs data discussed above emerged some remarkable differences regarding the selectivity for some *cis* and *trans* isomers. While methylstyrene showed similar TOFs for both *cis* and *trans* alkenes, in the case of 2-octene and stilbene considerable differences resulted. Oxidation of *trans*-stilbene proceeded  $\approx 2.7$  times faster than oxidation of *cis*-stilbene. On the contrary epoxidation of *cis*-2-octene resulted  $\approx 4.9$  times faster than epoxidation of *trans*-octene. The presence of a H bond between a Ru=O group and the hydrogen atom next to the double bond could affect the orientation of the substrate molecule around the metals core generating a more favorable approach for some isomers respect to others. The hindering of substituents and the lack of hydrogen atoms in suitable orientation explains the lower activity toward the oxidation of substrates like triphenylethylene, 1-octene and stilbene. DFT calculations have been carried out in order to estimate the transition state energy for the processes.

## DFT Calculations.

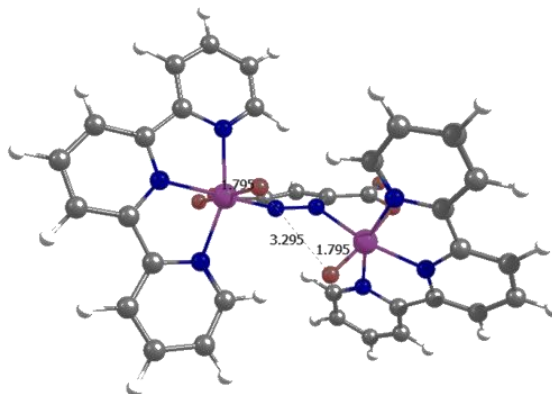
As shown in figure 6 the TOF values obtained experimentally resulted strongly influenced by the electronic properties and steric hindrance imposed by the substrate. Also, important differences were detected among different isomers of the same substrate. These gaps were minimum for the *cis* and *trans* isomers of  $\beta$ -methylstyrene but significant for the couple of isomers of the 2-octene (Figure 11).



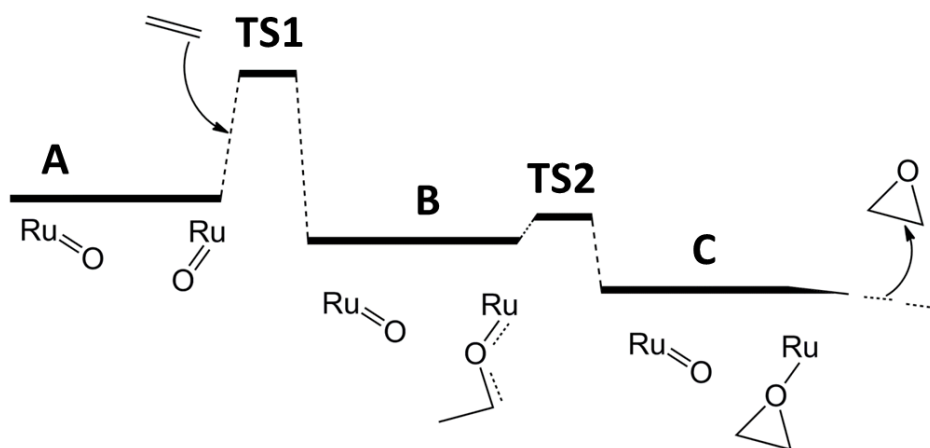
**Figure 11.** TOFs expressed in  $\text{TN} \cdot \text{min}^{-1}$  for epoxidation of *cis* and *trans* alkenes with  $2^+$ .

These data, together with the stereospecific nature of the catalyst, furnish an important starting point for the investigation of the approach and mechanism of epoxidation reaction catalyzed by  $2^+$ . For that purpose we performed Density Functional Theory (DFT) calculations of the catalytic epoxidation of *cis* and *trans* isomers of the three substrates mentioned above. A schematic draw of the studied mechanism is showed in Scheme 3, where with **A** is indicated

the starting active species represented in Figure 12, and with **B** and **C** the proposed intermediate species for the epoxide formation.



**Figure 12.** Optimized structure of the starting active  $\{O=Ru^{IV}-Ru^{IV}=O\}^+$  species, **A**, (distance in Å).

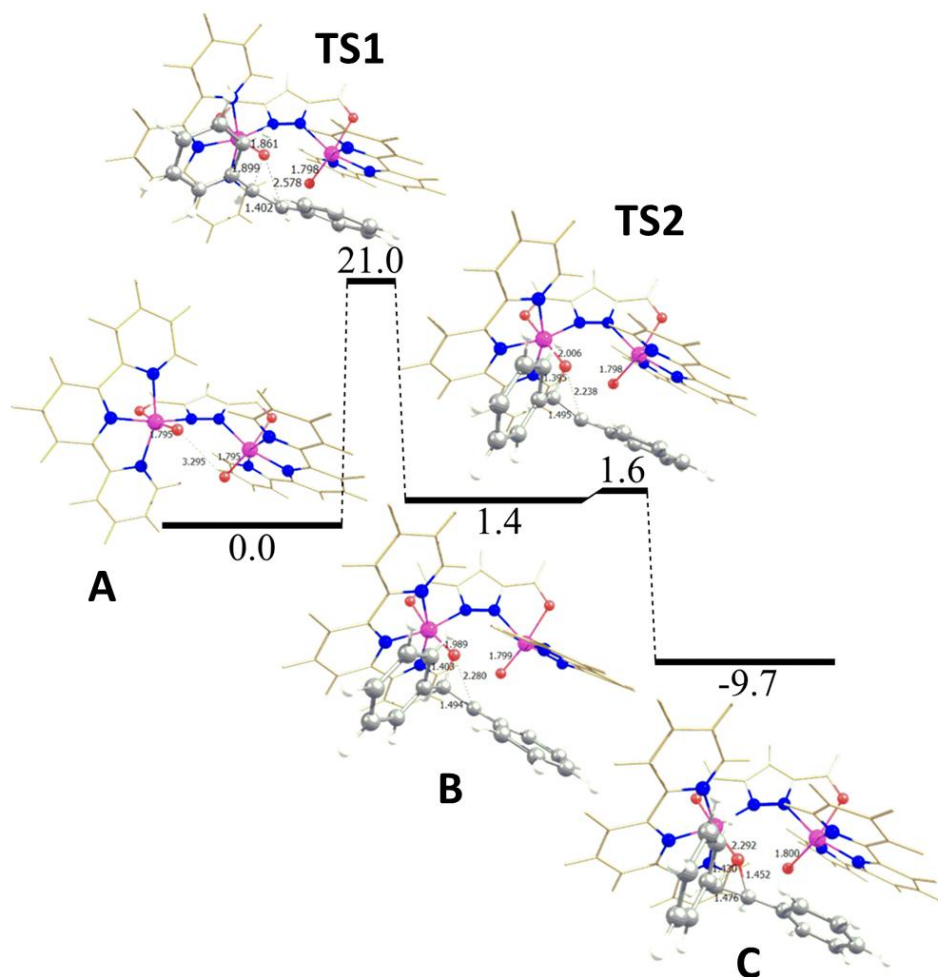


**Scheme 3.** Studied catalytic mechanism (simplified for the sake of clarity).

According to the electrochemical study presented in the previous section **A** has been as starting active species. It consists in a  $\{O=Ru^{IV}-Ru^{IV}=O\}^+$  species positively charged and a quintuplet ground multiplicity state. Reaction with the double bond of an alkene passes from a low barrier transition state (Scheme 3,

## Ru dinuclear complexes containing the pyrazole-3,5-dicarboxylic acid ligand

**TS1**) to form an intermediate with a Ru=O-C bond (**B**). In this species the second C atom of the double bond does not bond to the metal giving to **B** a radicalic character. To close the epoxide ring a second energy barrier corresponding to the transition state **TS2** and multiplicity crossing have to be overcome to form species **C** with triplet ground state multiplicity. The very low energetic gap between **B** and **TS2** (see Table 6) calculated for each substrate likely explains the stereospecificity of catalyst **2<sup>+</sup>** since its overcome implies a fast ring closure before a C-C bond rotation that would lead to the formation of the *trans* isomer. After liberation of the epoxide from **C**, species **A** is regenerated by coordination of a water molecule and oxidation to {O=Ru<sup>IV</sup>-Ru<sup>IV</sup>=O}<sup>+</sup>. This step might not be a barrierless process, however it was out of the scope for the present study because the step that forces the stereoselectivity is related to the barrier of the first transition state **TS1**. The substrate-catalyst adducts **B** calculated for each substrate presented weak C-O interactions with distance of about 4-5 Å between the O atom of one Ru<sup>IV</sup>=O group and C atom of the double bond of the alkene. These intermediates resulted thermodynamically not stable and rapidly overcome the energy barrier of **TS2** to form **C**. The lowest reaction pathway for the epoxidation of each substrate, both *cis* and *trans*, has been calculated. In Figure 13 the overall species involved in the oxidation of *cis*-stilbene by **2<sup>+</sup>** are shown.



**Figure 13.** Reaction pathway for the epoxidation of *cis*-stilbene with  $2^+$  (distance in Å)

Species **A** displays a quintuplet multiplicity as ground state with a weak O-O interaction between the oxygen atoms of the Ru=O groups. The corresponding structure with a triplet multiplicity state is 13.8 kcal/mol higher in energy. On the other hand the *cis* alkenes isomer are always less stable than the *trans* by 5.3, 2.6 and 1.2 kcal/mol for stilbene,  $\beta$ -methylstyrene, and 2-octene

## Ru dinuclear complexes containing the pyrazole-3,5-dicarboxylic acid ligand

respectively. It is interesting to mention that the transition state **TS1** in Figure 13 shows an initial C-O bond distance between the O atom of one Ru<sup>IV</sup>=O group and C atom of the double bond of the alkene of 1.899 Å that decreases until a value of 1.403 in the radical species **B** and then reaches the values of 1.430 and 1.454 Å for the epoxidized species **C**. At the same time the R-O bond distance corresponds to 1.795 Å in **A**, 1.989 Å in **B**, and finally at 2.292 Å in **C**.

In Table 6 the energy data for the six most stable reaction pathways are presented. These results highlight a trend in the value **TS1** that increases from *cis*- $\beta$ -methylstyrene, to stilbene, and reaches a maximum for 2-octene. A similar tendency resulted for the energy values of the radical species **B** but changes markedly for the epoxidized species **C**, among which the *cis*-octene one resulted the most stable. It is worth to mention that the crossing of multiplicity takes place after the radical species **B** for both 2-octene and  $\beta$ -methylstyrene, but in the case of stilbene **B** prefers the triplet multiplicity.

**Table 6.** Relative energies of the most stable epoxidation pathways in kcal/mol.

substrate	A	TS1	B	TS2	C
<i>cis</i> -stilbene	0.0	21.0	1.4	1.6	-9.7
<i>trans</i> -stilbene	0.0	20.3	7.9	9.1	-6.6
<i>cis</i> - $\beta$ -methylstyrene	0.0	18.4	0.4	3.8	-10.7
<i>trans</i> - $\beta$ -methylstyrene	0.0	18.1	2.5	4.3	-10.4
<i>cis</i> -2-octene	0.0	22.8	10.5	11.1	-14.2
<i>trans</i> -2-octene	0.0	24.9	11.9	12.5	-13.8

Having a look at the **TS1** values presented in Table 6 the resulting trend is in agreement with the experimental data of the epoxidation reaction catalyzed by 2<sup>+</sup>. As expected *cis* and *trans* stilbene present a difference in energy (0.7

kcal/mol) in favor of the oxidation of the *trans* isomers while for the 2-octene couple the energetic gap of 2.1 kcal/mol is dramatically in favor of the oxidation of the *cis* isomer in according with the experimental data that showed a TOF for the epoxidation of *cis*-2-octene almost 5 times higher than the one for the oxidation of *trans*-2-octene (Figure 11). Lastly the 0.3 kcal/mol that separate the **TS1**s for the epoxidation of *cis* and *trans*- $\beta$ -methylstyrene are reasonably in agreement with the similar catalytic results obtained experimentally. The **TS1** representations for all the substrates studied are reported in Figure S19.

In Table 7 is resumed the study of the decomposition energy for each substrate. This analysis consists of splitting the binding energy between the catalyst and the substrate into the deformation and the interaction energies. The interaction energy,  $E_{\text{intr}}$  is the energy product of the interaction of the frozen geometries of both fragments in the optimized species, whereas the deformation energy,  $E_{\text{def}}$  is the energy necessary to modify the structures of both fragments when they are free to the geometry of optimized species. The deformation energy is made of the sum of the  $E_{\text{def}}$  of the catalysts and the  $E_{\text{def}}$  of the substrate. Comparing the **TS1** of stilbene results that the *trans* isomer has a lower barrier because of having a less positive interaction energy, being the deformation energy very similar for both conformations. For  $\beta$ -methylstyrene the barriers are quite similar, with a difference of 0.3 kcal/mol between the *cis* and *trans* isomers, which is lower than the 0.7 kcal/mol and for stilbene. It is interesting to note that the *trans*- $\beta$ -methylstyrene has higher deformation energy but lower interaction energy respect to the *cis* isomers. The values balance into similar BE values. Finally for the non-arylic substrate, 2-octene, the deformation energy is similar, but the **TS1** of the *trans* isomer is disfavored because of the interaction energy. Also, the low stability of species



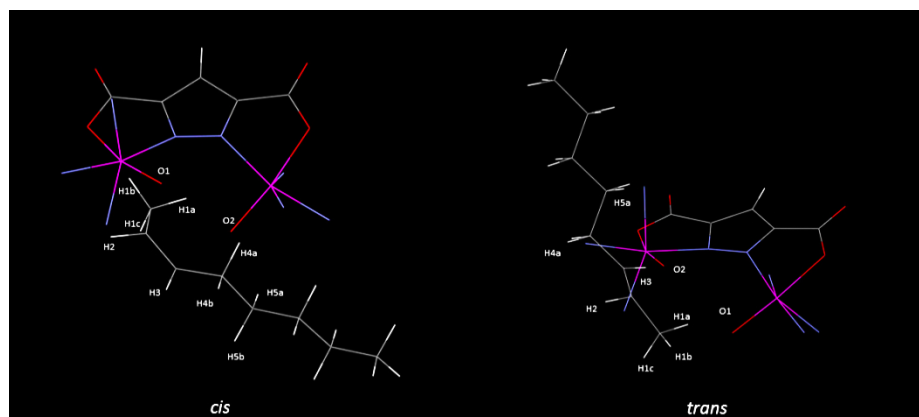
**Ru dinuclear complexes containing the pyrazole-3,5-dicarboxylic acid ligand**

**B** in the oxidation of 2-octene can be easily explained by the lack of groups, like the phenyl ring of  $\beta$ -methylstyrene and stilbene, able to delocalize the unpaired electrons.

**Table 7.** Energy decomposition analysis, values in kcal/mol.  $E_{\text{def catalyst}}$  = deformation energy of the catalyst.  $E_{\text{def substrate}}$  = deformation energy of the substrate.  $E_{\text{def}} = E_{\text{def catalyst}} + E_{\text{def substrate}}$ .  $E_{\text{int}}$  = interaction energy. BE = barriers energy.

		$E_{\text{def catalyst}}$	$E_{\text{def substrate}}$	$E_{\text{def}}$	$E_{\text{int}}$	BE
<i>cis</i> -stilbene	<b>TS1</b>	4.4	7.7	12.1	8.9	21.0
	<b>B</b>	11.7	31.3	43.0	-41.6	1.4
	<b>TS2</b>	13.2	27.5	40.7	-39.1	1.6
	<b>C</b>	35.7	15.9	51.6	-61.3	-9.7
<i>trans</i> -stilbene	<b>TS1</b>	4.7	7.9	12.6	7.7	20.3
	<b>B</b>	12.9	41.5	54.4	-46.4	7.9
	<b>TS2</b>	18.7	22.2	39.7	-31.8	9.1
	<b>C</b>	39.5	18.1	57.6	-64.2	-6.6
<i>cis</i> - $\beta$ -methylstyrene	<b>TS1</b>	1.5	9.4	10.9	7.5	18.4
	<b>B</b>	9.1	48.8	57.9	-57.5	0.4
	<b>TS2</b>	19.5	18.4	37.9	-34.1	3.8
	<b>C</b>	34.2	16.0	50.2	-60.9	-10.7
<i>trans</i> - $\beta$ -methylstyrene	<b>TS1</b>	2.8	9.0	11.8	6.2	18.1
	<b>B</b>	9.0	34.0	43.0	-40.5	2.5
	<b>TS2</b>	18.1	21.9	41.0	-36.7	4.3
	<b>C</b>	30.8	16.4	47.2	-57.6	-10.4
<i>cis</i> -2-octene	<b>TS1</b>	3.7	7.6	11.3	11.5	22.8
	<b>B</b>	10.6	56.8	67.4	-56.9	10.5
	<b>TS2</b>	13.5	25.7	39.2	-28.1	11.1
	<b>C</b>	29.8	16.0	45.8	-60.0	-14.2
<i>trans</i> -2-octene	<b>TS1</b>	2.2	8.9	11.1	13.8	24.9
	<b>B</b>	10.7	34.2	44.9	-33.0	11.9
	<b>TS2</b>	14.3	25.5	39.8	-27.3	12.5
	<b>C</b>	34.4	17.0	51.4	-65.2	-13.8

Lastly an investigation of the distances between the oxygen atoms of the Ru=O groups and the most close H atoms of the alkene in **TS1**s has been done in order to individuate some possible sites for hydrogen bonds. For each **TS1** distances in the range of 2.2-3.0 Å, suitable for hydrogen bonding, have been found between the Ru=O groups and the H of the alkene (Table 8-12). In this approach the double bond of the substrate interacts through a C-O bond with one Ru=O group and through a hydrogen bond with the oxygen atom second R=O group that thus fixes the structure. This could be evaluated as a further hint for the explanation of the stereospecific nature of **2<sup>†</sup>**. Likely the presence of these bonds would avoid the C-C rotation favoring even more the fast ring closure proposed above. Considering the example of the *cis* and *trans*-octene the distance O1-H1b (2.353 Å) in the *trans* isomer is much shorter than the O2H3 distance in *cis*-octene resulting in a stronger interaction and thus in a higher stabilization of **TS1**. The energetic barrier would then results higher and the kinetic of reaction slower (Figure 13 and Tables 8 and 9). Similarly, the lack of a suitable distance for hydrogen bond between O2 and H4 in the **TS1** of *trans*-stilbene epoxidation makes its kinetic faster than the one of *cis*-stilbene epoxidation which **TS1** is stabilized by O1H3 (2.592 Å) hydrogen bond (Figure 15 and Tables 12 and 13).



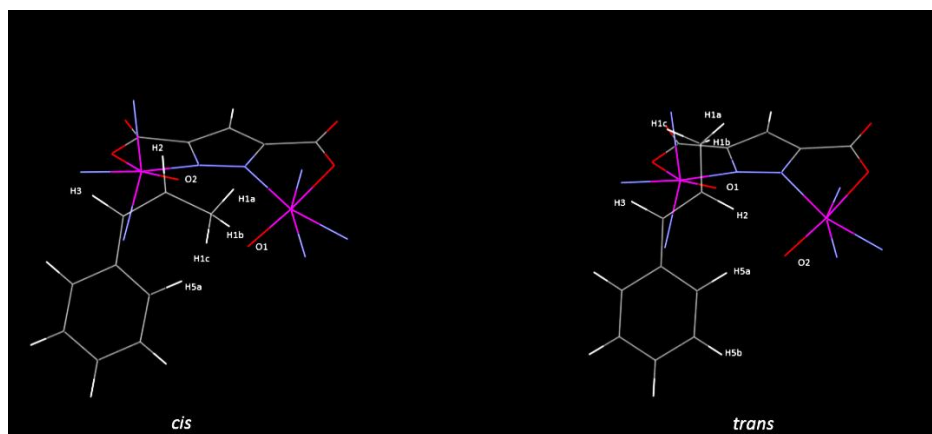
**Figure 13.** TS1 of the epoxidation of *cis* and *trans*-2-octene.

**Table 8.** Distance in (Å) of closest H atoms and Ru=O for TS1 of *cis*-2-octene.

<i>cis</i> -2-octene			
bond distance (Å) < 3 Å		bond distance (Å) > 3 Å	
O1-H2	2.270	O2-H4a	3.200
O2-H5b	2.340	O1-H1c	3.591
O1-H1b	2.630	O2-H5b	3.817
O1-H1a	2.731	O2-H4b	4.427
O2-H3	2.984		

**Table 9.** Distance in (Å) of closest H atoms and Ru=O for TS1 of *trans*-2-octene.

<i>trans</i> -2-octene			
bond distance (Å) < 3 Å		bond distance (Å) > 3 Å	
O2-H2	2.248	O1-H1a	3.103
O1-H1b	2.353	O2-H3	3.152
		O2-H5a	3.256
		O2-H4a	3.337
		O1-H1c	4.018



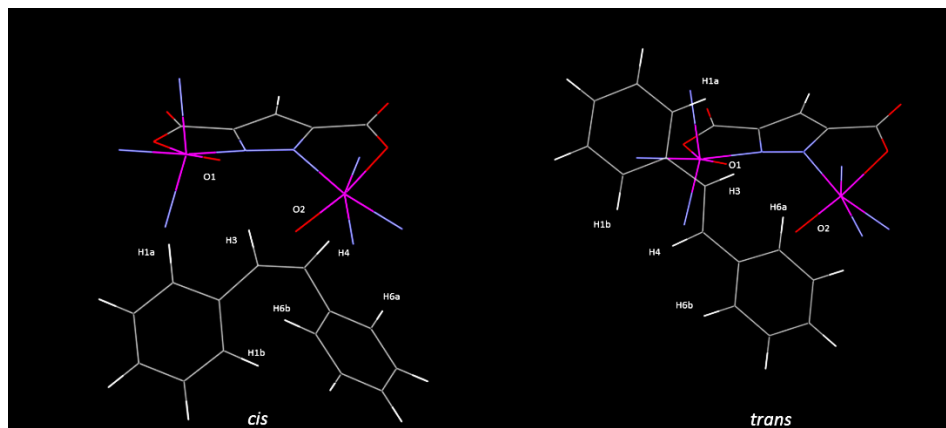
**Figure 14.** TS1 of the epoxidation of *cis* and *trans*- $\beta$ -methylstyrene.

**Table 10.** Distance in ( $\text{\AA}$ ) of closest H atoms and Ru=O for TS1 of *cis*- $\beta$ -methylstyrene.

<i>cis</i> - $\beta$ -methylstyrene			
bond distance ( $\text{\AA}$ ) < 3 $\text{\AA}$		bond distance ( $\text{\AA}$ ) > 3 $\text{\AA}$	
O2-H2	2.224	O2-H5a	3.028
O1-H1b	2.312	O2-H1a	3.120
O2-H1b	2.372	O2-H3	3.257
O1-H5a	2.719	O2-H1c	3.484

**Table 11.** Distance in ( $\text{\AA}$ ) of closest H atoms and Ru=O for TS1 of *trans*- $\beta$ -methylstyrene.

<i>trans</i> - $\beta$ -methylstyrene			
bond distance ( $\text{\AA}$ ) < 3 $\text{\AA}$		bond distance ( $\text{\AA}$ ) > 3 $\text{\AA}$	
O1-H2	2.145	O1-H1c	3.117
O1-H1a	2.542	O1-H3	3.370
O2-H5a	2.596	O1-H1b	3.595
O1-H5a	2.670	O2-H2	3.656



**Figure 15.** TS1 of the epoxidation of *cis* and *trans*-stilbene.

**Table 12.** Distance in (Å) of closest H atoms and Ru=O for TS1 of *cis*-stilbene.

<i>cis</i> -stilbene			
bond distance (Å) < 3 Å		bond distance (Å) > 3 Å	
O2-H4	2.248	O1-H5a	3.274
O2-H6b	2.535	O1-H4	3.877
O1-H3	2.592	O2-H6a	4.203
O2-H3	2.868	O2-H1b	4.215

**Table 13.** Distance in (Å) of closest H atoms and Ru=O for TS1 of *trans*-stilbene.

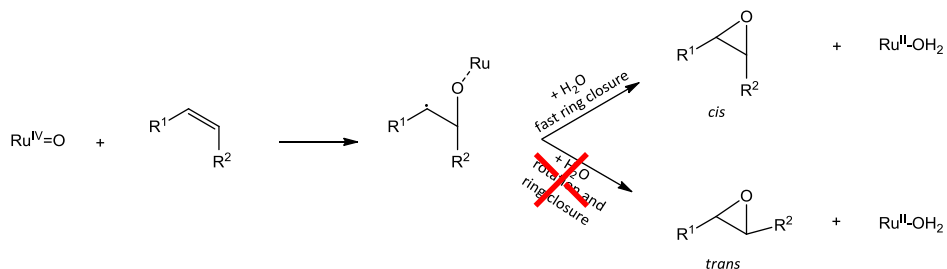
<i>trans</i> -stilbene			
bond distance (Å) < 3 Å		bond distance (Å) > 3 Å	
O1-H4	2.155	O1-H3	3.151
O1-H6b	2.795	O2-H1b	3.421
		O2-H4b	3.852
		O2-H1a	4.021
		O1-H6a	4.046

#### IV. iv. Conclusions

A new ruthenium dinuclear acetato bridge complex **1** containing the bridging ligand pyrazole-3,5-dicarboxylic acid has been prepared and characterized. Its efficiency as redox catalyst has been tested in the oxidation of water and olefins. The formation of a bis-aqua species **2<sup>+</sup>** has been demonstrated by electrochemical study in aqueous media. The activity toward the oxidation of double bond in the presence of (diacetoxyiodo)benzene has been deeply investigated for a series of alkenes with different geometric and electronic properties leading to important information about the mechanism of the reaction. The elevated turnover numbers and turnover frequencies obtained have been compared with the data of epoxidation reactions catalyzed by the analogous 6 member ring based complex  $\{[\text{Ru}^{\text{II}}(\text{trpy})(\text{H}_2\text{O})_2(\mu\text{-dcpd})]\}^{2+}$  described in Chapter III. **2<sup>+</sup>** resulted a highly active catalyst for the oxidation of both cyclic and linear alkenes with TOFs up to  $6.7 \text{ TN}\cdot\text{s}^{-1}$  and TN up to 17000. Electrochemical studies in the presence of styrene clearly demonstrated that a  $\text{Ru}^{\text{IV}}\text{Ru}^{\text{IV}}$  bis-oxo complex is the active species in the epoxidation reaction. In order to explain the elevated performance and stereospecificity of **2<sup>+</sup>** a supramolecular catalytic approach mediated by hydrogen bond which leads to a stabilization of the catalyst-substrate intermediate has been proposed. DFT calculations of the epoxidation process of 3 different alkenes, both *cis* and *trans* isomers, have been performed. The best transition states have been individuated and discussed in terms of energy and bond lengths. The data obtained by DFT calculations were strongly in agreement with the experimental results and likely point towards a mechanism of a radical path where the ring closing that generates the final epoxide is, possibly due also to

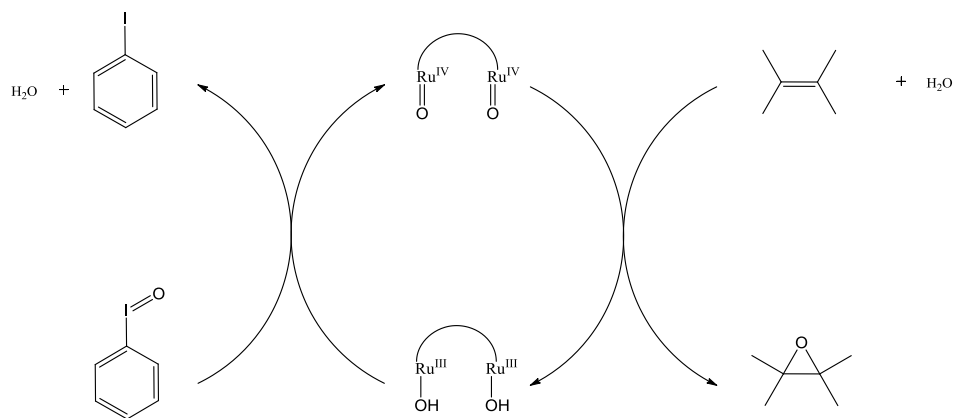
**Ru dinuclear complexes containing the pyrazole-3,5-dicarboxylic acid ligand**

the presence of hydrogen bonds, much faster than the C-C rotation of the generated radical (Scheme 4).



**Scheme 4.** Proposed reaction pathway for the epoxidation of *cis*- $\beta$ -methylstyrene by  $\text{Ru}^{\text{IV}}=\text{O}$ .

In conclusion the catalytic cycle proposed for the epoxidation of alkenes catalyzed by  $\mathbf{2}^{2+}$  is showed in Scheme 5.



**Scheme 5.** Proposed global catalytic reaction paths for the epoxidation of alkenes catalyzed by  $\mathbf{2}^{2+}$  in the presence of an excess of  $\text{PhI}(\text{OAc})_2$  and water.

## IV. v. Associated content

### Supportin Information

X-Ray crystallographic data in CIF format, additional spectroscopic, electrochemical and DFT data.

## IV. vi. Acknowledgements

DFT calculations were performed by Dr. Albert Poater Teixidor of the University of Girona (UDG).



## IV. vii. References

- (1) Meeuwissen, J.; Reek, J. N. H. *Nat Chem* **2010**, *2*, 615.
- (2) Koblenz, T. S.; Wassenaar, J.; Reek, J. N. H. *Chem. Soc. Rev.* **2008**, *37*, 247.
- (3) Yoshizawa, M.; Klosterman, J. K.; Fujita, M. *Angew. Chem., Int. Ed.* **2009**, *48*, 3418.
- (4) Brown, C. J.; Miller, G. M.; Johnson, M. W.; Bergman, R. G.; Raymond, K. N. *J. Am. Chem. Soc.* **2011**, *133*, 11964.
- (5) Breslow, R.; Zhang, X.; Huang, Y. *J. Am. Chem. Soc.* **1997**, *119*, 4535.
- (6) Yang, J.; Breslow, R. *Angew. Chem., Int. Ed.* **2000**, *39*, 2692.
- (7) Fang, Z.; Breslow, R. *Org. Lett.* **2006**, *8*, 251.
- (8) Das, S.; Incarvito, C. D.; Crabtree, R. H.; Brudvig, G. W. *Science* **2006**, *312*, 1941.
- (9) Lee, S. J.; Cho, S.-H.; Mulfort, K. L.; Tiede, D. M.; Hupp, J. T.; Nguyen, S. T. *J. Am. Chem. Soc.* **2008**, *130*, 16828.
- (10) Wyler, R.; de, M. J.; Rebek, J., Jr. *Angew. Chem.* **1993**, *105*, 1820.
- (11) Jonsson, S.; Odille, F. G. J.; Norrby, P.-O.; Waernmark, K. *Chem. Commun.* **2005**, 549.
- (12) Smejkal, T.; Breit, B. *Angew. Chem., Int. Ed.* **2008**, *47*, 3946.
- (13) Lu, Y.; Johnstone, T. C.; Arndtsen, B. A. *J. Am. Chem. Soc.* **2009**, *131*, 11284.
- (14) Fackler, P.; Berthold, C.; Voss, F.; Bach, T. *J. Am. Chem. Soc.* **2010**, *132*, 15911.
- (15) Sullivan, B. P.; Calvert, J. M.; Meyer, T. J. *Inorg. Chem.* **1980**, *19*, 1404.
- (16) Data collection with APEX II versions v1.0-22, Madison, Wisconsin, USA.
- (17) Data reduction with Bruker SAINT versions V.2.10(2003), Madison, Wisconsin, USA.
- (18) SADABS: V.2.10(2003); V2008 and V2008/1 Bruker (2001). Bruker AXS Inc., M., Wisconsin, USA. Blessing *Acta Cryst.* **1995**, *A51*, 33.
- (19) TWINABS Version 2008/4 Bruker AXS; Blessing *Acta Cryst.* **1995**, *A51*, 33.
- (20) Sheldrick, G. M. S. v. V. a. *Acta Cryst.* **2008**, *A64*, 112.
- (21) SQUEEZE implemented in Platon: Spek, A. L. *J. Appl. Cryst.* **2003**, *36*.
- (22) M. J. Frisch, G. W. Trucks; H. B. Schlegel; G. E. Scuseria; M. A. Robb; J. R. Cheeseman; G. Scalmani; V. Barone; B. Mennucci; G. A. Petersson; H. Nakasdfstsuji; M. Caricato; X. Li; H. P. Hratchian; A. F. Izmaylov; J. Bloino; G. Zheng; J. L. Sonnenberg; M. Hada; M. Ehara; K. Toyota; R. Fukuda; J. Hasegawa; M. Ishida; T. Nakajima; Y. Honda; O. Kitao; H.

- Nakai; T. Vreven, J. A. Montgomery, Jr., J. E. Peralta, F. Ogliaro, M. Bearpark, J. J. Heyd, E. Brothers, K. N. Kudin, V. N. Staroverov, R. Kobayashi, J. Normand, K. Raghavachari, A. Rendell, J. C. Burant; S. S. Iyengar; J. Tomasi; M. Cossi; N. Rega; J. M. Millam; M. Klene; J. E. Knox; J. B. Cross; V. Bakken; C. Adamo; J. Jaramillo; R. Gomperts; R. E. Stratmann; O. Yazyev; A. J. Austin; R. Cammi; C. Pomelli; J. W. Ochterski; R. L. Martin; K. Morokuma; V. G. Zakrzewski; G. A. Voth; P. Salvador; J. J. Dannenberg; S. Dapprich; A. D. Daniels; Ö. Farkas; J. B. Foresman; J. V. Ortiz; J. Cioslowski; D. J. Fox *Gaussian 09*; Gaussian, Inc.: Wallingford CT, **2009**.
- (23) Zhao, Y.; Truhlar, D. G. *J. Chem. Phys.* **2006**, *125*, 194101/1.
- (24) Schaefer, A.; Horn, H.; Ahlrichs, R. *J. Chem. Phys.* **1992**, *97*, 2571.
- (25) Kuechle, W.; Dolg, M.; Stoll, H.; Preuss, H. *J. Chem. Phys.* **1994**, *100*, 7535.
- (26) Leininger, T.; Nicklass, A.; Stoll, H.; Dolg, M.; Schwerdtfeger, P. *J. Chem. Phys.* **1996**, *105*, 1052.
- (27) Haeussermann, U.; Dolg, M.; Stoll, H.; Preuss, H.; Schwerdtfeger, P.; Pitzer, R. M. *Mol. Phys.* **1993**, *78*, 1211.
- (28) Zhao, Y.; Truhlar, D. G. *Theor. Chem. Acc.* **2008**, *120*, 215.
- (29) Barone, V.; Cossi, M. *J. Phys. Chem. A* **1998**, *102*, 1995.
- (30) Tomasi, J.; Persico, M. *Chem. Rev.* **1994**, *94*, 2027.
- (31) Laurent, F.; Plantalech, E.; Donnadieu, B.; Jimenez, A.; Hernandez, F.; Martinez-Ripoll, M.; Biner, M.; Llobet, A. *Polyhedron* **1999**, *18*, 3321.
- (32) Romero, I.; Rodriguez, M.; Llobet, A.; Collomb-Dunand-Sauthier, M.-N.; Deronzier, A.; Parella, T.; Stoeckli-Evans, H. *Dalton* **2000**, 1689.
- (33) Rodriguez, M.; Romero, I.; Llobet, A.; Deronzier, A.; Biner, M.; Parella, T.; Stoeckli-Evans, H. *Inorg. Chem.* **2001**, *40*, 4150.
- (34) Sens, C.; Rodriguez, M.; Romero, I.; Llobet, A.; Parella, T.; Benet-Buchholz, J. *Inorg. Chem.* **2003**, *42*, 8385.
- (35) Sens, C.; Rodriguez, M.; Romero, I.; Llobet, A.; Parella, T.; Sullivan, B. P.; Benet-Buchholz, J. *Inorg. Chem.* **2003**, *42*, 2040.
- (36) Sala, X.; Poater, A.; Romero, I.; Rodriguez, M.; Llobet, A.; Solans, X.; Parella, T.; Santos, T. M. *Eur. J. Inorg. Chem.* **2004**, 612.
- (37) Sala, X.; Romero, I.; Rodriguez, M.; Llobet, A.; Gonzalez, G.; Martinez, M.; Benet-Buchholz, J. *Inorg. Chem.* **2004**, *43*, 5403.
- (38) Sens, C.; Romero, I.; Rodriguez, M.; Llobet, A.; Parella, T.; Benet-Buchholz, J. *J. Am. Chem. Soc.* **2004**, *126*, 7798.
- (39) Katz, N. E.; Fagalde, F.; Lis, d. K. N. D.; Mellace, M. G.; Romero, I.; Llobet, A.; Benet-Buchholz, J. *Eur. J. Inorg. Chem.* **2005**, 3019.

## Ru dinuclear complexes containing the pyrazole-3,5-dicarboxylic acid ligand

- (40) Katz, N. E.; Romero, I.; Llobet, A.; Parella, T.; Benet-Buchholz, J. *Eur. J. Inorg. Chem.* **2005**, 272.
- (41) Mola, J.; Rodriguez, M.; Romero, I.; Llobet, A.; Parella, T.; Poater, A.; Duran, M.; Sola, M.; Benet-Buchholz, J. *Inorg. Chem.* **2006**, *45*, 10520.
- (42) Serrano, I.; Sala, X.; Plantalech, E.; Rodriguez, M.; Romero, I.; Jansat, S.; Gomez, M.; Parella, T.; Stoeckli-Evans, H.; Solans, X.; Font-Bardia, M.; Vidjayacoumar, B.; Llobet, A. *Inorg. Chem.* **2007**, *46*, 5381.
- (43) Dakkach, M.; Lopez, M. I.; Romero, I.; Rodriguez, M.; Atlamsani, A.; Parella, T.; Fontrodona, X.; Llobet, A. *Inorg. Chem.* **2010**, *49*, 7072.
- (44) Mola, J.; Dinoi, C.; Sala, X.; Rodriguez, M.; Romero, I.; Parella, T.; Fontrodona, X.; Llobet, A. *Dalton Trans.* **2011**, *40*, 3640.
- (45) Roeser, S.; Farras, P.; Bozoglian, F.; Martinez-Belmonte, M.; Benet-Buchholz, J.; Llobet, A. *ChemSusChem* **2011**, *4*, 197.
- (46) Sens, C.; Romero, I.; Rodríguez, M.; Llobet, A.; Parella, T.; Benet-Buchholz, J. *J. Am. Chem. Soc.* **2004**, *126*, 7798.
- (47) Muray, E.; Illa, O.; Castillo, J. A.; Alvarez-Larena, A.; Bourdelande, J. L.; Branchadell, V.; Ortuno, R. M. *J. Org. Chem.* **2003**, *68*, 4906.
- (48) Kumar, D.; de, V. S. P.; Shaik, S. *Chem.-Eur. J.* **2005**, *11*, 2825.
- (49) Baciocchi, E.; Boschi, T.; Cassioli, L.; Galli, C.; Jaquinod, L.; Lapi, A.; Paolesse, R.; Smith, K. M.; Tagliatesta, P. *Eur. J. Org. Chem.* **1999**, 3281.
- (50) Zona, T. A.; Goodman, J. L. *J. Am. Chem. Soc.* **1995**, *117*, 5879.
- (51) Srinivasan, K.; Michaud, P.; Kochi, J. K. *J. Am. Chem. Soc.* **1986**, *108*, 2309.

UNIVERSITAT ROVIRA I VIRGILI

NEW RUTHENIUM, MANGANESE AND COBALT DINUCLEAR COMPLEXES AS REDOX CATALYSTS.

UNFOLDING THE ESSENTIAL STEPS FOR THE GENERATION OF SOLAR FUELS

Carlo Di Giovanni

Dipòsit Legal: T. 1429-2012

UNIVERSITAT ROVIRA I VIRGILI

NEW RUTHENIUM, MANGANESE AND COBALT DINUCLEAR COMPLEXES AS REDOX CATALYSTS.






UNFOLDING THE ESSENTIAL STEPS FOR THE GENERATION OF SOLAR FUELS

Carlo Di Giovanni

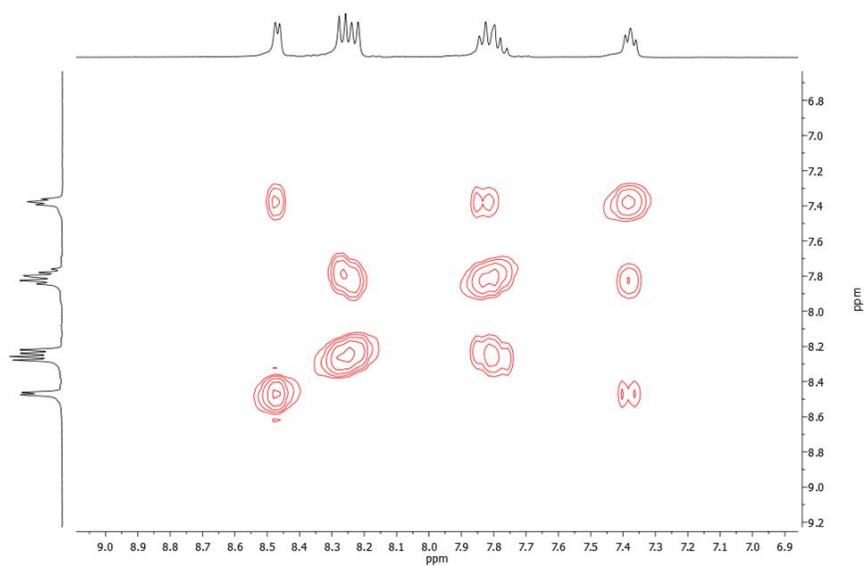
Dipòsit Legal: T. 1429-2012

# Chapter IV

## Supporting Information

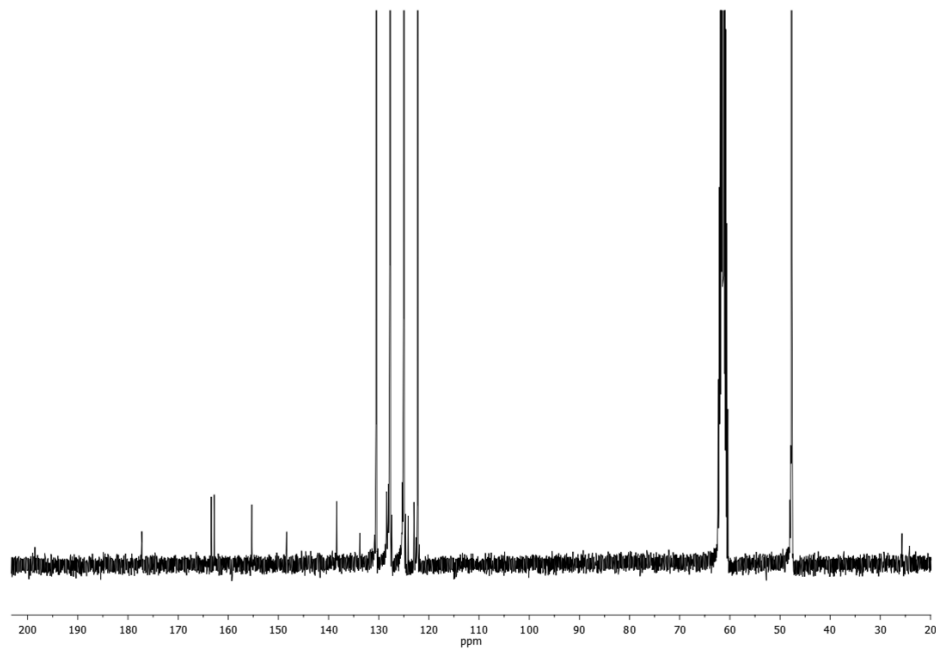
-  *NMR Characterization of 1: Figure SI1- Figure SI5*
-  *ESI-MS of 1: Figure SI6*
-  *DPV of 1 after catalytic epoxidation experiment: Figure SI7*
-  *Substrate concentration dependence of  $i_{pa}$*
-  *TS1 of the epoxidation process of the *cis* and *trans* alkenes*



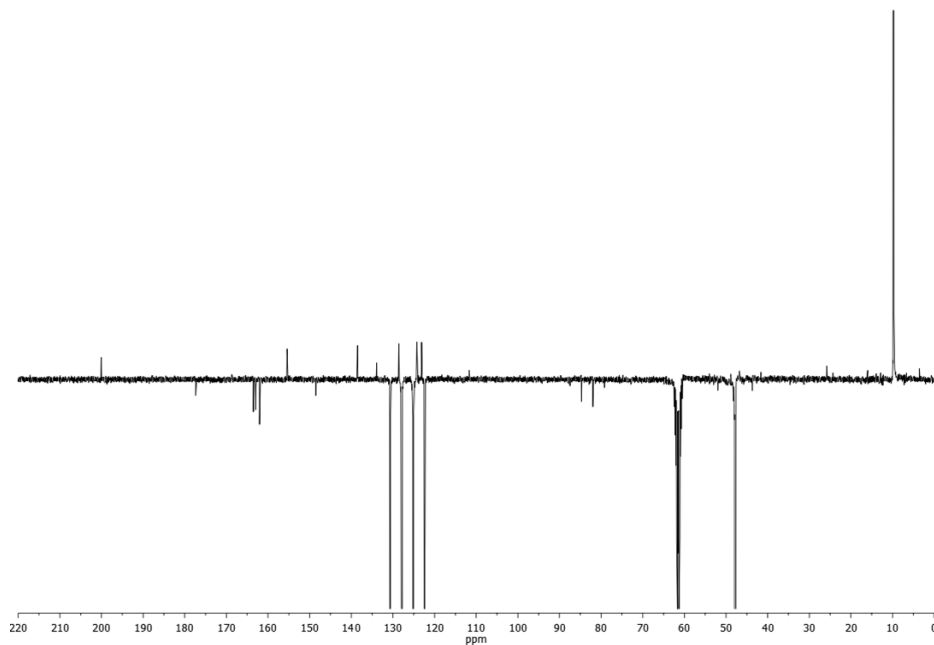


**Figure S11.** COSY of **1** (400 MHz, 298 K,  $\text{CF}_3\text{CD}_2\text{OD}$ ).





**Figure SI2.**  $^{13}\text{C}$ -NMR of **1** (100 MHz, 298 K,  $\text{CF}_3\text{CD}_2\text{OD}$ ).



**Figure S13.** DEPTQ-135 of **1** (100 MHz, 298 K,  $\text{CF}_3\text{CD}_2\text{OD}$ ).

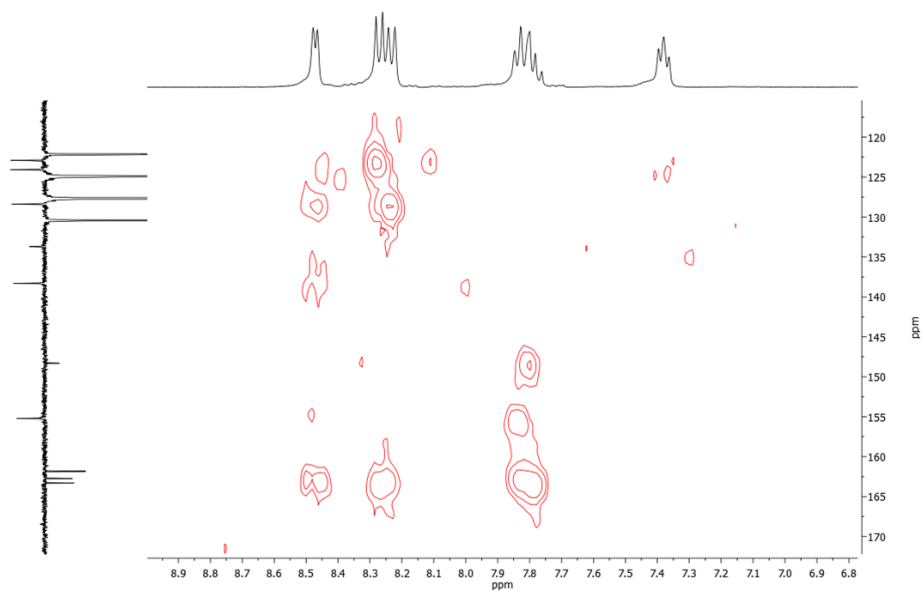
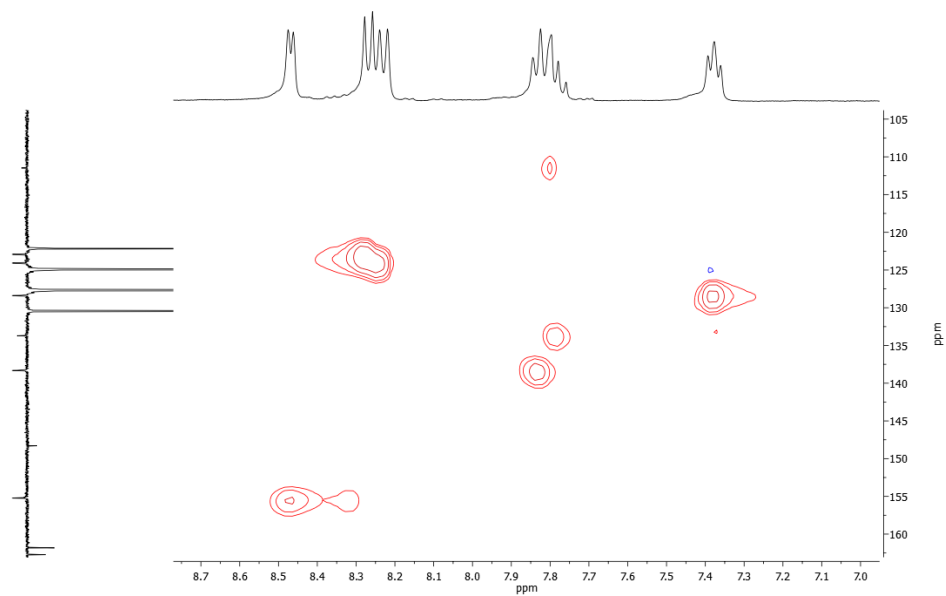


Figure SI4. HMBC of **1** (298 K,  $\text{CF}_3\text{CD}_2\text{OD}$ ).



**Figure S15.** HSQC of **1** (298 K,  $\text{CF}_3\text{CD}_2\text{OD}$ ).

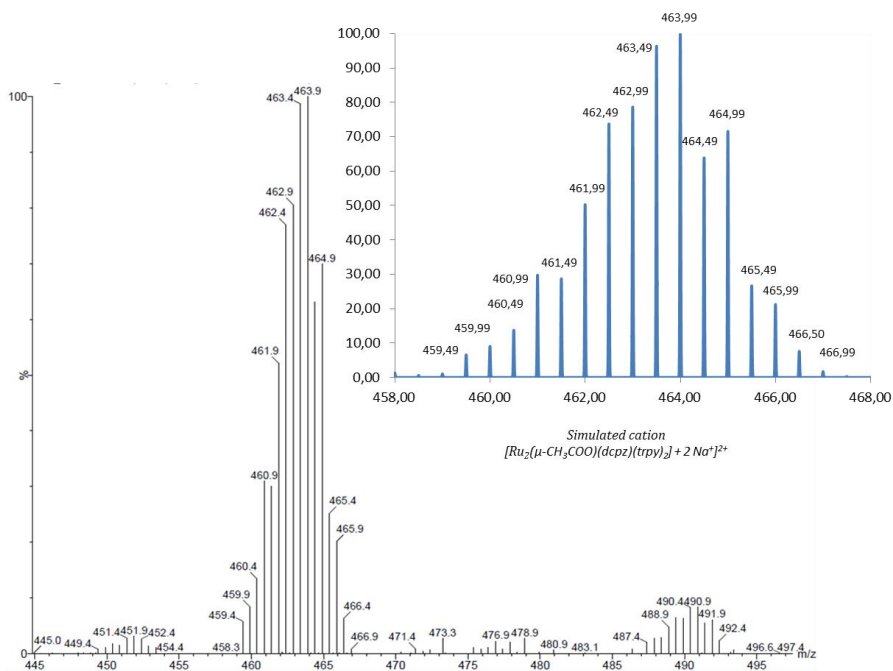
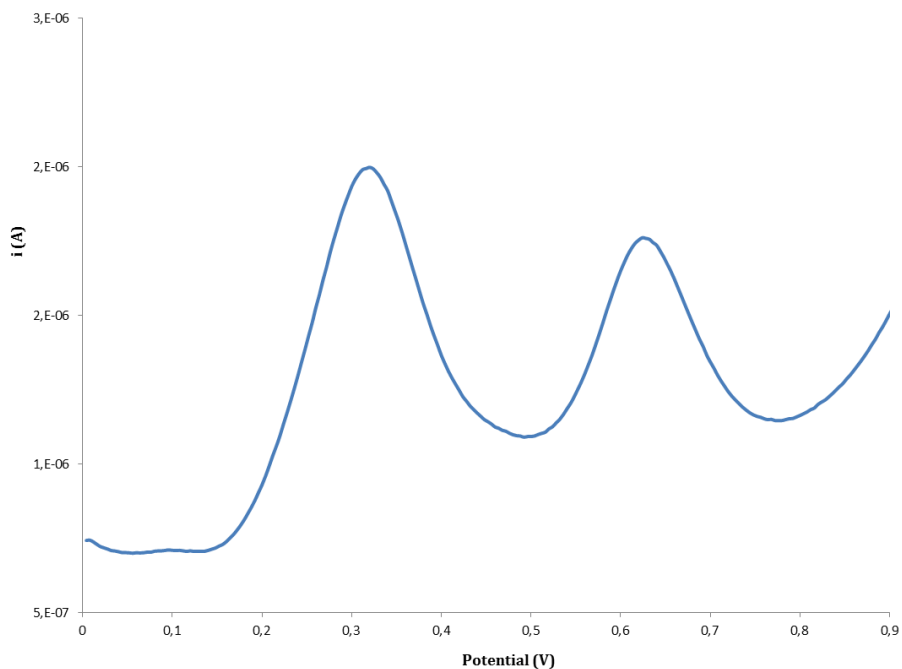
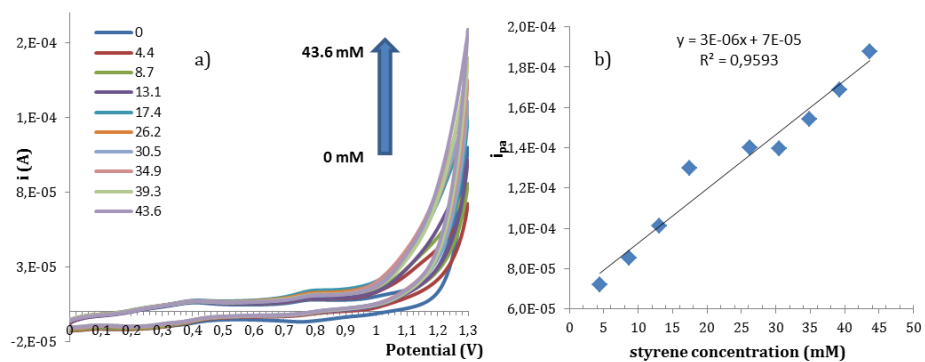


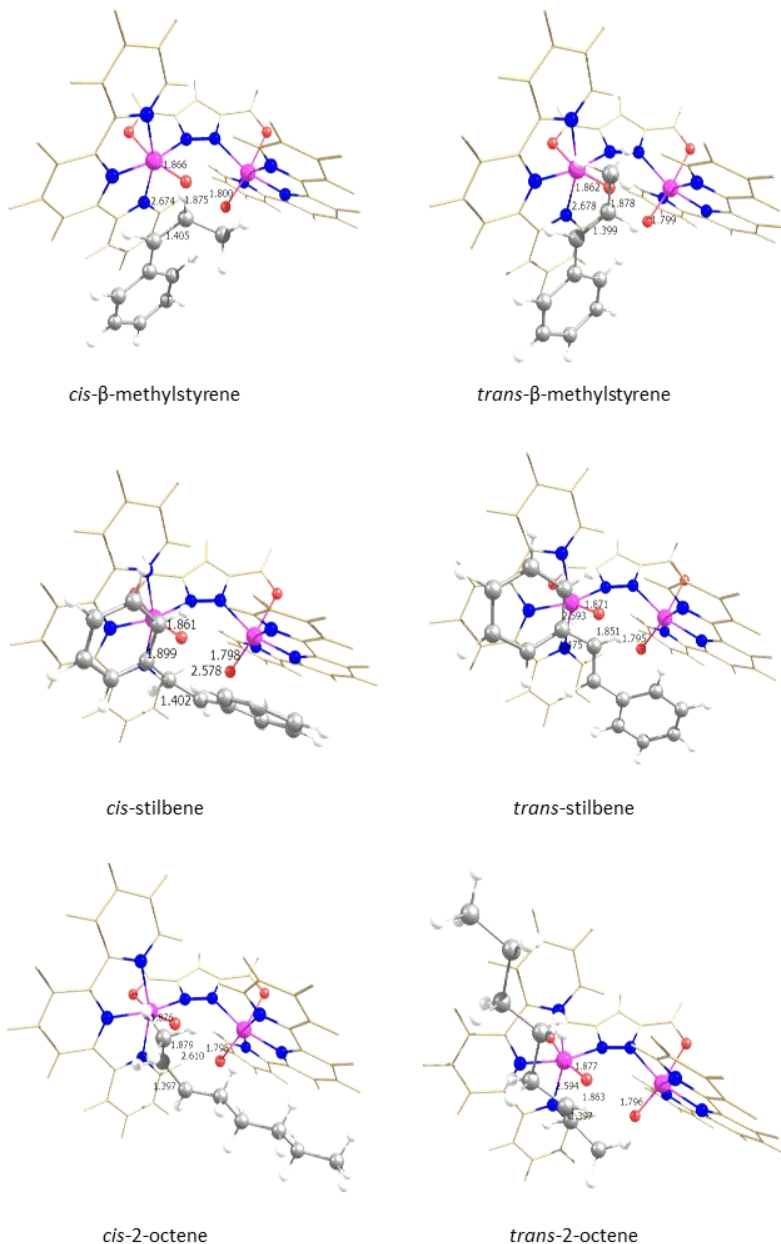
Figure S16. ESI-MS of 1 in MeOH.



**Figure SI7.** DPV of **1** after catalytic epoxidation of *cis*- $\beta$ -methylstyrene in  $\text{CH}_2\text{Cl}_2:\text{CH}_3\text{CH}_2\text{OH}$  (1:1), 0.1 M TBAH vs SSCE. (conditions of catalysis: **1** (1 mM) in dichloromethane/ethanol (1:1, 1 mL), alkene (2 M),  $\text{PhI}(\text{OAc})_2$  (4 M),  $\text{H}_2\text{O}$  (4 M). **1** was precipitated by addition of ether, filtered, washed with diethyl ether and dried).



**Figure S18.** Concentration dependence of  $i_{pa}$  in the electrochemical oxidation of styrene catalyzed by **1** a) cyclic voltammograms at different concentration of styrene b) plot of  $i_{pa}$  vs [styrene].



**Figure SI9.** TS1 of the epoxidation process of the *cis* and *trans* conformations of the  $\beta$ -methylstyrene, stilbene and 2-octene substrates (distances in Å).



UNIVERSITAT ROVIRA I VIRGILI

NEW RUTHENIUM, MANGANESE AND COBALT DINUCLEAR COMPLEXES AS REDOX CATALYSTS.

UNFOLDING THE ESSENTIAL STEPS FOR THE GENERATION OF SOLAR FUELS

Carlo Di Giovanni

Dipòsit Legal: T. 1429-2012

# Chapter V

A new dinuclear manganese bis-aqua complex containing the pyrazole-3,5-dicarboxylic acid ligand . Structural, magnetic characterization and application in the oxidation of *cis*- $\beta$ -methylstyrene

- i. Introduction*
- ii. Experimental Section*
- iii. Results and discussion*
- iv. Conclusions*
- v. Associated content*
- vi. Acknowledgements*
- vii. References*



## V. i. Introduction

Manganese complexes have been largely described as efficient catalysts for alkenes oxidation with different oxidants<sup>1-5</sup>. Peracetic acid is an environmentally friendly oxidant that only generates acetic acid as by-product. Although, this oxidant shows lower content of active oxygen compared to O<sub>2</sub> and H<sub>2</sub>O<sub>2</sub> (See Table 2, Chapter 1), and it is comparatively more expensive than H<sub>2</sub>O<sub>2</sub>. The epoxidation of alkenes by peracetic acid is often characterized by low selectivity, long reaction time and the employment of high temperature. For these reasons the development of an efficient catalyst for epoxidation with peracetic acid is of great interest in organic chemistry. The activity and selectivity of catalysts are largely influenced by the nature of the ligands. Mononuclear manganese complexes are usually labile and easily undergo ligand dissociation catalysis. However, the dinuclear complexes are often not stable and dissociate into mononuclear species. The use of multidentate ligands can enhance the stability. The pyrazole-3,5-dicarboxylic acid ligand, H<sub>3</sub>dcpz, has been already described to provide several possibilities in creating supramolecular architectures via  $\pi$ - $\pi$  interactions, hydrogen bonding and bridging between “bricks” *via* carboxylate groups<sup>6</sup>. Thanks to the 4 coordination sites, dcpz<sup>3-</sup> can coordinate as a mono-, bi- or tetradentate ligand and can act to link together metal centres through a number of bridging modes generating coordination polymers. This bridging attitude has been also demonstrated to modulate the magnetic properties via different coupling pathways<sup>7</sup>.

In Chapter IV a ruthenium dinuclear catalyst based on pyrazole-3,5-dicarboxylic acid as bridging ligand highly, active in epoxidation of olefins in presence of (diacetoxyiodo)benzene, has been presented and supramolecular catalytic

## Mn dinuclear complex containing the pyrazole-3,5-dicarboxylic acid ligand

approach has been also proposed and supported by DFT calculation. In this chapter a new dinuclear manganese bis-aqua complex containing the  $\text{dcpz}^{3-}$  ligand and two terpyridine ligands will be presented together with the synthesis of a derived polymer. The dinuclear complex, with formula  $\{[\text{Mn}^{\text{II}}(\text{trpy})(\text{H}_2\text{O})]_2(\mu\text{-dcpz})\}^+$ , **1**<sup>+</sup> or **MnPYZ**, has been characterized by electrochemical techniques, X-Ray diffraction and its magnetic properties have been studied. The catalytic activity has been tested with regard to the epoxidation of *cis*- $\beta$ -methylstyrene with peracetic acid. Full conversion and moderated selectivity has been obtained in short time reaction and with full retention of the initial *cis*-configuration. A crystal structure of species **2** made up a by one dimeric molecule complex and polymeric complex, which its smallest fragment contains 4 manganese atoms, will be also presented.

## V. ii. Experimental section

**Materials.** All reagents used in the present work were obtained from Aldrich Chemical Co. or Alfa Aesar and were used without further purification. Synthesis-grade organic solvents were obtained from SDS and were routinely degassed with argon. Methanol (MeOH) was distilled over MgI, ethanol was dried with a 3.5 Å molecular sieve, and acetonitrile, dichloromethane (DCM), hexane, and diethyl ether were used from the SPS. High-purity deionized water was obtained by passing distilled water through a nanopure Milli-Q water purification system.  $[\text{Mn}^{\text{II}}\text{Cl}_2(\text{trpy})]^{8-}$  were prepared as described in the literature. All synthetic manipulations were routinely performed under an argon atmosphere using Schlenk and vacuum-line techniques.

$\{[\text{Mn}^{\text{II}}(\text{trpy})(\text{H}_2\text{O})]_2(\mu\text{-dcpz})\}^+(\text{Hdcpz})_{0.5}, [\mathbf{1}(\text{dcpz})_{0.5}]$ . 200 mg (0.557 mmol) of  $\text{MnCl}_2(\text{trpy})$  were dissolved in 180 mL of methanol and stirred under Argon. A solution of 48 mg (0.276 mmol) of pyrazole-3,5-dicarboxylic acid monohydrate in 5 mL of methanol and 1 mL of water was added followed by 120  $\mu\text{L}$  of triethylamine (0.861 mmol). The addition of the base leads to the prompt change of the color from pale yellow to deep yellow. The solution was stirred at room temperature for 3 hours during which a pale yellow precipitate forms. The suspension was stored overnight in the fridge. The filtered s was washed with diethyl ether and dried under vacuum. Yield: 150 mg (96%). Anal. Calcd for  $(\text{C}_{35}\text{H}_{27}\text{Mn}_2\text{N}_8\text{O}_6)_2 \cdot \text{C}_5\text{H}_2\text{N}_2\text{O}_4 \cdot \text{H}_2\text{O}$  : C, 52.89; H, 3.43; N, 14.80. Found C 52.81; H 3.51; N 14.07.

**Equipment and Measurements.** . All electrochemical experiments were performed in a PAR 263A EG&G potentiostat or in an IJ-Cambria HI-660 potentiostat, using a three-electrode cell. Glassy carbon (3 mm diameter) from BAS was used as the working electrode, a platinum wire as the auxiliary

## μ<sub>2</sub>-Ru dinuclear complex containing the pyrazole-3,5-dicarboxylic acid ligand

electrode, and SSCE as the reference electrode. Cyclic voltammograms were recorded at a 100 mV·s<sup>-1</sup> scan rate. The complexes were dissolved in previously degassed MeCN containing the necessary amount of (n-Bu<sub>4</sub>N)(PF<sub>6</sub>), used as the supporting electrolyte, to yield a 0.1 M ionic strength solution. All E<sub>1/2</sub> values reported in this work were estimated from cyclic voltammetry (CV) as the average of the oxidative and reductive peak potentials (E<sub>p,a</sub> + E<sub>p,c</sub>)/2 or from differential pulse voltammetry (DPV; pulse amplitudes of 0.05 V, pulse widths of 0.05 s, sampling width of 0.02 s, and a pulse period of 0.1 s). Unless explicitly mentioned, the concentrations of the complexes were approximately 1 mM. Epoxidation catalytic experiments were analyzed in an Agilent 6890N gas chromatograph coupled to a mass selective detector with ionization by electronic impact and in an Agilent 6890 with a FID detector using a HP5 column. In a typical experiment the catalyst (2.1 mg, 2.5 μmol, final concentration = 2.3 mM) the alkene (33 μL, 250 μmol, final concentration = 230 mM), and dodecane (10 μL, 44 μmol, final concentration = 44 mM) as internal standard, were mixed together in anhydrous MeCN (final volume = 1 mL). The flask was then cooled in an ice bath. Afterwards, 32% (v/v) peracetic acid (110 μL, 500 μmol, final concentration = 460 mM) was added *via* syringe over 3 min under stirring (final volume ≈ 1.1 mL). After 2 additional minutes, the reaction vessel was taken out of the ice bath (this is taken as the starting point of the catalysis) and allowed to progressively warm to RT. GC conditions: initial temperature 40 °C for 10 min, ramp rate variable for each substrate (typically from 10 °C/min to 20 °/min), final temperature 250 °C, injection temperature 220 °C, detector temperature 250°C. Yield of epoxide and substrate conversion were calculated with regard to the initial concentration of substrate.

$$\text{Substrate conversion} = \frac{[\text{substrate}]_{\text{initial}} - [\text{substrate}]_{\text{final}}}{[\text{substrate}]_{\text{initial}}} \cdot 100.$$

$$\text{Yield epoxide} =$$

$$\frac{\{[\text{epoxide}]_{\text{final}}/[\text{substrate}]_{\text{initial}}\}}{[\text{epoxide}]_{\text{final}}/\{[\text{substrate}]_{\text{initial}}-[\text{substrate}]_{\text{final}}\}} \cdot 100. \quad \text{Epoxide selectivity} =$$

**Single-Crystal X-ray Structure Determination.** *Crystal Preparation.* Crystals for **1**<sup>+</sup> were grown by the slow evaporation of a chloroform/ethanol solution of the complex. All measured crystals were prepared under inert conditions immersed in perfluoropolyether as the protecting oil for manipulation.

*Data collection:* Crystal structure determinations for **1**<sup>+</sup> and **2** were carried out using a Bruker-Nonius diffractometer equipped with an APEX 2 4K CCD area detector, a FR591 rotating anode with MoK<sub>α</sub> radiation, Montel mirrors as monochromator and an Oxford Cryosystems low temperature device Cryostream 700 plus (*T* = -173 °C). Full-sphere data collection was used with  $\omega$  and  $\varphi$  scans. *Programs used:* Data collection APEX-2<sup>9</sup>, data reduction Bruker Saint<sup>10</sup> V/.60A and absorption correction SADABS<sup>11</sup> or TWINABS<sup>12</sup>.

*Structure Solution and Refinement:* Crystal structure solution was achieved using direct methods as implemented in SHELXTL<sup>13</sup> and visualized using the program XP. Missing atoms were subsequently located from difference Fourier synthesis and added to the atom list. Least-squares refinement on *F*<sup>2</sup> using all measured intensities was carried out using the program SHELXTL. All non-hydrogen atoms were refined including anisotropic displacement parameters. In order to avoid highly disordered solvent molecules the program SQUEEZE<sup>14</sup> was used.

The asymmetric unit of **1** is made up by one molecule of the, a half free additional dicarboxylic acid (shared with the neighboring asymmetric unit) and 9.75 molecules of water. The free dicarboxylic acid is disordered in two orientations located over a center of inversion. Although hydrogen atoms are extremely difficult to localize in this case it seems that the free dicarboxylic acid has a charge of -2 which corresponds to -1 for each asymmetric unit/complex.



## Mn dinuclear complex containing the pyrazole-3,5-dicarboxylic acid ligand

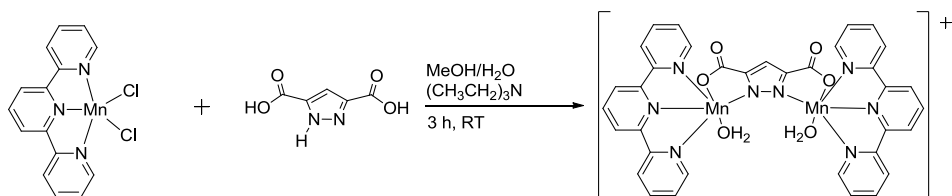
In consequence each Mn atom in the complex should have a charge of +2. The 9.75 water molecules are located partially disordered in eleven positions. Since the major part of the hydrogen atoms of the water molecules could not be clearly identified, they were added to fixed positions maintaining the right distance and angle to the attached oxygen atom. Due to the high number of water molecules, the orientation of some of the hydrogen atoms could not be appropriately corrected and some A and B alert in the check cif remained due to too short H---H distances. The structure has a R1 value of 6.37 %. The asymmetric unit of **2** is made up by one dimeric molecule complex having water molecules linked to the Mn atoms, one polymeric complex which its smallest fragment contains 4 manganese atoms and two tridentate ligands, three chlorine anions and twenty free water molecules in asymmetric unit. One of chlorine anions is disordered in two positions (ratio 50:50). The structure has a R1 value of 9.47 %.

**Magnetic susceptibility study.** Variable-temperature magnetic susceptibility data for compound **1** were obtained with a Quantum Design MPMS-XL SQUID magnetometer at the "Unitat de Mesures Magnètiques" of the Universitat de Barcelona. Pascal's constants were used to estimate diamagnetic corrections to the molar paramagnetic susceptibility, and an empirical correction was applied for the sample holder.

### V. iii. Results and discussion

#### Synthesis

The synthetic procedure followed for the synthesis of **1**<sup>+</sup> is outlined in Scheme 1.



**Scheme 1.** Synthetic pathway

When a solution of  $[\text{Mn}^{\text{II}}\text{Cl}_2(\text{trpy})]$  in methanol was mixed to a solution of pyrazole dicarboxylic acid monohydrate in methanol the mixture acquired a deep yellow color. The addition of triethylamine, which role is to deprotonate the ligand, provoked the formation of a fine precipitate corresponding to the bis-aqua complex **1**<sup>+</sup>.

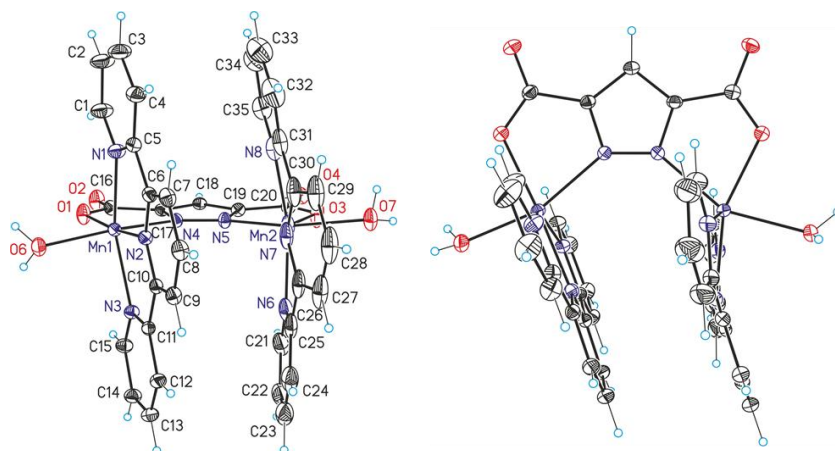
#### Solid state structure

The crystal structure of **1**<sup>+</sup> (Figure 1) shows a dinuclear complex with distorted octahedral geometry. The two manganese ions stay on the same plane of the pyrazole-3,5-dicarboxylate ligand. Each manganese is coordinated to the bridging ligand by one nitrogen atom and one oxygen atom. The octahedral coordination is completed by a terpyridine ligand and one aqua molecule. The latter present an *out,out* orientation with the two terpyridine on a *quasi*-parallel disposition. Each asymmetric unit of **1**<sup>+</sup> contains one molecule of dimer and half pyrazole-3,5-dicarboxylic acid molecule protonated on the N of the five-membered ring. The ligand acts therefore as counter ion in two neighboring asymmetric unit providing two negative charges in all. The Mn–

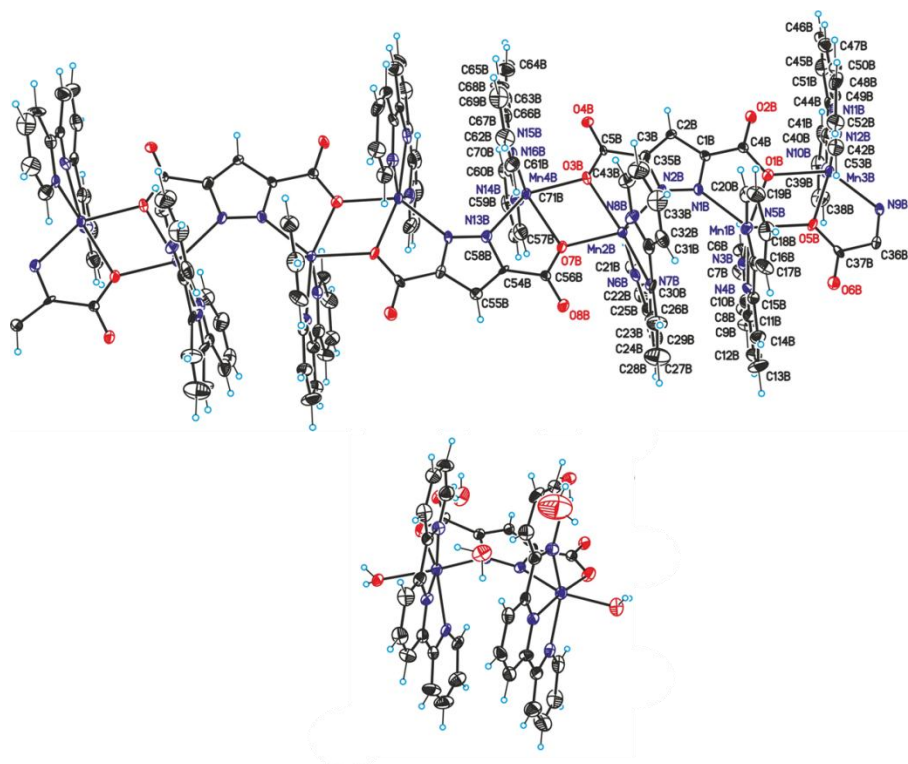
## Mn dinuclear complex containing the pyrazole-3,5-dicarboxylic acid ligand

Mn distance of 4.667 Å in  $\mathbf{1}^+$  is longer than other hexacoordinate dinuclear  $\text{Mn}^{\text{II}}$  compounds with chloro and acetato bridges<sup>15-18</sup>. The Mn-O<sub>aqua</sub> and Mn-N<sub>trpy</sub> bond distances are comparable to those found for similar Mn(II) complexes<sup>19-22</sup>.

When an aqueous solution of  $\mathbf{1}^+$  was treated with an excess of LiCl the dinuclear complex recrystallizes with one dimeric molecule complex having water and one polymeric complex which its smallest fragment contains 4 manganese atoms and two tridentate ligands, three chlorine anions and twenty free water molecules in asymmetric unit ( $\mathbf{2}$ , Figure 2). Here, the basic building block of  $\mathbf{1}^+$  can be linked to form 1-D chain through the O atoms of the carboxylate groups. The infinite chains pack together forming layers alternating with dinuclear molecules (Figure S11). In this new structure the Mn-Mn distance of 4.498 Å resulted shorter than in the dimer species. Crystal data and selected bond distances and angles for  $\mathbf{1}^+$  and  $\mathbf{2}$  are reported in table 1 and Table 2, respectively.



**Figure 1.** Ortep plots (ellipsoid at 50% probability) X-Ray structure of  $\mathbf{1}^+$  with labeling scheme.



**Figure 2.** Ortep plots (ellipsoid at 30% probability) X-ray structure of **2**.

## Mn dinuclear complex containing the pyrazole-3,5-dicarboxylic acid ligand

**Table 1.** Crystal Data for compounds **1<sup>+</sup>** and **2**.

	<b>1<sup>+</sup></b>		<b>2</b>	
Empirical formula	C <sub>37.50</sub> H <sub>47</sub> Mn <sub>2</sub> N <sub>9</sub> O <sub>17.75</sub>		C105H113Cl3Mn6N24O34	
Formula weight	1017.72		2691.18	
Temperature	100(2) K		100(2) K	
Wavelength	0.71073 Å		0.71073 Å	
Crystal system	Triclinic		Triclinic	
Space group	P-1		P-1	
Unit cell dimensions	a = 10.9557(6) Å	α = 90.866(2)°	a = 15.1837(12) Å	α = 102.039 (4)°
	b = 13.8952(8) Å	β = 107.3630(10)°	b = 15.8323(12) Å	β = 97.036(4)°
	c = 15.9305(10) Å	γ = 105.959(2)°	c = 25.628(2) Å	γ = 95.890(4)°
Volume	2212.9(2) Å <sup>3</sup>		5927.5(8) Å <sup>3</sup>	
Z	2		2	
Density (calculated)	1.527 Mg/m <sup>3</sup>		1.508 Mg/m <sup>3</sup>	
Absorption coefficient	0.656 mm <sup>-1</sup>		0.776 mm <sup>-1</sup>	
F(000)	1054		2769	
Crystal size	0.20 x 0.15 x 0.15 mm <sup>3</sup>		0.30 x 0.01 x 0.01 mm <sup>3</sup>	
Theta range for data collection	1.53 to 36.54 °.		1.36 to 25.57 °.	
Index ranges	-17 ≤ h ≤ 18, -22 ≤ k ≤ 22, -26 ≤ l ≤ 26		-18 ≤ h ≤ 18, -18 ≤ k ≤ 19, -31 ≤ l ≤ 31	
Reflections collected	19413		44586	
Independent reflections	15025 [R(int) = 0.0359]		21888 [R(int) = 0.0848]	
Completeness to theta = 25.40 °	0.889 %		0.985 %	
Absorption correction	Empirical		Empirical	
Max. and min. transmission	0.9081 and 0.8801		0.9923 and 0.8005	
Refinement method	Full-matrix least-squares on F <sup>2</sup>		Full-matrix least-squares on F <sup>2</sup>	
Data / restraints / parameters	19413 / 79 / 741		21888 / 68 / 1690	
Goodness-of-fit on F <sup>2</sup>	1046		1.065	
Final R indices [I > 2σ(I)]	R1 = 0.0637, wR2 = 0.1607		R1 = 0.0947, wR2 = 0.2110	
R indices (all data)	R1 = 0.0834, wR2 = 0.1725		R1 = 0.1720, wR2 = 0.2429	
Largest diff. peak and hole	1.696 and -1047 e.Å <sup>-3</sup>		1.071 and -0.962 e.Å <sup>-3</sup>	

**Table 2.** Selected metric parameters for complex 1<sup>+</sup>.

Selected bond (Å)		Selected Angle (°)	
Mn(1)-O(6)	2.1495	O(6)-Mn(1)-N(2)	172.97(6)
Mn(1)-O(1)	2.1654	N(2)-Mn(1)-N(4)	108.30(6)
Mn(1)-N(1)	2.2575	N(5)-Mn(2)-N(7)	126.37(7)
Mn(1)-N(2)	2.2168	N(7)-Mn(2)-O(7)	79.21(6)
Mn(1)-N(3)	2.2747	Mn(1)-N(4)-N(5)-Mn(2) <sup>a</sup>	-3.7(3)
Mn(1)-N(4)	2.2176		

<sup>a</sup> Torsion angle that involves the two N atoms belonging to the pyrazoledicarboxylate-bridged group and the two metal centers.

**Table 3.** Selected metric parameters for complex 2.

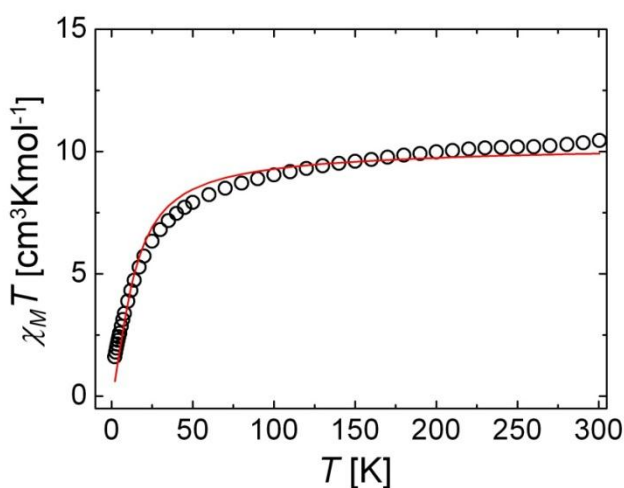
Selected bond (Å)			
Mn(4B)-N(13B)	2.175(7)	Mn(1B)-O(5B)	2.188(6)
Mn(4B)-O(7B)	2.237(6)	Mn(3B)-N(9B)	2.178(7)
Mn(4B)-O(3B)	2.159(5)	Mn(3B)-O(1B)	2.137(6)
Mn(2B)-N(2B)	2.166(7)	Mn(3B)-O(5B)	2.271(6)
Mn(2B)-O(7B)	2.138(6)	Mn(4B)-Mn(2B)	3.566
Mn(2B)-O(3B)	2.267(6)	Mn(2B)-Mn(1B)	4.498
Mn(1B)-N(1B)	2.191(7)	Mn(1B)-Mn(3B)	3.594
Mn(1B)-O(1B)	2.227(6)		
Selected Angle (°)			
Mn(4B)-O(3B)-Mn(2B)			107.3(2)
Mn(2B)-O(7B)-Mn(4B)			109.1(2)
Mn(3B)-O(1B)-Mn(1B)			110.8(2)
Mn(1B)-O(5B)-Mn(3B)			107.4(2)
Mn(1B)-N(1B)-N(2B)-Mn(2B) <sup>a</sup>			-5.27(13)

<sup>a</sup> Torsion angle that involves the two N atoms belonging to the pyrazoledicarboxylate-bridged group and the two metal centers

## Mn dinuclear complex containing the pyrazole-3,5-dicarboxylic acid ligand

**Magnetic properties**

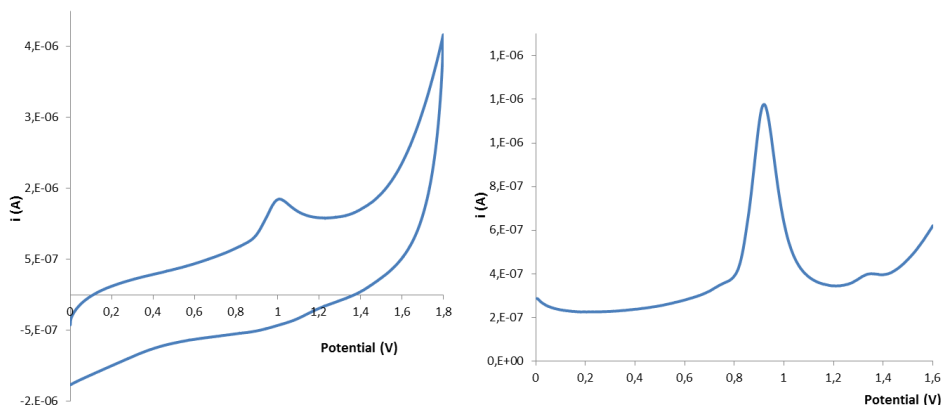
The temperature-dependent magnetic susceptibility for complex  $\mathbf{1}^+$  has been investigated under a constant field of 0.5T. In Figure 3 is presented a plot of  $\chi_M T$  vs T and a fit using the Van Vleck equation for the following Hamiltonian of the magnetic energy coupling ( $H = -2JS_1S_2$ ;  $S_1 = S_2 = 5/2$ ). The fit was performed with a TIP (Temperature Independent Paramagnetism) of  $4 \times 10^{-4} \text{ cm}^3 \text{ mol K}^{-1}$ . The results from the fit are:  $J = -0.97 \text{ cm}^{-1}$  and  $g = 2.15$ . The value of  $\chi_M T$  at 300 K resulted around  $9 \text{ cm}^3 \cdot \text{K} \cdot \text{mol}^{-1}$ , close to the expected value for two  $\text{Mn}^{\text{II}}$  ions ( $8.75 \text{ cm}^3 \cdot \text{K} \cdot \text{mol}^{-1}$ )<sup>23</sup>. On decreasing the temperature, the  $\chi_M T$  values fall considerably indicating an antiferromagnetic coupling.



**Figure 3.**  $\chi_M T$  vs T plot for  $\mathbf{1}^+$  (the solid line is the best fit to the experimental data).

### Redox properties

The oxidation potentials of compounds  $1^+$  has been determined by cyclic voltammetry in  $\text{CH}_3\text{CN}$  (0.1 M  $[(n\text{-Bu})_4\text{N}]\text{PF}_6$ ). The cyclic and the differential pulse voltammograms are shown in Figure 4. One irreversible oxidation peak at  $E = 1.00$  V has been detected.

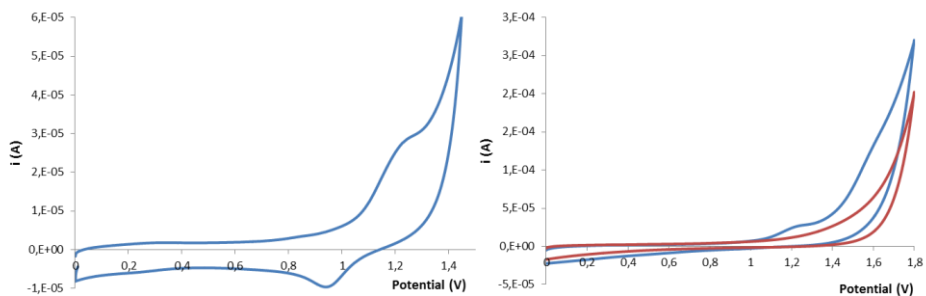


**Figure 4.** CV and DPV of  $1^+$  in MeCN ( 0.1 M TBAH).

In pH 1 triflic acid 0.1 M aqueous solution one reversible wave has been detected at  $E_{1/2} = 1.058$  V (Figure 5a). When a higher potential of 1.8 V is applied a weak electrocatalytical wave appears from potential  $E = 1.4$  V. The reverse scan did not present any wave for reduction pointing toward a change in the structure of  $1^+$  (Figure 5b). A second wave can be detected by DPV at  $E = 1.47$  V (Figure SI2).



Mn dinuclear complex containing the pyrazole-3,5-dicarboxylic acid ligand



**Figure 5.** Cyclic voltammograms at different potential range for  $1^+$  at pH = 1.0 in 0.1 M triflic acid aqueous solution. Background in red color.

### Catalytic epoxidation

Catalytic activity of  $\mathbf{1}^+$  was investigated in the epoxidation *cis*- $\beta$ -methylstyrene using commercial peracetic acid (32% v/v) as the oxidant. After 10 min of reaction the substrate resulted fully converted with a yield of epoxide corresponding to 64 % (Table 4, Entry 1). Phenylacetone was also detected as by-product with a yield of 33 %. A second catalytic experiment has been carried on reducing the excess of oxidant to 1.2 equivalents respect to the substrate. In this case the conversion reduced to 67% but the selectivity of epoxide maintained similar value (Table 4, Entry 1). On the contrary less ketone was detected indicating a competitive direct oxidation of the substrate by peracetic acid as possible source of the ketone. Results in terms of conversion, yield and selectivity are presented in Table 4. No epoxidation occurred in the absence of catalyst.

**Table 4.** Epoxidation of *cis*- $\beta$ -methylstyrene with peracetic acid catalyzed by  $\mathbf{1}^+$ .

Entry	Initial concentration (M)			Substrate Conversion (%) <sup>b</sup>	[Epoxide], M; (Selectivity %) <sup>c,f</sup>	[ketone], M; (selectivity %) <sup>d</sup>	TN <sup>e</sup>
	$\mathbf{1}^+$	substrate	oxidant				
1	$2.3 \cdot 10^{-3}$	0.230	0.460	100	0.15 (65)	0.08 (34)	65
2	$2.3 \cdot 10^{-3}$	0.230	0.276	67	0.10 (66)	0.04 (28)	43

<sup>a</sup>Reaction conditions:  $\mathbf{1}^+$  (2.1 mg, 2.5  $\mu$ mol, final concentration = 2.3 mM), *cis*- $\beta$ -methylstyrene (33  $\mu$ L, 250  $\mu$ mol, final concentration = 230 mM), dodecane (10  $\mu$ L, 44  $\mu$ mol, final concentration = 44 mM), anhydrous MeCN (final volume = 1 mL). The flask was then cooled in an ice bath. Afterwards, 32% (v/v) peracetic acid (110  $\mu$ L, 500  $\mu$ mol, final concentration = 460 mM) was added *via* syringe over 3 min under stirring (final volume  $\approx$  1.1 mL). <sup>b</sup>Substrate conversion =  $\{[\text{substrate}]_{\text{initial}} - [\text{substrate}]_{\text{final}}\} / [\text{substrate}]_{\text{initial}} \cdot 100$ . <sup>c</sup>Epoxide selectivity =  $[\text{epoxide}]_{\text{final}} / \{[\text{substrate}]_{\text{initial}} - [\text{substrate}]_{\text{final}}\} \cdot 100$ . <sup>d</sup>ketone selectivity =  $[\text{ketone}]_{\text{final}} / \{[\text{substrate}]_{\text{initial}} - [\text{substrate}]_{\text{final}}\} \cdot 100$ . <sup>e</sup>TN is the turnover number with regard to epoxide. <sup>f</sup>100% of *cis*-epoxide. Blank experiment without catalyst  $\mathbf{1}^+$  did not produced epoxide.

## V. iv. Conclusions

In this chapter the synthesis and the characterization of a new robust dinuclear manganese complex **1**<sup>+</sup> has been described and discussed. The catalytic activity of **1**<sup>+</sup> has been investigated in the oxidation of *cis*- $\beta$ -methylstyrene with peracetic acid resulting in a moderated efficiency as epoxidation catalyst. The solid state structure showed an unexpected *out, out* orientation of the aqua ligands that resulted unfavorable from a catalytic point of view because avoids a potential cooperation of the two Mn<sup>IV</sup>=O active sites. Despite that, the presence of labile aqua ligands in *out* position, favors, in solution, the substitution of the latter and the coordination by O atoms of the carboxylic groups of adjacent molecules of dimers leading to the formation of a polymeric structure, **2**, constituted of chains of tetranuclear units. The magnetic properties of **1**<sup>+</sup> have been preliminary investigated in terms of measurement of the temperature dependence of magnetic susceptibility indicating antiferromagnetic properties of the dimer. The magnetic properties of **2** are under investigation in order to compare the electron coupling between the dinuclear species and the polymeric one, which takes advantages of further carboxylic bridging groups.

## V. v. Associated content

### Supporting Information

X-Ray crystallographic data in CIF format, additional spectroscopic and electrochemical data.

## V. vi. Acknowledgements

Magnetic susceptibility measurements have been done by Dr. Guillem Aromí at the “Unitat de Mesures” of the University of Barcelona.

## V. vii. References

- (1) Berkessel, A.; Frauenkron, M.; Schwenkreis, T.; Steinmetz, A.; Baum, G.; Fenske, D. *J. Mol. Catal. A: Chem.* **1996**, *113*.
- (2) Irie, R.; Hosoya, N.; Katsuki, T. *Synlett.* **1994**.
- (3) Battioni, P.; Renaud, J. P.; Bartoli, J. F.; Reina-Artiles, M.; Fort, M.; Mansuy, D. *J. Am. Chem. Soc.* **1988**, *110*, 8462.
- (4) Zhang, W.; Loebach, J. L.; Wilson, S. R.; Jacobsen, E. N. *J. Am. Chem. Soc.* **1990**, *112*, 2801.
- (5) Garcia-Bosch, I.; Company, A.; Fontrodona, X.; Ribas, X.; Costas, M. *Org. Lett.* **2008**, *10*, 2095.
- (6) King, P.; Clerac, R.; Anson, C. E.; Powell, A. K. *Dalton Trans.* **2004**, 852.
- (7) King, P.; Clérac, R.; Anson, C. E.; Coulon, C.; Powell, A. K. *Inorg. Chem.* **2003**, *42*, 3492.
- (8) Mantel, C.; Baffert, C.; Romero, I.; Deronzier, A.; Pecaut, J.; Collomb, M.-N.; Duboc, C. *Inorg. Chem.* **2004**, *43*, 6455.
- (9) Data collection with APEX II versions v1.0-22, Madison, Wisconsin, USA.
- (10) Data reduction with Bruker SAINT versions V.2.10(2003), Madison, Wisconsin, USA.
- (11) SADABS: V.2.10(2003); V2008 and V2008/1 Bruker (2001). Bruker AXS Inc., M., Wisconsin, USA. Blessing *Acta Cryst.* **1995**, *A51*, 33.
- (12) TWINABS Version 2008/4 Bruker AXS; Blessing *Acta Cryst.* **1995**, *A51*, 33.
- (13) Sheldrick, G. M. S. v. V. a. *Acta Cryst.* **2008**, *A64*, 112.
- (14) SQUEEZE implemented in Platon: Spek, A. L. *J. Appl. Cryst.* **2003**, *36*.

Ru<sup>II</sup> dinuclear complex containing the pyrazole-3,5-dicarboxylic acid ligand

- (15) van, A. G. A.; Mohamadou, A.; Driessen, W. L.; de, G. R.; Tanase, S.; Reedijk, J. *Polyhedron* **2004**, *23*, 2387.
- (16) Qi, C.-M.; Sun, X.-X.; Gao, S.; Ma, S.-L.; Yuan, D.-Q.; Fan, C.-H.; Huang, H.-B.; Zhu, W.-X. *Eur. J. Inorg. Chem.* **2007**, 3663.
- (17) Romero, I.; Collomb, M.-N.; Deronzier, A.; Llobet, A.; Perret, E.; Pecaut, J.; Le, P. L.; Latour, J.-M. *Eur. J. Inorg. Chem.* **2001**, 69.
- (18) Rich, J.; Rodriguez, M.; Romero, I.; Vaquer, L.; Sala, X.; Llobet, A.; Corbella, M.; Collomb, M.-N.; Fontrodona, X. *Dalton Trans.* **2009**, 8117.
- (19) Walesa-Chorab, M.; Stefankiewicz, A. R.; Ciesielski, D.; Hnatejko, Z.; Kubicki, M.; Klak, J.; Korabik, M. J.; Patroniak, V. *Polyhedron* **2011**, *30*, 730.
- (20) Baffert, C.; Romero, I.; Pecaut, J.; Llobet, A.; Deronzier, A.; Collomb, M.-N. *Inorg. Chim. Acta* **2004**, *357*, 3430.
- (21) Chen, C.; Zhu, H.; Huang, D.; Wen, T.; Liu, Q.; Liao, D.; Cui, J. *Inorg. Chim. Acta* **2001**, *320*, 159.
- (22) Fernandez, G.; Corbella, M.; Alfonso, M.; Stoeckli-Evans, H.; Castro, I. *Inorg. Chem.* **2004**, *43*, 6684.
- (23) Gomez, V.; Corbella, M. *Eur. J. Inorg. Chem.* **2009**, 4471.

UNIVERSITAT ROVIRA I VIRGILI

NEW RUTHENIUM, MANGANESE AND COBALT DINUCLEAR COMPLEXES AS REDOX CATALYSTS.

UNFOLDING THE ESSENTIAL STEPS FOR THE GENERATION OF SOLAR FUELS

Carlo Di Giovanni

Dipòsit Legal: T. 1429-2012

UNIVERSITAT ROVIRA I VIRGILI

NEW RUTHENIUM, MANGANESE AND COBALT DINUCLEAR COMPLEXES AS REDOX CATALYSTS.




UNFOLDING THE ESSENTIAL STEPS FOR THE GENERATION OF SOLAR FUELS

Carlo Di Giovanni

Dipòsit Legal: T. 1429-2012

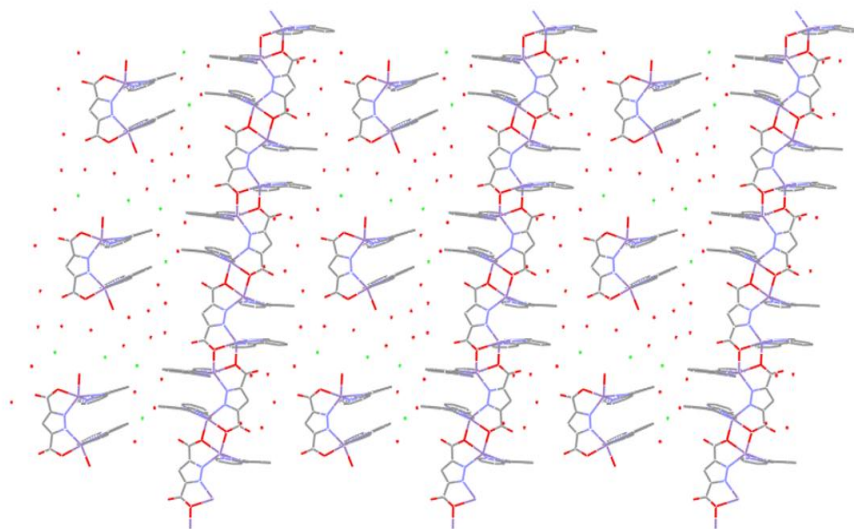
# Chapter V

## Supporting Information

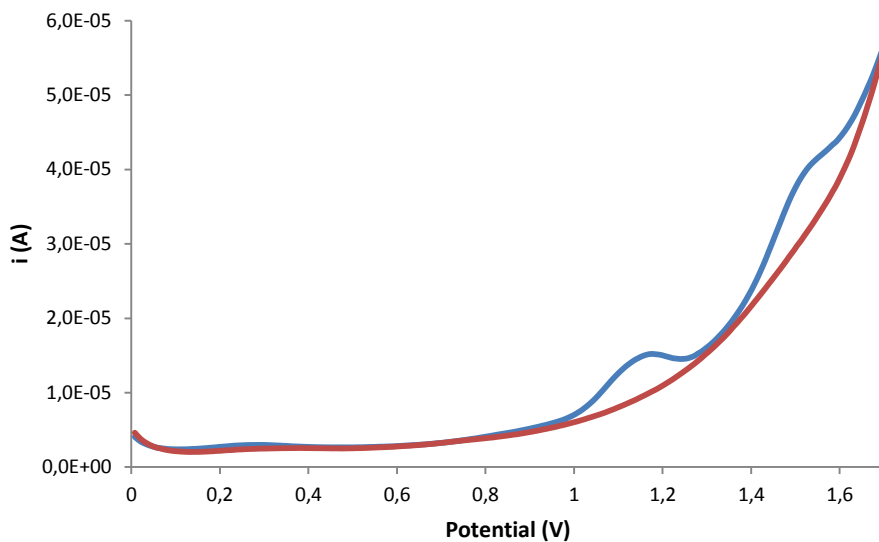
-  *X-Ray structure packing of 2:*
-  *DPV of 1<sup>+</sup> in triflic acid:*
-  *Catalytic epoxidation of cis-β-methylstyrene with 1<sup>+</sup>*



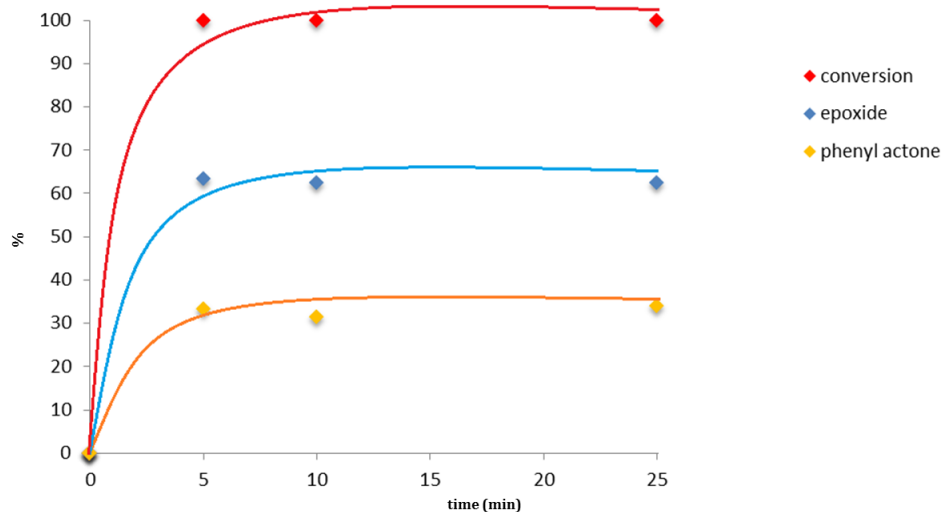




**Figure S11.** X-Ray structure, packing of **2**.



**Figure S12.** Differential pulse voltammogram for  $1^+$  at pH = 1.0 in 0.1 M triflic acid aqueous solution. Background in red color.



**Figure S13.** Reaction conditions:  $\mathbf{1}^+$  (2.1 mg, 2.5  $\mu\text{mol}$ , final concentration = 2.3 mM), *cis*- $\beta$ -methylstyrene (33  $\mu\text{L}$ , 250  $\mu\text{mol}$ , final concentration = 230 mM), dodecane (10  $\mu\text{L}$ , 44  $\mu\text{mol}$ , final concentration = 44 mM), anhydrous MeCN (final volume = 1 mL). The flask was then cooled in an ice bath. Afterwards, 32% (v/v) peracetic acid (110  $\mu\text{L}$ , 500  $\mu\text{mol}$ , final concentration = 460 mM) was added *via* syringe over 3 min under stirring (final volume  $\approx$  1.1 mL).

Substrate conversion =  $\frac{[\text{substrate}]_{\text{initial}} - [\text{substrate}]_{\text{final}}}{[\text{substrate}]_{\text{initial}}} \cdot 100$ . Epoxide selectivity =  $\frac{[\text{epoxide}]_{\text{final}}}{[\text{substrate}]_{\text{initial}} - [\text{substrate}]_{\text{final}}} \cdot 100$ . ketone selectivity =  $\frac{[\text{ketone}]_{\text{final}}}{[\text{substrate}]_{\text{initial}} - [\text{substrate}]_{\text{final}}} \cdot 100$ .

UNIVERSITAT ROVIRA I VIRGILI

NEW RUTHENIUM, MANGANESE AND COBALT DINUCLEAR COMPLEXES AS REDOX CATALYSTS.

UNFOLDING THE ESSENTIAL STEPS FOR THE GENERATION OF SOLAR FUELS

Carlo Di Giovanni

Dipòsit Legal: T. 1429-2012

# Chapter VI

Synthesis and characterization of a new  
polypyridyl decadentate ligand, L.  
Preparation of cobalt dinuclear complexes  
based on L and investigation of their  
catalytic activity

- i. Introduction*
- ii. Experimental Section*
- iii. Results and discussion*
- iv. Conclusions*
- v. Associated content*
- vi. Acknowledgements*
- vii. References*



## VI. i. Introduction

The d-block of the periodic table is defined as the section that encloses the elements, from group 3 to group 12, in which the d-subshells are being filled with electrons. Among this group, the peculiarity of having a partially filled d-electron shell in one of its common oxidation states outlines a new subset of elements called *transition metals*.

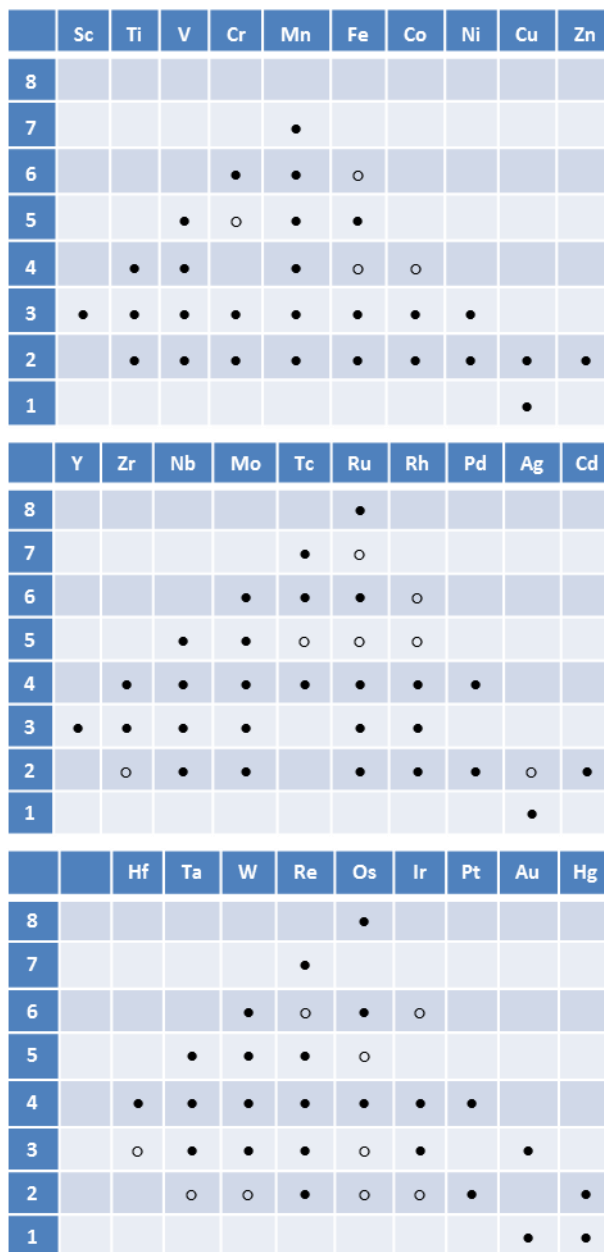
Transition metals have certain characteristics in common that are not generally shared by other metals (including zinc and scandium). Some of these properties are:

- the variety of stable oxidation states,
- the formation of compounds with different geometries,
- the good conductivity of heat and charge,
- the elevate melting point,
- the formation of coloured compounds (except Sc(III) and Ti(IV))
- the catalytic activity.

Transition metals exhibit multiple oxidation states (Figure 1) ; this is due to the fact that slight increases in ionization energy separate the different losses of electrons, leading to the formation of ions with different positive charges. These cations present low energy unfilled d orbitals that can accept pairs of electrons from *ligands* generating a dative bond. The new species metal-ligand is called *complex-ion*. The ability to accept electrons from ligands, and the wide variety of possible oxidation states are the responsible of the factor responsible of the catalytic activity of transition metals complexes in redox reactions.



New polypyridyl decadentate ligand and related Co complexes



**Figure 1.** Oxidation states of transition metals, empty marks represent the less common species.

Thanks to the stability of adjacent oxidation states and to the significant advantage given by the absence of unpaired electrons, the synthetic methodologies for second-row metals complexes result more advanced than those for paramagnetic organometallic complexes of the first row in which NMR spectroscopy is considered the best characterization technique.

These factors, together with the high catalytic performance, made of the *precious metals* the first choice in several industrial catalyzed processes while the drawbacks associated with the handling (instability toward air, moisture and thermal conditions) and the lower stability of oxidation states relegated first row's metal complexes in the background.

### **The octahedral geometry**

The design of ligands able to impose specific coordination geometry is the starting point for the reactivity study of metal complexes. The advantage of having rigid structure with a well-defined geometry and reduced number of labile coordination site confer higher stability to metal complexes upon red-ox processes leading to easier mechanistic studies and intermediates identification.

Not many pentadentate ligands are able to induce an octahedral geometry to transition metals<sup>1-4</sup>. 2,6-(bis-(bis-2-pyridyl)-methoxymethane)pyridine ligand, PY5, has been described as efficient flexible ligand for coordination of first row transition metal ions<sup>5</sup>. Complexes based on PY5 and its derivatives have found application in different areas, from magnetism to catalysis<sup>6-11</sup>.

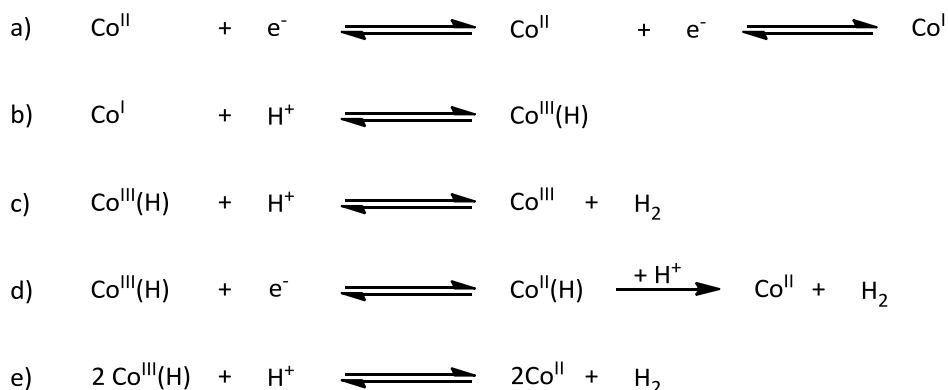
When the octahedral geometry wants to be extended to dinuclear complexes the common strategy is to design a bridging ligand able to link, structurally and electronically, the two metal centers on the same plane and employ further ligands for reaching the pentacoordination on both the metal ions. This

procedure often increases the flexibility at the expense of the strength of the structure.

### Proton reduction

As already mentioned the search of a non-carbon and abundant source of hydrogen is a challenge for chemists. Fe-Ni and Fe-Fe hydrogenases produce dihydrogen in water at close to the thermodynamic potential of -0.41 V vs the normal hydrogen electrode (NHE) at pH 7<sup>12-16</sup>. However, the existence of a catalyst, based on a cheap and earth-abundant metal capable, to reduce protons to hydrogen at low overpotential is still the main drawback in this field. Pt is the most efficient catalyst for the hydrogen production, but its low abundance and high cost prohibit its large scale use. DuBois and co-workers reported that Ni and Co phosphines exhibit high turnover frequencies (TOFs) of 103–105 s<sup>-1</sup> at low overpotentials (50–400 mV)<sup>17-21</sup>. Co diglyoximes also have been described to operate at low overpotentials with high rates<sup>22-28</sup>. More recently, polypyridine Co complexes reported by Chang<sup>29,30</sup> and Gray<sup>31</sup> have been shown to catalyze H<sub>2</sub> evolution from aqueous systems.

Despite of the advances achieved in terms of catalytic efficiency the mechanism for hydrogen production is still controversial. In the case of molecular cobalt catalysts mechanisms involving cobalt hydride formation (Scheme 1 a and b) have been proposed<sup>22,23,26,32-34</sup>. The latter can then evolve through different possible pathways as shown in (Scheme 1 c-e).



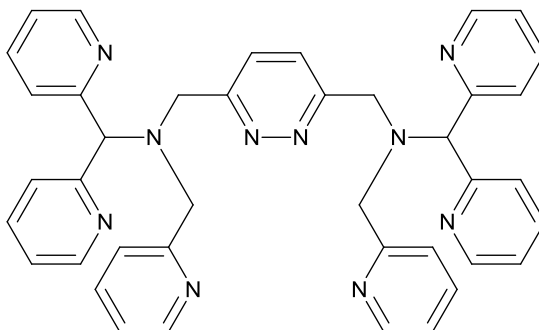
**Scheme 1.** Proposed mechanisms for cobalt hydride formation and H<sub>2</sub> evolution.

Recently Savéant and coworkers unambiguously demonstrated that the electrochemical proton reduction catalyzed by the chelator cobalt complex Co[dpg]<sub>3</sub>(BF<sub>4</sub>)<sub>2</sub>BF<sub>4</sub> (where dpg is diphenylglyoxime), leads to the formation of cobalt nanoparticles on the electrode surface. These nanoparticles have been proven to be the active species in the hydrogen production<sup>35</sup>.

In this chapter the synthesis and the characterization of a new polypyridyl decadentate ligand, shown in Figure 2, is presented. The ligand has been designed to furnish a rigid and flexible scaffold for ions of the first row transition metals. A six-member heterocyclic ring directly link the two metal centers imposing the distance between them. Two tertiary amines symmetrically extend from this central unit supplying a further coordination site. A dipyridyl group and a more flexible methylpyridyl unit complete, for both side, the pentacoordination leaving to each metal a sixth coordination site free for accommodate small ligands such as chloro, acetonitrile, water or bridging group like hydroxo and peroxy. The ligand owns a C<sub>2v</sub> symmetry as

## New polypyridyl decadentate ligand and related Co complexes

confirmed by the  $^1\text{H-NMR}$  spectra (Figure 5). Two possible isomers can result from the coordination of two metal ions depending on the orientation, *cis* or *trans*, of the two methylpyridyl groups.



**Figure 2.** Polypyridyl decadentate ligand, **L**

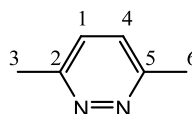
The synthesis and characterization of two dinuclear cobalt complexes containing the decadentate ligand will be also presented. Latest some results of a preliminary study of the electrocatalytic activity of these complexes toward the oxidation of water and the reduction of proton will be discussed.

## VI. ii. Experimental section

**Materials.** All reagents used in the present work were obtained from Aldrich Chemical Co. or Alfa Aesar and were used without further purification. Synthesis-grade organic solvents were obtained from SDS and were routinely degassed with argon. Methanol (MeOH) was distilled over  $Mg/I_2$ , ethanol was dried with a 3.5 Å molecular sieve, and acetonitrile, dichloromethane (DCM), hexane, and diethyl ether were used from the SPS. High-purity deionized water was obtained by passing distilled water through a nanopure Milli-Q water purification system.  $Co(OTf)_2$  was prepared as described in the literature. All synthetic manipulations were routinely performed under an argon atmosphere using Schlenk and vacuum-line techniques.

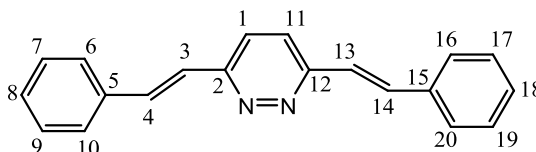
## New polypyridyl decadentate ligand and related Co complexes

**3,6-Dimethylpyridazine (1):** 19.98 g (0.175 mol) of acetylacetone and 9 g (0.180 mol) of hydrazine monohydrate were dissolved in 200 mL of absolute



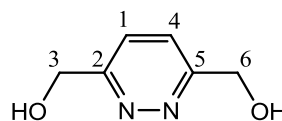
ethanol and refluxed for 30 min. The ethanol was evaporated leading to green oil. 200 mL of toluene were added, and then 1.40 g of 10% Pd on Carbon was slowly added at room temperature. The solution was then refluxed overnight. After filtration the toluene was evaporated to give 17.6 g (93%) of product as green oil.  $^1\text{H-NMR}$  (400 MHz,  $\text{CDCl}_3$ )  $\delta$  7.20 (s, 2H; H1, H4), 2.66 (s, 6H; H3, H6).

**3,6-Distyrylpyridazine (2):** 0.742 g of  $\text{ZnCl}_2$ , 7.42 g of **1** (68.6 mmol) and 22 mL (3 eq) of freshly distilled benzaldehyde



were mixed and let reflux for 2 h under Ar. After this time the benzaldehyde/water azeotrope was slowly distilled in a Dean-Stark trap. The resulting black solid was filtered and washed with cold ethanol (or acetone) and dried. Yield, 51%.  $^1\text{H-NMR}$  (400 MHz,  $\text{DMSO-d}_6$ )  $\delta$  8.02 (s, 2H; H1, H11), 7.80 (d,  $J = 16.5$  Hz, 2H; H3, H13), 7.76 – 7.71 (m, 4H; H6, H10, H16, H20), 7.50 (d,  $J = 16.5$  Hz, 2H; H4, H14), 7.45 (t,  $J = 7.4$  Hz, 4H; H7, H9, H17, H19), 7.40–7.33 (m, 2H; H8, H18).

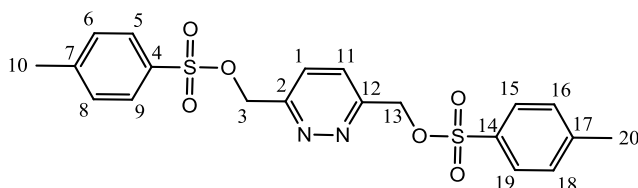
**3,6-Di(hydroxymethyl)pyridazine (3):** Ozone was bubbled through a suspension of 2.5 g (8.8 mmol) of **2** at  $-78$  °C in methanol (300 mL) until all the solid



dissolves. Excess of ozone was then removed by degassing the solution with nitrogen, and an excess of sodium borohydride (1g, 26 mmol, 3 equivalents) was added maintaining  $-78$  °C. The reaction mixture was then warmed to ambient temperature and filtered. After evaporation of the methanol under

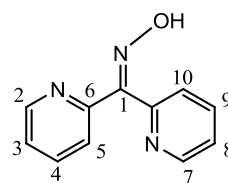
vacuum the crude product was purified by chromatography (silica; washed with dichloromethane and eluted with dichloromethane/methanol 3:1) allowing the isolation of the product as yellow oil in 75% yield. The purity of the product was confirmed by proton NMR.  $^1\text{H-NMR}$  (400 MHz,  $\text{DMSO-d}_6$ )  $\delta$  7.72 (s, 2H; H1, H4), 4.74 (s, 4H; H3, H6).

### 3,6-Bis(tosyloxymethyl)pyridazine (**5**):



A solution of *p*-toluenesulfonyl chloride (1.52 g, 8 mmol) in THF (11 mL) was added to a solution of **3** (0.56 g, 4 mmol) and NaOH (0.5 g, 12.5 mmol) in a mixture of water (11 mL) and THF (11 mL). After stirring at 25°C for 3 h, the solution was concentrated by partial evaporation of the solvent, which resulted in the precipitation of the product as a white solid. The product was isolated by filtration to give **5** (1.61 g, 90% yield).  $^1\text{H-NMR}$  (400 MHz,  $\text{CDCl}_3$ )  $\delta$  7.84 (d,  $J = 8.2$  Hz, 4H; H5, H9, H15, H19), 7.67 (s, 2H; H1, H11), 7.38 (d,  $J = 8.1$  Hz, 4H; H6, H8, H16, H18), 5.37 (s, 4H; H3, H13), 2.47 (s, 6H; H10, H20).

*Di-2-pyridyl ketone oxime* (**6**): Di-2-pyridyl ketone (5 g, 27 mmol) and hydroxylamine hydrochloride (2.91 g, 42 mmol) were dissolved in 10 mL of ethanol. Sodium hydroxide (5.5 g, 137.5 mmol) was slowly added to the

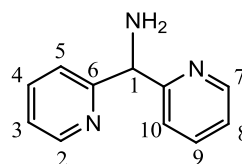


solution with stirring over a period of 90 min, during which time the solution turned dark orange and a white precipitate formed. The solution was heated at reflux for 10 min and cooled to room temperature. The reaction mixture was treated with water (20 mL) and concentrated HCl (10 mL), and the ethanol was



removed by rotary evaporation to yield a dark red solution. The product was precipitated by addition of saturated aqueous sodium carbonate (20 mL), isolated by vacuum filtration. The crude oxime, a white solid, was used in the next step without further purification.  $^1\text{H-NMR}$  (400 MHz,  $\text{CDCl}_3$ )  $\delta$  16.18 (br s, 1H; OH), 8.69-8.57 (m, 2H; H2, H7), 7.92-7.75 (m, 3H; H5, H4, H9), 7.65 (dt,  $J = 8.2, 1.0$  Hz, 1H; H10), 7.45 (ddd,  $J = 7.6, 5.0, 1.1$  Hz, 1H, H8), 7.39-.29 (m, 1H; H3).

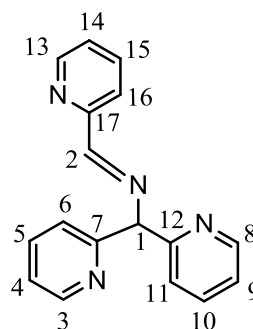
*Di-(2-pyridyl)methylamine (7)*: Oxime **6** (5 g, 25 mmol),  $\text{NH}_4\text{OAc}$  (3.40 g, 44 mmol),  $\text{NH}_3$  (28% aqueous, 75 mL), EtOH (100 mL) and  $\text{H}_2\text{O}$  (50 mL) were mixed and heated at 80 °C. Zn dust (7.47 g, 114.3 mmol) was



added in small portions over 30 min. The resulting mixture was refluxed for 3 h and then stirred at room temperature overnight. The mixture was filtered to remove the solids, which were washed with MeOH and  $\text{H}_2\text{O}$ . The filtrate was concentrated to yield an aqueous solution that was made strongly alkaline with aqueous 10 M NaOH. The amine was extracted with  $\text{CH}_2\text{Cl}_2$  and the organic phase was then washed with brine, dried over  $\text{Na}_2\text{SO}_4$  and concentrated under vacuum to afford the product as pale yellow oil; yield: 3.66 g (79%). Spectral data were in accordance with those previously reported.  $^1\text{H-NMR}$  (400 MHz,  $\text{CDCl}_3$ )  $\delta$  8.64-8.49 (m, 2H; H2, H7), 7.62 (td,  $J = 7.7, 1.8$  Hz, 2H; H4, H9), 7.38 (d,  $J = 7.9$  Hz, 2H; H5, H10), 7.14 (ddd,  $J = 7.4, 4.9, 1.0$  Hz, 2H; H3, H8), 5.32 (s, 1H; H1), 2.22 (br s, 2H,  $\text{NH}_2$ ).

*N*-[di(2-pyridinyl)methylidene]-*N*-(2-pyridinylmethyl)amine (**8**):

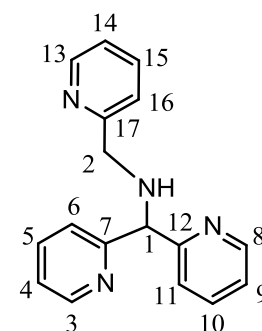
Freshly distilled pyridine-2-carboxaldehyde (2.0 mL, 21 mmol) was added to **7** (3.7 g, 20 mmol) and vigorously shaken. The mixture was then allowed to stand for 2 hours. The white solid was collected and washed with cyclohexane to remove traces of unreacted starting material to give 5.15 g (yield: 94%) of **8**. Spectral data were compared with those



reported.  $^1\text{H-NMR}$  (400 MHz,  $\text{CDCl}_3$ )  $\delta$  8.67-8.64 (m, 1H; H13), 8.63 (s, 1H; H2), 8.60-8.56 (m, 2H; H3, H8), 8.22 (d,  $J = 7.9$  Hz, 1H; H16), 7.76 (td,  $J = 7.6, 1.4$  Hz, 1H; H15), 7.68 (td,  $J = 7.7, 1.8$  Hz, 2H; H10, H5), 7.57 (d,  $J = 7.9$  Hz, 2H; H11, H6), 7.32 (ddd,  $J = 7.5, 4.8, 1.2$  Hz, 1H; H14), 7.16 (ddd,  $J = 7.4, 4.9, 1.1$  Hz, 2H; H9, H4), 6.01 (s, 1H; H1).

*N*-[di(2-pyridinyl)methyl]-*N*-(2-pyridinylmethyl)amine (**9**):

To a solution of **8** (5.15 g, 19 mmol) in dry methanol (70 mL) was added  $\text{NaBH}_4$  (1.78 g, 47 mmol) in small portions. After stirring at room temperature for 2 hours HCl (aq) was added until the  $\text{pH} < 2$ . After stirring for 30 min 5 N NaOH (aq) was added until the  $\text{pH} > 9$ . The methanol was evaporated leading and aqueous solution that was extracted with ethyl acetate. The

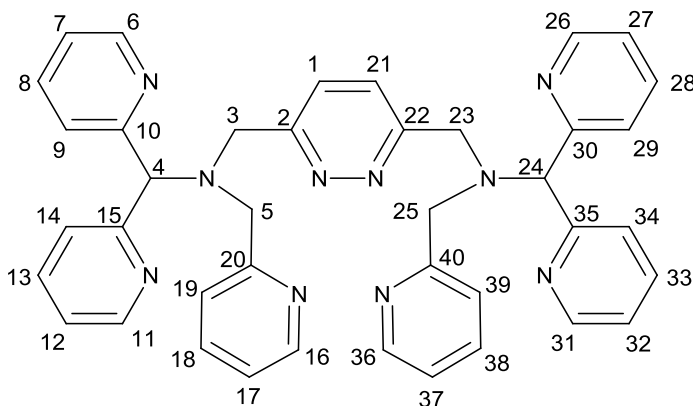


organic phase was then washed with brine and dried on  $\text{MgSO}_4$ . Evaporation of the solvent gave 5.14 g (yield: 98%) of **9**.

$^1\text{H-NMR}$  (400 MHz,  $\text{CDCl}_3$ )  $\delta$  8.55 (d,  $J = 4.7$  Hz, 2H; H8, H3), 8.53 (d,  $J = 4.9$  Hz, 1H; H13), 7.64-7.56 (m, 3H; H10, H5, H15), 7.46 (d,  $J = 7.3$  Hz, 2H; H11, H6), 7.34 (d,  $J = 7.7$  Hz, 1H; H16), 7.15-7.08 (m, 3H; H9, H4, H14), 5.15 (s, 1H; H15).

## New polypyridyl decadentate ligand and related Co complexes

*N,N'*-(pyridazine-3,6-diylbis(methylene))bis(1,1-di(pyridin-2-yl)-*N*-(pyridin-2-ylmethyl)methanamine), (**L**):



**9** (6.19 g, 22 mmol) and  $\text{Na}_2\text{CO}_3$  (25 g, 236 mmol) were dissolved in dry MeCN (70 mL) and warmed at 50 °C under Ar. A solution of **4** (5 g, 11 mmol) in dry MeCN (150 mL) was added. The resulting solution was heated at reflux during 6 hours under Ar. The crude was purified by chromatography (silica; washed with dichloromethane and eluted with dichloromethane/methanol 20:1) to give 3.2 g (yield: 44%) of pure product.

$^1\text{H-NMR}$  (400 MHz,  $\text{CDCl}_3$ )  $\delta$  8.63-8.51 (m, 4H; H6, H11, H26, H31), 8.45 (d,  $J = 4.7$  Hz, 2H; H16, H36), 7.70 (s, 2H; H1, H21), 7.68-7.61 (m, 8H; H8, H9, H13, H14, H28, H29, H33, H34), 7.58-7.47 (m, 4H; H18, H19, H38, H39), 7.17-7.09 (m, 4H; H7, H12, H27, H32), 7.06-6.97 (m, 2H; H17, H37), 5.26 (s, 2H; H4, H24), 4.10 (s, 4H; H3, H23), 3.92 (s, 4H; H5, H25).  $^{13}\text{C-NMR}$  (100 MHz,  $\text{CDCl}_3$ )  $\delta$  160.64 (C2, C22), 159.84 (C10, C15, C30, C35), 159.47 (C20, C40), 149.44 (C6, C11, C26, C31), 149.18 (C16, C36), 136.50 (C9, C14, C29, C34), 136.46 (C19, C39), 127.11 (C1, C21), 124.29 (C8, C13, C28, C33), 123.46 (C18, C38), 122.36 (C7, C12, C27, C32), 122.02 (C17, C37), 72.59 (C4, C24), 57.79 (C5, C25), 55.45 (C3, C23).

ESI-MS: Two major peaks were detected at  $m/z = 657$  corresponding to  $[\text{M}+\text{H}]^+$  and at  $m/z = 679$  corresponding to  $[\text{M}+\text{Na}]^+$ .

$\{[Co^{II}(L)(OTf)_2]\}(OTf)_2 \cdot 5H_2O$ , [**10(OTf)**] $_2 \cdot 5H_2O$ ]. The whole synthesis has been carried out inside the glove box under a N<sub>2</sub> atmosphere. 80 mg of [Co(OTf)<sub>2</sub>] $\cdot$ 0.5 MeCN (0.211 mmol) and 70 mg of **L** (0.105 mmol) were dissolved in 2 mL of MeCN and warmed at 60 °C. The solution was stirred for 3 h at this temperature and then filtered on cotton for removing unreacted starting materials. The product was precipitated by addition of diethyl ether. The initial precipitate, in form of oil, was scratched until that a light brown solid was obtained. The solid was then dried under vacuum for one night.

Anal. Calcd for C<sub>44</sub>H<sub>36</sub>Co<sub>2</sub>F<sub>12</sub>N<sub>10</sub>O<sub>12</sub>S<sub>4</sub> $\cdot$ 5H<sub>2</sub>O: C, 36.17 ; H, 3.17, N, 9.59; S, 8.78.

Found: C, 36.38; H, 3.09; N, 9.26; S, 8.48.

$\{[Co_2(O-O)L]\}(OTf)_4$ , [**13(OTf)**] $_4$ ]: 30 mg of [**10(OTf)**] $_2 \cdot 5H_2O$  were left under aerobic condition for one night. The red solid obtained was recrystallized from ethanol/diethyl ether leading to the formation of dark orange crystals.

<sup>1</sup>H-NMR (400 MHz, CD<sub>3</sub>CN) δ 10.48 (d, *J* = 7.0 Hz, 1H; H40), 9.23 (d, *J* = 5.6 Hz, 1H; H34), 8.14 – 7.06 (m, 2H; H32, H31), 8.02 (td, *J* = 7.7 Hz, 1.44 Hz, 1H; H38), 7.95 – 7.88 (m, 2H; H26, H27), 7.76 (s, 1H; H2), 7.68-7.58 (m, 2H; H39, H33), 7.39 (d, *J* = 8.8 Hz, 1H; H37), 7.05 (d, *J* = 6.5 Hz, 1H; H29), 6.86 (s, 1H; H24), 6.79 (td, *J* = 6.54 Hz, 1.68 Hz, 1H; H28), 5.55 (d, *J* = 19.8 Hz, 1H; H35A), 5.50 (d, *J* = 20.39 Hz, 1H; H5A), 5.31 (d, *J* = 19.8 Hz, 1H; H35B), 5.21 (d, *J* = 20.39 Hz, 1H; H5B). <sup>13</sup>C-NMR (100 MHz, CD<sub>3</sub>CN) δ 177.02 (C1), 167.62 (C36), 158.17 (C25, C30), 154.53 (C29), 154.12 (C34), 154.07 (C40), 143.57 (C32), 143.25 (C26), 142.35 (C38), 132.51 (C2), 138.34 (C33), 127.34 (C28), 127.21 (C39), 126.94 (C31), 126.41 (C27), 123.86 (C37), 78.11 (C24), 67.27 (C35), 66.05 (C5).

**Equipment and Measurements.** All electrochemical experiments were performed in a PAR 263A EG&G potentiostat or in an IJ-Cambria HI-660 potentiostat, using a three-electrode cell. Glassy carbon (3 mm diameter) from

BAS was used as the working electrode, a platinum wire as the auxiliary electrode, and SSCE or a  $\text{Ag}/\text{Ag}^+$  (0.1 M TBAD-0.01M  $\text{AgNO}_3$  in MeCN) as the reference electrode. Cyclic voltammograms were recorded at a  $100 \text{ mV}\cdot\text{s}^{-1}$  scan rate. The complexes were dissolved in previously degassed MeCN containing the necessary amount of  $(n\text{-Bu}_4\text{N})(\text{PF}_6)$ , used as the supporting electrolyte, to yield a 0.1 M ionic strength solution. All  $E_{1/2}$  values reported in this work were estimated from cyclic voltammetry (CV) as the average of the oxidative and reductive peak potentials  $(E_{p,o} + E_{p,c})/2$  or from differential pulse voltammetry (DPV; pulse amplitudes of 0.05 V, pulse widths of 0.05 s, sampling width of 0.02 s, and a pulse period of 0.1 s). Unless explicitly mentioned, the concentrations of the complexes were approximately 1 mM. A 400 MHz Bruker Avance II spectrometer and a Bruker Avance 500 MHz were used to carry out NMR spectroscopy at room temperature. Samples were run in acetonitrile- $d_3$ . Elemental analyses were performed using a Carlo Erba CHMS EA-1108 instrument provided by the Chemical Analysis Service of the Universitat Autònoma de Barcelona (CAS-UAB).

#### **Single-Crystal X-Ray Structure Determination.** *Crystal Preparation.*

Crystals of  $[\mathbf{11}(\text{PF}_6)_4]$  were grown under strictly dry and anaerobic conditions by slow evaporation of an acetonitrile solution of  $\mathbf{10}^{2+}$  at  $-30 \text{ }^\circ\text{C}$ . The addition of a drop of a saturated  $\text{NH}_4\text{PF}_6$  methanol solution resulted necessary for the growth of suitable crystals for X-Ray diffraction. Crystals of  $[\mathbf{12}(\text{OTf})_4]$  were grown by diffusion of hexane on a solution of  $\mathbf{10}^{2+}$  in benzonitrile (crystals grew in the glove box but were measured long time after getting them out, partial oxidation had taken place and the crystal had taken an orange color). Crystals of  $[\mathbf{13}(\text{OTf})_4]$  were obtained by slow diffusion of diethyl ether on a solution of  $[\mathbf{13}(\text{OTf})_4]$  in ethanol.

*Data collection:* Crystal structure determinations for complexes **11**<sup>4+</sup>, **12**<sup>4+</sup> and **13**<sup>4+</sup> were carried out using a Bruker-Nonius diffractometer equipped with an APPEX 2 4K CCD area detector, a FR591 rotating anode with MoK<sub>α</sub> radiation, Montel mirrors as monochromator and an Oxford Cryosystems low temperature device Cryostream 700 plus ( $T = -173$  °C). Full-sphere data collection was used with  $\omega$  and  $\varphi$  scans. *Programs used:* Data collection APEX-2, data reduction Bruker Saint V/.60A and absorption correction SADABS or TWINABS.

*Structure Solution and Refinement:* Crystal structure solution was achieved using direct methods as implemented in SHELXTL and visualized using the program XP. Missing atoms were subsequently located from difference Fourier synthesis and added to the atom list. Least-squares refinement on  $F^2$  using all measured intensities was carried out using the program SHELXTL. All non-hydrogen atoms were refined including anisotropic displacement parameters. In order to avoid highly disordered solvent molecules the program SQUEEZE was used.

The asymmetric unit of **11**<sup>2+</sup> contains one molecule complex, four PF<sub>6</sub> anions and 3 and half molecules of acetonitrile. One of the acetonitrile molecules is disordered over a center of inversion (50:50). The structure has a R1 value of 6,28 %. The asymmetric unit of **12**<sup>4+</sup> contains one molecule of the complex, four triflate anions and some highly disordered solvent molecules (probably benzonitrile). In the main molecule complex one of the decadentate ligand rests is disordered in inverted positions (ratio 57:43). Three of the four triflate anions are disordered in two positions (ratios 55:45, 71:29, 68:32). The crystal structure contains also an undetermined number of solvent molecules which are highly disordered. In order to avoid the highly disordered solvent molecules the program SQUEEZE was applied leading to a refined model with a

R1 value of 8.22 % in which the solvent molecules were removed. The asymmetric unit of  $\mathbf{13}^{4+}$  contains one molecule of the complex, four triflate anions and three highly disordered alcohol. Two of the triflate anions are disordered in two positions (ratios: 51:49 and 69:41). The R1 value is of 9.31 %.

*Proton reduction.* All the electrochemical proton reduction experiments were performed in an IJ-Cambria HI-660 potentiostat, using a three-electrode cell. Glassy carbon (3 mm diameter) from BAS was used as the working electrode, a platinum wire as the auxiliary electrode, and SSCE as the reference electrode. All the experiments were performed under  $N_2$  atmosphere through a slight flow of gas. *Acid concentration dependence.* 2.1 mg (1.44  $\mu\text{mol}$ ) of  $[\mathbf{10}(\text{OTf})_2 \cdot 5\text{H}_2\text{O}]$  were transferred in a vial inside the glovebox and sealed. 7.18 mL of previously degassed acetonitrile containing the necessary amount of (n-Bu<sub>4</sub>N)(PF<sub>6</sub>), used as the supporting electrolyte, to yield a 0.1 M ionic strength solution, were transfer in the vial under  $N_2$  atmosphere. The final concentration of  $\mathbf{10}^{2+}$  was of 0.2 mM. Cyclic voltammograms were recorded at a 100  $\text{mV} \cdot \text{s}^{-1}$  scan rate. A first voltammogram in absence of acid was recorded to determine  $i_p$ . Aliquots of 6  $\mu\text{L}$  ( $7.835 \cdot 10^{-5}$  mol, final concentration = 21 mM) trifluoroacetic acid 99% were added and the current at -0.99 V vs SSCE was measured to determine  $i_c$ . The glassy carbon working electrode was cleaned on a MicroPolish Powder (0.05 micron, washed with water and acetone and dry after each measure. *Scan rate dependence:* 4.0 mg (2.74  $\mu\text{mol}$ ) of  $[\mathbf{10}(\text{OTf})_2 \cdot 5\text{H}_2\text{O}]$  were transferred in a vial inside the glovebox and sealed. 13.7 mL of previously degassed acetonitrile containing the necessary amount of (n-Bu<sub>4</sub>N)(PF<sub>6</sub>), used as the supporting electrolyte, to yield a 0.1 M ionic strength solution, were transfer in the vial under  $N_2$  atmosphere. The final concentration of  $\mathbf{10}^{2+}$  was of 0.2 mM. Cyclic voltammograms were recorded at

different scan rate from  $200 \text{ mV}\cdot\text{s}^{-1}$  to  $10 \text{ mV}\cdot\text{s}^{-1}$ . The glassy carbon working electrode was cleaned as described above after each measure.

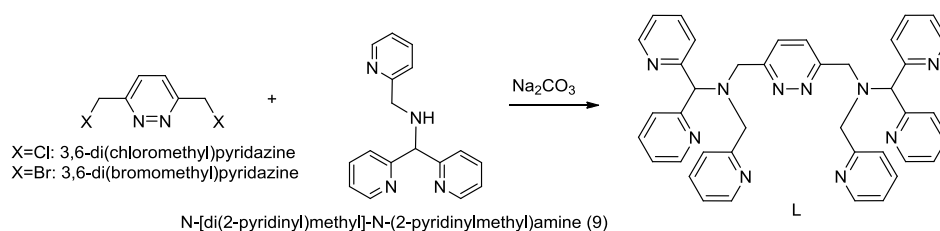
*Water oxidation.* All the controlled potential electrolysis (CPE), electrocatalysis, CVs and DPVs before and after the electrocatalytic experiment of water oxidation were performed in a two compartment cell closed with a septum-sealed adapter using a Bio-Logic potentiostat/galvanostat and EC-Lab software. A FTO slide ( $1 \text{ cm}^2$ ) connected to a tin wire was used as working electrode, platinum grid as the auxiliary electrode and an aqueous  $\text{Ag}/\text{Ag}^+$  (KCl 3 M) as the reference electrode. The oxygen concentration of the headspace of the compartment containing the working electrode was monitored with a Clark's fast-response oxygen micro-electrode needle sensor (OX-N, 40 mm needle length, 1.1 mm diameter, 90% response time  $<10 \text{ s}$ ) commercialized by Unisense A/S. In a typical experiment 0.70 mg ( $0.5 \text{ }\mu\text{mol}$ , final concentration 0.1 mM) of  $\mathbf{13}^{4+}$  were dissolved in 5 mL of pH 2.1 phosphate buffer (0.1 M,  $I = 0.052$ ). Controlled potential electrolysis was performed on the stirred solution at 1.80 V vs  $\text{Ag}/\text{Ag}^+$ .



## VI. iii. Results and discussion

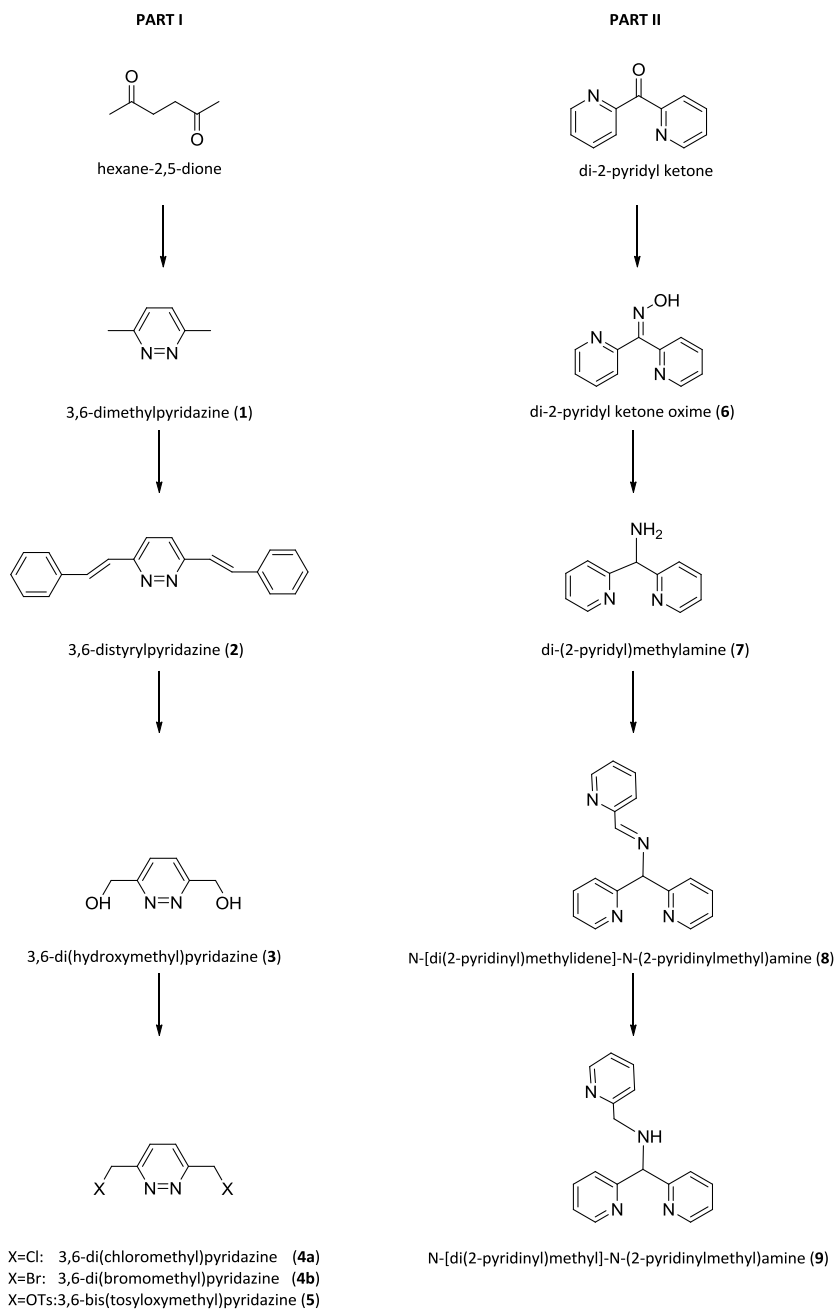
### Synthesis of the ligand

As mentioned above the pyridazine based ligand has been chosen as bridging ligand for insuring the coordination of two metal centres. A symmetrical disubstitution in *orto* to N atoms has been operated for binding the remaining 8 coordination sites. According to this design the preparation of the decadentate ligand  $L_1$  has been planned as the condensation between two species: a halopyridazine and a secondary amine as indicated below:



**Scheme 2.** Synthesis of  $L$ .

The good tendency of chloro and bromo as leaving groups would have led to an easy attack by the deprotonated ternary amine. The synthesis of the two precursors is showed in the following scheme.

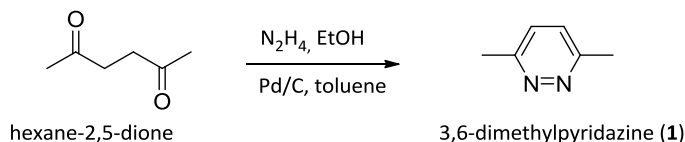


**Scheme 3.** Synthetic pathway for L.

## New polypyridyl decadentate ligand and related Co complexes

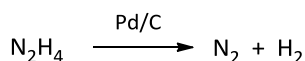
### Part I

The pyridazine cycle, in which two methyl groups are *para* to each other, was prepared by the route referenced by Wiley<sup>36</sup> starting from hexane-2,5-dione (scheme 4):



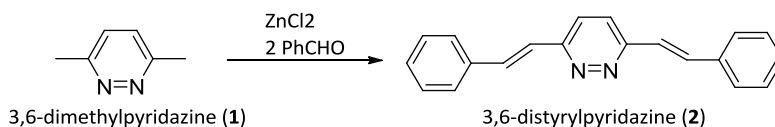
**Scheme 4.** Synthesis of **1**.

The role of Palladium is to accelerate the decomposition of excess of hydrazine by the reaction:



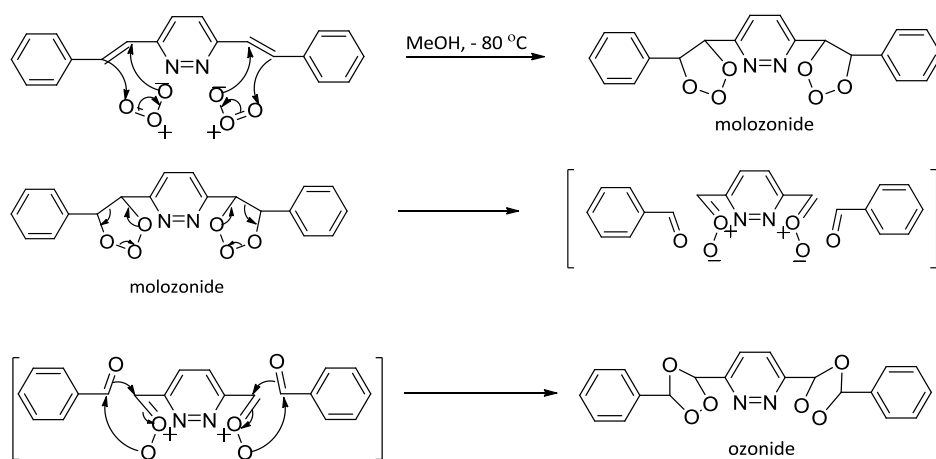
**Scheme 5.** Hydrazine decomposition.

Distyrylpyridazine was obtained from the condensation of **1** with benzaldehyde<sup>36</sup> in accordance with the following scheme:



**Scheme 6.** Synthesis of **2**.

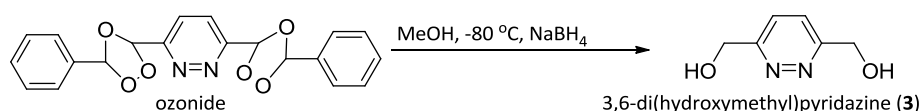
Bubbling ozone into a suspension of **2** in methanol at  $-80^\circ\text{C}$  generates the formation of the molozonide intermediate that rearranges to the ozonide form (Scheme 7).



**Scheme 7.** Mechanism of ozonolysis.

The functional group of an ozonide is a trioxolane ring structure with a five-member C-O-O-C-O ring. Ozonides are explosive compounds that are usually not isolated but treated at low temperature.

Reduction with an excess of  $\text{NaBH}_4$  finally gives the 3,6-di(hydroxymethyl)pyridazine (**3**) (Scheme 8)<sup>37</sup>



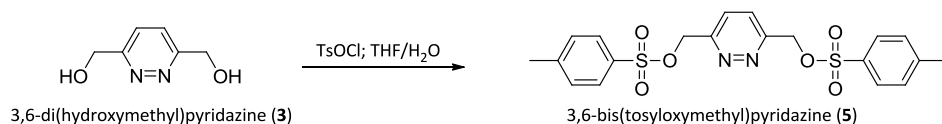
**Scheme 8.** Break of ozonide and formation of **3**.

Initially the substitution of the two hydroxyl groups of **3** with good leaving groups as  $\text{Cl}$  or  $\text{Br}^-$  (**4a** and **4b**) has been planned in order to provide a suitable site for the attack **9**. For this purpose several attempts of the reaction of **3** with thionyl chloride has been operated changing solvent ( $\text{CHCl}_3$ ,  $\text{MeOH}/\text{CHCl}_3$ , DMF) and time of reaction. All the experiments did not give the desired 3,6-di(chloromethyl)pyridazine, therefore the analogous substitution with bromo

## VI New polypyridyl decadentate ligand and related Co complexes

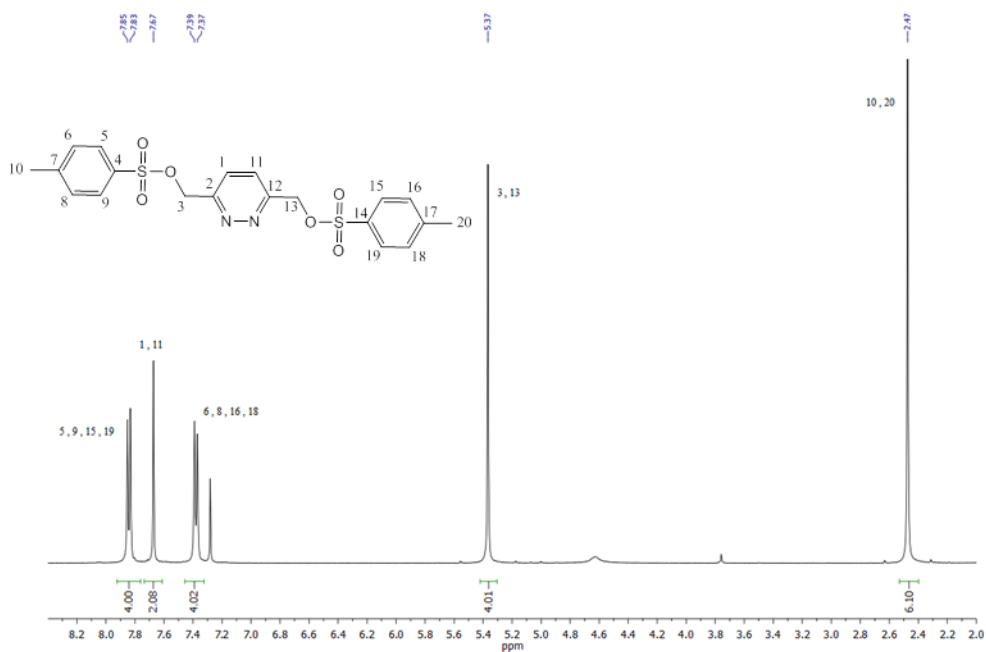
has been tried. The reaction was tested using  $PB_3$  as reactant in  $CCl_4$  or  $C_2H_4Cl_2$ , but in both cases the substitution did not proceed. Given that the main problem seemed to be the solubility of **3** in organic solvents (commonly used in chlorination and bromination reactions) another attempt has been made using  $HBr$  48% as reactant<sup>38</sup>. Unfortunately it did not lead to the desired product.

Finally, a room temperature reaction with *p*-toluenesulfonyl chloride in a water/tetrahydrofuran mixture, led to the formation of 3,6-bis(tosyloxymethyl)pyridazine (**5**) in good yields<sup>39</sup>. The tosyl group represents another good option as leaving group (Scheme 9).



**Scheme 9.** Synthesis of **5**.

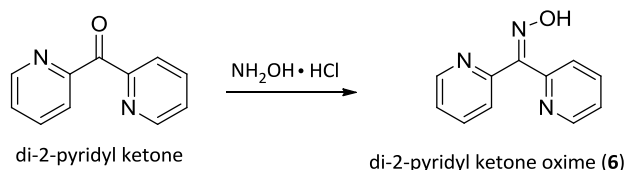
The  $^1H$ -NMR spectra of **5** (Figure 3), compared with reported one<sup>39</sup>, confirmed the purity of the compound.



## Part II

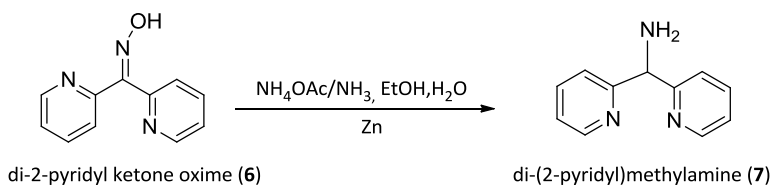
On the other hand the synthesis of the second precursor, the secondary amine, has been carried out as planned.

Again a ketone is the starting material for the preparation<sup>40</sup>. Di-2-pyridyl ketone reacted almost quantitatively with hydroxylamine hydrochloride giving the relative ketoxime, **6**, (Scheme 10).



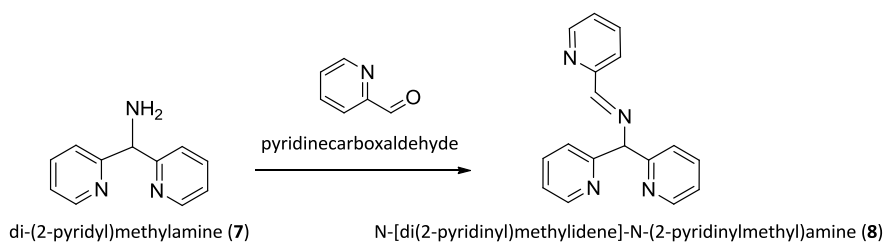
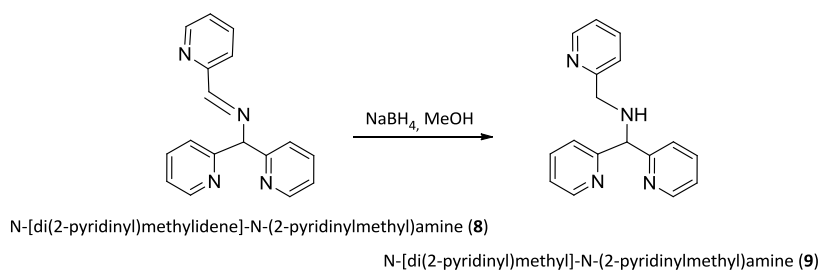
**Scheme 10.** Synthesis of **6**.

Reduction of **6** with Zn gave the di-(2-pyridyl)methylamine (**7**) as described<sup>41</sup> (Scheme 11).



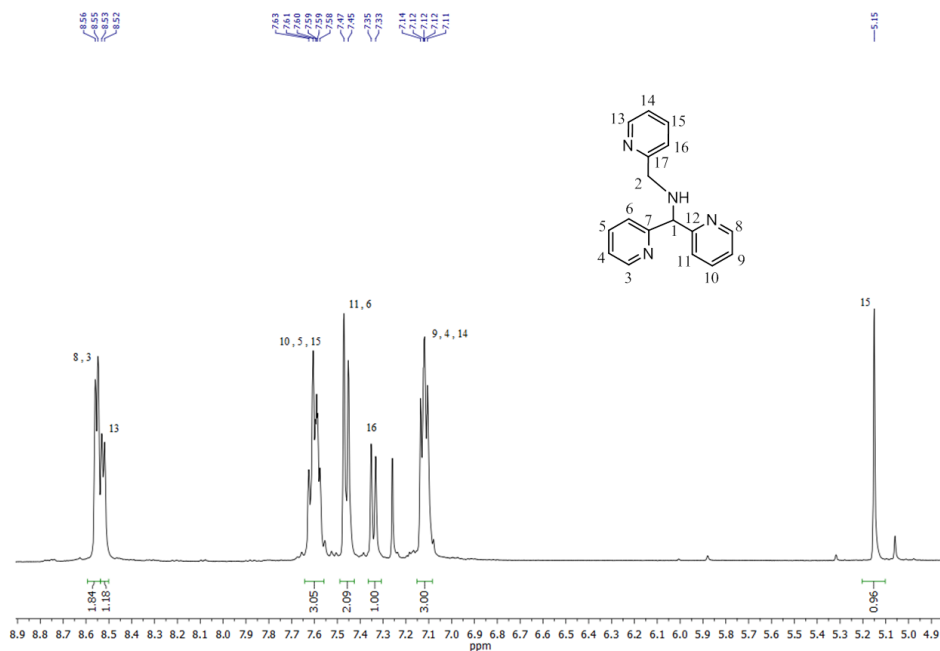
**Scheme 11.** Synthesis of **7**.

The following step was fundamental for the modification of the final ligand. Condensations with functionalized aldehyde could be carried out with high yield<sup>42,43</sup>. Reaction of **7** with pyridine-2-carboxaldehyde gave the relative imine **8**, which is reduced in the next by NaBH<sub>4</sub> to the desired amine<sup>42</sup> **9** (Scheme 12 and 13).

**Scheme 12.** Synthesis of **8**.**Scheme 13.** Synthesis of **16**.

In figure 4 the spectra of **9** is shown; all the peaks have been assigned and compared with reported data.

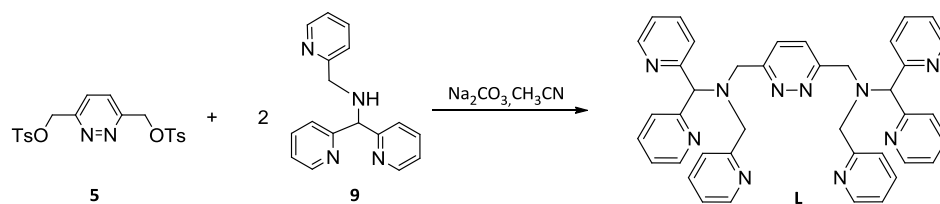




**Figure 4.**  $^1\text{H-NMR}$  spectra of **9** (400 MHz, 298 K,  $\text{CDCl}_3$ ).

### Part III

The final step of the synthesis consists in the condensation of the two precursors **5** and **9**. The reaction is carried out in dry acetonitrile in the presence of an excess of  $\text{Na}_2\text{CO}_3$  (Scheme 14).

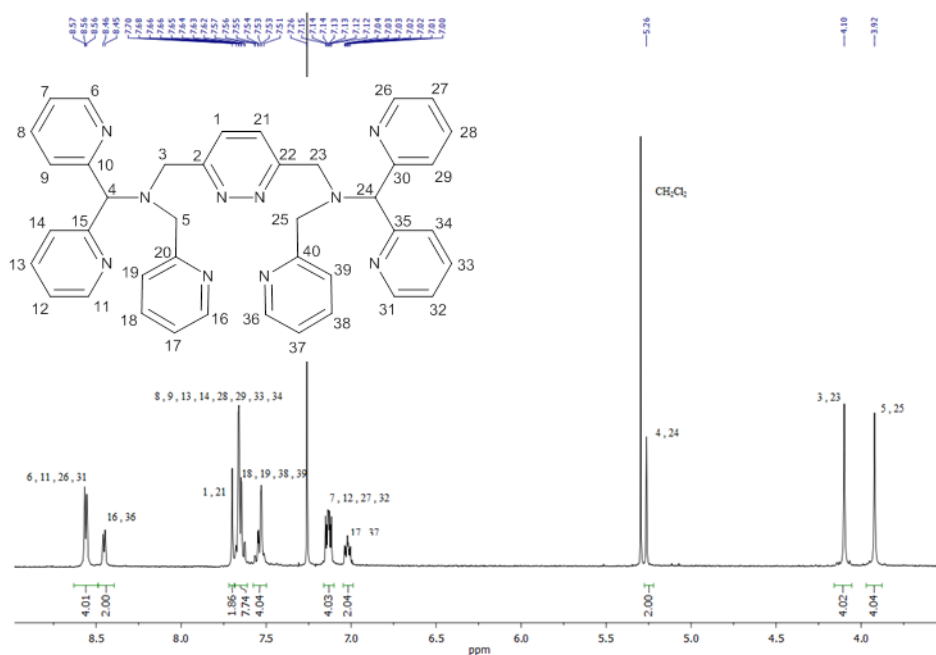


**Scheme 14.** Synthesis of  $N,N'$ -(pyridazine-3,6-diylbis(methylene))bis(1,1-di(pyridin-2-yl)- $N$ -(pyridin-2-ylmethyl) methanamine) **L**.

The crude is then purified by chromatography resulting in 40% yield of pure product. The moderate yield obtained is mainly due:

- the competition with the monosubstitution reaction
- the instability of **5**<sup>39</sup>
- the efficiency of Na<sub>2</sub>CO<sub>3</sub> in deprotonating the amine

The product has been characterized by 1D and 2D NMR and mass spectroscopy. All the <sup>1</sup>H and <sup>13</sup>C signals were unambiguously assigned as shown in Figure 5 and Figure 6.



**Figure 5.** <sup>1</sup>H-NMR spectra of **L** (400 MHz, 298 K, CDCl<sub>3</sub>).

In the aromatic section of <sup>1</sup>H-NMR (Figure 5) the characteristic peaks of H atoms of pyridyl groups were found. In particular the two doublets of H6 (H11) and H16 were easily noticed at δ 8.56 and δ 8.45 respectively. On the other hand, in the aliphatic area, three singlets were found as expected. At δ 5.26 the singlet corresponding to one proton was assigned to H4, while the peak of H3 was found at δ 4.10 through the interaction with H1 detected by NOESY



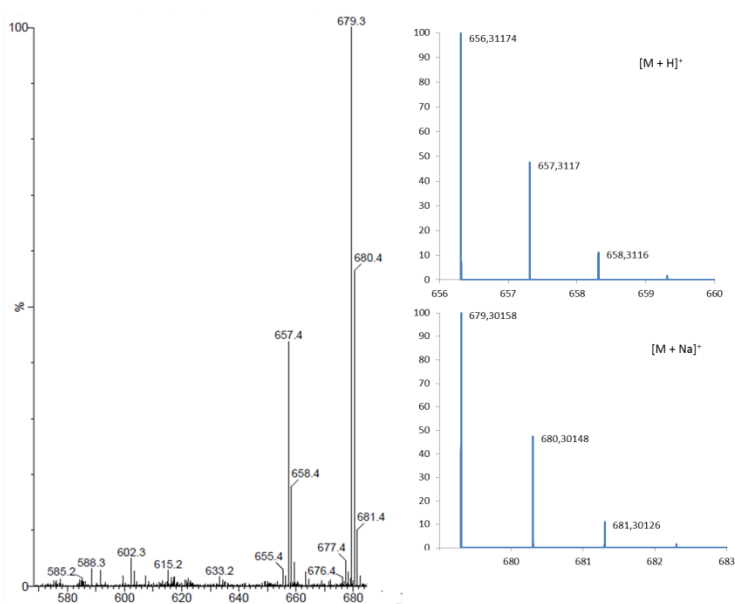


Figure 7. ESI-MS (CH<sub>3</sub>OH) of L.

### Synthesis of $\{[\text{Co}^{\text{II}}_2(\text{L})(\text{OTf})_2]\}(\text{OTf})_2$ , **10**.

The whole synthesis of the dinuclear Co(II) complex containing **L** was performed inside a glove box under  $\text{N}_2$  atmosphere in order to avoid aerobic oxidation. An acetonitrile solution of **L** was mixed with an acetonitrile solution containing two equivalents of  $[\text{Co}(\text{OTf})_2]$  and warmed at  $50\text{ }^\circ\text{C}$  for 3 hours. The mixture was then filtered and the product precipitated as triflate complex by addition of diethyl ether. The pale yellow solid obtained was then dried and analyzed by ESI-MS (Figure 8). The resulting spectra agreed with a dinuclear complex with formula  $\{[\text{Co}^{\text{II}}_2(\text{L})(\text{OTf})_2]\}(\text{OTf})_2$ , [**10**(**OTf**)<sub>2</sub>], confirming the II,II oxidation states for the two metals centers. As shown in Figure 8, peaks of mono- double- and triple-charged species were detected and compared with their simulated pattern. However the lack of solid state structure impeded a description, beyond the speculative character, of the disposition of the ligand and the triflate ions inside the coordination sphere.

As expected **10**<sup>2+</sup> is highly sensitive to aerobic conditions both in solid state and in solution resulting in a clear change of color from yellow pale to orange.

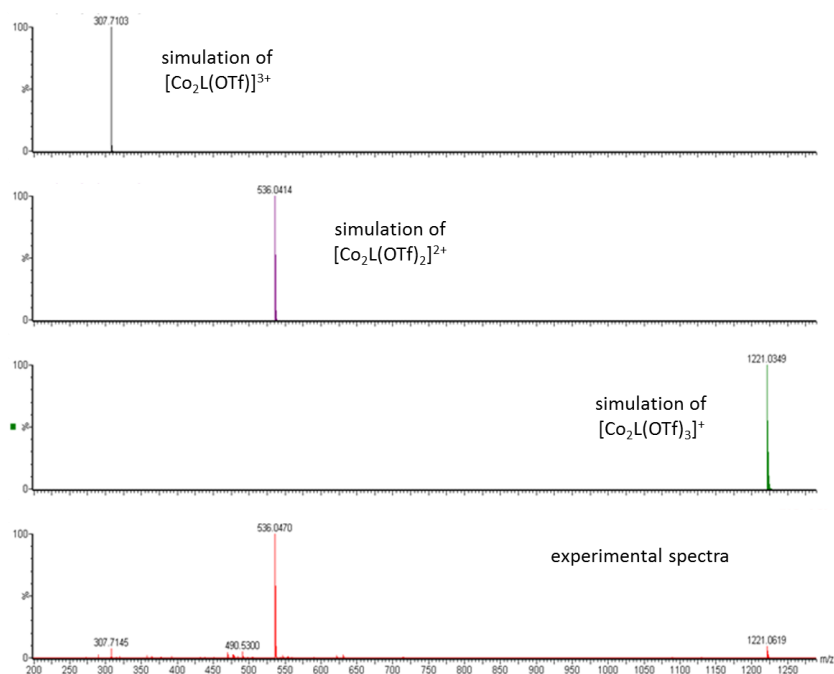
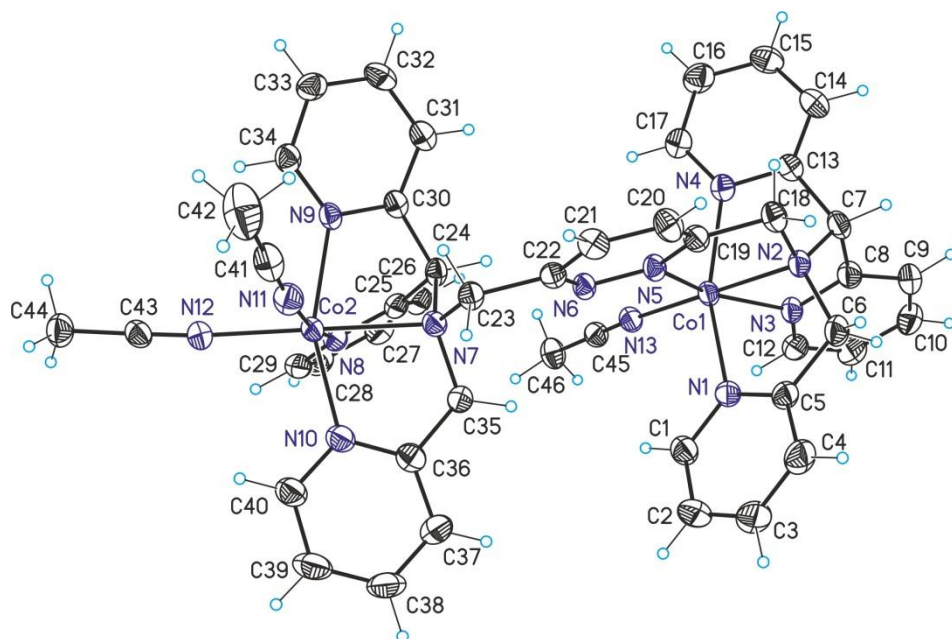


Figure 8. ESI-MS (MeCN) of  $[10(OTf)_2]$ .

### Solid state structure

The characterization of **10** and its oxidized forms has been completed through elemental analysis, electrochemistry and X-Ray diffraction. Three X-Ray structures have been obtained from crystals grown in different conditions. Under strictly dry and anaerobic conditions a  $Co^{II}Co^{II}$  complex,  $[11(PF_6)_4]$ , has been obtained by slow evaporation of an acetonitrile solution of  $10^{2+}$  at  $-30\text{ }^\circ\text{C}$ . The addition of a drop of a saturated  $NH_4PF_6$  methanol solution resulted necessary for the growth of suitable crystals for X-Ray diffraction. The two metal centers present both hexacoordination but, unexpectedly, the ligand resulted partially decoordinated in the N6 of the pyridazine moiety. Three molecules of acetonitrile fulfil the coordination sphere while four  $PF_6^-$  act as counter ions. Likely, the flexibility of the ligand, given by the  $CH_2$  groups and

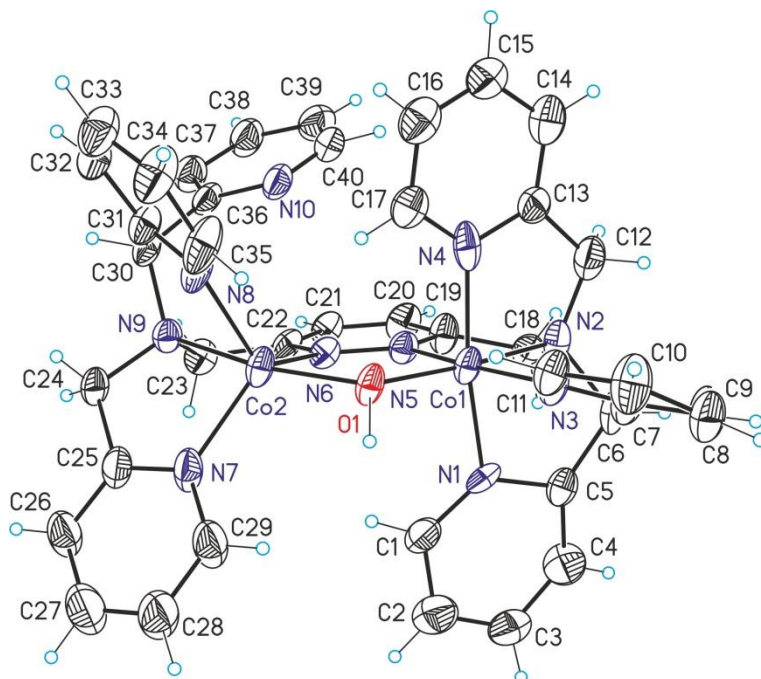
the free rotation of the tertiary amine, leads to the formation in solution of a mixture of structural isomers in which the ligand and solvent compete for the coordination sites of the metal ions. The Co-N bond distances were similar to those of similar dinuclear cobalt(II) complexes<sup>44</sup>. The ortep plot of **11**<sup>4+</sup> is shown in figure 9.



**Figure 9.** Ortep plot (ellipsoid at 50% probability) X-Ray structure of **11**<sup>4+</sup>.

Some yellow crystals were also obtained by slow diffusion of hexane on a solution of **10**<sup>2+</sup> in benzonitrile (crystals grew in the glove box but were measured long time after getting them out, partial oxidation had taken place and the crystal had taken an orange color). This structure showed a hydroxo bridge between the two Co centers (**[12(OTf)<sub>4</sub>]**, Figure 10). The number of counter ions and the bond distances of the indicated a different oxidation state for the two metal atoms. The most surprising feature of this structure was the pentacoordination of the cobalt atom in the oxidation state +2, given

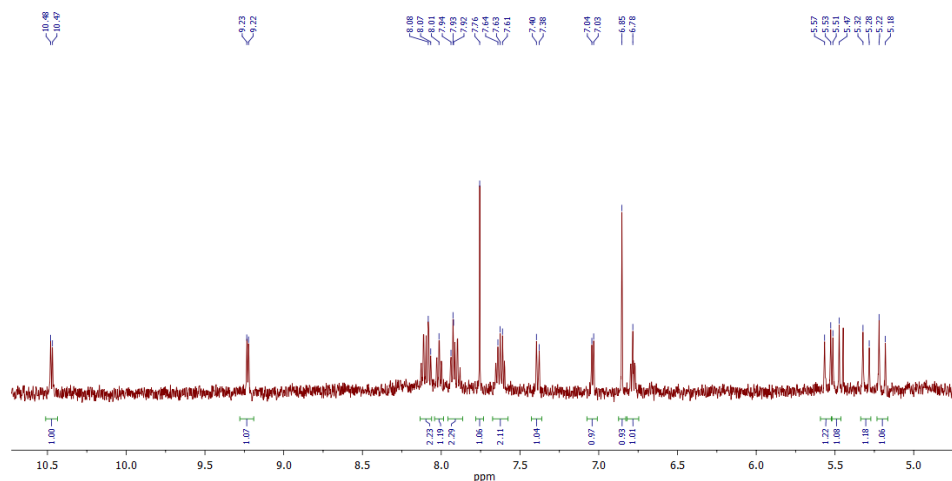
that N10 of one pyridyl group resulted decoordinates. Lastly, the presence of very small amount of water in the crystallization solvent resulted in the coordination of the six coordination site by the same.



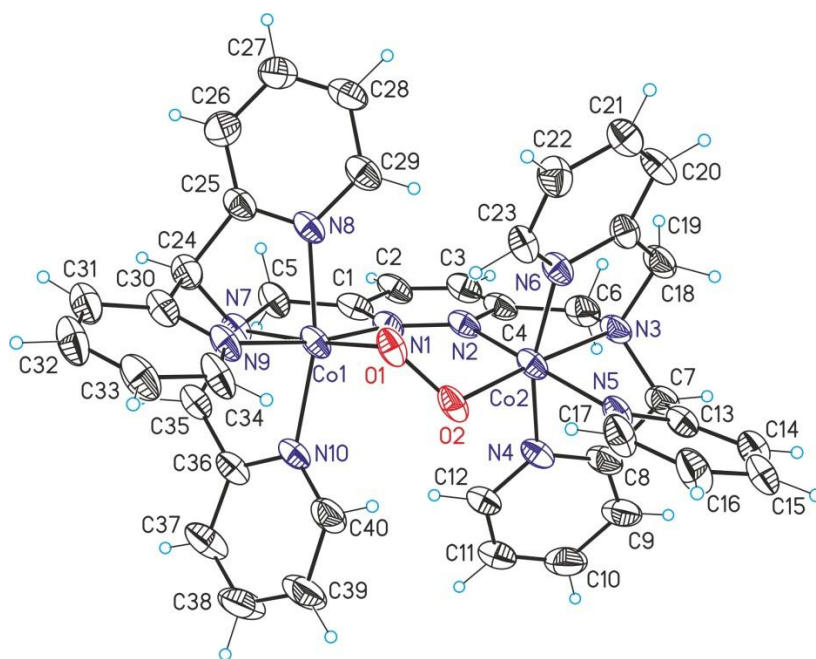
**Figure 10.** Ortep plot (ellipsoid at 50% probability) X-Ray structure of  $12^{4+}$ .

Lastly, in order to characterize the oxidized species,  $[10(OTf)_2]$  was let under aerobic condition in solid state for one night and then dissolved in ethanol. After addition of diethyl ether a dark orange solid was obtained and characterized by  $^1H$ -NMR. The proton NMR spectra showed a highly pure symmetric and diamagnetic compound pointing at a  $Co^{III}Co^{III}$  species ( $13^{4+}$ , Figure 11). Slow diffusion of diethyl ether on a solution of  $[13(OTf)_4]$  in ethanol gave suitable crystals for X-Ray diffraction. The oxidized compound consisted of a peroxobridge dinuclear  $Co^{III}Co^{III}$  complex (Figure 12). Both the metal centers showed hexacoordination and similar bond distances.





**Figure 11.** <sup>1</sup>H-NMR **13**<sup>4+</sup> (400 MHz, 298 K, CD<sub>3</sub>CN).



**Figure 12.** Ortep plot (ellipsoid at 50% probability) X-Ray structure of **13**<sup>4+</sup>.

Co-N bond distances of the **13**<sup>4+</sup> are within the range of expected for Co<sup>III</sup> octahedral complexes<sup>45,46</sup>. The Co-O and O-O bond distances were similar to

those of previously described cobalt(III) dinuclear peroxo-bridged complexes<sup>47</sup>.

Crystallographic data and selected bond distances and angles are reported in Table 1 and 2.

**Table 1.** Crystal Data for compounds **11<sup>4+</sup>** and **12<sup>4+</sup>** and **13<sup>4+</sup>**.

	<b>11<sup>4+</sup></b>		<b>12<sup>4+</sup></b>		<b>13<sup>4+</sup></b>	
Empirical formula	C <sub>106</sub> H <sub>111</sub> Co <sub>4</sub> F <sub>48</sub> N <sub>33</sub> P <sub>8</sub>		C <sub>44</sub> H <sub>37</sub> Co <sub>2</sub> F <sub>12</sub> N <sub>10</sub> O <sub>13</sub> S <sub>4</sub>		C <sub>46.50</sub> H <sub>43.50</sub> Co <sub>2</sub> F <sub>12</sub> N <sub>10</sub> O <sub>15.25</sub> S <sub>4</sub>	
Formula weight	3242.76		1387.94		1460.51	
Temperature	100(2)K		100(2)K		100(2)K	
Wavelength	0.71073 Å		0.71073 Å		0.71073 Å	
Crystal system	Triclinic		Triclinic		Monoclinic	
Space group	P-1		P-1		C2/c	
Unit cell dimensions	a = 11.38(9) Å	α = 81.21(2)°	a = 14.24(16) Å	α = 71.27(3)°	a = 35.08(3) Å	α = 90.00°
	b = 13.07(8) Å	β = 89.17(3)°	b = 14.85(16) Å	β = 72.10(3)°	b = 12.85(9) Å	β = 121.12(2)°
	c = 22.92(17) Å	γ = 87.44(2)°	c = 18.06(19) Å	γ = 72.37(3)°	c = 30.21(3) Å	γ = 90.00°
Volume	3368.1(4) Å <sup>3</sup>		3356.3(6) Å <sup>3</sup>		11668.5(18) Å <sup>3</sup>	
Z	1		2		8	
Density (calculated)	1.599 Mg/m <sup>3</sup>		1.373 Mg/m <sup>3</sup>		1.663 Mg/m <sup>3</sup>	
Absorption coefficient	0.704 mm <sup>-1</sup>		0.710 mm <sup>-1</sup>		0.824 mm <sup>-1</sup>	
F(000)	1638		1402		5924	
Crystal size	0.10 x 0.04 x 0.03 mm <sup>3</sup>		0.09 x 0.03 x 0.03 mm <sup>3</sup>		0.20 x 0.20 x 0.10 mm <sup>3</sup>	
Theta range for data collection	0.90 to 28.30 °		1.80 to 25.07 °		1.36 to 25.10 °	
	-15 <= h <= 14		-16 <= h <= 16		-41 <= h <= 40	
Index ranges	-12 <= k <= 17		-17 <= k <= 17		-15 <= k <= 13	
	-29 <= l <= 30		-21 <= l <= 21		-35 <= l <= 35	
Reflections collected	47446		52490		70489	
Independent reflections	16237 [R(int) = 0.0360]		11795 [R(int) = 0.0616]		10283 [R(int) = 0.0696]	
Completeness to theta = 28.30°	0.968 %		0.991 %		0.988 %	
Absorption correction	Empirical		Empirical		Empirical	
Max. and min. transmission	1.00 and 0.92		1.00 and 0.91		0.9221 and 0.8525	
Refinement method	Full-matrix least-squares on F <sup>2</sup>		Full-matrix least-squares on F <sup>2</sup>		Full-matrix least-squares on F <sup>2</sup>	
Data/restraints/parameters	16237/0/917		11795/303/963		10283/146/887	
Goodness-of-fit on F <sup>2</sup>	1.060		1.034		1.057	
Final R indices [I > 2σ(I)]	R1 = 0.0628 wR2 = 0.1519		R1 = 0.0822 wR2 = 0.2302		R1 = 0.0931 wR2 = 0.2582	
R indices (all data)	R1 = 0.0907 wR2 = 0.1648		R1 = 0.1282 wR2 = 0.2565		R1 = 0.1574 wR2 = 0.3215	
Largest diff. peak and hole	1.086 and -0.477 e.Å <sup>-3</sup>		1.049 and -0.689 e.Å <sup>-3</sup>		1.635 and -0.969 e.Å <sup>-3</sup>	

## New polypyridyl decadentate ligand and related Co complexes

**Table 2.** Selected metric parameters for compounds **11<sup>4+</sup>** and **12<sup>4+</sup>** and **13<sup>4+</sup>**.

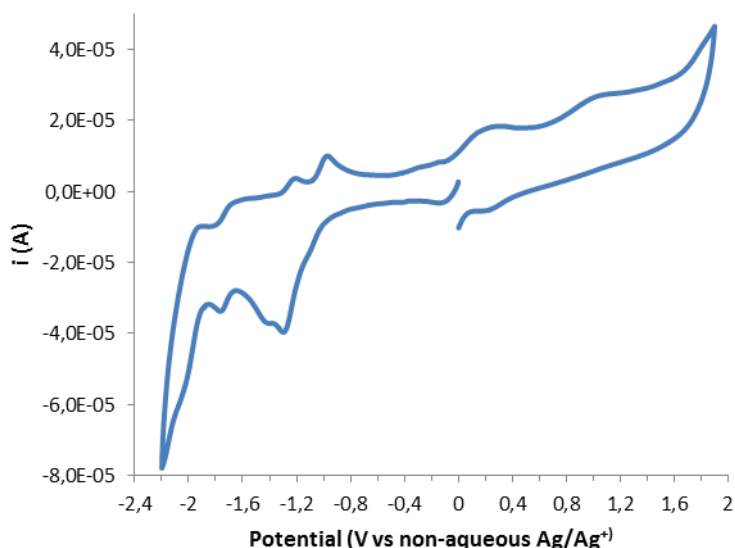
<b>11<sup>4+</sup></b>		<b>12<sup>4+</sup></b>		<b>13<sup>4+</sup></b>	
<b>Bond distances (Å)</b>		<b>Bond distances (Å)</b>		<b>Bond distances (Å)</b>	
Co(1)-Co(2)	7.723	Co(1)-Co(2)	3.336	Co(1)-Co(2)	3.740
Co(1)-N(1)	1.340(5)	Co(1)-N(1)	1.926(10)	Co(1)-N(10)	1.972(7)
Co(1)-N(2)	2.146(3)	Co(1)-N(2)	1.926(13)	Co(1)-N(7)	1.990(7)
Co(1)-N(3)	2.161(3)	Co(1)-N(3)	1.919(12)	Co(1)-N(9)	1.923(7)
Co(1)-N(4)	2.118(3)	Co(1)-N(4)	1.961(12)	Co(1)-N(8)	1.969(7)
Co(1)-N(5)	2.105(3)	Co(1)-N(5)	1.896(4)	Co(1)-N(1)	1.961(6)
Co(1)-N(13)	2.169(3)	Co(1)-O(1)	1.890(3)	Co(1)-O(1)	1.864(6)
Co(2)-N(6)	-	Co(2)-N(6)	2.054(4)	Co(2)-N(2)	1.962(8)
Co(2)-N(7)	2.224(3)	Co(2)-N(9)	2.216(4)	Co(2)-N(3)	1.989(7)
Co(2)-N(8)	2.128(3)	Co(2)-N(8)	2.041(5)	Co(2)-N(4)	1.959(8)
Co(2)-N(9)	2.106(3)	Co(2)-N(10)	-	Co(2)-N(5)	1.925(8)
Co(2)-N(10)	2.074(3)	Co(2)-N(7)	2.009(5)	Co(2)-N(6)	1.959(7)
Co(2)-N(11)	2.172(3)	Co(2)-O(1)	1.963(3)	Co(2)-O(2)	1.843(5)
Co(2)-N(12)	2.067(3)			O(1)-O(2)	1.418(9)
<b>Angles (°)</b>		<b>Angles (°)</b>		<b>Angles (°)</b>	
N(3)-Co(1)-N(5)	159.19(11)	N(3)-Co(1)-N(5)	170.3(5)	N(1)-Co(1)-N(9)	168.0(3)
N(1)-Co(1)-N(4)	159.33(12)	N(1)-Co(1)-N(4)	177.4(4)	N(8)-Co(1)-N(10)	165.6(3)
N(2)-Co(1)-N(13)	175.58(12)	N(2)-Co(1)-O(1)	175.8(4)	N(1)-Co(1)-O(1)	95.8(3)
N(5)-Co(1)-N(13)	104.37(12)	N(5)-Co(1)-O(1)	91.68(17)	N(7)-Co(1)-O(1)	175.4(3)
N(6)-N(5)-Co(1)	122.9(2)	N(6)-N(5)-Co(1)	121.7(3)	N(2)-N(1)-Co(1)	126.6(5)
N(5)-N(6)-Co(2)	-	N(5)-N(6)-Co(2)	119.2(3)	N(1)-N(2)-Co(2)	126.9(5)
Co(1)-N(5)-N(6)-Co(2) <sup>a</sup>	-	Co(1)-N(5)-N(6)-Co(2) <sup>a</sup>	7.5(5)	Co(1)-N(1)-N(2)-Co(2) <sup>a</sup>	18.1(10)

<sup>a</sup> Torsion angle that involves the two N atoms belonging to the pyridazine-bridged group and the two metal centers.

### Redox properties

The redox properties of the complex  $10^{2+}$  and  $13^{4+}$  were investigated by cyclic voltammetric technique. In the case of complex  $10^{2+}$  all the measurements have been carried on inside the glovebox under a  $N_2$  atmosphere using a glassy carbon electrode as the working electrode, a platinum wire as the counter electrode and a  $Ag/Ag^+$  electrode in a solution 0.1 M TBAD and 0.01 M  $AgNO_3$  in MeCN as the reference electrode. Four waves are observed at negative potential which correspond to the first one-electron reduction of  $10^{2+}$  to the Co(I)-Co(II) species at  $-1.27$  V (vs  $Ag/Ag^+$ ) and the second one-electron reduction to the Co(I)-Co(I) complex at  $-1.39$  V. The third and the fourth waves could be assigned to the reduction of the two metal centres to oxidation state (0) or, more likely, to some processes that involve on the organic ligand.

The low reversibility of the waves not necessarily indicates the complex decomposition but could be an evidence of the variability of the coordination environment of the Co centres while varying their oxidation state. The oxidative part of the voltammogram is characterized by two waves at 0.25 V and 1.03 V assigned to the one electron oxidation from  $Co^{II}Co^{II}$  to the  $Co^{III}Co^{III}$  species.

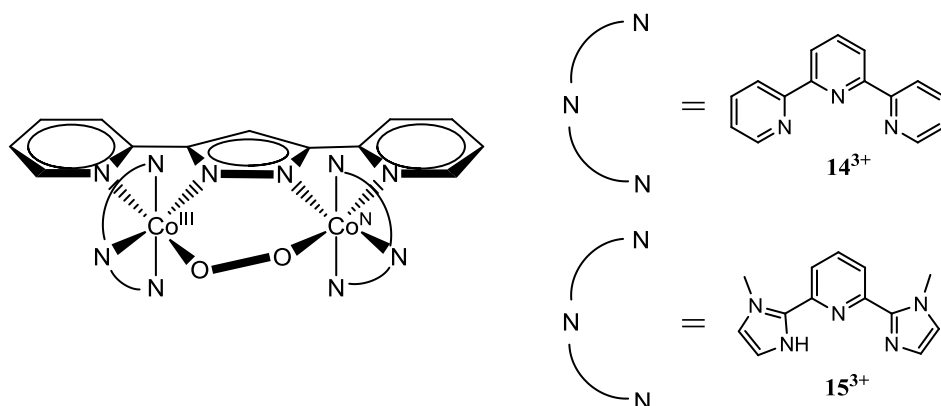


**Figure 13.** Cyclic voltammogram of  $10^{2+}$  in MeCN (0.1 M TABPF<sub>6</sub>) registered inside the glovebox; working electrode: glassy carbon; counter electrode: Pt; reference electrode: Ag/Ag<sup>+</sup> electrode in a solution 0.1 M TBAD and 0.01 M AgNO<sub>3</sub> in MeCN; scan rate 100 mV/s; starting at 0 V toward negative potential.

The redox properties of  $13^{4+}$  have been investigated in a pH 2.1 phosphate buffer solution using an FTO slide (1 cm<sup>2</sup>) connected to a tin wire as the working electrode, a platinum wire as the auxiliary electrode and an aqueous Ag/Ag<sup>+</sup> (KCl 3 M) as the reference electrode. The acidic conditions have been chosen in order to avoid formation of catalytically active heterogeneous cobalt oxide films or nanoparticles (unstable with respect to hydrolysis below pH 3-4)<sup>47,48</sup>.

The cyclic voltammogram shows an irreversible wave at  $E_p = 1.57$  V vs Ag/Ag<sup>+</sup> (1.79 vs NHE) assigned to the one electron oxidation of Co<sup>III</sup>Co<sup>III</sup> complex to the Co<sup>IV</sup>Co<sup>III</sup> species (Figure 15). This value was compared to those reported for two

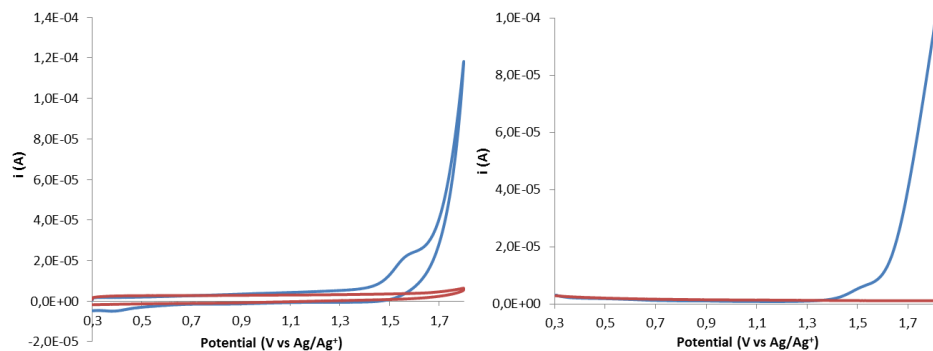
similar dinuclear cobalt peroxo-bridge complexes<sup>47</sup>. Complexes **14**<sup>3+</sup> and **15**<sup>3+</sup>, represented in Figure 14, show a one electron oxidation wave for the oxidation couple  $\text{Co}^{\text{IV,III}}/\text{Co}^{\text{III,III}}$  at  $E_p = 1.56$  and  $1.45$  V vs NHE. The  $\Delta E$  of 230 and 340 mV between these systems and complex **13**<sup>4+</sup> is probably due to the electron-donating nature of the bis(2-pyridyl)-3,5-pyrazolate bridging ligand (bpp) and the bis(N-methylimidazolyl)pyridine ( $\text{Me}_2\text{bimpy}$ ) respect to the neutral decadentate ligand.



**Figure 14.** Structure of **14**<sup>3+</sup> and **15**<sup>3+</sup>.

An electrocatalytical wave was detected from  $E > 1.6$  V vs  $\text{Ag}/\text{Ag}^+$  and assigned to the oxidation of water. Differential pulse voltammetry showed (Figure 15) that this wave starts just after the first oxidation to  $\text{Co}^{\text{IV}}\text{Co}^{\text{III}}$  species. This likely suggests the presence of a  $\text{Co}^{\text{IV}}\text{Co}^{\text{IV}}$  species responsible for the catalytic reaction.

New polypyridyl decadentate ligand and related Co complexes



**Figure 15.** Cyclic voltammogram (left) and differential pulse voltammogram (right) of  $\mathbf{13}^{4+}$  in pH 2.1 phosphate buffer (0.1 M); working electrode: FTO slide ( $1 \text{ cm}^2$ ); counter electrode: Pt; reference electrode: aqueous  $\text{Ag}/\text{Ag}^+$  electrode; scan rate 100 mV/s, background in red line.

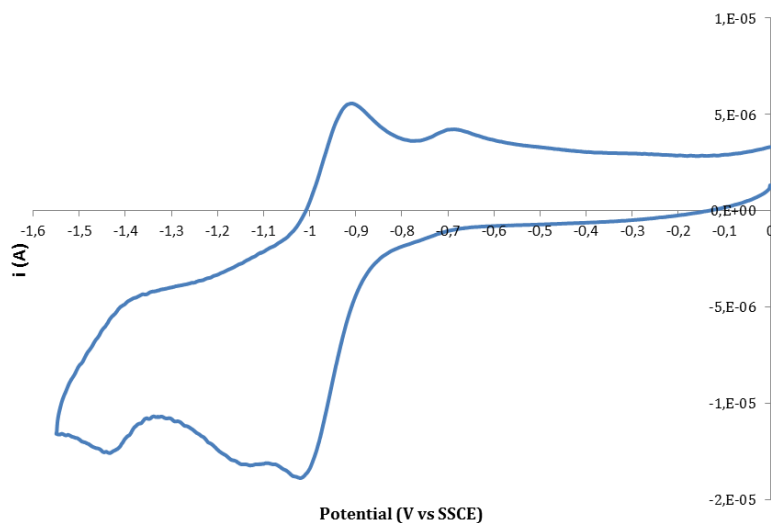
### Catalytic activity

The efficiency in catalysis of the cobalt dinuclear complexes containing **L** have been investigated both for electrochemical proton reduction and water oxidation. The results of these preliminary studies are showed and discussed below.

#### *Catalysis of proton reduction*

The reduction chemistry of  $\mathbf{10}^{2+}$  has been investigated by cyclic voltammetry. All the experiment were performed in well degassed acetonitrile under strictly  $\text{N}_2$  atmosphere to avoid aerobic oxidation of  $\mathbf{10}^{2+}$ . A glassy carbon electrode was used as the working electrode, a platinum wire as the auxiliary electrode and SSCE as the reference electrode; all the CVs were recorded at scan rate of  $100 \text{ mV}\cdot\text{s}^{-1}$ . The cyclic voltammogram of  $\mathbf{10}^{2+}$  in acetonitrile shows two close quasi-reversible waves at  $E_{1/2} = 0.854$  and  $1.017 \text{ V}$  vs SSCE (Figure 16). These waves have been assigned to the successive one electron reduction process of the two metal centers from  $\text{Co}^{\text{II}}\text{Co}^{\text{II}}$  to  $\text{Co}^{\text{I}}\text{Co}^{\text{I}}$ . A third wave, likely corresponding to the generation of the  $\text{Co}^0\text{Co}^{\text{I}}$  species has been detected at  $E_p = 1.412 \text{ V}$  vs SSCE.





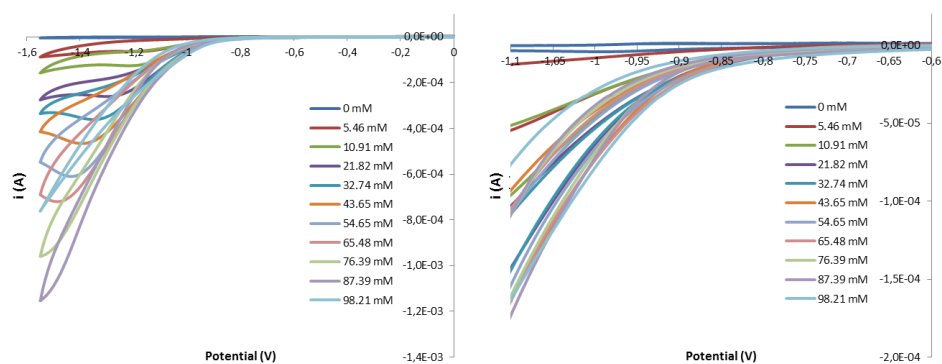
**Figure 16.** Cyclic voltammogram of  $10^{2+}$  in MeCN (0.1 M TBAPF<sub>6</sub>); working electrode: glassy carbon; counter electrode: Pt; reference electrode: SSCE; scan rate 100mV/s. Starting at 0 V toward negative potential.

The catalytic activity of  $10^{2+}$  versus proton reduction was tested using degassed trifluoroacetic acid (TFA) as acid source. Figure 17 shows successive cyclic voltammograms of a 0.2 mM solution of  $10^{2+}$  in acetonitrile with increasing concentrations of TFA. A catalytic wave for the reduction of protons is observed from a potential of ca -0.90 V vs SSCE, corresponding to an overpotential of  $\approx$  400 mV determined using the method of Evans<sup>49</sup>:

$$E_{TFA}^0 = E_{H^+}^0 - \left(2.303 \frac{RT}{F}\right) pK_{a,TFA} \quad (1)$$

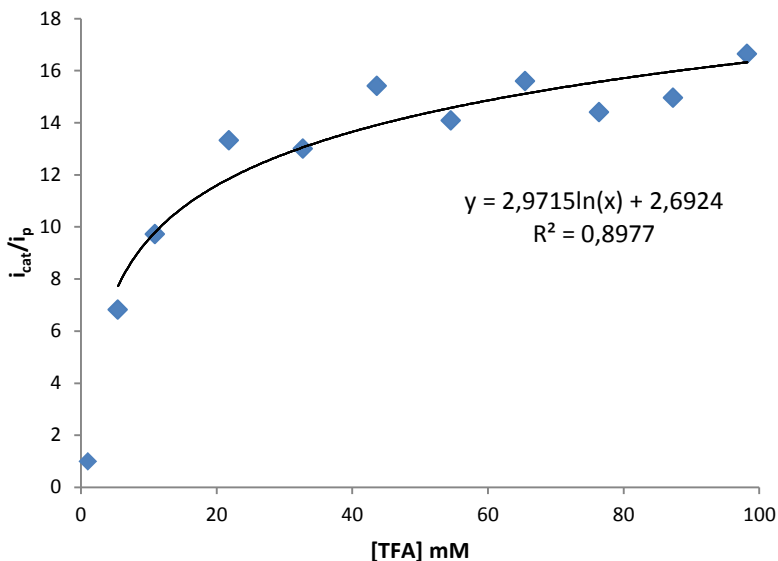
where  $E_{TFA}^0$  is the standard reduction potential for TFA in acetonitrile (-0.51 V vs SCE)<sup>50</sup>,  $E_{H^+}^0$  is the standard potential for the solvated H<sup>+</sup>/H<sub>2</sub> couple in MeCN<sup>51</sup>, R is the ideal gas constant (8.314472 J·K<sup>-1</sup>·mol<sup>-1</sup>), T is the temperature in Kelvin, F is the Faraday constant (96487 C·mol<sup>-1</sup>) and  $pK_{a,TFA}$  is the dissociation constant for TFA (12 in MeCN)<sup>52</sup>. This value is comparable to those

obtained with analogous monometallic Co(II) complexes described in the literature<sup>30,50,53</sup>.



**Figure 17.** Successive cyclic voltammograms of 0.2 mM solution of  $10^{2+}$  in MeCN (0.1 M TBAPF<sub>6</sub>) at increasing concentrations of TFA. Working electrode: glassy carbon; counter electrode: Pt; reference electrode: SSCE; scan rate 100mV/s. Starting at 0 V toward negative potential (left). Zoom of potential range (-0.6 V)-(-1.1 V) (right).

The  $i_{cat}/i_p$  vs [TFA] (where  $i_{cat}$  is the current intensity in the presence of acid and  $i_p$  is the current intensity without acid), reported in Figure 18 for  $i_{cat}$  at  $E = -0.99$  V vs SSCE, corresponding to the  $E_p$  of the first reduction wave, increases with sequential increments of acid added reaching a *plateau* for [TFA] > 70 mM.



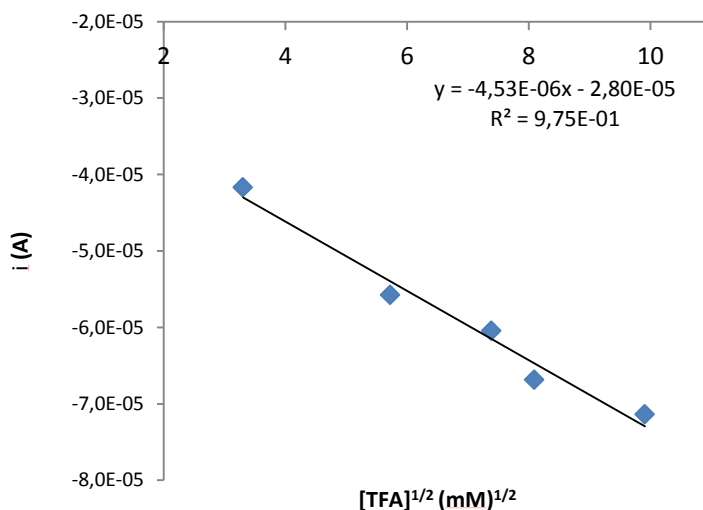
**Figure 18.** Dependence of  $i_{cat}/i_p$  at -0.99 V on [TFA].. Experimental conditions:  $10^{2+}$  (0.2 mM), [TFA] = 0-210 mM, MeCN (0.1 M TBAPF<sub>6</sub>), GC WE, Pt CE, SSCE RE, 100 mV/s.

The rate constant value  $k$  for the proton reduction catalysis can be estimated from the plots of the  $i_{cat}$  vs the square root of the acid concentration according to equation<sup>54</sup>:

$$i_{cat} = nFA[cat]D^{\frac{1}{2}}k^{\frac{1}{2}}[TFA]^{\frac{1}{2}} \quad (2)$$

where  $i_{cat}$  is the current intensity at - 0.99 V vs SSCE,  $n$  is the number of electrons involved in the catalysis,  $F$  is the Faraday constant,  $A$  is the surface area of the working electrode in cm<sup>2</sup>,  $[cat]$  is the concentration of catalyst in mol/cm<sup>3</sup>,  $D$  is the diffusion coefficient of the catalyst in cm<sup>2</sup>/s, and  $[TFA]$  is the concentration of acid in mol/cm<sup>3</sup>.

The plot of  $i_{\text{cat}}$  vs  $[\text{TFA}]^{1/2}$  shows a linear trend when the acid concentration is higher than 11 mM (Figure 19). Under kinetic control conditions the slope is proportional to  $k^{1/2}$ .



**Figure 19.** Dependence of  $i_{\text{cat}}$  at -0.99 V on  $[\text{TFA}]^{1/2}$ . Experimental conditions:  $\mathbf{10}^{2+}$  (1 mM),  $[\text{TFA}] = 0\text{-}210$  mM, MeCN (0.1 M TBAPF<sub>6</sub>), GC WE, Pt CE, SSCE RE, 100 mV/s.

In order to estimate the value of the rate constant the  $A \cdot D^{1/2}$  product was calculated from the peak current prior the addition of acid according to the following equation<sup>54</sup>:

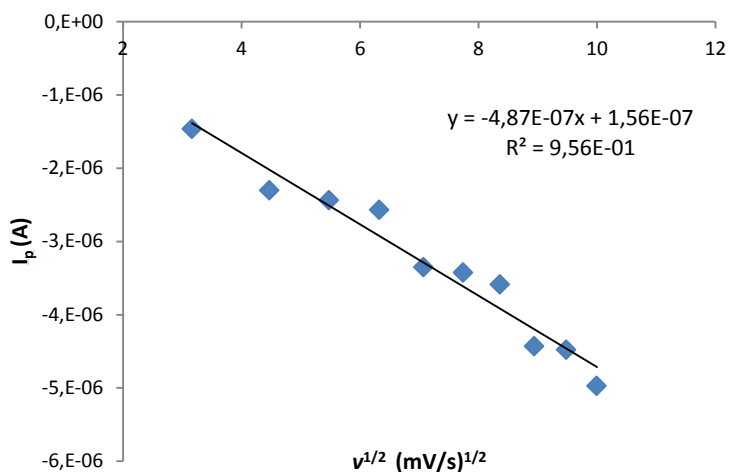
$$i_p = (2.69 \cdot 10^5) n^{3/2} A D^{1/2} [cat] v^{1/2} \quad (3)$$

where  $i_p$  is the current intensity at -0.99 V ( $E_p$  vs SSCE of first reduction wave),  $n$  is the number of electrons involved in the electrochemical process,  $A$  is the surface area of the working electrode in  $\text{cm}^2$ ,  $D$  is the diffusion coefficient of

## VI New polypyridyl decadentate ligand and related Co complexes

the catalyst in  $\text{cm}^2/\text{s}$ ,  $[\text{cat}]$  in the is the concentration of catalyst in  $\text{mol}/\text{cm}^3$  and  $v$  is the scan rate in  $\text{V}/\text{s}$ .

If a linear relationship for  $i_p$  vs  $v^{1/2}$  is obtained the slope is proportional to  $AD^{1/2}$ . As shown in Figure 20 the plot of  $i_p$  vs the square root of the scan rate, presented a good linear trend for a range of scan rate from 100  $\text{mV}/\text{s}$  to 10  $\text{mV}/\text{s}$ .



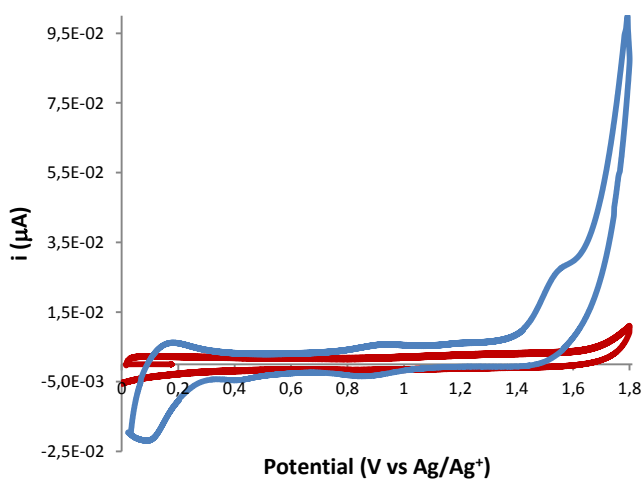
**Figure 20.** Dependence of  $i_{\text{cat}}$  at  $-0.99 \text{ V}$  on  $v^{1/2}$ . Experimental conditions:  $\mathbf{10^{2+}}$  ( $0.2 \text{ mM}$ ),  $v = 10\text{-}200 \text{ V}/\text{s}$ ,  $\text{MeCN}$  ( $0.1 \text{ M TBAPF}_6$ ), GC WE, Pt CE, SSCE RE.

Combining the values obtained from equations 2 and 3 a rate constant of ca  $168 \text{ M}^{-1}\text{s}^{-1}$  has been calculated for the proton reduction catalyzed by  $\mathbf{10^{2+}}$  in  $\text{MeCN}$  in the presence of TFA as proton source.

### Catalysis of water oxidation

In order to test the catalytic activity of  $13^{4+}$  toward the oxidation of water a controlled potential electrolysis was performed in a two compartments cell on a stirred aqueous solution of  $13^{4+}$  and oxygen evolution was detected by using a Clark's oxygen needle sensor. For this experiment 5 mL a 0.1 mM solution of  $13^{4+}$  in pH 2.1 phosphate buffer (0.1 M) were used. A FTO slide of  $1\text{ cm}^2$  surface was used as the working electrode, a platinum grid as the counter electrode and an aqueous  $\text{Ag}/\text{Ag}^+$  electrode as the reference electrode.

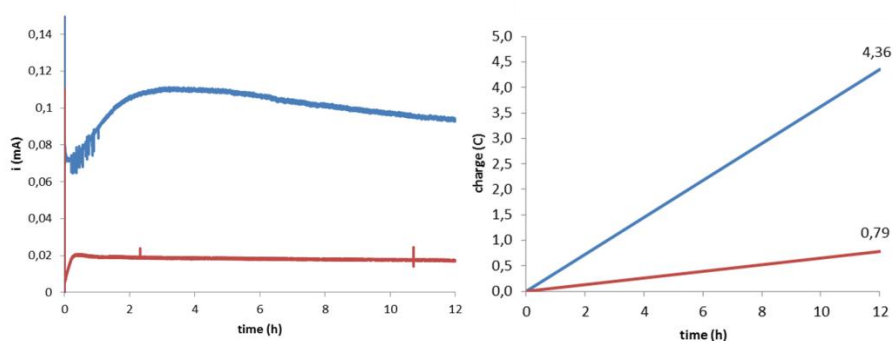
Cyclic voltammograms were registered before and after the electrolysis showing important change in the electrochemistry of  $13^{4+}$ . Before the bulk experiment (Figure 21) a wave was observed at  $E_p = 1.57$ , as already described above. Sweeping the potential back to 0 V a reduction wave corresponding to the  $\text{Co}^{\text{III,III/III,II}}$  was detected.



**Figure 21.** Cyclic voltammogram of  $13^{4+}$  (0.1 mM) in pH 2.1 phosphate buffer (0.1 M); working electrode before controlled electrolysis experiment (blue line); working electrode: FTO slide ( $1\text{ cm}^2$ ) counter electrode: Pt grid; reference electrode: aqueous  $\text{Ag}/\text{Ag}^+$  electrode; scan rate 100 mV/s, background in red line.

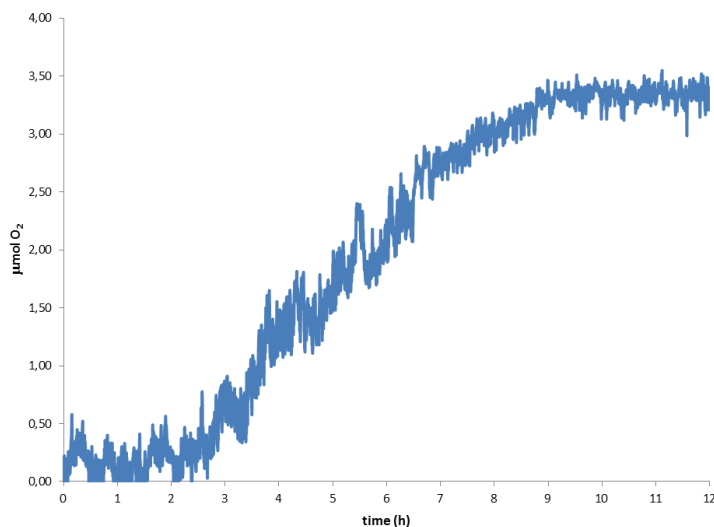
## New polypyridyl decadentate ligand and related Co complexes

For the electrolysis experiment a potential of 1.80 V vs  $\text{Ag}/\text{Ag}^+$  has been applied for 12 hours and. A blank experiment has been performed for the same duration and the charge measured used as baseline for the catalytic experiment. Figure 22 shows the current vs time plot for the described experiment and the corresponding charge passed. The Faraday efficiency, described as the ratio between the amount of charge employed for the chemical reaction and the total charge passed resulted of 36.5%.



**Figure 22.** Controlled potential electrolysis at 1.8 V vs  $\text{Ag}/\text{Ag}^+$  of  $\mathbf{13}^{4+}$  (0.1 mM) in pH 2.1 phosphate buffer (0.1 M); working electrode: FTO slide ( $1 \text{ cm}^2$ ) before controlled; counter electrode: Pt grid; reference electrode: aqueous  $\text{Ag}/\text{Ag}^+$  electrode; total time 12 hours. Current (mA) vs time (h) plot (left); Charge (C) vs time (h) plot (right). Background in red.

Oxygen evolution measured with a Clark electrode resulted of  $\approx 3.4 \mu\text{mol}$  of  $\text{O}_2$ , corresponding to  $\approx 6.8 \text{ TN}$  (Figure 23).

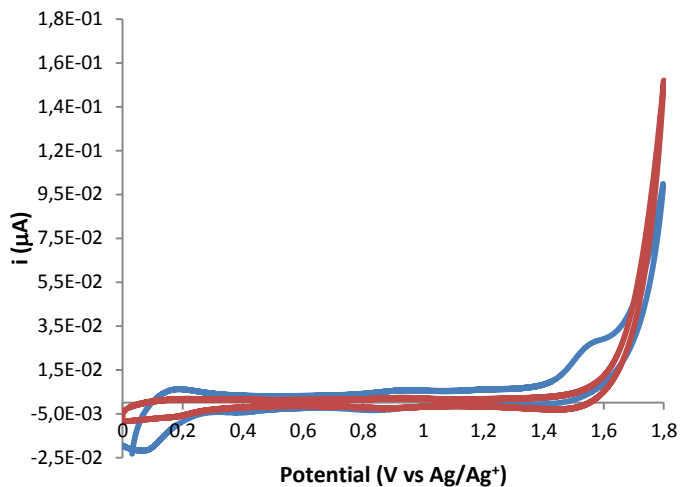


**Figure 23.** Oxygen evolution measured with a Clark electrode during controlled potential electrolysis at 1.8 V vs Ag/Ag<sup>+</sup> of **13**<sup>4+</sup> (0.1 mM) in pH 2.1 phosphate buffer (0.1 M); working electrode: FTO slide (1 cm<sup>2</sup>) before controlled; counter electrode: Pt grid; reference electrode: aqueous Ag/Ag<sup>+</sup> electrode; total time 12 hours.

However the cyclic voltammogram registered after the electrolysis resulted different from the initial one. Both Co<sup>IV,III/III,III</sup> and Co<sup>III,III/III,II</sup> redox couples disappeared while a slightly higher electrocatalytic wave is maintained at E ≈ 1.8 V. This is probably an indication of the decomposition of the initial species and formation of a new one responsible of the O<sub>2</sub> generation.



## New polypyridyl decadentate ligand and related Co complexes



**Figure 23** Cyclic voltammogram of  $13^{4+}$  (0.1 mM) in pH 2.1 phosphate buffer (0.1 M); working electrode: FTO slide ( $1 \text{ cm}^2$ ) after 12 hours controlled electrolysis experiment (red line); counter electrode: Pt grid; reference electrode: aqueous  $\text{Ag}/\text{Ag}^+$  electrode; scan rate 100 mV/s, CV before bulk experiment in blue line.

## VI. iv. Conclusion

In this chapter a new polypyridyl ligand with ten coordination sites **L** has been presented. The synthesis and the characterization of **L** has been outlined and discussed. A new dinuclear cobalt complex [**10(OTf)<sub>2</sub>**] containing **L** has been prepared. Full characterization by X-Ray diffraction, elemental analysis, <sup>1</sup>H-NMR spectroscopy and electrochemical techniques has been carried on in order to characterize complexes **10<sup>2+</sup>**, **11<sup>4+</sup>**, **12<sup>4+</sup>** and **13<sup>4+</sup>** confirming the high stability of **L** as bridging among different oxidation states of the two metal centers. Cobalt complexes based on **L** have been proven to be active catalysts for both electrochemical proton reduction and water oxidation. **10<sup>2+</sup>** have been tested in the electrochemical proton reduction in the presence of trifluoroacetic acid as proton source resulting an active catalyst for H<sub>2</sub> generation with an overpotential of ≈ 400 mV and a rate constant *k* of 161 M<sup>-1</sup>s<sup>-1</sup>. Peroxo-bridged complex **13<sup>4+</sup>** has been tested as catalyst for the electrochemical water oxidation via controlled potential electrolysis at 1.8 V vs Ag/Ag<sup>+</sup>. Oxygen evolution has been detected during 12 hours with a TN of 6.8 and a Faraday efficiency of 36.5 %. However indications of a possible decomposition of the catalyst were obtained via electrochemical study. Further studies of the catalytic properties of complexes **10<sup>2+</sup>** and **13<sup>4+</sup>** will be carried on in order to investigate the mechanism of generation of O<sub>2</sub> and H<sub>2</sub> and optimize a system for the generation of solar fuels.

## VI. v. Associated content

### Supporting Information

X-Ray crystallographic data in CIF format, additional spectroscopic and electrochemical data.

## VI. vi. Acknowledgements

The cobalt dinuclear complex **10(OTf)<sub>2</sub>** has been synthesized as described by Dr. X. Sala (University Autònoma of Barcelona) and Dr. M. Nippe (University of Berkeley). ESI-MS spectra presented in Figure 8 has been registered by Dr. Sala and Dr. Nippe in Berkeley University.

## VI. vii. References

- (1) Grohmann, A.; Knoch, F. *Inorg. Chem.* **1996**, *35*, 7932.
- (2) Tamagaki, S.; Kanamaru, Y.; Ueno, M.; Tagaki, W. *Bull. Chem. Soc. Jpn.* **1991**, *64*, 165.
- (3) Lubben, M.; Meetsma, A.; Wilkinson, E. C.; Feringa, B.; Que, L., Jr. *Angew. Chem., Int. Ed. Engl.* **1995**, *34*, 1512.
- (4) Roelfes, G.; Lubben, M.; Chen, K.; Ho, R. Y. N.; Meetsma, A.; Genseberger, S.; Hermant, R. M.; Hage, R.; Mandal, S. K.; Young, V. G., Jr.; Zang, Y.; Kooijman, H.; Spek, A. L.; Que, L.; Feringa, B. L. *Inorg. Chem.* **1999**, *38*, 1929.
- (5) Klein Gebbink, R. J. M.; Jonas, R. T.; Goldsmith, C. R.; Stack, T. D. P. *Inorg. Chem.* **2002**, *41*, 4633.
- (6) Smith, J. M.; Long, J. R. *Inorg. Chem.* **2010**, *49*, 11223.
- (7) Jonas, R. T.; Stack, T. D. P. *J. Am. Chem. Soc.* **1997**, *119*, 8566.
- (8) Goldsmith, C. R.; Jonas, R. T.; Stack, T. D. P. *J. Am. Chem. Soc.* **2002**, *124*, 83.
- (9) Freedman, D. E.; Jenkins, D. M.; Iavarone, A. T.; Long, J. R. *J. Am. Chem. Soc.* **2008**, *130*, 2884.
- (10) Karunadasa, H. I.; Chang, C. J.; Long, J. R. *Nature* **2010**, *464*, 1329.
- (11) Zadrozny, J. M.; Freedman, D. E.; Jenkins, D. M.; Harris, T. D.; Iavarone, A. T.; Mathoniere, C.; Clerac, R.; Long, J. R. *Inorg. Chem.* **2010**, *49*, 8886.
- (12) Fontcilla-Camps, J. C.; Ragsdale, S. W. *Adv. Inorg. Chem.* **1999**, *47*, 283.
- (13) Adams, M. W. *Biochim. Biophys. Acta* **1990**, *1020*, 115.
- (14) Darensbourg, M. Y.; Lyon, E. J.; Smee, J. J. *Coord. Chem. Rev.* **2000**, *206-207*, 533.
- (15) Adams, M. W. W.; Stiefel, E. I. *Science* **1998**, *282*, 1842.
- (16) Peters, J. W.; Lanzilotta, W. N.; Lemon, B. J.; Seefeldt, L. C. *Science* **1998**, *282*, 1853.
- (17) Helm, M. L.; Stewart, M. P.; Bullock, R. M.; DuBois, M. R.; DuBois, D. L. *Science* **2011**, *333*, 863.
- (18) Kilgore, U. J.; Roberts, J. A. S.; Pool, D. H.; Appel, A. M.; Stewart, M. P.; DuBois, M. R.; Dougherty, W. G.; Kassel, W. S.; Bullock, R. M.; DuBois, D. L. *J. Am. Chem. Soc.* **2011**, *133*, 5861.
- (19) Wiedner, E. S.; Yang, J. Y.; Dougherty, W. G.; Kassel, W. S.; Bullock, R. M.; DuBois, M. R.; DuBois, D. L. *Organometallics* **2010**, *29*, 5390.
- (20) Wilson, A. D.; Newell, R. H.; McNevin, M. J.; Muckerman, J. T.; Rakowski, D. M.; DuBois, D. L. *J. Am. Chem. Soc.* **2006**, *128*, 358.

## VI New polypyridyl decadentate ligand and related Co complexes

- (21) Rakowski, D. M.; DuBois, D. L. *Acc. Chem. Res.* **2009**, *42*, 1974.
- (22) Hu, X.; Brunswig, B. S.; Peters, J. C. *J. Am. Chem. Soc.* **2007**, *129*, 8988.
- (23) Dempsey, J. L.; Brunswig, B. S.; Winkler, J. R.; Gray, H. B. *Acc. Chem. Res.* **2009**, *42*, 1995.
- (24) Hu, X.; Cossairt, B. M.; Brunswig, B. S.; Lewis, N. S.; Peters, J. C. *Chem. Commun.* **2005**, 4723.
- (25) Baffert, C.; Artero, V.; Fontecave, M. *Inorg. Chem.* **2007**, *46*, 1817.
- (26) Razavet, M.; Artero, V.; Fontecave, M. *Inorg. Chem.* **2005**, *44*, 4786.
- (27) Fourmond, V.; Jacques, P.-A.; Fontecave, M.; Artero, V. *Inorg. Chem.* **2010**, *49*, 10338.
- (28) Jacques, P.-A.; Artero, V.; Pecaut, J.; Fontecave, M. *Proc. Natl. Acad. Sci. U. S. A.* **2009**, *106*, 20627.
- (29) Sun, Y.; Bigi, J. P.; Piro, N. A.; Tang, M. L.; Long, J. R.; Chang, C. J. *J. Am. Chem. Soc.* **2011**, *133*, 9212.
- (30) Bigi, J. P.; Hanna, T. E.; Harman, W. H.; Chang, A.; Chang, C. J. *Chem. Commun.* **2010**, *46*, 958.
- (31) Stubbert, B. D.; Peters, J. C.; Gray, H. B. *J. Am. Chem. Soc.* **2011**, *133*, 18070.
- (32) Connolly, P.; Espenson, J. H. *Inorg. Chem.* **1986**, *25*, 2684.
- (33) Pantani, O.; Anxolabehere-Mallart, E.; Aukauloo, A.; Millet, P. *Electrochem. Commun.* **2006**, *9*, 54.
- (34) Solis, B. H.; Hammes-Schiffer, S. *Inorg. Chem.* **2011**, *50*, 11252.
- (35) Anxolabéhère-Mallart, E.; Costentin, C.; Fournier, M.; Nowak, S.; Robert, M.; Savéant, J.-M. *J. Am. Chem. Soc.* **2012**, *134*, 6104.
- (36) Wiley, R. H. *J. Macromol. Sci. Chem.* **1987**, *24*, 1183.
- (37) Picot, A., Texas A&M University, **2004**.
- (38) Eggert, J. P. W.; Lüning, U. *Eur. J. Org. Chem.* **2007**, 6046.
- (39) Picot, A.; Gabbaï, F. P. *Tetrahedron Lett.* **2002**, *43*, 11.
- (40) Chang, J.; Plummer, S.; Berman, E. S. F.; Striplin, D.; Blauch, D. *Inorg. Chem.* **2004**, *43*, 1735.
- (41) Nájera, C.; Gil-Moltó, J.; Karlström, S. *Adv. Synth. Catal.* **2004**, *346*, 1798.
- (42) Roelfes, G.; Branum, M. E.; Wang, L.; Que, L.; Feringa, B. L. *J. Am. Chem. Soc.* **2000**, *122*, 11517.
- (43) G. J. Ligtenbarg, A.; L. Spek, A.; Hage, R.; L. Feringa, B. *J. Chem. Soc. Dalton* **1999**, 659.
- (44) Fukuzumi, S.; Mandal, S.; Mase, K.; Ohkubo, K.; Park, H.; Benet-Buchholz, J.; Nam, W.; Llobet, A. *J. Am. Chem. Soc.* **2012**, *134*, 9906.

- (45) Datta, A.; Huang, J.-H.; Machura, B. *J. Chem. Crystallogr.* **2012**, *42*, 691.
- (46) Thakurta, S.; Butcher, R. J.; Pilet, G.; Mitra, S. *J. Mol. Struct.* **2009**, *929*, 112.
- (47) Rigsby, M. L.; Mandal, S.; Nam, W.; Spencer, L. C.; Llobet, A.; Stahl, S. *S. Chem. Sci.* **2012**.
- (48) Gerken, J. B.; McAlpin, J. G.; Chen, J. Y. C.; Rigsby, M. L.; Casey, W. H.; Britt, R. D.; Stahl, S. S. *J. Am. Chem. Soc.* **2011**, *133*, 14431.
- (49) Felton, G. A. N.; Glass, R. S.; Lichtenberger, D. L.; Evans, D. H. *Inorg. Chem.* **2006**, *45*, 9181.
- (50) Rose, M. J.; Gray, H. B.; Winkler, J. R. *J. Am. Chem. Soc.* **2012**, *134*, 8310.
- (51) Felton, G. A. N.; Glass, R. S.; Lichtenberger, D. L.; Evans, D. H. *Inorg. Chem.* **2006**, *45*, 9181.
- (52) Eckert, F.; Leito, I.; Kaljurand, I.; Kuett, A.; Klamt, A.; Diedenhofen, M. *J. Comput. Chem.* **2009**, *30*, 799.
- (53) Dempsey, J. L.; Brunschwig, B. S.; Winkler, J. R.; Gray, H. B. *Acc. Chem. Res.* **2009**, *42*, 1995.
- (54) Bard, A. J.; Faulkner, L. R. *Electrochemical Methods: fundamentals and applications*, Dianhuaxue Bianjibu **2001**, *7*, 255.

UNIVERSITAT ROVIRA I VIRGILI

NEW RUTHENIUM, MANGANESE AND COBALT DINUCLEAR COMPLEXES AS REDOX CATALYSTS.

UNFOLDING THE ESSENTIAL STEPS FOR THE GENERATION OF SOLAR FUELS

Carlo Di Giovanni

Dipòsit Legal: T. 1429-2012

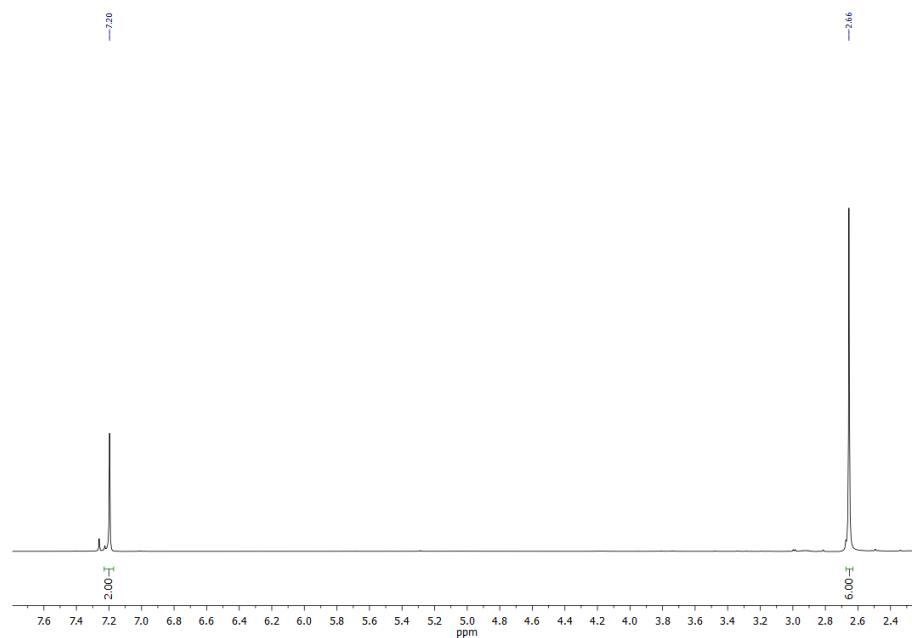
# Chapter VI

## Supporting Information

- *<sup>1</sup>H-NMR spectra of 1, 2, 3, 6, 7, 8 : FigSI1-SI6*
- *NMR characterization of L : FigSI7-SI10*
- *NMR Characterization of 13<sup>+</sup> : Figure SI11- Figure SI13*
- *CV of 10<sup>2+</sup> in MeCN in the presence of TFA, scan rate dependence: FigureSI14*







**Figure SI1.**  $^1\text{H-NMR}$  of **1** (400 MHz, 298 K,  $\text{CDCl}_3$ ).

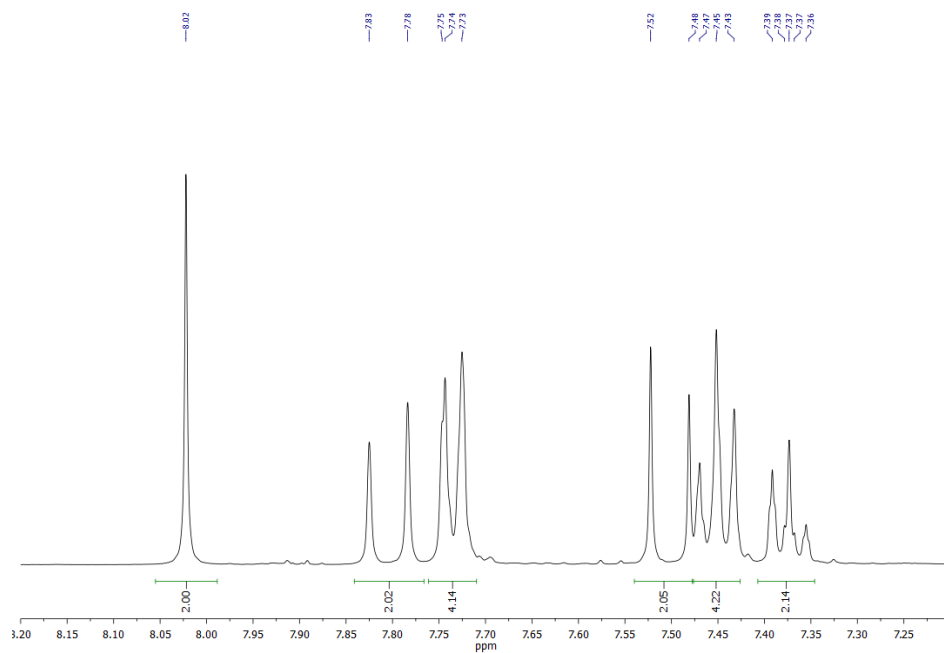
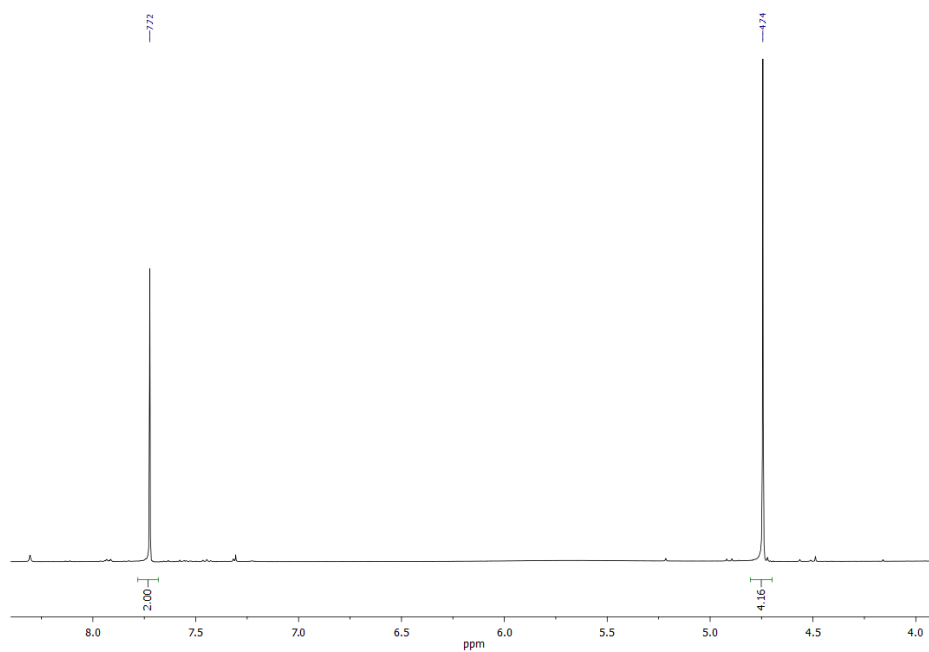


Figure S12.  $^1\text{H-NMR}$  of **2** (400 MHz, 298 K,  $\text{DMSO-d}_6$ ).



**Figure S13.**  $^1\text{H-NMR}$  of **3** (400 MHz, 298 K,  $\text{DMSO-d}_6$ ).

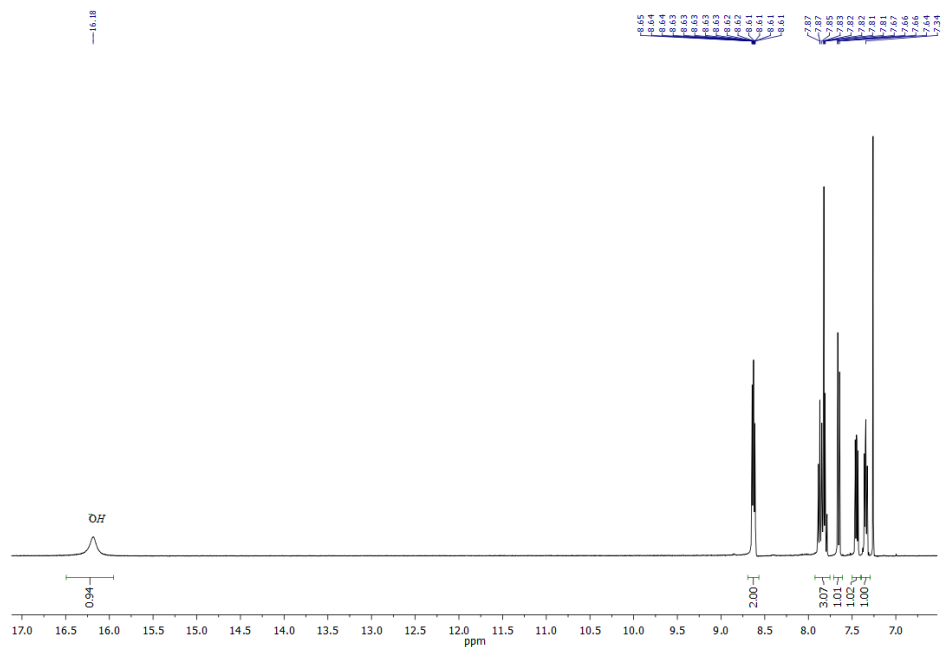
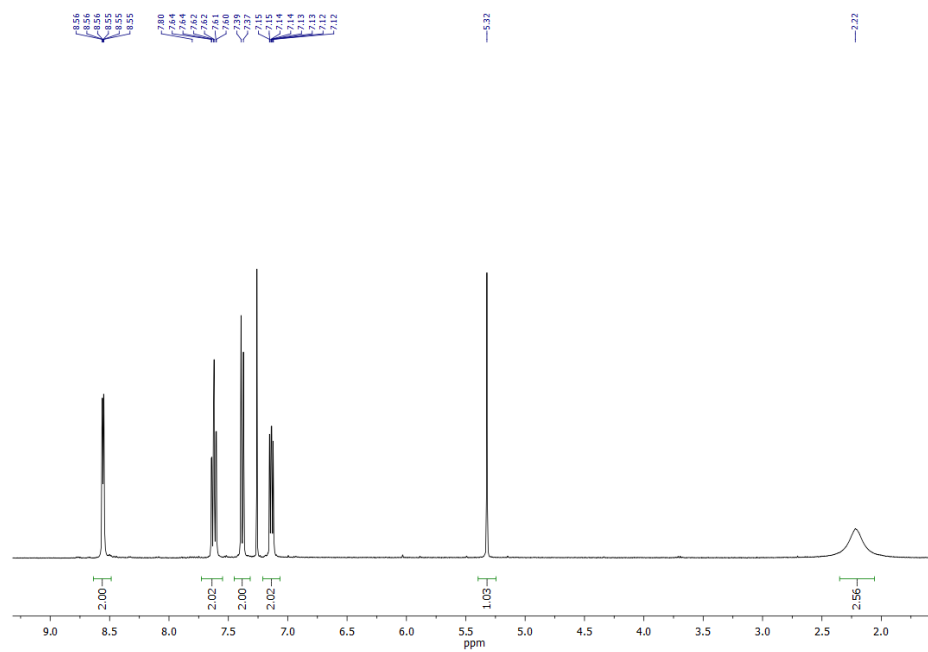
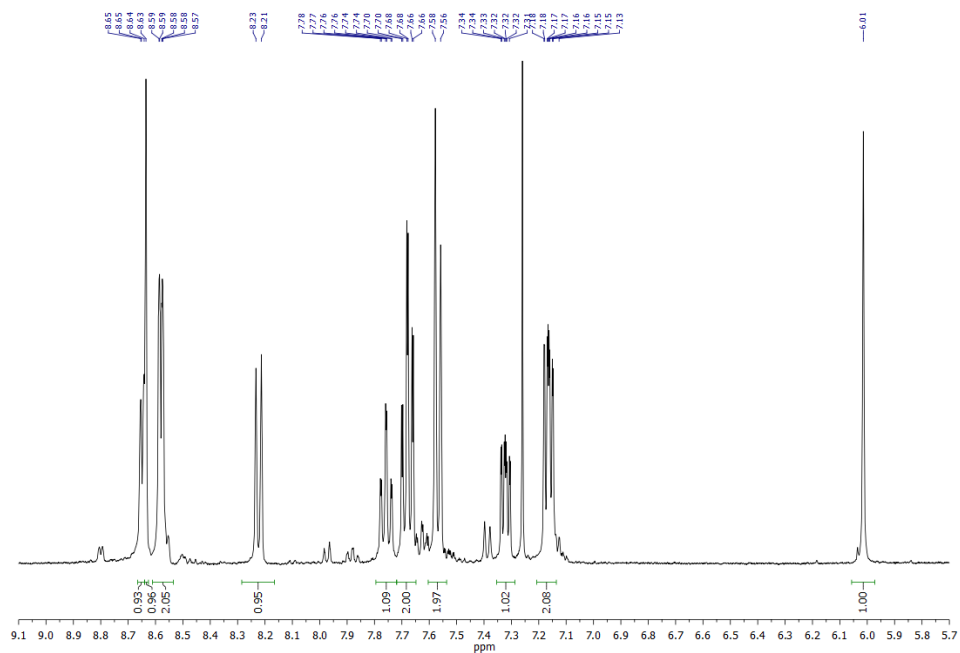
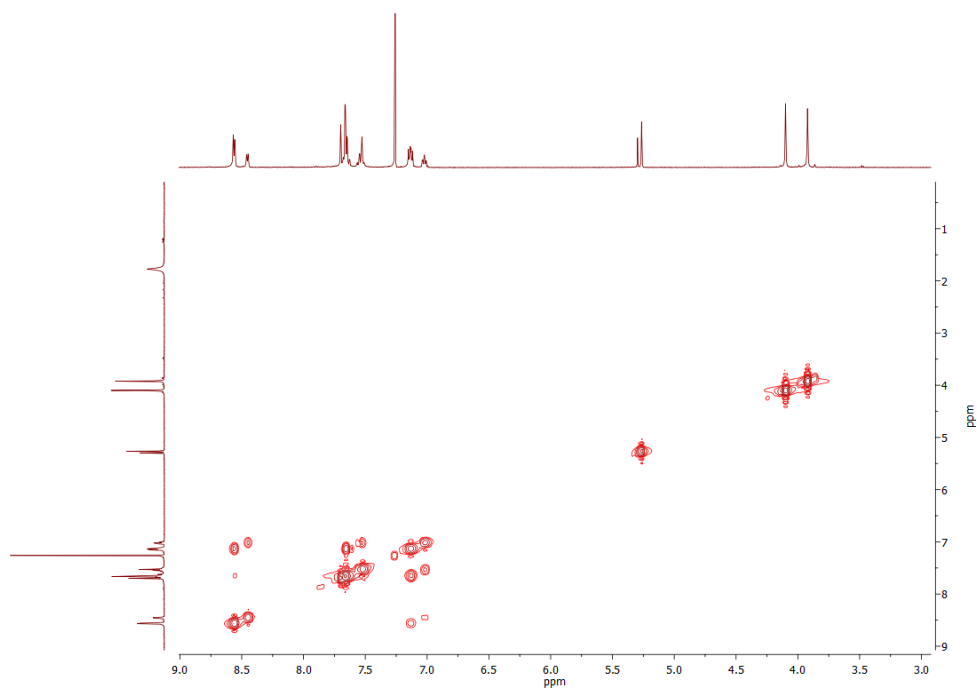


Figure S14.  $^1\text{H-NMR}$  of **6** (400 MHz, 298 K,  $\text{CDCl}_3$ ).



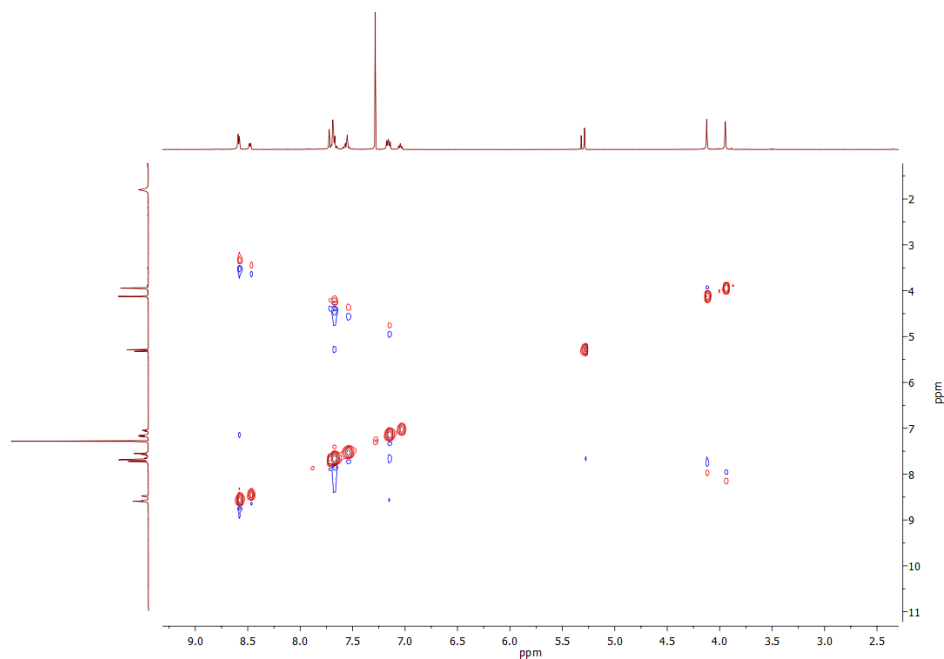
**Figure S15.**  $^1\text{H-NMR}$  of **7** (400 MHz, 298 K,  $\text{CDCl}_3$ ).



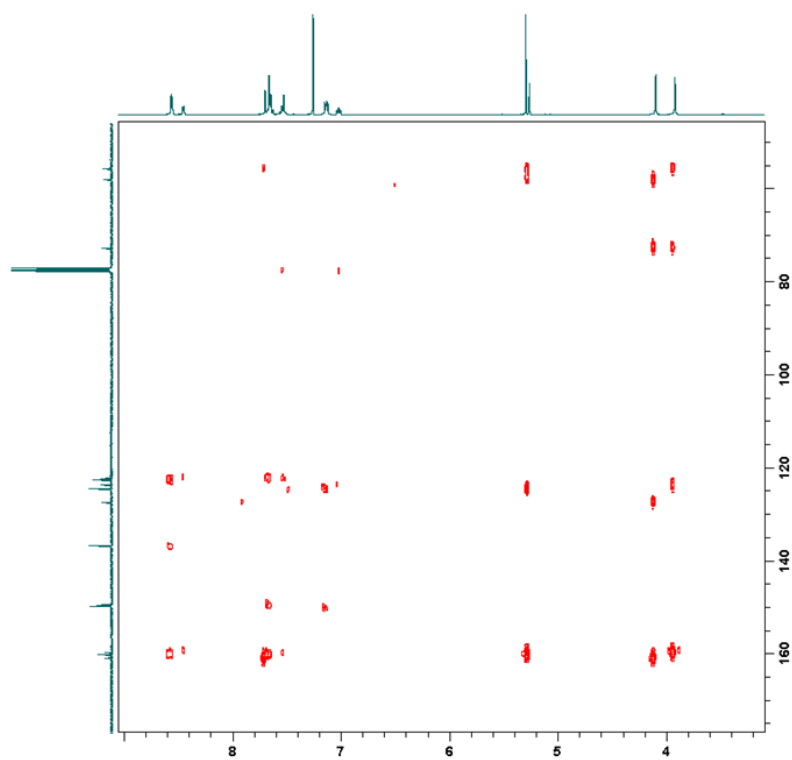


**Figure SI7.** COSY of L (400 MHz, 298 K, CDCl<sub>3</sub>).





**Figure S18.** NOESY of L (400 MHz, 298 K, CDCl<sub>3</sub>).



**Figure SI9.** HMBC of L (298 K, CDCl<sub>3</sub>).

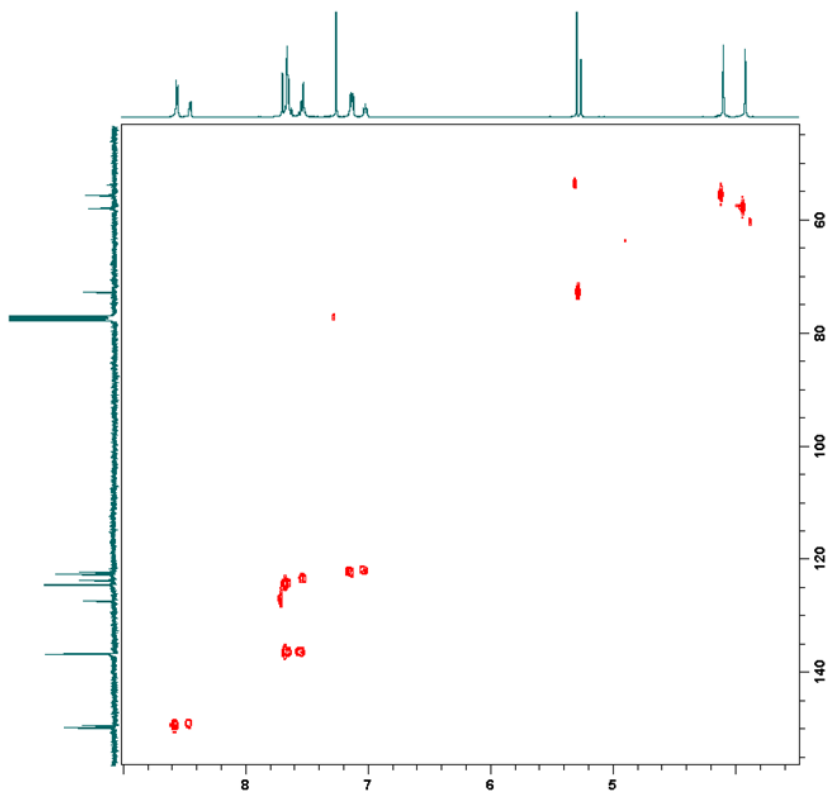
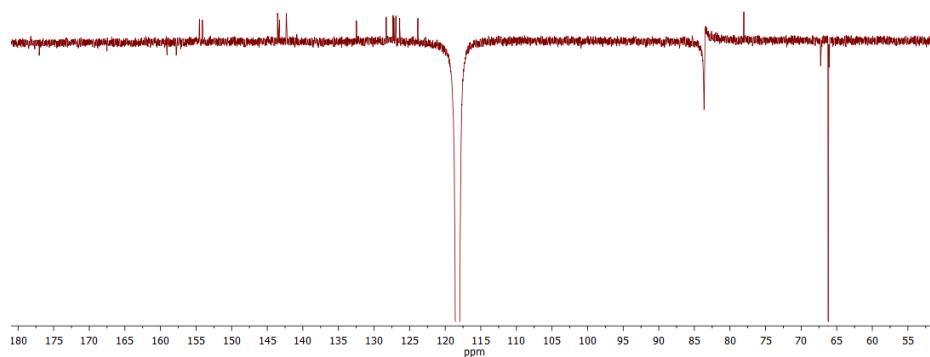


Figure S110. HMQC of L (298 K, CDCl<sub>3</sub>).



**Figure S111.** DEPTQ-135 of  $13^{4+}$  (100 MHz, 298 K,  $CD_3CN$ ).

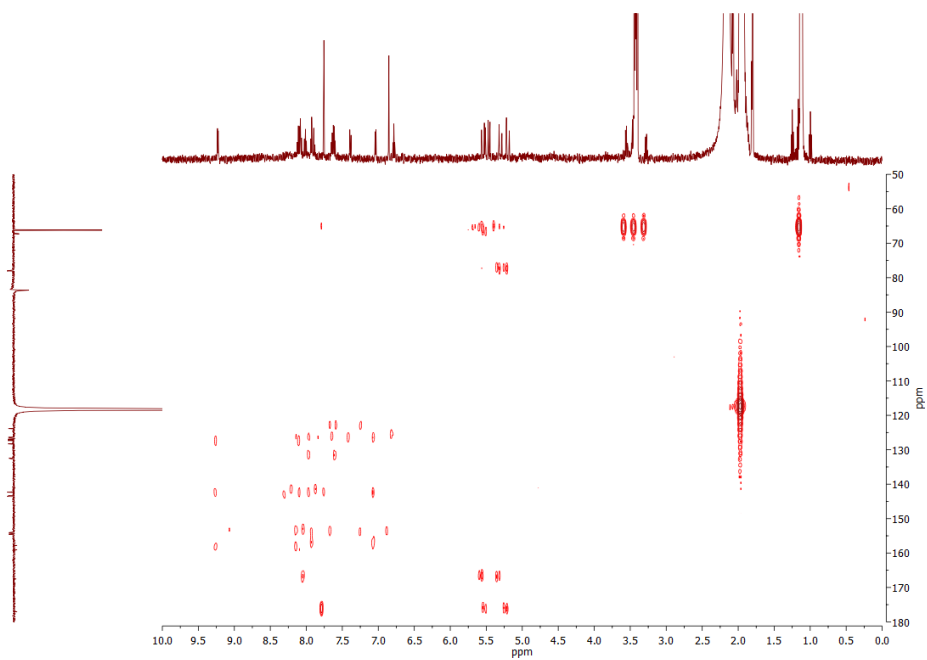
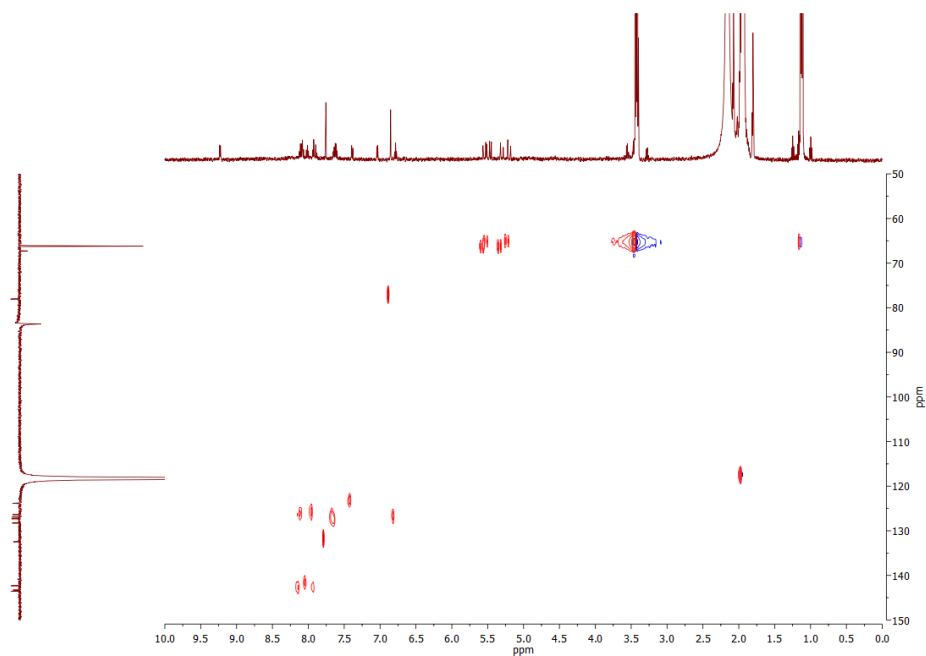
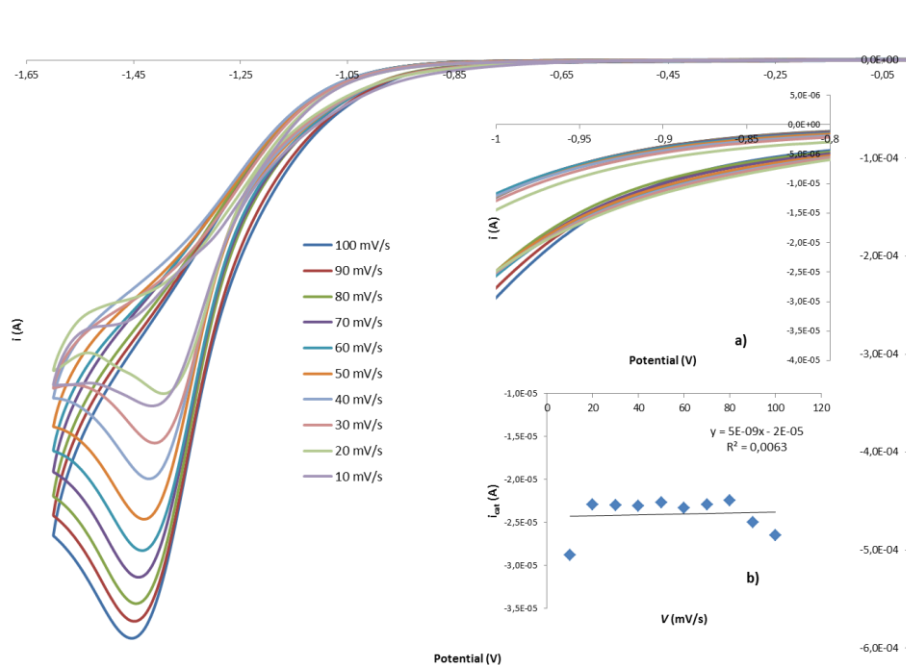


Figure S112. HMBC of  $13^{4+}$  (298 K,  $CD_3CN$ ).



**Figure SI13.** HSBC of  $13^{4+}$  (298 K,  $CD_3CN$ ).



**Figure S114.** Successive cyclic voltammograms of 0.2 mM solution of  $10^{2+}$  in MeCN (0.1 M TBAPF<sub>6</sub>) with [TFA] = 70 mM. Experimental conditions:  $10^{2+}$  (0.2 mM),  $v = 10$ -200 V/s, MeCN (0.1 M TBAPF<sub>6</sub>), GC WE, Pt CE, SSCE RE. Insert a) zoom of potential range (-1.0 V)-(-0.7 V). Insert b) Dependence of  $i_{cat}$  at -0.99 V on  $v$ .

UNIVERSITAT ROVIRA I VIRGILI

NEW RUTHENIUM, MANGANESE AND COBALT DINUCLEAR COMPLEXES AS REDOX CATALYSTS.

UNFOLDING THE ESSENTIAL STEPS FOR THE GENERATION OF SOLAR FUELS

Carlo Di Giovanni

Dipòsit Legal: T. 1429-2012



UNIVERSITAT ROVIRA I VIRGILI

NEW RUTHENIUM, MANGANESE AND COBALT DINUCLEAR COMPLEXES AS REDOX CATALYSTS.

UNFOLDING THE ESSENTIAL STEPS FOR THE GENERATION OF SOLAR FUELS

Carlo Di Giovanni

Dipòsit Legal: T. 1429-2012

# Chapter VII

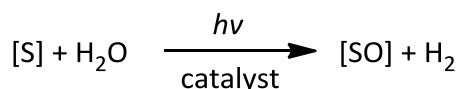
## Assembly of a cell for artificial photosynthesis via two-electron oxidation processes

- i. Introduction*
- ii. Experimental Section*
- iii. Photochemical oxidation of organic substrate*
  - iii. i. Results and discussion*
  - iii. ii. Conclusions*
- iv. Assembly of a system for photochemical sulfide oxidation and proton reduction*
  - iv. i. Results and discussion*
  - iv. ii. Conclusions*
- v. Associated content*
- vi. Acknowledgments*
- vii. References*



## VII. i. Introduction

In previous chapters the importance of the development of an efficient photocatalytic water splitting system has been remarked as an answer to the global energy demand and the employment of a “green” source of energy. On the other side the design of a photocatalytic system for organic synthesis has attracted very little attention until now<sup>1</sup>. Generally oxygenation reactions are performed in chlorinated solvents and in presence of strong chemical oxidants but the use of water as solvent and at the same time oxygen source represents an ideal clean alternative (Scheme 1).



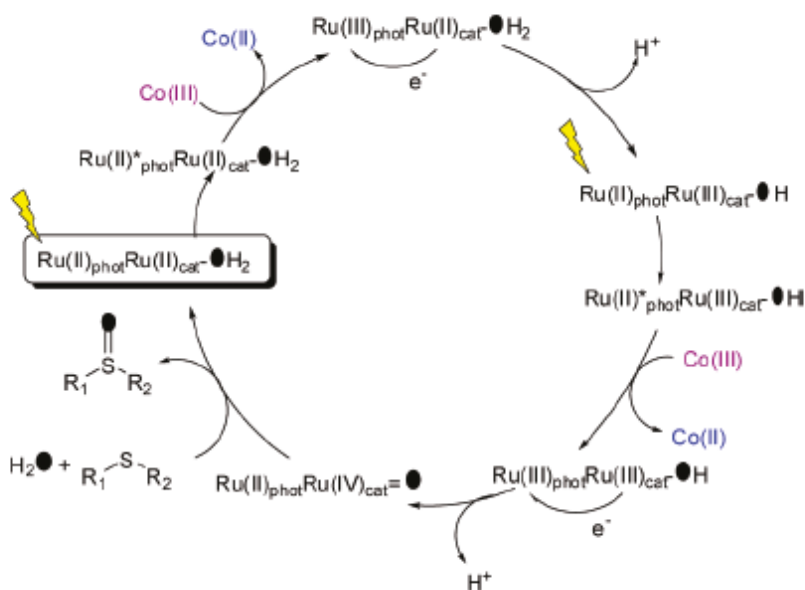
**Scheme. 1.** Oxygenation of organic substrate.

Therefore, very recently, a wide range of organic compounds like benzene, alkenes, alcohol and sulfides, received strong attention as suitable substrates for photocatalytic two-electron oxidations in water<sup>1-5</sup>. Nam and Fukuzumi recently presented the photocatalytic oxygenation of water soluble organic substrates, like *para*-styrene sulfonate using a manganese porphyrins as catalyst, [Ru(bpy)<sub>3</sub>]<sup>2+</sup> as photosensitizer and [Co(NH<sub>3</sub>)Cl]<sup>2+</sup> as sacrificial electron acceptor<sup>6</sup>. Elevated TN and TOF and nearly 100% of quantum efficiency have been obtained in phosphate buffer solution (pH 7.4). Labelling experiment confirmed that water is the oxygen source. Sun and co-workers later published the photocatalytic oxygenation of thioanisole and *p*-methoxythioanisole in high yield using ruthenium mononuclear catalysts, [Ru(bpy)<sub>3</sub>]<sup>2+</sup> as photosensitizer and [Co(NH<sub>3</sub>)Cl]<sup>2+</sup> as sacrificial electron acceptor<sup>4</sup>. In most of these cases, a ruthenium polypyridyl complex is

VII Artificial photosynthesis via two-electron oxidation processes

employed as catalyst, a  $[\text{Ru}(\text{bpy})_3]^{2+}$  derivate acts as photosensitizer and a Co or Pt compound is used as final sacrificial electron acceptor.

In other cases the bimolecular system catalyst-photosensitizer is replaced by a dyad constituted of a photosensitizer covalently bound to a polypyridyl ruthenium fragment<sup>7,8</sup>. Ménage reported the synthesis of a ruthenium-based dyad able to catalyze selective sulfide oxygenation<sup>7</sup>. A mechanistic pathway has been also proposed according to electrochemical and photophysical results obtained. Likely, the absorption of two photons by the photosensitizer fragment initiates two PCET processes from the  $\text{Ru}^{\text{II}}$  active site to the  $\text{Co}^{\text{III}}$  sacrificial acceptor that lead to the formation of  $\text{Ru}^{\text{IV}}=\text{O}$  species responsible of the oxygen atom transfer to the substrate (Figure 1).



**Figure 1.** Mechanistic pathway for photochemical sulfide oxygenation.

In both bimolecular and dyad examples high selectivities and turnover numbers have been obtained increasing the interest for light-driven oxidation reactions

using water as oxygen atom source. Given that protons and electrons are the only by-products of these reactions, the replacement of the commonly used electron acceptors is the final step for the assembly of a cell able to run organic reactions and produce  $H_2$  at the same time. However, in homogeneous systems, studies of water splitting have been generally carried out separately employing sacrificial oxidants and reductants while the combination of water oxidation and proton reduction in a homogeneous system remains a great challenge. Recently Zhao and co-workers reported a homogeneous multicomponent system for photocatalytic oxygenation of hydrocarbons and the production of  $H_2$ <sup>9</sup>. The use of two photosensitizers seems to be the key for the coupling of the two systems giving one of the first examples of a full-working photochemical cell for water oxidation and proton reduction where all components are in homogeneous phase.

In this chapter is reported the design and the optimization of a photocatalytic system based on the highly active catalyst  $\{[Ru^{II}(trpy)]_2(\mu-OOCMe)(\mu-dcpz)\}^+$  (where  $dcpz^{3-}$  is the pyrazole-3,5-dicarboxylate anion;  $trpy$  is 2,2':6',2''-terpyridine), **1**, described in Chapter IV. Its photocatalytic activity has been tested toward the oxygenation of different substrates in water, employing different photosensitizers, sacrificial acceptors and pH conditions.

After optimization of the photocatalytic conditions several attempts have been done for merging this system with a photochemical proton reduction catalysts, based on cobaloxime or hydrogenase, with the intention of set up an assembly for homogeneous artificial photosynthesis.

## VII. ii. Experimental section

**Materials.** All reagents used in the present work were obtained from Aldrich Chemical Co. or TCI chemicals and were used without further purification. Synthesis-grade organic solvents were obtained from SDS and were routinely degassed with argon. Ethanol was dried with a 3.5 Å molecular sieves, and acetonitrile, dichloromethane (DCM), hexane, and diethyl ether were used from the SPS. High-purity deionized water was obtained by passing distilled water through a nanopure Milli-Q water purification system.

**Equipment and Measurements.** All electrochemical experiments were performed in a PAR 263A EG&G potentiostat or in an IJ-Cambria HI-660 potentiostat, using a three-electrode cell. Glassy carbon (3 mm diameter) from BAS was used as the working electrode, a platinum wire as the auxiliary electrode, and SSCE as the reference electrode. Cyclic voltammograms were recorded at a  $100 \text{ mV}\cdot\text{s}^{-1}$  scan rate. The complexes were dissolved in previously degassed MeCN containing the necessary amount of  $(n\text{-Bu}_4\text{N})(\text{PF}_6)$ , used as the supporting electrolyte, to yield a 0.1 M ionic strength solution. All  $E_{1/2}$  values reported in this work were estimated from cyclic voltammetry (CV) as the average of the oxidative and reductive peak potentials  $(E_{p,a} + E_{p,c})/2$  or from differential pulse voltammetry (DPV; pulse amplitudes of 0.05 V, pulse widths of 0.05 s, sampling width of 0.02 s, and a pulse period of 0.1 s). Unless explicitly mentioned, the concentrations of the complexes were approximately 1 mM. A 400 MHz Bruker Avance II spectrometer and a Bruker Avance 500 MHz were used to carry out NMR spectroscopy at room temperature. Samples were run in  $\text{D}_2\text{O}$  and  $\text{CDCl}_3$ .

*General procedure for photochemical oxidation of organic substrates.* The photochemical experiments involved a three-component system: catalyst,

photosensitizer and sacrificial electron acceptor dissolved in 2 mL of a 50 mM phosphate buffer solution (pH 7.04). Irradiation was carried out with a 150 W xenon arc lamp equipped with a 400 nm cut-off filter to remove UV and IR radiation. The intensity of the radiation was approximately  $0.3 \text{ W}\cdot\text{cm}^{-2}$ . In a typical photocatalytic experiment of oxidation of sodium *para*-styrene sulfonate **1** (25  $\mu\text{L}$  of 4 mM solution of **1** in trifluoroethanol; final concentration = 0.05 mM), **P1** (0.16 mg,  $2\cdot 10^{-7}$  mol, final concentration = 0.1 mM),  $[\text{Co}(\text{NH}_3)_5\text{Cl}]\text{Cl}_2$  (20 mg,  $8\cdot 10^{-5}$  mol, final concentration = 40 mM), Sodium *para*-styrene sulfonate (4.12 mg,  $2\cdot 10^{-2}$  mol, final concentration = 10 mM) were mixed together in a vial covered from light and 2 mL of pH = 7 phosphate buffer in  $\text{D}_2\text{O}$ , a small amount of 3-(trimethylsilyl)-1-propanesulfonic acid sodium salt (DSS) was added as internal reference. Aliquots of 0.5 mL were taken before the irradiation, after 3 and 12 hours of irradiation and a  $^1\text{H-NMR}$  spectra was registered. Yield was calculated by integration of the substrate, epoxide and DSS. Yield =  $\{[\text{epoxide}]/[\text{DSS}]\}/\{[\text{alkene}]_0/[\text{DSS}]_0\}$  (where  $[\text{alkene}]_0$  and  $[\text{DSS}]_0$  are the initial concentration of sodium *para*-styrene sulfonate and DSS). Signals of epoxide were confirmed by comparison with the spectra of the *para*-styrene oxide sulfonate synthesized as described<sup>10</sup>. In a typical photocatalytic experiment of oxidation of thioanisole **1** (20  $\mu\text{L}$  of 4 mM solution of **1** in trifluoroethanol;  $8.0\cdot 10^{-8}$  mol, final concentration = 0.02 mM), **P1** (0.61 mg,  $8\cdot 10^{-7}$  mol, final concentration = 0.2 mM),  $[\text{Co}(\text{NH}_3)_5\text{Cl}]\text{Cl}_2$  (20 mg,  $8\cdot 10^{-5}$  mol, final concentration = 20 mM) in a total volume of 4 mL of pH = 5.5  $\text{SiF}_6^{2-}/\text{HCO}_3^-$  buffer), thioanisole (9.4  $\mu\text{L}$ ,  $8\cdot 10^{-5}$  mol, final concentration = 20 mM), DMF (4  $\mu\text{L}$ ,  $5.1\cdot 10^{-5}$  mol, 13 mM). The mixture was irradiated with visible light for 30 minutes and then extracted with dichloromethane ( $3\cdot 10$  mL) and the organic phase evaporated.  $^1\text{H-NMR}$  in  $\text{CDCl}_3$  was registered and compared



with the described spectra of sulfoxide<sup>4</sup>. Calculation of the yield of epoxide was made using the DMF peak as internal reference.

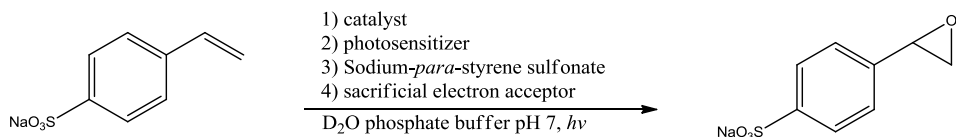
*General procedure for assembly of photocatalytic H<sub>2</sub> production particles. 2* (0.1 mL of a 2.0 mM aqueous solution of **2** in water,  $2.0 \cdot 10^{-7}$  mol, final concentration = 0.045 mM) was added slowly to a stirred (volume of stir bar: 0.15 mL) dispersion of TiO<sub>2</sub> nanoparticles (5 mg) and **1** (0.088 mg, 0.1 μmol, final concentration = 0.022 mM) in 4.3 mL of buffer (100 mM, pH 7) in a Pyrex pressure reaction vessel (total volume 9.5 mL). After 10 minutes, **P3**(Br)<sub>2</sub> (0.1 mL of a 1.0 mM aqueous solution,  $1.0 \cdot 10^{-7}$  mol, final concentration = 0.022 mM) was added dropwise to the stirred mixture of **2**-modified TiO<sub>2</sub> nanoparticles. After 15 min, thioanisole (10 μL, 85 μmol, final concentration = 19 mM) was added and the reaction vessel was sealed tightly with a rubber septum. The stirred and light-protected reaction vessel was purged with 2% CH<sub>4</sub> in N<sub>2</sub> for 15 min prior light experiments. Methane acts as an internal standard for H<sub>2</sub> quantification. The reaction vessel was thermostated with a water circulator connected to a water-jacketed reservoir at 25 °C.

*Photocatalytic H<sub>2</sub> and sulfoxide production.* Photocatalytic experiments were performed with either a slide projector light source (Kodak Carousel S-AV 1010) featuring a 250 W (24 V) tungsten halogen lamp (Philips, light intensity  $45 \text{ mW} \cdot \text{cm}^{-2}$  measured using a Melles Griot Broadband Power/Energy Meter 13PEM001) or with a Solar Light Simulator (Newport Oriel, 150 W,  $100 \text{ mW} \cdot \text{cm}^{-2}$ ) equipped with an air mass 1.5 global filter. IR irradiation was filtered in all experiments with a water filter, and the UV irradiation was filtered with a 420 nm cut-off filter (UQG Optics), unless otherwise noted (UV experiments). To reduce the light intensity to  $20 \text{ mW} \cdot \text{cm}^{-2}$  a neutral density filter with 20% transmission was used in one of the experiments. The amount of photo-generated H<sub>2</sub> was detected and quantified by headspace gas analysis with an

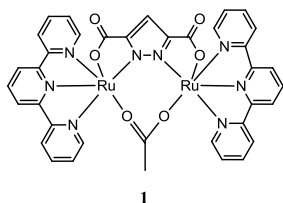
Agilent 7890A Series gas chromatograph (GC) equipped with a 5 Å molecular sieve column ( $N_2$  carrier gas at a flow rate of approximately  $3 \text{ mL}\cdot\text{min}^{-1}$ ). The column temperature was held isothermally at  $40 \text{ }^\circ\text{C}$ , and a thermal conductivity detector was used. The instrument was calibrated with various known amounts of  $H_2$  against  $CH_4$  and the linearity and stability of the instrument and method were checked regularly. The total irradiation time for each light experiment was 4 h, with  $10 \text{ }\mu\text{L}$  aliquots of the headspace gas removed for GC analysis after 0, 0.5, 1, 1.5, 2, 3 and 4 h (and 5, 6, 7, 8 and 24 h for the long-term experiment). After irradiation time the suspension was extracted three times with  $CH_2Cl_2$  and the organic fraction dried with  $MgSO_4$ . After evaporation of the solvent the residue was analyzed by  $^1\text{H-NMR}$  in  $CDCl_3$ , in order to quantify the amounts of final product and initial substrate.

### VII. iii. Photochemical oxidation of organic substrate

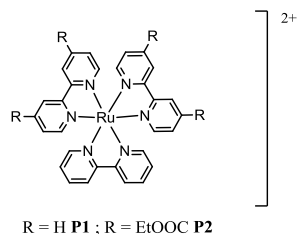
In order to test the photocatalytic activity of **1** toward the oxidation of organic substrates, a three component homogeneous system consisting of **1**, a photosensitizer, a catalyst and a sacrificial electron acceptor was selected. A representation of the photocatalytic oxidation of sodium *para*-styrene sulfonate is outlined in Schemes 2.



catalyst:



photosensitizer:

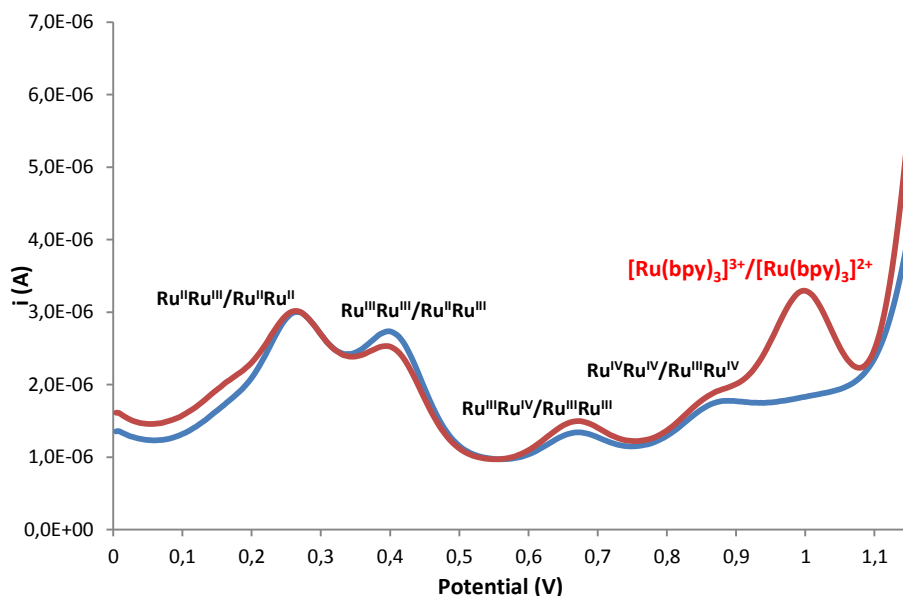


sacrificial electron acceptor: Co[(NH<sub>3</sub>)<sub>5</sub>Cl]Cl<sub>2</sub>

**Scheme 2.** Scheme of the photocatalytic epoxidation of sodium *para*-styrene sulfonate catalyzed by **1**.

### VII.iii.i. Results and discussion

Complex **1** has been described in Chapter IV as an active catalyst for alkenes oxidation in organic solvents in the presence of (diacetoxyiodo)benzene as terminal oxidant. Electrochemical studies and DFT calculation validated the proposed mechanism of formation of a  $\text{Ru}^{\text{IV}}\text{Ru}^{\text{IV}}$  di-oxo species responsible of the oxygen transfer to the C=C double bond. The elevated turnover frequency of oxidation reaction catalyzed by **1** influenced our decision to choice this catalyst for a photochemical system in which short lifetime of photo-induced species is usually a limiting factor. To generate the active species of **1**, four electrons have to be removed from the same molecule of catalyst by the photogenerated oxidant  $[\text{Ru}^{\text{III}}(\text{bpy})_3]^{3+}$  in order to form a di-oxo  $\text{Ru}^{\text{IV}}\text{Ru}^{\text{IV}}$  species. A differential pulse voltammogram of **1** in pH 2.0 triflic acid, has been registered in the presence of a small excess of  $[\text{Ru}(\text{bpy})_3](\text{ClO}_4)_2$ ,  $[\text{P1}(\text{ClO}_4)_2]$  (Figure 2). A pH independent wave of the one electron oxidation of the photosensitizer has been detected at 1.0 V vs SSCE, which is around 100 mV over the oxidation of the  $\text{Ru}^{\text{III}}\text{Ru}^{\text{IV}}$  species to  $\text{Ru}^{\text{IV}}\text{Ru}^{\text{IV}}$  complex.



**Figure 2.** DPV of **1** in pH 2.0 triflic acid 0.1 M. **1** (blue line), **1** + **P1** (red line); working electrode: glassy carbon, counter electrode: Pt, reference electrode: SSCE.

In a typical photocatalytic experiment **1** (25  $\mu\text{L}$  of 4 mM solution of **1** in trifluoroethanol;  $1.0 \cdot 10^{-7}$  mol, final concentration = 0.05 mM), **P1** (0.16 mg,  $2 \cdot 10^{-7}$  mol, final concentration = 0.1 mM),  $[\text{Co}(\text{NH}_3)_5\text{Cl}]\text{Cl}_2$  (20 mg,  $8 \cdot 10^{-5}$  mol, final concentration = 40 mM), Sodium *para*-styrene sulfonate (4.12 mg,  $2 \cdot 10^{-2}$  mol, final concentration = 10 mM) were mixed together in a vial covered from light and 2 mL of pH 7.0 phosphate buffer in  $\text{D}_2\text{O}$ , a small amount of 3-(trimethylsilyl)-1-propanesulfonic acid sodium salt (DSS) was added as internal reference. An aliquot of 0.5 mL were taken and a  $^1\text{H-NMR}$  spectra was registered (Figure SI1). After 3 hours of irradiation with visible light 20 TN of *para*-styrene oxide were obtained (Table 1, Entry 1). Overloading of Co(III) sacrificial acceptor led to a higher TN in the presence of the same amounts of catalyst and photosensitizer (Table 1, Entry 2). In contrast, an increment of the

concentration of photosensitizer did not affect markedly the activity (Table 1, Entry 3). When  $[\text{Ru}(\text{bpy})(\text{dcbpy})_2]^{2+}$  (where  $\text{dcbpy} = 4,4'-(\text{COOEt})_2\text{bpy}$ ) (**P2**, 0.23 mg,  $2 \cdot 10^{-7}$  mol, final concentration = 0.1 mM) was employed as photosensitizer 28 TN were obtained (Table 1, Entry 4). By reducing the concentration of **1** the highest TN of 65 was obtained (Table 1, entry 5). On the contrary, the use of other sacrificial acceptor like  $\text{K}_2\text{PtCl}_6$  and  $\text{Na}_2\text{S}_2\text{O}_8$  did not produce epoxide at all (Table 1, Entries 6-8). Lastly the change of buffer and pH slightly affect the catalytic performance (Table 1, Entry 9).

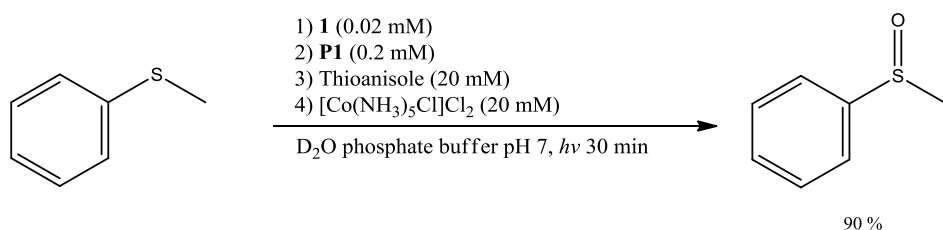
**Table 1.** Photocatalytic oxidation of Sodium *para*-styrene sulfonate with **1**

Entry	Catalyst [mM]	Photosensitizer [mM]	Sacrificial acceptor [mM]	Buffer	Product (TN)
1	<b>1</b> [0.05]	<b>P1</b> [0.1]	Co[(NH <sub>3</sub> ) <sub>5</sub> Cl]Cl <sub>2</sub> [40]	Phosphate, pH 7	20
2	<b>1</b> [0.05]	<b>P1</b> [0.1]	Co[(NH <sub>3</sub> ) <sub>5</sub> Cl]Cl <sub>2</sub> [80]	Phosphate, pH 7	40
3	<b>1</b> [0.05]	<b>P1</b> [0.2]	Co[(NH <sub>3</sub> ) <sub>5</sub> Cl]Cl <sub>2</sub> [40]	Phosphate, pH 7	22
4	<b>1</b> [0.05]	<b>P2</b> [0.1]	Co[(NH <sub>3</sub> ) <sub>5</sub> Cl]Cl <sub>2</sub> [40]	Phosphate, pH 7	28
5	<b>1</b> [0.01]	<b>P2</b> [0.1]	Co[(NH <sub>3</sub> ) <sub>5</sub> Cl]Cl <sub>2</sub> [40]	Phosphate, pH 7	65
6	<b>1</b> [0.05]	<b>P1</b> [0.1]	K <sub>2</sub> PtCl <sub>6</sub>	Phosphate, pH 7	0
7	<b>1</b> [0.05]	<b>P2</b> [0.1]	K <sub>2</sub> PtCl <sub>6</sub>	Phosphate, pH 7	0
8	<b>1</b> [0.05]	<b>P2</b> [0.1]	Na <sub>2</sub> S <sub>2</sub> O <sub>8</sub>	Phosphate, pH 7	0
9	<b>1</b> [0.05]	<b>P1</b> [0.1]	Co[(NH <sub>3</sub> ) <sub>5</sub> Cl]Cl <sub>2</sub> [40]	SiF <sub>6</sub> <sup>2-</sup> -HCO <sub>3</sub> <sup>-</sup> , pH 5.8	19

Reaction conditions: total volume = 2 mL of pH 7 phosphate buffer in D<sub>2</sub>O; aliquots analyzed by <sup>1</sup>H-NMR before irradiation, after 3 hours of irradiation and after 12 hours irradiation. Yield = {[epoxide]/[DSS]}/{[alkene]<sub>0</sub>/[DSS]<sub>0</sub>} (where [alkene]<sub>0</sub> and [DSS]<sub>0</sub> are the initial concentration of sodium *para*-styrene sulfonate and DSS). Irradiation was carried out with a 150 W Xenon arc lamp equipped with a 400 nm cut-off filter to remove UV and IR radiation. The intensity of the radiation was approximately 0.3 W·cm<sup>2</sup>. Control experiments without light and/or catalyst did not produce epoxide in detectable amounts.

More promising results were obtained in the sulfoxidation of thioanisole to methyl sulfoxide (Scheme 3). In the presence of **1** (20 μL of 4 mM solution of **1** in trifluoroethanol; 8.0·10<sup>-8</sup> mol, final concentration = 0.02 mM), **P1** (0.61 mg, 8·10<sup>-7</sup> mol, final concentration = 0.2 mM), [Co(NH<sub>3</sub>)<sub>5</sub>Cl]Cl<sub>2</sub> (20 mg, 8·10<sup>-5</sup> mol, final concentration = 20 mM) in a total volume of 4 mL of pH = 5.5 SiF<sub>6</sub><sup>2-</sup>/HCO<sub>3</sub><sup>-</sup> buffer), DMF (4 μL, 5.1·10<sup>-5</sup> mol, 13 mM) as internal reference, thioanisole (9.4

$\mu\text{L}$ ,  $8 \cdot 10^{-5}$  mol, final concentration = 20 mM) was converted to sulfoxide in 90% yield, corresponding to 450 TN after 30 minutes of irradiation by visible light (Figure SI2). No overoxidation to sulfone was detected. Control experiments showed negligible amounts of product with no catalyst or photosensitizer or light.



**Scheme 3.** Scheme of the photocatalytic sulfoxidation of thioanisole catalyzed by **1**.



### VII.iii.ii. Conclusions

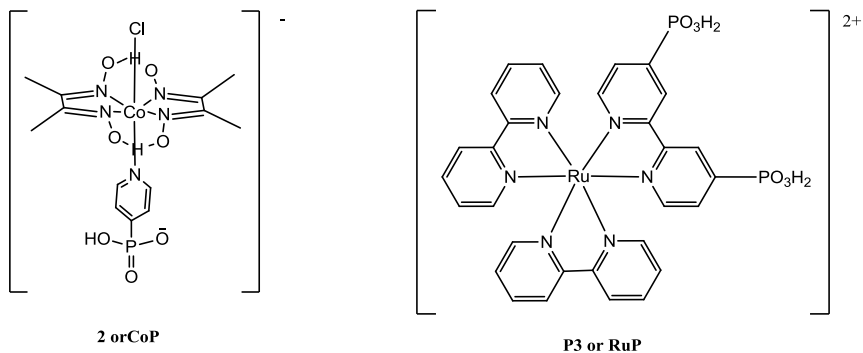
In the first part of this chapter it has been described the assembly of an efficient photochemical system for the oxidation of organic substrates constituted of a catalyst, a photosensitizer and a sacrificial electron acceptor. The ruthenium dinuclear complex **1**, described in Chapter IV as highly efficient catalyst for the epoxidation in organic solvents of alkenes, has been now demonstrated to be also an active catalyst for the photochemical epoxidation of the *para*-styrene sulfonate and sulfoxidation of thioanisole using water as oxidant under visible light. Under optimized conditions a max TN of 65 for the epoxide of styrene and 450 for the sulfoxide of thioanisole have been obtained. The latter result represents a valid starting point for the design of a clean and efficient method for selective large scale sulfoxidation. Moreover the high catalytic performance for the oxygenation of the sulfur atom, in terms yield and reaction time, makes the **1/P1** system an attractive candidate for the assembly of a cell for photochemical H<sub>2</sub> production.

## VII. iv. Assembly of a system for photochemical sulfide oxidation and proton reduction

In the second part of this chapter the results of the experimental project carried out in the group of Dr Erwin Reisner, at the University of Cambridge, are summarized.

This group has recently developed a heterogeneous photochemical system for proton reduction. TiO<sub>2</sub> nanoparticles were successfully functionalized with [Ru(bpy)<sub>2</sub>(dppbpy)]Br<sub>2</sub> (where dppbpy is 4,4'-(PO<sub>3</sub>H<sub>2</sub>)bpy), (**P3**(Br)<sub>2</sub>, Figure 3), and with a cobaloxime based catalyst, [Co<sup>III</sup>Cl(dmgh)<sub>2</sub>(pyridine)](Et<sub>3</sub>NH) (**2**(Et<sub>3</sub>NH) or **CoP**(Et<sub>3</sub>NH), Figure 3). One of the advantages of employing TiO<sub>2</sub> nanoparticles is to provide a fast electron transfer from the photoexcited photosensitizer to the catalyst reducing electronic recombination. The system, in the presence of an excess of triethanolamine (TEOA) as sacrificial electron donor, has been described to generate H<sub>2</sub> at pH 7 under irradiation of visible light<sup>11,12</sup>.

The aim of this collaboration was to assemble a cell for artificial photosynthesis for simultaneous sulfoxidation and H<sup>+</sup> reduction. **1** (Scheme 2) was chosen as catalyst for the oxidative part thanks to its high photocatalytic performance in thioanisole sulfoxidation. For the hydrogen production **2** and *Db* [NiFeSe]-H hydrogenase enzyme, described by Reisner and co-workers<sup>11-13</sup>, were tested. Both of these catalysts work in heterogeneous systems based on dispersed TiO<sub>2</sub> nanoparticles: the cobaloxime, as well as the photosensitizer **P3**, is attached through phosphonic linkage groups while hydrogenase has itself high affinity for the titanium oxide surface.



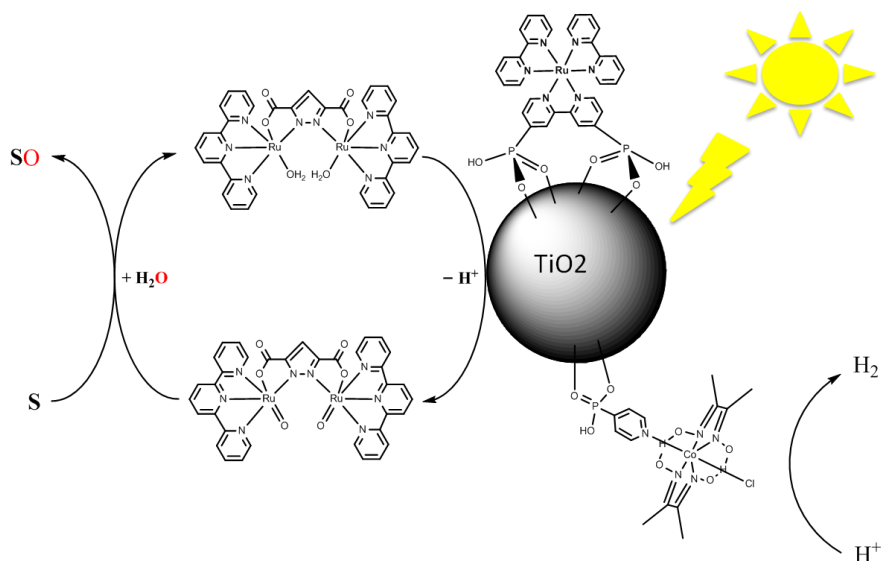
**Figure 3.** Structure of **2** and **P3**.

### VII.iv.i. Results and Discussion

#### [CoCl(dmgh)<sub>2</sub>(POOOH-pyridine)]<sup>+</sup>, CoP

Figure 4 shows the setup of the cell for the photocatalytic oxidation of an organic substrate and simultaneous H<sub>2</sub> generation.

In order to avoid any possible interaction with the TiO<sub>2</sub> nanoparticles a buffer made of non-coordinative species and able to maintain the pH above 6 (in order to maintain the catalytic activity of **2**<sup>11</sup>) has to be employed. For that reason the SiF<sub>6</sub><sup>-</sup>/HCO<sub>3</sub><sup>-</sup> couple was preferred to the H<sub>2</sub>PO<sub>4</sub><sup>-</sup>/HPO<sub>4</sub><sup>2-</sup> considering the high affinity of phosphate group for TiO<sub>2</sub> sites<sup>11</sup>. Photoinduced H<sub>2</sub> production, catalyzed by **2** in the presence of **P3** and TEOA, has been monitored in a SiF<sub>6</sub><sup>-</sup>/HCO<sub>3</sub><sup>-</sup> aqueous buffer at different concentration. H<sub>2</sub> generation resulted inhibited for concentration of HCO<sub>3</sub><sup>-</sup> = 30 mM, while no effect on the TN was detected for concentration of HCO<sub>3</sub><sup>-</sup> = 2 mM (Figure S13).



**Figure 4.** Scheme of the cell for the simultaneous photocatalytic sulfoxidation of thioanisole and proton production catalyzed by **1** and **2**.

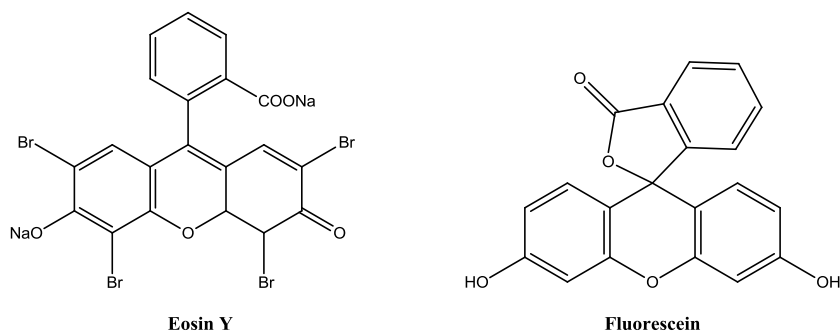
In a typical photocatalytic experiment **2** (0.1 mL of a 2.0 mM aqueous solution of **2** in water,  $2.0 \cdot 10^{-7}$  mol, final concentration = 0.045 mM) was first added to a stirred suspension of 5 mg of TiO<sub>2</sub> nanoparticles in 4.3 mL of SiF<sub>6</sub><sup>2-</sup>/HCO<sub>3</sub><sup>-</sup> (pH 7, 5 mM). After 30 minutes stirring, **1** (0.088 mg, 0.1 μmol, final concentration = 0.022 mM) was added and the reaction vessel was covered from light. The photosensitizer **P3** (0.1 mL of a 1.0 mM aqueous solution,  $1.0 \cdot 10^{-7}$  mol, final concentration = 0.022 mM) was added dropwise to the stirred and light-protected solution that was then stirred for 15 minutes more. Final addition of thioanisole (10 μL, 85 μmol, final concentration = 19 mM) was made and the whole system was purged with 2% CH<sub>4</sub> in N<sub>2</sub>. The vessel was then irradiated by visible light and aliquots of gas were taken and analyzed by GC. Under these conditions neither hydrogen nor sulfoxide was generated. The reactions conditions have been therefore modified in order to find the “Achilles heel” of the system and summarized below:

- The concentration of **2** used was varied in a range between 0.022 mM and 0.13 mM in order to test conditions of excess of **2** respect to **1** and *vice versa*.
- The concentration of **P3** was increased from 0.022 mM to 0.067 mM.
- The amount of TiO<sub>2</sub> nanoparticles was increased to 15 mg together with three-fold amount of **2** and **P3** in order to increase the activity of the system and the overall concentration respect to **1**.
- The photosensitizer was omitted and UV light applied in order to use the conduction band electrons of TiO<sub>2</sub> and **1** as hole scavenger

Also, other photosensitizers, like fluorescein (Figure 5), or mixture of photosensitizer/electron carrier, like methyl viologen, were tested. Sodium *para*-styrene sulfonate was also tested as substrate. All the experiment carried

out did not produce hydrogen in quantifiable amounts. Sulfoxide has been detected in some experiments, but never more than 4% yield (all the experimental data are sorted in Table SI1)

In order to check the proper functioning of the oxidative process some control experiments have been performed for the sulfoxidation reaction of thioanisole with **1** and different photosensitizers using  $[\text{Co}(\text{NH}_3)_5\text{Cl}]\text{Cl}_2$  as sacrificial electron acceptor. When **P3**/ $\text{TiO}_2$  was used a yield of 84% of sulfoxide was obtained (Table 2, Entry 2); unexpectedly, in the absence of  $\text{TiO}_2$  nanoparticles the yield decreased to a value of 6.7 % (Table 2, Entry 1). The organic dye Eosin Y (Figure 5) was also tested as photosensitizer resulting in a yield of epoxide of 9.7 %. The results of these catalytic experiments are reported in Table 2.



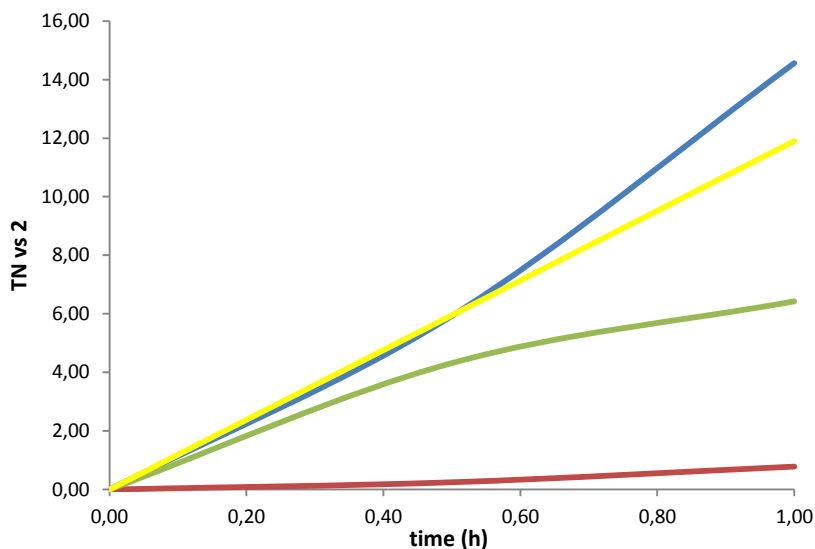
**Figure 5.** Structure of organic dye Eosin Y and Fluorescein.

**Table 2.** Photochemical oxidation of thioanisole with **1** and  $[\text{Co}(\text{NH}_3)_5\text{Cl}]\text{Cl}_2$ .

Entry	TiO <sub>2</sub> (mg)	<b>1</b> (mM)	Photosensitizer (mM)	Product yield (%)	Sulfoxide (mM)
1	-	<b>1</b> (0.12)	<b>P3</b> (0.12)	6.7	0.9
2	5	<b>1</b> (0.022)	<b>P3</b> (0.045)	84	11.4
3	-	<b>1</b> (0.022)	Eosin Y (0.32)	9.7	1.3

Reaction conditions:  $[\text{Co}(\text{NH}_3)_5\text{Cl}]\text{Cl}_2$  (30 mg, 0.12 mmol, final concentration = 30 mM), thioanisole (9.4  $\mu\text{L}$ , 0.08 mmol, final concentration = 20 mM), 4 mL total volume of  $\text{SiF}_6/\text{HCO}_3$  (pH = 7). 4 h irradiation with visible light.

Once excluded that an inhibition of the catalytic activity of **1** by **P3**/TiO<sub>2</sub> it was tested if **2** could be affected by the presence of **1** and thioanisole. For this control experiment, the catalytic H<sub>2</sub> production in standard conditions (**2** = 0.044 mM, **P3** = 0.022 mM, TEOA = 0.1 M, pH 7) was compared with the gas evolution in the presence of **1** and thioanisole. In Figure 6 the plot of TN of H<sub>2</sub> (respect **2**) vs time is presented. In blue line is plotted the H<sub>2</sub> in standard conditions. In the presence of **1** (0.22 mM) and thioanisole (19 mM) H<sub>2</sub> generation resulted totally inhibited (Figure 6, red line). In the absence of **1** the efficiency resulted reduced of ca 50% due to the presence of thioanisole (19 mM) (Figure 6, green line). Lastly in the absence of thioanisole, just a slight decrease in the performance of **2** was detected in the presence of **1** (0.022 mM).

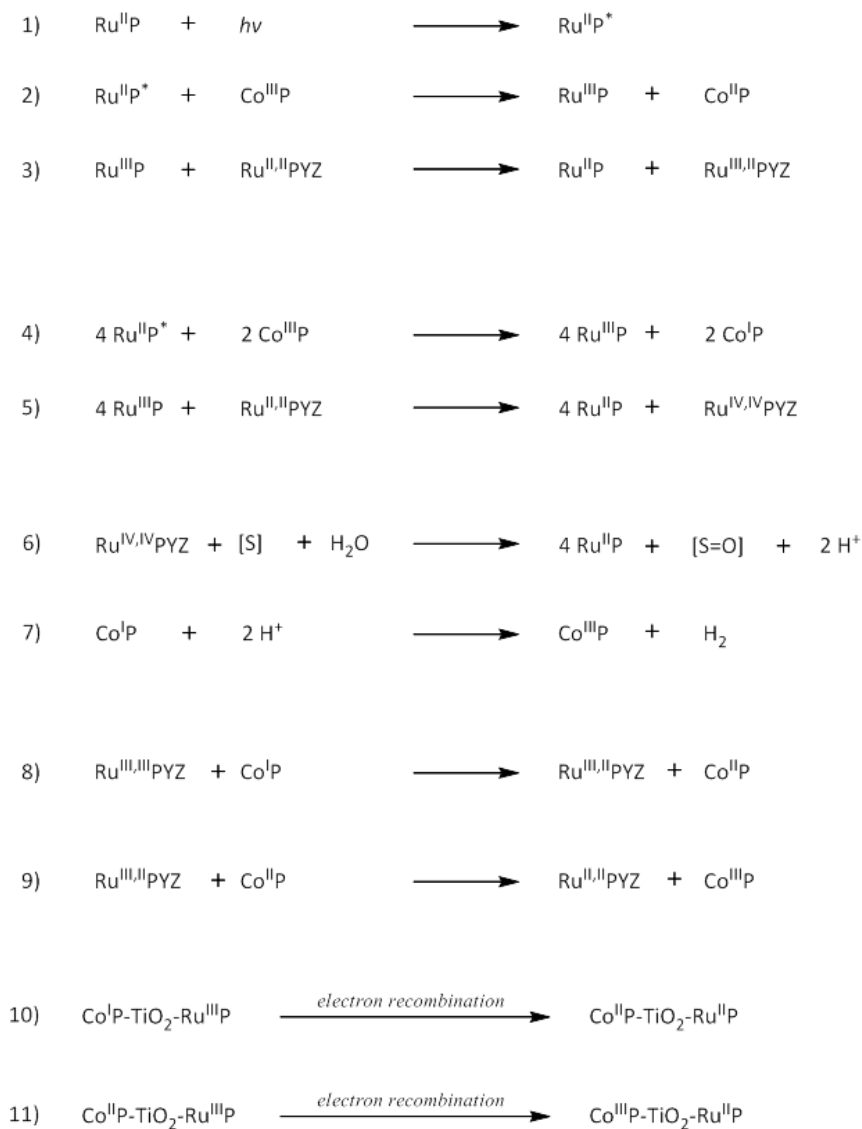


**Figure 6.** Hydrogen evolution (TN respect to **2**) catalyzed by **2** ( $4.4 \cdot 10^{-5}$  M) in the presence of **P3** ( $2.2 \cdot 10^{-5}$  M) and TEOA (0.1 M) under visible light in a pH 7  $\text{SiF}_6^{2-}/\text{HCO}_3^-$  (blue line). In the presence of **1** ( $2.2 \cdot 10^{-4}$  M) and thioanisole (19 mM) (red line). In the presence of thioanisole (19 mM) (green line). In the presence of **1** ( $2.2 \cdot 10^{-5}$  M) (yellow line).

These effects could be explained in terms of electron transfer according to the pathway illustrated in scheme 4, where CoP corresponds to **2**, RuP to **P3**, RuPYZ to **1**.



VII Artificial photosynthesis via two-electron oxidation processes



**Scheme. 4.** Proposed pathway for inhibition process.

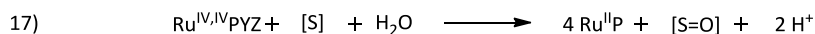
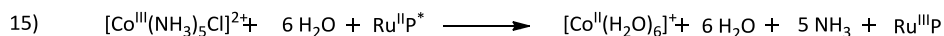
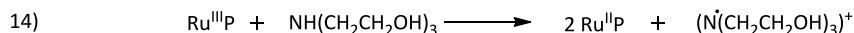
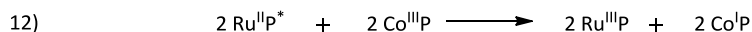
In Scheme 4 the first step 1) consists in the generation of the photoexcited species **Ru<sup>II</sup>P\*** by irradiation of the photosensitizer **Ru<sup>II</sup>P**. In reaction 2) the photogenerated **Ru<sup>II</sup>P\*** reduces **Co<sup>III</sup>P** to **Co<sup>II</sup>P** via a one electron process leading to the oxidized form of the photosensitizer **Ru<sup>III</sup>P**. The latter acts then

as oxidant generating  $\text{Ru}^{\text{III,II}}\text{PYZ}$  through a one electron oxidation of  $\text{Ru}^{\text{II,II}}\text{PYZ}$  as outlined in 3). Theoretically, further reductions and oxidations of  $\text{Co}^{\text{II}}\text{P}$  and  $\text{Ru}^{\text{III,II}}\text{P}$  by  $\text{Ru}^{\text{II}}\text{P}^*$  and  $\text{Ru}^{\text{III}}\text{P}$  should lead to the formation of  $\text{Co}^{\text{I}}\text{P}$  and  $\text{Ru}^{\text{IV,IV}}\text{P}$  according to the net reactions 4) and 5). The latter are supposed to be the catalytic active species for proton reduction and oxidation of organic substrates as shown in 6) and 7). However, the lack of  $\text{H}_2$  evolution during the whole experiment suggests some alternative pathways:

- a.*  $\text{Ru}^{\text{III,III}}\text{PYZ}$  is too strong an oxidant and oxidizes  $\text{Co}^{\text{I}}\text{P}$  to  $\text{Co}^{\text{II}}\text{P}$  before it could reduce protons (8 in Scheme 4).
- b.* Even  $\text{Ru}^{\text{III,II}}\text{PYZ}$  could be able to oxidize  $\text{Co}^{\text{I}}\text{P}$  to  $\text{Co}^{\text{II}}\text{P}$  before a new photogenerated  $\text{Ru}^{\text{II}}\text{P}^*$  forms  $\text{Co}^{\text{I}}\text{P}$  (9 in Scheme 4).
- c.* The electron recombination processes from  $\text{Co}^{\text{II}}\text{P-TiO}_2\text{-Ru}^{\text{III}}\text{P}$  or  $\text{Co}^{\text{I}}\text{P-TiO}_2\text{-Ru}^{\text{III}}\text{P}$  (10 and 11 in Scheme 4) could be faster than the oxidation reaction 3).

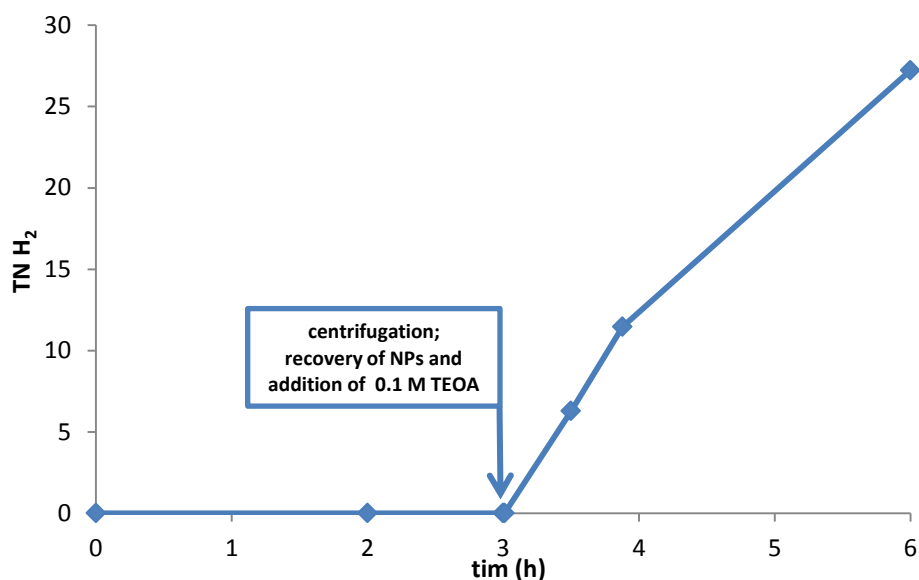
The sacrificial nature of TEOA and  $[\text{Co}(\text{NH}_3)_5\text{Cl}]\text{Cl}_2$  that, after donating or accepting electrons, undergo into irreversible decompositions<sup>14,15</sup> (Scheme 5, 12-17) ensures the proper working of the independent systems.

Artificial photosynthesis via two-electron oxidation processes



**Scheme 5.** Photochemical proton reduction and organic substrate oxidation with sacrificial electron donor (TEOA) and sacrificial electron acceptor.

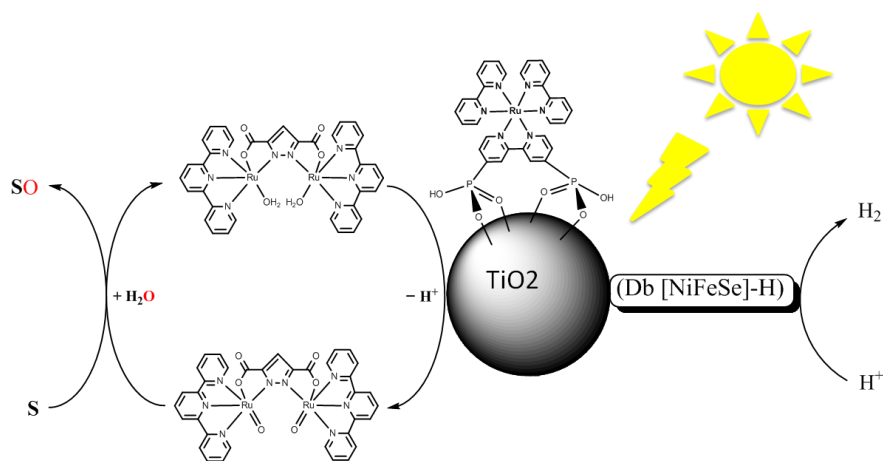
An electronic deactivation process like the one described in Scheme 4 should not affect the integrity of the catalysts. To check this hypothesis a nanoparticles recovery experiment has been performed. A catalytic experiment with **1** (0.022 mM), **2** (0.044 mM), **P3** (0.022 mM), TiO<sub>2</sub> (5 g), thioanisole (3.8 mM) was set up by following the procedure described above and irradiated for 3 hours with visible light. No H<sub>2</sub> was detected during this time. The mixture was then centrifuged and the nanoparticles recovered and treated with 4.5 mL of pH 7 TEOA 0.1 M solution and irradiated with visible light for 3 hours more. Generation of H<sub>2</sub> was suddenly detected.



**Figure 7.** Catalytic experiment and NPs recovery: **2** ( $4.4 \cdot 10^{-5}$  M), **P3** ( $2.2 \cdot 10^{-5}$  M), TiO<sub>2</sub> (5 mg), **1** ( $2.2 \cdot 10^{-5}$  M), thioanisole ( $3.78 \cdot 10^{-3}$  M), irradiation with visible light for 3 h. After centrifugation the recovered nanoparticles were treated with 4.5 mL of a 0.1 M solution of TEOA (pH 7) and irradiated again for 3 hours more.

### ***Db*-[NiFeSe]-hydrogenase, H<sub>2</sub>ase**

The use of an enzyme in the place of a cobaloxime assures higher TOF for H<sup>+</sup> reduction and a wider pH range but requires a strict control of some parameters of the reaction like the absence of oxygen and the stirring rate. A schematic representation of the system for simultaneous photocatalytic oxidation of an organic substrate and H<sub>2</sub> generation is showed below:



**Figure 8.** Scheme of the cell for photocatalytic sulfoxidation of thioanisole and H<sub>2</sub> production catalyzed by **1** and H<sub>2</sub>ase.

In a typical experiment **1** (0.088 mg, 0.1 μmol, final concentration = 0.022 mM) was first added to a stirred suspension of 5 mg of TiO<sub>2</sub> nanoparticles in 4.4 mL of SiF<sub>6</sub><sup>2-</sup>/HCO<sub>3</sub><sup>-</sup> (pH 7, 5 mM). After 10 minutes stirring the system was purged with 2% CH<sub>4</sub> in N<sub>2</sub>. H<sub>2</sub>-ase (8 μL of 5 mM solution, 40 pmol, final concentration 8.9 μM). After stirring for 15 minute the vessel was covered from light and **P3** (0.1 mL of a 2 mM aqueous solution, 0.2 μmol, final concentration = 0.044 mM). Thioanisole (10 μL, 85 μmol, final concentration = 19 mM) was lastly added the reaction vessel irradiated with visible light.

Both H<sub>2</sub> and Sulfoxide were detected from this experiment but the values disagreed (S=O > H<sub>2</sub>). Also, control experiment in the absence of **1** produced even more H<sub>2</sub> indicating the presence of small amounts of an electron donor in solution. This electron donor could be a residual buffer or another component from the synthesis of the hydrogenase<sup>16</sup>.

The amount of sulfoxide detected in the control experiment was in the limit of quantifiability, however the higher amount of H<sub>2</sub> produced makes difficult any interpretation of the data. The results in terms of TN of H<sub>2</sub> and sulfoxide are reported in Table 3.

**Table 3.** Catalytic data for simultaneous H<sub>2</sub> generation and thioanisole oxidation catalyzed by H<sub>2</sub>-ase and **1**.

Product	catalytic experiment		blank experiment	
	S=O	H <sub>2</sub>	S=O	H <sub>2</sub>
concentration	0.044 mM	0.014 mM	0.009 mM	0.029 mM
TN vs <b>1</b>	2	0.64		
TN vs P3	10	3.21	2	6.5
TN vs H <sub>2</sub> -ase	5000	1600	1000	3250

Catalytic conditions: **1** ( $2.2 \cdot 10^{-5}$  M), H<sub>2</sub>-ase (8.9 μM), P3 ( $4.4 \cdot 10^{-5}$  M), thioanisole ( $19 \cdot 10^{-3}$  M), irradiation with visible light for 5 h. H<sub>2</sub> detected by GC. Sulfoxide detected by NMR.

## VII.iv.ii. Conclusions

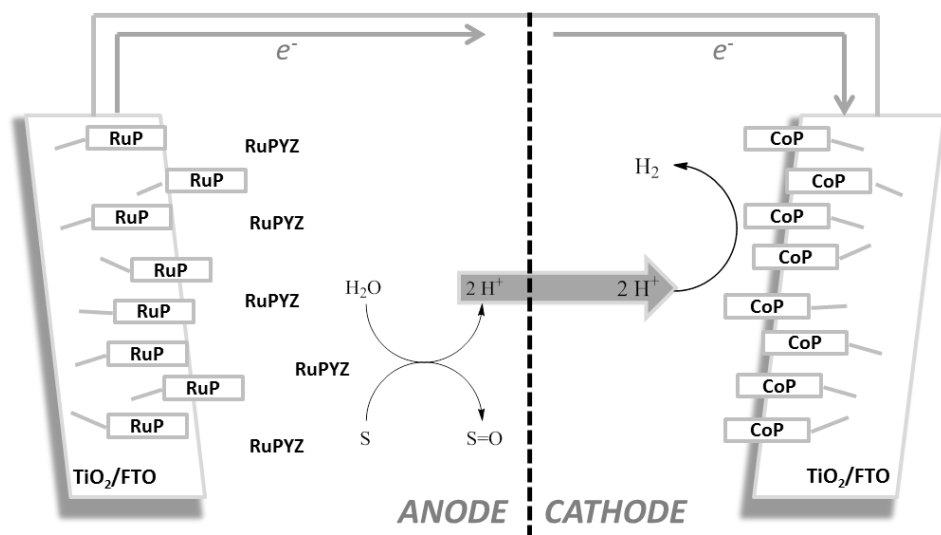
In this second part of the chapter has been presented one of the first attempts of assembly a cell for artificial photosynthesis with no sacrificial components. Several modifications of the reaction conditions have been operated in order to trigger the photocatalytic red/ox processes. Both semi-reactions have been individually proven to work in the same reaction conditions, nevertheless when merged in one photocatalytic system both reactions resulted inhibited.

The lack, or the presence just in traces, of  $H_2$  suggest that a sort of interaction between the two catalysts lies at the bottom of the inactivity of the whole cell.

The most likely quenching process is the oxidation of **2** by **1**. In other terms the reduced species  $Co^I$  is a better substrate for the oxidized  $Ru^{IV}=O$  species than thioanisole. In the case of hydrogenase, the high activity and the sterical hindrance around its active site, allow a slightly functioning of the cell in both reduction and oxidation. Nevertheless the mismatch between the values of two products and the unexpected activity measured in the control experiment makes difficult an interpretation of the resulting data.

In conclusion, **1** and **2** work properly at the same conditions when employed individually but lose their catalytic activity regard sulfoxidation and proton reduction when mixed together. Assuming that a red-ox quenching process like the one described above is the cause of the system collapse, a two compartments cell like the one shown in Figure 9 could be an efficacious option. An anode, constituted of an aqueous solution of **RuPYZ** and thioanisole and a FTO/ $TiO_2$  slide with supported **RuP**, would work, under visible light irradiation, as sulfoxidation system and source of protons which would be the only species able to pass through the membrane. In the cathode the electrons from photoexcited photosensitizer would reduce the supported **CoP**. Once

reached the oxidation state of active species the catalyst would reduce the protons generating  $H_2$ . In the whole process **RuPYZ** and **CoP** would be physically separated and the fast electron transfer ensured by FTO/ $TiO_2$  support would prevent any recombination process.



**Figure 9.** Scheme of a two compartment cell for simultaneous photochemical sulfoxidation and proton reduction with **1** and **2**.



## VII. v. Associated content

### Supporting Information

Additional spectroscopic and experimental data.

## VII. vi. Acknowledgements

C. D. G. is grateful to Dr. Pau Farràs for the help in setting up the system for the photochemical epoxidation. The experiments for the assembly of the cell have been performed in the laboratory of Dr. Erwin Reisner in Cambridge University.

C. D. G. is grateful to Dr. Reisner and his group for the help during the stay in his lab.

## VII. vii. References

- (1) Guillo, P.; Hamelin, O.; Batat, P.; Jonusauskas, G.; McClenaghan, N. D.; Ménage, S. *Inorg. Chem.* **2012**, *51*, 2222.
- (2) Chen, W.; Rein, F. N.; Scott, B. L.; Rocha, R. C. *Chem. Eur. J.* **2011**, *17*, 5595.
- (3) Kalita, D.; Radaram, B.; Brooks, B.; Kannam, P. P.; Zhao, X. *ChemCatChem* **2011**, *3*, 571.
- (4) Li, F.; Yu, M.; Jiang, Y.; Huang, F.; Li, Y.; Zhang, B.; Sun, L. *Chem Commun.* **2011**, *47*, 8949.
- (5) Ohkubo, K.; Kobayashi, T.; Fukuzumi, S. *Angew. Chem. Int. Ed.* **2011**, *50*, 8652.
- (6) Fukuzumi, S.; Kishi, T.; Kotani, H.; Lee, Y.-M.; Nam, W. *Nat Chem* **2011**, *3*, 38.
- (7) Hamelin, O.; Guillo, P.; Loiseau, F. d. r.; Boissonnet, M.-F.; Ménage, S. *Inorg. Chem.* **2011**, *50*, 7952.
- (8) Chen, W.; Rein, F. N.; Rocha, R. C. *Angew. Chem. Int. Ed.* **2009**, *48*, 9672.
- (9) Singh, W. M.; Pegram, D.; Duan, H.; Kalita, D.; Simone, P.; Emmert, G. L.; Zhao, X. *Angew. Chem. Int. Ed.* **2012**, *51*, 1653.
- (10) Yao, H.; Richardson, D. E. *J. Am. Chem. Soc.* **2000**, *122*, 3220.
- (11) Lakadamyali, F.; Reisner, E. *Chem. Commun.* **2011**, *47*, 1695.
- (12) Lakadamyali, F.; Kato, M.; Reisner, E. *Faraday Discuss.* **2012**, *155*, 191.
- (13) Reisner, E.; Powell, D. J.; Cavazza, C.; Fontecilla-Camps, J. C.; Armstrong, F. A. *J. Am. Chem. Soc.* **2009**, *131*, 18457.
- (14) Probst, B.; Rodenberg, A.; Guttentag, M.; Hamm, P.; Alberto, R. *Inorg. Chem.* **2010**, *49*, 6453.
- (15) Sun, L.; Hammarstrom, L.; Akermark, B.; Styring, S. *Chem. Soc. Rev.* **2001**, *30*, 36.
- (16) Hatchikian, E. C.; Bruschi, M.; Le Gall, J. *Biochem. Biophys. Res. Co.* **1978**, *82*, 451.

UNIVERSITAT ROVIRA I VIRGILI

NEW RUTHENIUM, MANGANESE AND COBALT DINUCLEAR COMPLEXES AS REDOX CATALYSTS.






UNFOLDING THE ESSENTIAL STEPS FOR THE GENERATION OF SOLAR FUELS

Carlo Di Giovanni

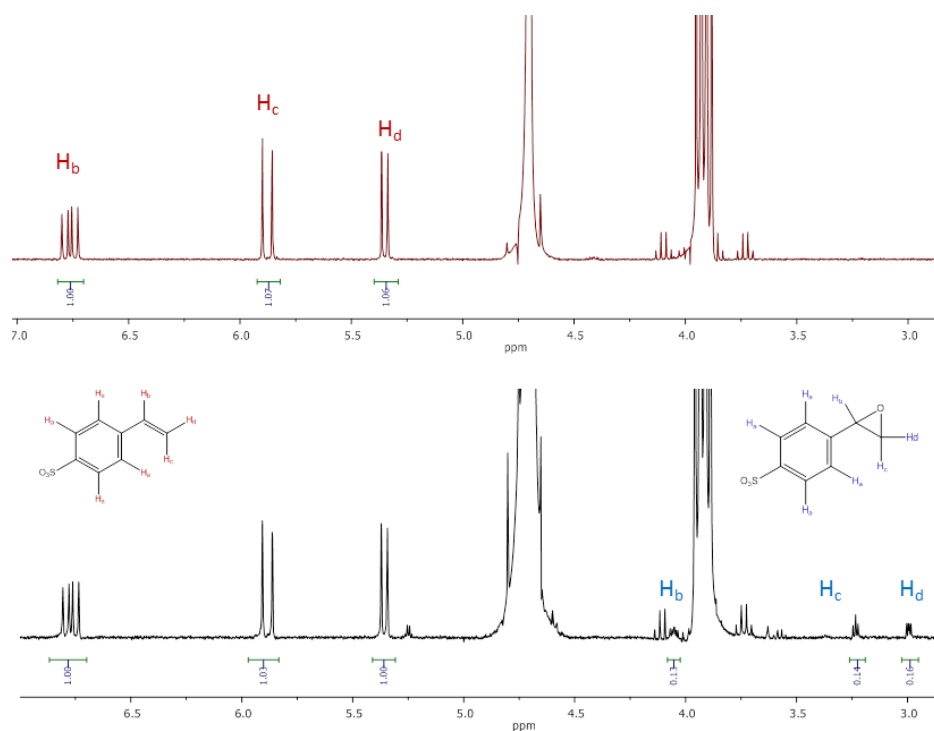
Dipòsit Legal: T. 1429-2012

# Chapter VII

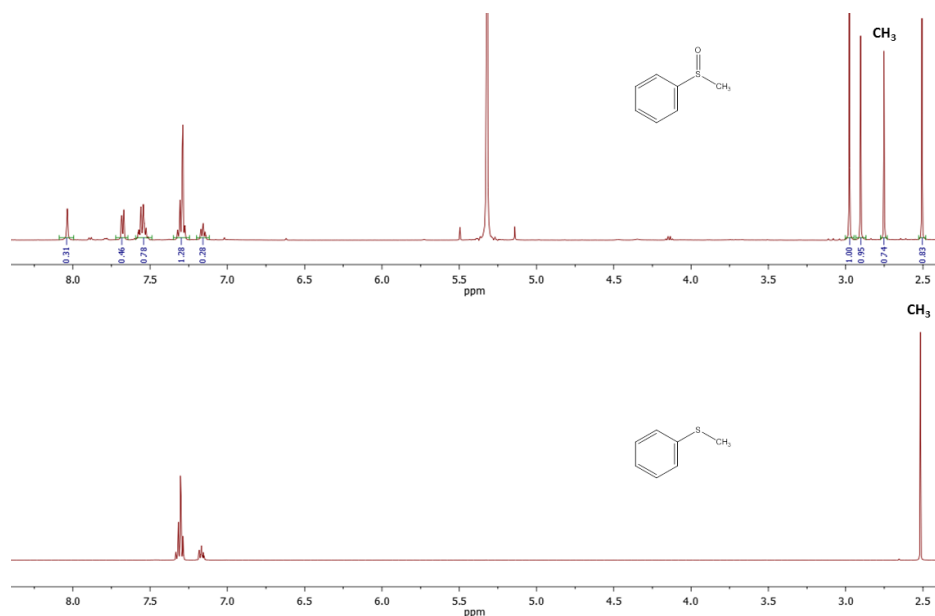
## Supporting Information

-  *<sup>1</sup>H-NMR of photocatalytic oxidation of sodium para-styrene sulfonate with **1**: Figure SI1*
-  *<sup>1</sup>H-NMR of photocatalytic oxidation of thioanisole with **1**: Figure SI2*
-  *Hydrogen production catalyzed by **2**, dependence on  $[\text{HCO}_3^-]$ : Figure SI3*
-  *Photocatalytic experiment with **CoP**: Table SI1*
-  *Photocatalytic experiment with **H<sub>2</sub>-ase**: Table SI2*

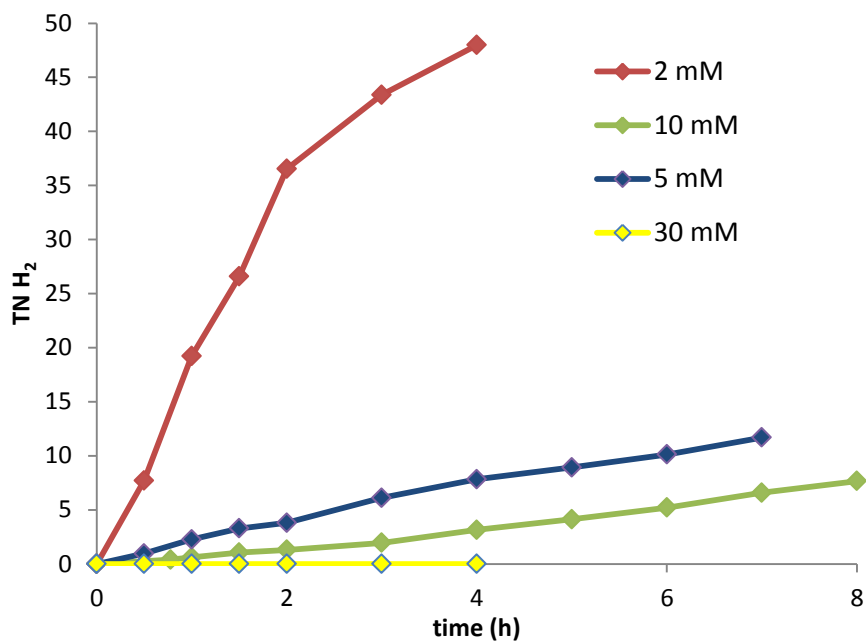




**Figure S11.** <sup>1</sup>H-NMR of photocatalytic oxidation of sodium *para*-styrene sulfonate with **1** (400 MHz, 298 K, D<sub>2</sub>O). Reaction conditions: **1** (25 μL of 4 mM solution of **1** in trifluoroethanol; 1·10<sup>-7</sup> mol, final concentration = 0.05 mM), **P1** (0.16 mg, 2·10<sup>-7</sup> mol, final concentration = 0.1 mM), [Co(NH<sub>3</sub>)<sub>5</sub>Cl]Cl<sub>2</sub> (20 mg, 8·10<sup>-5</sup> mol, final concentration = 40 mM), Sodium *para*-styrene sulfonate (4.12 mg, 2·10<sup>-2</sup> mol, final concentration = 10 mM), DSS as internal reference. Total volume = 2 mL of pH = 7 phosphate buffer in D<sub>2</sub>O). Irradiation for 3 hours with a 150 W Xenon arc lamp equipped with a 400 nm cut-off filter to remove UV and IR radiation. The intensity of the radiation was approximately 0.3 W/cm<sup>2</sup>. Yield = {[epoxide]/[DSS]}/{[alkene]<sub>0</sub>/[DSS]<sub>0</sub>} (where [alkene]<sub>0</sub> and [DSS]<sub>0</sub> are the initial concentration of sodium *para*-styrene sulfonate and DSS. (up, time = 0; down, time = 3h).



**Figure S12.** <sup>1</sup>H-NMR of photocatalytic oxidation of sodium thioanisole with **1** (400 MHz, 298 K, CDCl<sub>3</sub>). Reaction conditions: **1** (20 μL of 4 mM solution of **1** in trifluoroethanol; 8·10<sup>-8</sup> mol, final concentration = 0.02 mM), **P1** (0.61 mg, 8·10<sup>-7</sup> mol, final concentration = 0.2 mM), [Co(NH<sub>3</sub>)<sub>5</sub>Cl]Cl<sub>2</sub> (20 mg, 8·10<sup>-5</sup> mol, final concentration = 20 mM), thioanisole (9.4 μL, 8·10<sup>-5</sup> mol, final concentration = 20 mM), DMF (4 μL, 5.1·10<sup>-5</sup> mol, 13 mM) as internal reference. Total volume = 4 mL pH 5.5 SiF<sub>6</sub><sup>2-</sup>/HCO<sub>3</sub><sup>-</sup> buffer. Irradiation for 30 min with a 150 W Xenon arc lamp equipped with a 400 nm cutoff filter to remove UV and IR radiation. The solution was then extracted with dichloromethane (3 · 10 mL) and the organic phase evaporated. (up, catalytic experiment; down, <sup>1</sup>H-NMR in CDCl<sub>3</sub>, of commercial thioanisole).



**Figure SI3.** Hydrogen production catalyzed by **2** ( $4.4 \cdot 10^{-5}$  M) in the presence of **3P** ( $2.2 \cdot 10^{-5}$  M) and TEOA (0.1 M) under visible light in a pH 7  $\text{SiF}_6^{2-}/\text{HCO}_3^-$ . Dependence on  $[\text{HCO}_3^-]$ .



**Table SI1.** Photocatalytic experiment with CoP. (1/2)

Reductant ( $\mu\text{mol}$ )	TiO <sub>2</sub> (mg)	Photosensitizer ( $\mu\text{mol}$ )	Oxidant ( $\mu\text{mol}$ )	Buffer (pH)	Substrate ( $\mu\text{mol}$ )	hv	H <sub>2</sub>	Product ( $\mu\text{mol}$ )
CoP (0.2)	5	RuP (0.1)	TEOA	TEOA	-	vis	Yes	-
CoP (0.2)	5	RuP (0.1)	TEOA	TEOA + SiF <sub>6</sub> /HCO <sub>3</sub> (7)	-	vis	Yes	-
CoP (0.2)	5	RuP (0.1)	TEOA	TEOA + SiF <sub>6</sub> /B <sub>4</sub> O <sub>7</sub> (7)	-	vis	No	-
CoP (0.2)	5	RuP (0.1)	RuPYZ (1)	SiF <sub>6</sub> /HCO <sub>3</sub> (7)	-	vis	No	-
CoP (0.2)	5	RuP (0.1)	RuPYZ (0.5)	SiF <sub>6</sub> /HCO <sub>3</sub> (7)	-	vis	No	-
CoP (0.2)	5	RuP (0.1)	RuPDZ (1)	SiF <sub>6</sub> /HCO <sub>3</sub> (7)	-	vis	No	-
CoP (0.2)	5	RuP (0.1)	Bis/Tris	Bis/Tris (7)	-	vis	Yes	-
CoP (0.2)	5	RuP (0.1)	RuPYZ (1) TEOA	SiF <sub>6</sub> /HCO <sub>3</sub> (7)	17	vis	No Yes	-
CoP (0.2)	5	RuP (0.1) Ru(bpy) <sub>3</sub>	RuPYZ (1)	SiF <sub>6</sub> /HCO <sub>3</sub> (7)	-	vis	No traces	-
CoP (0.2)	5	Ru(bpy) <sub>3</sub> (1)	RuPYZ (1)	SiF <sub>6</sub> /HCO <sub>3</sub> (7)	-	vis	traces	-
CoP (0.2)	5	- Ru(bpy) <sub>3</sub>	RuPYZ (1)	SiF <sub>6</sub> /HCO <sub>3</sub> (7)	-	UV	No	-
CoP (0.2)	5	RuP (0.1)/MV <sup>2+</sup>	RuPYZ (1)	SiF <sub>6</sub> /HCO <sub>3</sub> (7)	-	vis	No	-
CoP (0.2)	5	Ru(bpy) <sub>3</sub> (1)/MV <sup>2+</sup>	RuPYZ (1)	SiF <sub>6</sub> /HCO <sub>3</sub> (7)	-	vis	No	-
CoP (0.2)	5	Ru(bpy) <sub>3</sub> (1) RuP (0.1)	TEOA	TEOA (7)	-	vis	No Yes	-
CoP (0.2)	5	RuP (0.1)	RuPYZ (1)	SiF <sub>6</sub> /HCO <sub>3</sub> (7)	-	vis	No	-
CoP (0.2)	5	RuP (0.2)	RuPYZ (0.1)	SiF <sub>6</sub> /HCO <sub>3</sub> (7)	80	vis	No	0.85
CoP (0.6)	15	RuP (0.3)	RuPYZ (0.1)	SiF <sub>6</sub> /HCO <sub>3</sub> (7)	85	vis	No	3.2
CoP (0.4)	10	RuP (0.2)	RuPYZ (0.45)	SiF <sub>6</sub> /HCO <sub>3</sub> (7)	85	vis	No	No
CoP (0.2)	5	-	RuPYZ (0.225)	SiF <sub>6</sub> /HCO <sub>3</sub> (7)	85	UV	No	0.32

*contd.*

**Table SI1.** Photocatalytic experiment with CoP. (2/2)

Reductant ( $\mu\text{mol}$ )	TiO <sub>2</sub> (mg)	Photosensitizer ( $\mu\text{mol}$ )	Oxidant ( $\mu\text{mol}$ )	buffer (pH)	Substrate ( $\mu\text{mol}$ )	h $\nu$	H <sub>2</sub>	Product ( $\mu\text{mol}$ )
CoP (0.2)	5	RuP (0.1)	TEOA	TEOA/CF <sub>3</sub> EtOH (7)	-	vis		-
CoP (0.2)	5	RuP (0.1) Ru(bpy) <sub>3</sub>	RuPYZ (1)	TEOA/CF <sub>3</sub> EtOH (7)	85	vis	No	0.3
CoP (0.2)	5	Fluorescein (2.9)	RuPYZ (0.11)	SiF <sub>6</sub> /HCO <sub>3</sub> (7)	85	vis	No	0.69
CoP (0.2)	-	Fluorescein (5.4)	RuPYZ (1.2)	CF <sub>3</sub> EtOH/SiF <sub>6</sub> /HCO <sub>3</sub> (7)	85	vis	No	-
CoP (0.6)	15	Ru(bpy) <sub>3</sub> (2.46) RuP (0.3)	RuPYZ (2.27)	SiF <sub>6</sub> /HCO <sub>3</sub> (7)	85	vis		-
CoP (0.6)	15	Ru(bpy) <sub>3</sub> (2.46)/RuP (0.3)	RuPYZ (2.27)	SiF <sub>6</sub> /HCO <sub>3</sub> (7)	85	vis	No	2,02
CoP (0.2)	5	RuP (0.1) Ru(bpy) <sub>3</sub> (1)	RuPYZ (5.1)	H <sub>2</sub> O (7)	85	vis	No No	
CoP (0.2)	5	Ru(bpy) <sub>3</sub> (1 $\mu\text{mol}$ )	RuPYZ (1 $\mu\text{mol}$ )	SiF <sub>6</sub> /HCO <sub>3</sub> (7)	85	vis	No	0.63
CoP (0.2)	5	RuP (0.1)	RuPYZ (1) TEOA	TEOA (7)	85	vis	0.78 (1h)	
CoP (0.2)	5	RuP (0.1)	TEOA	TEOA (7)	85	vis	6.43 (1h)	
CoP (0.2)	5	Ru(bpy) <sub>3</sub> (1) RuP (0.1)	RuPYZ (0.1)	SiF <sub>6</sub> /HCO <sub>3</sub> (7)	68	vis	No No	0.83
CoP (0.1)	5	-	RuPYZ (0.1)	SiF <sub>6</sub> /HCO <sub>3</sub> (7)	85	UV	No	
CoP (0.1)	5	RuP (0.1)	RuPYZ (0.1)	SiF <sub>6</sub> /HCO <sub>3</sub> (7)	10 (NaSS)	vis	No	
CoP (0.1)	5	RuP (0.1)	RuPYZ (0.1)/TEOA	TEOA (7)	-	vis	11.9 (1h)	

**Table SI2.** Photocatalytic experiments with **H<sub>2</sub>-ase**.

Reductant (pmol)	TiO <sub>2</sub> (mg)	Photosensitizer (μmol)	Oxidant (μmol)	buffer (pH)	Substrate (μmol)	hν	H <sub>2</sub> (μmol)	Product (μmol)
H <sub>2</sub> -ase (40)	-	RuP (0.1)/MV <sup>2+</sup>	1. RuPYZ (1) 2. TEOA	SiF <sub>6</sub> /HCO <sub>3</sub> (7)	-	vis	No No	-
H <sub>2</sub> -ase (40)	-	Ru(bpy) <sub>3</sub> (1)	RuPYZ (0.1)	SiF <sub>6</sub> /HCO <sub>3</sub> (7)	80	vis	No	No
H <sub>2</sub> -ase (40)	5	RuP (0.2)	RuPYZ (0.11)	SiF <sub>6</sub> /HCO <sub>3</sub> (7)	80	vis		0.4
H <sub>2</sub> -ase (40)	5	RuP (0.1)	RuPYZ (0.11)	SiF <sub>6</sub> /HCO <sub>3</sub> (7)	85	vis	0.108	No
H <sub>2</sub> -ase (40)	5	RuP (0.1)	RuPYZ (0.11)	SiF <sub>6</sub> /HCO <sub>3</sub> (6)	85	vis	0.043	0.45
H <sub>2</sub> -ase (40)	5	RuP (0.1)	RuPYZ (0.11)	SiF <sub>6</sub> /HCO <sub>3</sub> (6)	85	vis	n.q.	2.07
H <sub>2</sub> -ase (40)	5	RuP (0.1)	RuPYZ (0.22)	SiF <sub>6</sub> /HCO <sub>3</sub> (6.5)	85	vis		0.19
H <sub>2</sub> -ase (40)	5	RuP (0.1)	RuPDZ (0.1)	SiF <sub>6</sub> /HCO <sub>3</sub> (6.5)	85	vis		-
H <sub>2</sub> -ase (40)	5	RuP (0.1)	RuPYZ (0.1)	SiF <sub>6</sub> /HCO <sub>3</sub> (6.85)	85	vis	0.08	0.76
H <sub>2</sub> -ase (40)	5	RuP (0.02)	RuPYZ (0.1)	H <sub>2</sub> O (6.22)	85	vis	0.064	0.2

UNIVERSITAT ROVIRA I VIRGILI

NEW RUTHENIUM, MANGANESE AND COBALT DINUCLEAR COMPLEXES AS REDOX CATALYSTS.

UNFOLDING THE ESSENTIAL STEPS FOR THE GENERATION OF SOLAR FUELS

Carlo Di Giovanni

Dipòsit Legal: T. 1429-2012

UNIVERSITAT ROVIRA I VIRGILI

NEW RUTHENIUM, MANGANESE AND COBALT DINUCLEAR COMPLEXES AS REDOX CATALYSTS.

UNFOLDING THE ESSENTIAL STEPS FOR THE GENERATION OF SOLAR FUELS

Carlo Di Giovanni

Dipòsit Legal: T. 1429-2012

# Chapter VIII

## Summary and Conclusions



- Two new ruthenium dinuclear complexes containing the bridging pyridazine-3,6-dicarboxylic acid has been synthesized and fully characterized. The catalytic activity toward the oxidation of water and epoxidation of alkenes has been investigated.
- A new acetato-bridged ruthenium dinuclear complex containing the pyrazole-3,5-dicarboxylate bridging ligand has been synthesized and fully characterized. The catalytic activity of the bis-aqua complex, generated by hydrolysis of the acetato-bridge, was tested in epoxidation of alkenes resulting in high turnover number and turnover frequency. A mechanism based on a radical path favoured by supramolecular catalyst-substrate interactions has been proposed for the epoxidation reaction and supported by electrochemical data and DFT calculations.
- A new bis-aqua dinuclear manganese complex containing the pyrazole-3,5-dicarboxylate bridging ligand has been synthesized and characterized by X-Ray diffraction and susceptibility measurements. The epoxidation of *cis*- $\beta$ -methylstyrene with peracetic acid has been tested. A polymeric species has been also obtained by recrystallization of the dimer in presence of an excess of a chloride.
- A new polypyridyl decadentate ligand has been designed and synthesized. The ligand was fully characterized by  $^1\text{H-NMR}$  and  $^{13}\text{C-NMR}$ , EA and mass spectroscopy.



## VIII Summary and Conclusions

- A new dinuclear Co complexes containing a decadentate ligand has been prepared. Structural, spectroscopic and electrochemical characterization has been done. The complex was tested as redox catalyst for electrochemical proton reduction and water oxidation.
- A photocatalytic system for oxidation of alkenes and sulfides by a ruthenium dinuclear catalyst in water has been set up. Sodium-*para*-styrene sulfate and thioanisole have been oxidized in presence of  $[\text{Ru}(\text{bpy})_3]^{2+}$  and a cobalt sacrificial electron acceptor under visible light.
- A homogeneous system for simultaneous sulfoxidation and proton reduction has been set up and tested.

UNIVERSITAT ROVIRA I VIRGILI

NEW RUTHENIUM, MANGANESE AND COBALT DINUCLEAR COMPLEXES AS REDOX CATALYSTS.

UNFOLDING THE ESSENTIAL STEPS FOR THE GENERATION OF SOLAR FUELS

Carlo Di Giovanni

Dipòsit Legal: T. 1429-2012

UNIVERSITAT ROVIRA I VIRGILI

NEW RUTHENIUM, MANGANESE AND COBALT DINUCLEAR COMPLEXES AS REDOX CATALYSTS.

UNFOLDING THE ESSENTIAL STEPS FOR THE GENERATION OF SOLAR FUELS

Carlo Di Giovanni

Dipòsit Legal: T. 1429-2012